THE ROLE OF MECHANO-GROWTH FACTOR

IN SKELETAL MUSCLE INJURY

KENG TING, SUN

Ph.D

The Hong Kong Polytechnic University

2018

The Hong Kong Polytechnic University

Department of Rehabilitation Sciences

The Role of Mechano-growth Factor in Skeletal Muscle Injury

Keng Ting, SUN

A thesis submitted in partial fulfilment of the requirements for the degree of

Doctor of Philosophy

November, 2017

CERTIFICATE OF ORIGINALITY

I hereby declare that this thesis is my own work and that, to the best of my knowledge and belief, it reproduces no material previously published or written, nor material that has been accepted for the award of any other degree or diploma, except where due acknowledgement has been made in the text.

_____(Signed)

Keng Ting, SUN (Name of student)

ABSTRACT

Skeletal muscle regeneration is a well-orchestrated process involving regulated inflammatory response. Infiltrated myeloid cells, in particular macrophages, are implicated in the release of key soluble factors to modulate muscle inflammation. One such factor, insulin-like growth factor-1 (IGF-1) suppresses inflammatory cytokine expression and promotes anti-inflammatory macrophage polarization. However, IGF-1 exists in two isoforms and one of them IGF-1Ea was shown to be anti-inflammatory. Another isoform, mechano-growth factor (MGF) is structurally and functionally distinct from IGF-1Ea but it is unclear if MGF is implicated in muscle inflammation. In this thesis, we hypothesize that (i) the upregulation of MGF in injured muscle is associated with infiltration of myeloid cells including macrophages; and (ii) MGF can modulate inflammatory response during muscle injury.

We first examined the transcription of MGF in response to cardiotoxin (CTX)-induced muscle injury in vivo. MGF upregulation correlated with that of inflammatory cytokines and coincided with myeloid cell infiltration. Furthermore, myeloid cells isolated at the time of MGF upregulation in injured muscles, including neutrophils and macrophages, expressed MGF. These findings suggested that MGF is associated with muscle inflammatory response, particularly the infiltration of myeloid cells. It prompted us to examine the roles of MGF in modulating muscle inflammatory response.

We then investigated whether MGF could affect the expression of inflammatory markers and macrophage populations in muscle injury. At

day 5, MGF overexpression led to upregulation of inflammatory markers which coincided with prolonged but transient increase of pro-inflammatory macrophages. The prolonged presence of macrophages might contribute to the inflammatory marker upregulation. Muscle resident cells were also implicated in the upregulation of these markers because MGF overexpression in the absence of CTX-induced injury could increase their expression level, yet in lower magnitude relative to the injury context. We then studied whether the modulation of inflammatory response by MGF overexpression translated into changes in muscle regeneration. The number and cross-sectional area of regenerating myofibers and the expression of regeneration-related transcripts were, nevertheless, not altered by MGF overexpression.

This study highlights the roles of MGF in the expression of inflammatory markers and the modulation of macrophage resolution. The potential mechanisms of MGF in modulating inflammatory processes were discussed. To understand the role of MGF in muscle inflammation, future studies should examine the survival of pro-inflammatory macrophages. Although MGF expression did not seem to affect muscle regeneration outcomes, the current findings are novel and offer insights on the physiological roles of MGF in inflammatory response of muscle injury.

PUBLICATIONS

Manuscripts

1. Llano-Diez M, Cheng AJ, Jonsson W, Ivarsson N, Westerblad H, Sun V, Cacciani N, Larsson L & Bruton J (2016). Impaired Ca(2+) release contributes to muscle weakness in a rat model of critical illness myopathy. *Crit Care* **20,** 254.
2. Sun KT, Cheung KK, Yeung SS & Yeung EW. Role of mechano-growth factor in modulating inflammatory response to muscle injury. *In preparation.*

Book Chapter

1. Yeung EW, Cheung KK & Sun KT (2017). Biological role of TRPC1 in myogenesis, regeneration, and disease. In *The Plasticity of Skeletal Muscle*, ed. Sakuma K, pp. 211–230. Springer Singapore, Singapore.

Conference Presentations

1. Sun KT & Yeung EW (2015). "Involvement of mechano-growth factor in muscle regeneration and aging". Poster presented in *9th Pan-Pacific Conference on Rehabilitation cum 21st Annual Congress of Gerontology*, Hong Kong SAR.
2. Sun KT, Yeung EW, Yeung SS & Cheung KK (2015). "Regenerative capacity following muscle injury in mdx mice – Role of mechano-growth factor (MGF)". Poster presented in *14th Asian and Oceanian Myology Center Annual Scientific Meeting 2015*, Bangkok, Thailand.

ACKNOWLEDGEMENTS

I owe my deepest gratitude to my respectful chief supervisor, Dr. Ella W Yeung. With her full support, I can complete this challenging study with all the resources I need. With her coordination, I was granted the opportunity to learn and research in one of the most prestigious medical university, Karolinska Institutet in Sweden. Yet without her enthusiasm and experience in scientific research, I cannot determine and be competent to move forward on the research career path. It is always an honor for me to be her student.

I would also like to thank my co-supervisor Dr. Simon S Yeung, and the collaborators Dr. Shannon W Au, Dr. Parco M Siu and Dr. Bao-Ting Cheung for their useful advice and helpful technical supports.

Special thanks are given to Dr. Alex Cheung for his comments and suggestions on experimental design, data analyses and thesis writing. Thanks to my teammates for working side by side with me, Ms. Karena Wong, Ms. Lu Xia, Mr. Martin Wang and Ms. Rose Mirsafaei Rizi. I am also indebted to many colleagues for their technical expertise, including Mr. Sik-Cheung Siu, Mr. Ka-Keung Yip, Ms. Alice Au, Mr. Ping-Gor, Mr. Bjorn Tam and Ms. Iris Wong.

I am grateful to be mentored by Dr. Håkan Westerblad during my attachment in Karolinska Institutet. The care and sharing from Dr. Joseph Bruton and Dr. Arthur Cheng helped me overcome the hardest time living in a foreign country. I would also like to thank my colleagues in Karolinska Insitutet for their cheering and encouragement, Dr. Johanna Lanner,

Dr. Daniel Andersson, Ms. Maja Schlittler, Ms. Charlotte Gineste, Mr. Thomas Chaillou, Mr. Gianluigi Pironti, Mr. Niklas Ivarsson, Mr Maarten Steinz and Ms. Therese Cedervall.

I have to express my sincere gratitude to my dearest family. Thanks for your patience and consideration, Mr. and Mrs. Sun. Thank you to Mr. Jason Sun for taking care of our lovely parents when I was abroad and when I moved out.

Lastly, I am grateful to be in love with you, Mantra Tse. Thanks for marrying me and supporting me to pursue a PhD degree. Let's welcome our new family member, our energetic little Sun.

This study was supported by the Hong Kong Research Grants Council General Research Fund (PolyU 5635/12M).

TABLE OF CONTENTS

LIST OF FIGURES

LIST OF TABLES

ABBREVIATIONS

°C	degree Celsius
18S rRNA	Ribosomal RNA 18S
6-HIS tag/ peptide-HIS	Hexahistidine epitope tag/ 6-HIS-tagged peptide
7-AAD	7-aminoactinomycin D
aa	amino acid
Abs	Absorbance
ad lib	Ad libitum
AEBSF	4-(2-aminoethyl)-benzenesulfonyl fluoride hydrochloride
AF 647	Alexa Fluor 647
Akt	Protein kinase B
ANOVA	Analysis of variance
AREG	Amphiregulin
BB515	BD Horizon BB515
Bcl-X	B-cell lymphoma-2 like 1
bp	base pair
BSA	Bovine serum albumin
CAF	Centralized Animal Facilities
CCL2	C-C motif chemokine ligand 2
CCR2	C-C motif chemokine receptor 2
CD115	Monocyte marker; macrophage colony-stimulating factor 1 receptor
CD11b	Myeloid cell marker; Integrin alpha-M
CD206	M2 MP marker; Mannose receptor C-type 1

CD86	M1 MP marker; B-lymphocyte antigen B7-2
CMV	Cytomegalovirus (promoter)
CN myofibers	Centrally nucleated myofibers
CO_2	Carbon dioxide
CSA	Cross-sectional area
Ct/ dCt	Cycle of threshold/ delta cycle of threshold
CTX	Cardiotoxin
CX3CL1/ CX3CR1	Fractaline/ Fractalkine receptor
CXCL1	C-X-C motif chemokine ligand 1
DAMP	Damage associated molecular patterns
DAPI	4',6-diamidino-2-phenylindole
ddH_2O	Double-distilled water
DMEM	Dulbecco's Modified Eagle Medium
DNA/ cDNA	Deoxyribonucleic acid/ complementary deoxyribonucleic acid
DNase	Deoxyribonuclease
dNTP	Deoxyribonucleotide mix
DT/ DTR	Diphtheria toxin/ diphtheria toxin receptor
DTT	Dithiothreitol
ECM	Extracellular matrix
EDTA	Ethylenediaminetetraacetic acid
F4/80	Macrophage marker; epidermal growth factor-like module-containing mucin-like hormone receptor-like 1
FACS	Fluorescence-assisted cell sorting

FAP	Fibro-adipogenic progenitor cells
Fas/ FasL	Fas cell surface death receptor/ Fas Ligand
FBS	Fetal bovine serum
FL	Fluorochrome channel
FSC-H/ A	Forward scattering- height/ area
GAPDH	Glyceraldehyde 3-phosphate dehydrogenase
GFP	Green fluorescent protein
GM	Growth medium
H&E	Hematoxylin and eosin
HGF	Hepatocyte growth factor
High-SSC	High granularity
HMGB1	High-mobility group protein 1
IFNγ	Interferon γ
IFNγR1	M1 MP marker; Interferon gamma receptor 1
IGF	Insulin-like growth factor
IGF-1 and IGF-1R	Insulin-like growth factor-1 and the receptor
IGF-1Ea/ Eb	Insulin-like growth factor-1 Ea/ Eb isoform
IGF-2 and IGF-2R	Insulin-like growth factor-2 and the receptor
IGFBP	Insulin-like growth factor binding proteins
IgG	Immunoglobulin G
IHC	Immunohistochemistry
IL-1β/ 4/ 6/ 8/ 10/ 33	Interleukin-1β/ 4/ 6/ 8/ 10/ 33
IL-4Ra	M2 MP marker; Interleukin-4 receptor, alpha
iNOS	Induced nitric oxide synthase
IRS	Insulin receptor substrate protein

JNK	c-jun N-terminal kinase
kb	kilobase
kDa	kilodalton
LB	Luria-Bertani or lysogeny broth medium
Liq. N	Liquefied nitrogen
Ly6C	Infiltrating myeloid cell marker; Lymphocyte antigen 6 complex, locus C
Ly6G	Neutrophil marker; Lymphocyte antigen 6 complex, locus G
LysM	Lysozyme M
m/v	percentage mass per volume
M1 or M1 MP	Pro-inflammatory macrophages
M2 or M2 MP	Anti-inflammatory macrophages
MAPK	Mitogen activated protein kinases
M_{BSA}	Linear slope of standard curve established with BSA standards
$MgCl_2$	Magnesium chloride
MGF	Mechano-growth factor
MHC	Myosin heavy chain
MPC	Myogenic precursor cells
MRF	Myogenic regulatory factors
MRF4	Myogenic regulatory factor 4
Myf5	Myogenic factor 5
Myh3	Myosin heavy chain, embryonic form
Myh8	Myosin heavy chain, neonatal form

MyoD	Myogenic differentiation protein 1
Myog	Myogenin
NF-κB	Nuclear factor kappa B
NO	Nitric oxide
Oligo dT	Deoxythymidine oligomer
Pax7	Paired box 7
PBS	Phosphate buffer saline
PCR	Polymerase chain reaction
PE	Phycoerythrin
PECAM1	Platelet endothelial cell adhesion molecule 1
PE-Cy7	Phycoerythrin-cyanine 7 tandem dye
PI3K	Phosphatidylinositol-3 kinase
PKC	Protein kinase C
Pre-pro-IGF-1/ IGF-1Ea/ MGF	Pre-pro-peptide of IGF-1/ IGF-1Ea/ MGF
Pro-IGF-1/ IGF-1Ea/ MGF	Pro-peptide of IGF-1/ IGF-1Ea/ MGF
PSG	Penicillin-streptomycin-glutamine
Resident MP	Resident macrophages
RIPA	Radioimmunoprecipitation assay buffer
RNA/ mRNA	Ribonucleic acid/ messenger ribonucleic acid
RNase	Ribonuclease
RNasin	Ribonuclease inhibitor
ROS/ RNS	Reactive oxygen species and reactive nitrogen species
rpm	round per minute
RPS20	Ribosomal protein S20

RQ	Relative quantification
RT-qPCR	Real-time quantitative PCR
SDS-PAGE	Sodium dodecyl sulfate-polyacrylamide gel electrophoresis
SEM	Standard error of mean
SiglecF	Eosinophil marker; sialic acid-binding Ig-like lectin
SSC-A	Side scattering- area
STAT3	Signal transducer and activator of transcription 3
TA	Tibialis anterior
TBST	Tris-buffered saline plus 0.1% Tween 20
TGF-β	Transforming growth factor β
TLR-2/ 4	Toll-like receptor-2/ 4
TNF or TNF-α	Tumor necrosis factor or tumor necrosis factor-α
T_{reg}	Regulatory T cell
TUNEL	Terminal transferase-mediated dUTP nick end-labeling
v/v	percentage volume per volume
x g	times gravity

CHAPTER 1

General Introduction

1.1 INTRODUCTION

Skeletal muscle is the most abundant tissue in human body. It is specialized for contractility to serve many vital functions such as breathing (diaphragm), swallowing (tongue), eye (ocular muscles) and body movement (limb muscles). In recent years, skeletal muscle is also implicated in endocrine functions by releasing myokines (muscle-derived cytokines) in response to mechanical stimulation and metabolic stress (Nielsen & Pedersen, 2008; Miyatake *et al.*, 2016; Whitham & Febbraio, 2016; Lightfoot & Cooper, 2016). To maintain functional integrity, skeletal muscle demonstrates remarkable regenerating capacity when encountering injury. Skeletal muscle tissue stem cells, namely satellite cells, undergo myogenesis to become myocytes to repair or regenerate damaged tissues. Soluble factors derived from inflammatory cells are indispensable for satellite cell myogenesis (Tidball, 2017). Amongst the inflammatory cell-derived soluble factors, insulin-like growth factor-1 (IGF-1) exerts effects in promoting myogenesis and mediating inflammation in muscle regeneration (Pelosi *et al.*, 2007; Tidball & Welc, 2015; Tonkin *et al.*, 2015). In this study, we investigated the role of mechano-growth factor (MGF), one of the IGF-1 isoforms, in the modulation of skeletal muscle inflammatory response to regeneration.

1.2 SKELETAL MUSCLE

1.2.1 Structural and cellular components

Although the size, architecture and geometry of skeletal muscles vary considerably (see reviews; Spoor *et al.*, 1991; Kawakami *et al.*, 1998; Charles *et al.*, 2016), skeletal muscles ("muscle(s)" is used hereafter) possess similar structural and cellular components (Figure 1.1). Muscles are ensheathed with connective tissues epimysium and perimysium. Epimysium is the outermost layer enwrapping the muscle belly whereas perimysium is an extension from epimysium enveloping individual muscle fascicles. A muscle fascicle contains bundled myofibers in which each myofiber is a single, cylindrical multinucleated muscle cell. Besides, vessels and nerves located at the perimysial structure provide nutrients and transmit signal from central nervous system to myofibers respectively. In addition, satellite cells reside between the basement membrane and sarcolemma of myofibers (Mauro, 1961). Resident macrophages are located within epimysial and perimysial structures (Brigitte *et al.*, 2010). Interstitium, the space between myofibers, is where interstitial cells such as fibroblast and fibro-adipogenic progenitor cells (FAP) reside (Heredia *et al.*, 2013).

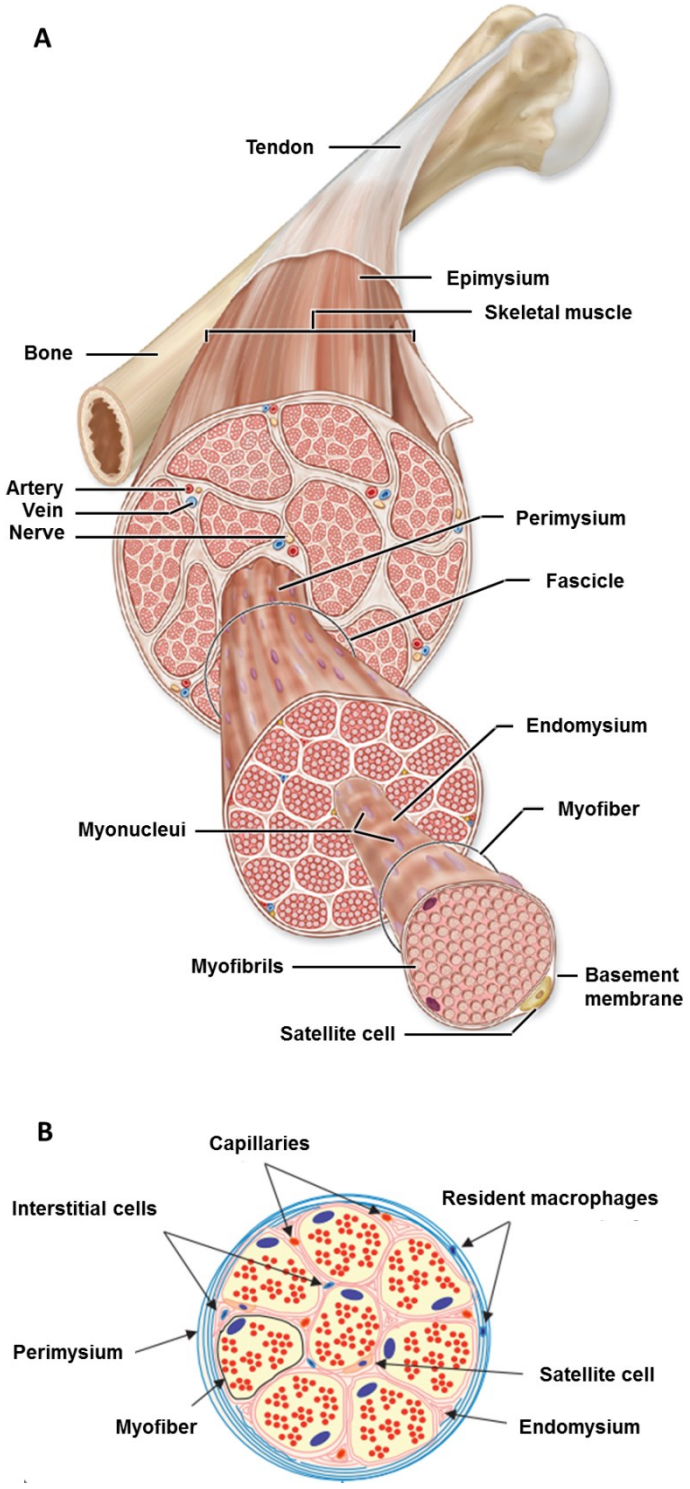

Figure 1.1 Structural and cellular components of skeletal muscle. (A) Organization of muscle tissue (adapted and modified from Mescher, 2013); (B) Cellular components within a fascicle (adapted and modified from Sciorati *et al.*, 2016).

1.2.2 Muscle injury

Any injury or damage to muscles (such as lacerations, contusions, strain injuries or toxin-mediated) leads to loss of contractility that compromises function (Swentik, 2016). For instance, toxin-mediated injury is mostly caused by venoms from snake bite and insect sting which are biochemically active to induce muscle lysis (Chiou *et al.*, 1993; Ownby *et al.*, 1993, 1997). Strain-induced injury is most frequent in sports such as sprinting and jumping which require repetitive eccentric muscle contractions (Järvinen *et al.*, 2005). Strain-induced injury may lead to tear and complete disruption of muscle tissue especially in athletic injuries. These injuries are acute in nature and is pathologically distinct from chronic injury that manifests persistent muscle inflammation, impeded muscle regeneration and tissue fibrosis (see reviews: Tidball, 2011; Swentik, 2016). From here on, "muscle injury" refers to acute muscle injury and chronic injury is not considered in this thesis.

1.2.3 Muscle regeneration by satellite cells

After muscle injury, myofiber necrosis may propagate from the injured site to the intact part along the damaged myofibers. As a protective mechanism, the damaged myofibers form contraction band to constrict damage propagation (Järvinen *et al.*, 2005). The injured site is then localized followed by regeneration process. To repair or regenerate the damaged tissue, it requires the participation and interaction of satellite cells and

inflammatory cells. The myogenic program of satellite cells is first described (Figure 1.2).

Since the identification of satellite cells in 1961 (Mauro, 1961), extensive investigation was carried out to characterize satellite cells in skeletal muscle including their origin, molecular identity, anatomical distribution and functional roles (see reviews: Yin *et al.*, 2013 and Ceafalan *et al.*, 2014). Satellite cells are indispensable for muscle regeneration (Sambasivan *et al.*, 2011; Relaix & Zammit, 2012). In non-injured muscle, satellite cells are mitotically quiescent and express marker paired box 7, or Pax7 (Tidball, 2011; Ceafalan *et al.*, 2014). Upon injury, satellite cells can be activated by hepatocyte growth factor (HGF) and receptor c-Met binding (Tatsumi *et al.*, 1998; Miller *et al.*, 2000). Activated satellite cells become mitogenic myoblasts and undergo proliferation.

Whether satellite cells continue proliferation, commit myogenic differentiation or return quiescence (self-renewal pathway) are governed by a number of transcription factors, namely myogenic regulatory factors (MRF) expressed in satellite cells. These MRF are myogenic factor 5 (Myf5), myogenic differentiation protein 1 (MyoD), myogenin (Myog) and myogenic regulatory factor 4 (MRF4) (Chargé & Rudnicki, 2004). Myoblasts co-express Pax7, Myf5 and MyoD but not Myog and MRF4. The predominance of Pax7 and Myf5 is suggested to be the determinant of satellite cell proliferation whereas that of MyoD is essential for myogenic differentiation (Sabourin *et al.*, 1999; Montarras *et al.*, 2000; Olguin *et al.*, 2007; Yin *et al.*, 2013). Part of the activated satellite cells switches off MyoD expression and returns quiescence to complete a self-renewal cycle.

Differentiation requires the downregulation of Pax7 and subsequent upregulation of Myog and MRF4 (Olguin *et al.*, 2007). Expression of muscle-specific genes like myofibrillar proteins (e.g. myosin and actin) is governed by Myog and MRF4 (Berkes & Tapscott, 2005). The terminally differentiated satellite cells are now called myocytes. Myocytes may fuse with existing myofibers to repair the damaged part or to fuse with other myocytes to regenerate myofibers *de novo* (Guttridge, 2012).

The expression of MRF in satellite cells during muscle regeneration is orchestrated by dynamic cell-cell interaction and autocrine or paracrine signals from the dynamic niche (see reviews: Yin *et al.*, 2013; Ceafalan *et al.*, 2014; Tidball, 2017). In particular, inflammation and the associated activities play pivotal roles in this process.

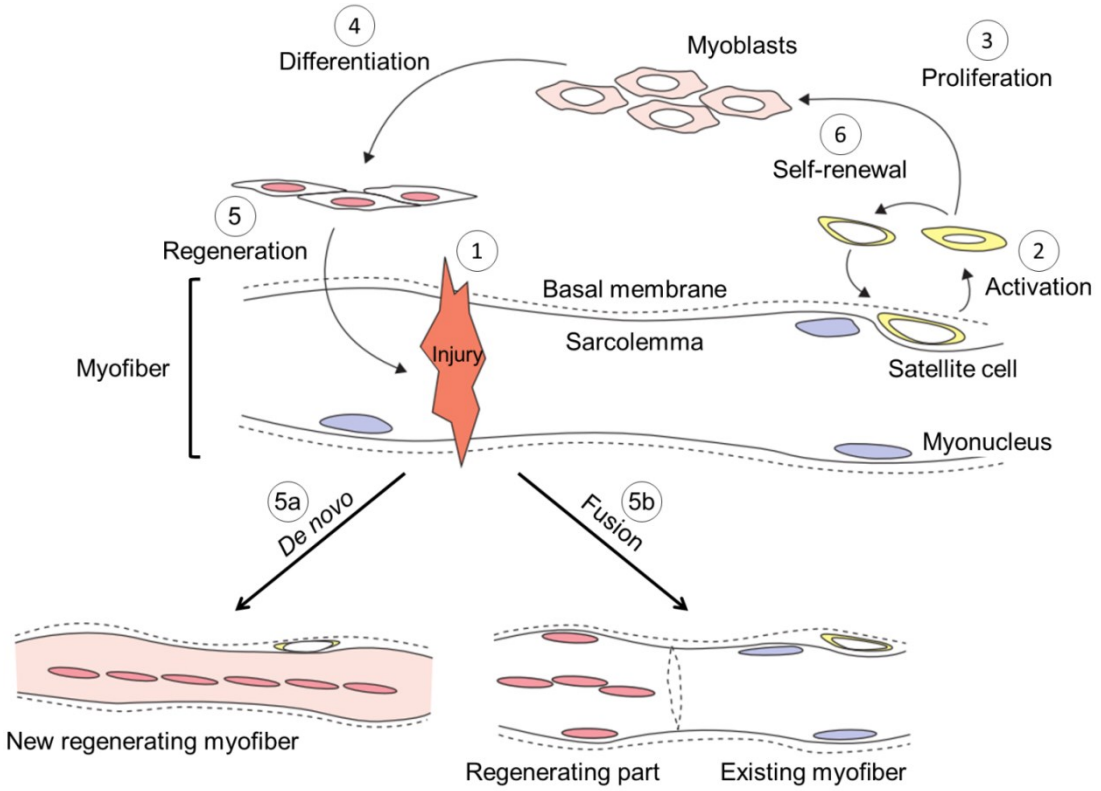

Figure 1.2 Muscle regeneration by satellite cells (adapted and modified from Guttridge, 2012). When a myofiber is injured (1), satellite cells associated with the injured myofiber are activated (2) and become myoblasts (3). The cells later differentiate into myocytes (4) and fuse together into myotube to regenerate the injured muscle (5). Myocytes may fuse into the newly formed myotube and result in *de novo* myofiber regeneration (5a). Or, the myotube may fuse and repair the existing myofiber (5b). Of note, central nuclei chain is observable in newly formed and regenerating myofibers which migrates to peripheral region in later regeneration process. Satellite cells possess self-renewal property. Part of the daughter cells quits from cell cycle and returns to quiescence stage (6).

1.3 INFLAMMATION

The participation of inflammatory cells in response to muscle injury was identified 60 years ago (Godman, 1957). Yet, only in past two decades, inflammatory response in muscle regeneration is beginning to be understood. Muscle inflammatory response involves often overlapping phases including initiation, perpetuation and resolution (Tidball & Villalta, 2010; Bentzinger *et al.*, 2013; Tidball, 2017). Each phase involves various inflammatory progenies and the associated activities. The essence of regulated muscle inflammatory response for proper muscle regeneration is highlighted. The inflammatory response coincides with satellite cell myogenesis. It is now evident that interaction of inflammatory cells and satellite cells is essential for muscle regeneration. Particularly, the mediation of various cell activities and survival depends on soluble factors derived from inflammatory cells in autocrine or paracrine manner (Tidball, 2017).

1.3.1 Innate inflammatory response

Innate immunity is the primordial defense system to provide rapid, non-antigen-specific response to homeostatic disruption. In this thesis, we only consider innate inflammatory response in the context of muscle injury without pathogen involvement. Typical innate inflammatory cells implicated in muscle regeneration are neutrophils and macrophages (Lacy & Stow, 2011). They develop from myeloid lineage and collectively designated as myeloid cells when appropriate.

Neutrophils are polymorphonuclear leukocytes or granulocytes specialized in phagocytosis. The granules are abundant in neutrophil cytoplasm, which include lysosomes containing hydrolytic enzymes to digest engulfed materials; and secretory vesicles carrying inflammatory cytokines synthesized during maturation or upon activation (Lacy & Stow, 2011). Neutrophils actively release reactive oxygen species and reactive nitrogen species (ROS/ RNS) such as nitric oxide (NO) and inflammatory cytokines to perpetuate the inflammatory response (Teixeira *et al.*, 2003; Butterfield *et al.*, 2006; Toumi *et al.*, 2006).

Monocytes infiltrate injured muscle and differentiate into macrophages that direct to the lesion sites under chemotactic gradient. Dependent on the niche, these exudate macrophages can be classified into pro-inflammatory macrophages (M1 MP) and anti-inflammatory macrophages (M2 MP) (Mills *et al.*, 2000). Of importance, macrophages can undergo polarization highlighting the phenotypic plasticity of macrophages in response to various niche factors (Tidball & Rinaldi, 2012). When tissue debris and necrosis are prevalent at early muscle injury, M1 MP persists at the injured site to perpetuate inflammation by releasing chemotactic factors and pro-inflammatory cytokines. At the later stage when tissue debris clearance has completed, M2 MP emerges to secrete various growth factors and anti-inflammatory cytokines to support tissue regeneration and inflammatory resolution. In addition to exudate macrophages, including M1 MP and M2 MP, there is a resident progeny in muscle called resident macrophages (resident MP) implicated in the initiation of inflammatory response (Brigitte *et al.*, 2010). Of note, the abbreviated term for

macrophages, “MP” is used for macrophages with specific phenotype and distinct functions (e.g. M1 MP, M2 MP and resident MP); and full term “macrophages” is used as a general description.

1.3.2 Muscle inflammatory response

The cellular players and processes involved in the muscle inflammatory response are depicted in Figure 1.3. Myeloid cells orchestrate the myogenic program of satellite cells in muscle regeneration. Although recent literature has discussed the involvement of T cells (Burzyn *et al.*, 2013; Schiaffino *et al.*, 2017), eosinophils (Heredia *et al.*, 2013) and stromal cells (FAP and fibroblasts) (Heredia *et al.*, 2013; Farup *et al.*, 2015) in mediating inflammatory response, they are not considered in this thesis.

The inflammatory response often includes several overlapping phases (Tidball & Rinaldi, 2012; Bentzinger *et al.*, 2013). It begins with the inflammatory phase characterized with initiation and perpetuation of inflammation. The initiation involves recruitment of myeloid cells and activation of satellite cells. In perpetuation, infiltrated myeloid cells enhance the inflammatory response to remove tissue debris and promote myoblast proliferation. The resolution phase subdivided into early and late resolution phases is required after clearance of necrotic tissue and apoptotic cells. The early resolution phase is characterized by the clearance of pro-inflammatory myeloid cells (e.g. neutrophils and M1 MP) and replacement by M2 MP. This phase is a critical turning point for mitogenic satellite cells to commit myogenic differentiation and become myocytes for repair or regeneration. As

for the late resolution phase, M2 MP is involved and resolved after supporting myogenic differentiation and tissue remodeling. The inflammatory response involved in each phase and interaction of inflammatory cells with satellite cells are described followed.

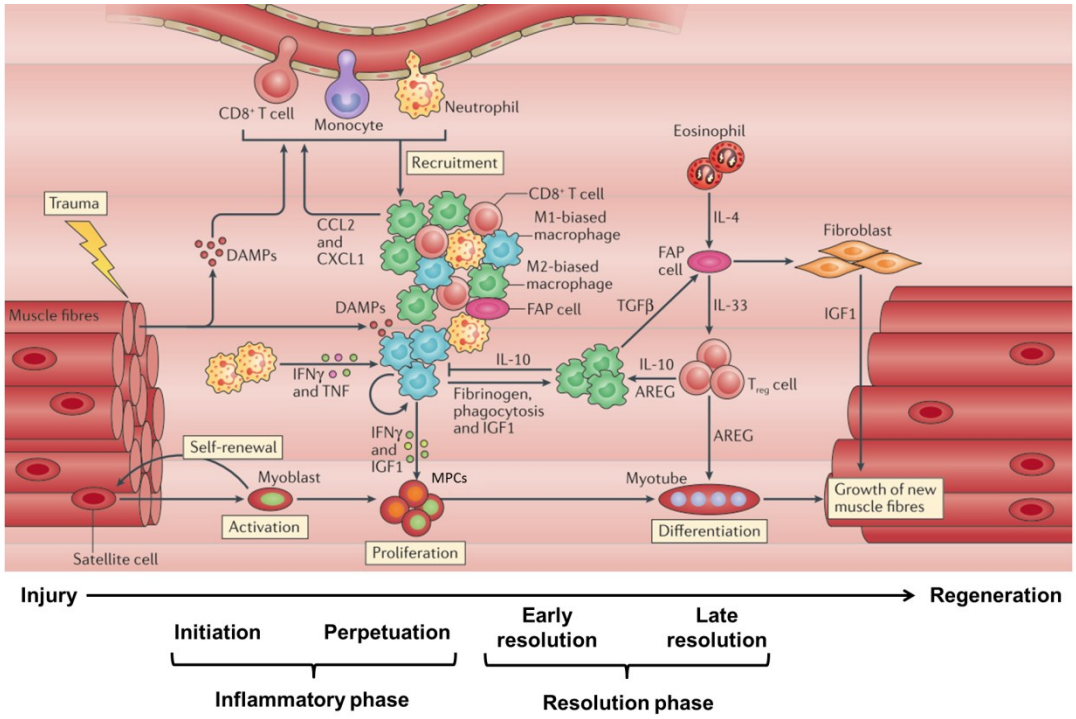

Figure 1.3 Cellular constituents of muscle inflammatory response (adapted and modified from Tidball, 2017). Infiltrating myeloid cells, including monocytes and neutrophils are the major cellular players of muscle inflammation. Neutrophils release pro-inflammatory factors like TNF to promote monocyte activation and polarization to pro-inflammatory (M1-biased) macrophages during the inflammatory phase. In resolution phase, anti-inflammatory (M2-biased) macrophages emerge and release key anti-inflammatory factor IL-10 to suppress the pro-inflammatory cell activities. Abbreviation for cells: FAP (fibro-adipogenic progenitor cells); MPC (myogenic precursor cells); and T_{reg} cell (regulatory T cell). Abbreviation for biomolecules: DAMP (damage associated molecular patterns); CCL2 (C-C motif chemokine ligand 2); CXCL1 (C-X-C motif chemokine ligand 1); IFNγ (interferon γ); TNF (tumor necrosis factor); IGF-1 (insulin-like growth factor-1); IL- (interleukin) 4/ 10/ 33; AREG (amphiregulin); and TGF-β (transforming growth factor β).

1.3.3 Initiation

The initiation of inflammation takes place immediately after injury with characteristic infiltration of myeloid cells. Although inflammatory cells are scarce in non-injured skeletal muscle, resident MP is enriched at epimysium and perimysium and plays a pivotal role in exudate myeloid cell recruitment. Resident MP is fusiform mononuclear cells expressing mature macrophage marker, epidermal growth factor-like module-containing mucin-like hormone receptor-like 1, or F4/80 (Brigitte *et al.*, 2010). Injured muscle releases damage associated molecular patterns (DAMP) for instance mitochondrial constituents (Zhang *et al.*, 2010*b*) and high-mobility group protein 1 (HMGB1) (Sciorati *et al.*, 2016). These can be recognized by resident MP via toll-like receptors (TLR) that leads to activation of nuclear factor kappa B (NF-κB) pro-inflammatory signaling cascade (Verstak *et al.*, 2009). Injured muscles from TLR-2 knockout (Mojumdar *et al.*, 2016) and TLR-4 knockout (Paiva-Oliveira *et al.*, 2017) mice demonstrated lower myeloid cell infiltration and impaired muscle regeneration.

Activated resident MP then releases neutrophil chemoattractants (e.g. C-X-C motif chemokine ligand 1, or CXCL1; and interleukin-8 or IL-8) and monocyte chemoattractants (e.g. C-C motif chemokine ligand 2, CCL2) to recruit exudate neutrophils and macrophages respectively (Brigitte *et al.*, 2010; Marino *et al.*, 2011). Using chimeric mice model, Brigitte *et al.*, (2010) demonstrated that the recruitment of exudate macrophages in response to ectopic tumor necrosis factor-α (TNF-α) and myotoxin treatment were severely inhibited for 93% and 77% by specific depletion of resident MP. CCL2 is the key chemokine for macrophage infiltration. The absence of

CCL2 signaling in CCL2 and the receptor CCR2 (C-C motif chemokine receptor 2) knockout models, abolishes macrophage infiltration into injured muscle and impairs muscle regeneration (Lu *et al.*, 2011*a*, 2011*b*). Besides the initiating role, resident MP can migrate from epimysium into the injured site and potentially participates in phagocytosis of tissue debris (Brigitte *et al.*, 2010). Intriguingly, the proliferative capacity of muscle resident MP increased when exudate macrophages were depleted by clodronate liposome, a reagent used to induce apoptosis of exudate macrophages (Côté *et al.*, 2013). The compensatory macrophage expansion from resident MP may account for the delayed but not abrogated muscle regeneration when clodronate liposome applied (Summan *et al.*, 2006). To summarize, resident MP is specialized for the initiation of inflammatory response to recruit exudate myeloid cells into injured skeletal muscle.

1.3.4 Perpetuation

Perpetuation refers to the progression of inflammatory response in which clearance of tissue debris is the major event set into place. In response to the chemotactic signals derived from activated resident MP, infiltration of myeloid cells appears sequentially (Tidball, 2017). The accumulation takes place first at the epimysium (Brigitte *et al.*, 2010). Myeloid cells migrate down the chemotactic gradient from epimysium toward the injured site and carries out specific functions. The roles of neutrophils and macrophages in inflammatory perpetuation are considered.

Neutrophils are the first wave of myeloid infiltrates. Its role in muscle regeneration is however controversial. Concurrent with phagocytosis of tissue debris, neutrophils undergo respiratory burst that synthesize maximal amount of NO via induced nitric oxide synthase (iNOS). It was suggested to enhance the removal of tissue debris (Teixeira *et al.*, 2003) and conversely, deteriorate muscle injury by enhancing myofiber lysis (Pizza *et al.*, 2001; Nguyen & Tidball, 2003; Dumont *et al.*, 2008). Neutrophils also release inflammatory cytokines to recruit (e.g. CCL2) and activate (e.g. IFNγ and TNF-α) macrophages, which are essential for muscle regeneration (Tidball & St Pierre, 1996; Teixeira *et al.*, 2003; Butterfield *et al.*, 2006; Toumi *et al.*, 2006; Pelletier *et al.*, 2010). Specific depletion of neutrophils by clone 1A8 anti-Ly6G (an antibody against the neutrophil marker, lymphocyte antigen 6 complex locus G or Ly6G) (Daley *et al.*, 2008), diminishes macrophage infiltration and inflammatory cytokine expression in exhaustively exercised muscle (Kawanishi *et al.*, 2016). However, the study did not examine the regeneration outcomes of the neutrophil-depleted animals. Of note, neutrophils are important in macrophage recruitment and activation whether neutrophil-derived NO beneficially promotes lysis of injured myofibers and debris removal; or detrimentally lyses intact myofibers causing secondary injury remains elusive.

Macrophages infiltrate injured muscle following neutrophil infiltration. Neutrophil-derived cytokines (e.g. TNF-α) activate infiltrated macrophages into M1 MP. M1 MP secretes similar profile of cytokines and chemokines, in an autocrine or paracrine manner, to feed-forward the recruitment and activation of macrophages (Stout *et al.*, 2005; Tidball *et al.*,

2014; Tidball, 2017). Inflammatory response is thus enhanced and perpetuated. With the collaboration of phagocytic neutrophils and M1 MP, cellular and tissue debris are phagocytized within 24 to 48 h from injury onset (Tidball, 2011, 2017). The essence of phagocytosis in muscle regeneration is demonstrated in a number of phagocyte depletion studies. The clearance of tissue debris and muscle regeneration were suspended when phagocytic infiltration was abolished (Arnold *et al.*, 2007). These studies utilized different methodologies including: (i) antibody against phagocytes (Teixeira *et al.*, 2003); (ii) administration of diphtheria toxin (DT) to CD11b (integrin alpha-M; myeloid cell-specific) promoter driven human diphtheria toxin receptor (DTR) transgenic mice model, i.e. CD11b-DTR mice (Arnold *et al.*, 2007); (iii) clodronate liposome-induced exudate macrophage apoptosis (Summan *et al.*, 2006; Côté *et al.*, 2013); and (iv) chemotaxis-associated gene knockout (e.g. CCL2 knockout) models (Lu *et al.*, 2011*a*, 2011*b*; Arnold *et al.*, 2015). Even though the depletion was not complete, the treatment sufficiently prolonged tissue debris clearance and resulted in fat deposition (Summan *et al.*, 2006).

Although neutrophils and macrophages are implicated in phagocytic activities, macrophages seem to be the major phagocytes in muscle regeneration. Neutrophils are likely to take a minor role in phagocytosis but involve in promoting macrophage functions (Nguyen & Tidball, 2003; Stout *et al.*, 2005; Tidball *et al.*, 2014; Tidball, 2017). In a study where neutrophil depletion was achieved by neutralizing antibody (clone RB6-8C5) showed persistent tissue necrosis (Teixeira *et al.*, 2003). However, the clone RB6-8C5 antibody used also reduced the infiltration of

macrophages (Teixeira *et al.*, 2003). Similar results could be achieved by depletion of myeloid cells (Arnold *et al.*, 2007). In later studies, specific abolishment of macrophages without reducing neutrophil infiltration repeated the deficit in debris phagocytosis and muscle regeneration (Segawa *et al.*, 2008; Lu *et al.*, 2011*a*; Arnold *et al.*, 2015). Collectively, perpetuation of inflammatory response to muscle injury involves neutrophils and M1 MP derived pro-inflammatory cytokines and phagocytic activities, in which macrophages play a more major role in muscle regeneration than neutrophils.

1.3.5 Resolution

Inflammatory resolution is characterized by inhibition of exudate myeloid cell recruitment and suppression of pro-inflammatory response from the early infiltrate. Neutrophils are generally resolved by spontaneous apoptosis in 1 to 2 days since its infiltration (Sciorati *et al.*, 2016). M1 MP is resolved following neutrophil resolution either by spontaneous apoptosis or polarization into M2 MP (Ortega-Gómez *et al.*, 2013; Gautier *et al.*, 2013; Sciorati *et al.*, 2016). The M2 polarization can be driven by engulfing apoptotic cells such as neutrophils and muscle cells (Fadok *et al.*, 1998, 2001; Arnold *et al.*, 2007; Tidball, 2017). The emergence of M2 MP is essential for inflammatory suppression. M2 MP characteristically expresses arginase-1 to metabolize L-arginine, which is the common substrate to iNOS expressed in M1 MP (Rath *et al.*, 2014). Production of NO and the pro-inflammatory effects consequently diminish. Hydrolytic products from arginase-1-mediated L-arginine digestion, polyamine and ornithine, are also essential for muscle regeneration and extracellular matrix (ECM) remodeling

(see review: Rath *et al.*, 2014). Furthermore, M2 MP releases the key anti-inflammatory cytokine, interleukin (IL)-10 to repress residual M1 activities by limiting pro-inflammatory cytokine and chemokine expression; and by promoting resided macrophages into M2 MP (Mills *et al.*, 2000; Meador *et al.*, 2008; Deng *et al.*, 2012). Recently, IGF-1 autocrine or paracrine signaling in macrophages are also implicated in the M2 polarization in addition to promoting muscle regeneration (Tonkin *et al.*, 2015). The anti-inflammatory property of IGF-1 has also been suggested (Pelosi *et al.*, 2007) implying potential roles of IGF-1 in mediating resolution phases. Details of IGF-1 in mediating inflammatory response are described in Section 1.4. Although M2 MP and the derived soluble factors are reparative and anti-inflammatory in nature, early initiation of M2 polarization leads to premature muscle differentiation and inefficient muscle regeneration (Perdiguero *et al.*, 2011). Together, it implies the significance of ordered inflammatory phases to muscle regeneration.

1.3.6 Interaction between satellite cells and myeloid cells

As indicated in Figure 1.3, myogenesis of satellite cells in response to muscle injury coincides with the inflammatory response. Interactions of myeloid cells with satellite cells are dependent on the inflammatory phases and the involved cellular players. Besides, numerous soluble factors including growth factors, cytokines and chemokines are implicated (see reviews: Tidball & Villalta, 2010; Farup *et al.*, 2015; Tidball, 2017). The typical soluble factors, their sources, targeting cells and functions are summarized in Table 1.1. Some of the critical interactions are highlighted.

At the initiation phase, exudate myeloid cells are recruited mainly by chemokines derived from resident MP (Brigitte *et al.*, 2010). Yet, activated satellite cells are suggested to participate in the early recruitment by releasing chemokines such as CCL2 (Chazaud *et al.*, 2003) and IL-8 (Marino *et al.*, 2011). Prior to myeloid cell infiltration, satellite cells at the injured site are activated by the local injury signals like cleaved HGF from disrupted ECM (Tatsumi *et al.*, 1998; Miller *et al.*, 2000). The upregulation of chemokine like CCL2 via IL-6 autocrine signaling in activated satellite cells contributes to the establishment of chemokine gradient (Chazaud *et al.*, 2003; Marino *et al.*, 2008; Deshmane *et al.*, 2009; Zhang *et al.*, 2013). The gradient guides exudate myeloid cells to accumulate at the epimysial structure and migrate to the injured site. Similarly, satellite cells at remote area of either the same injured myofibers or the adjacent myofibers can migrate towards the injured site down the same chemotactic gradient to enhance regeneration (Chazaud *et al.*, 2003; Deshmane *et al.*, 2009; Brigitte *et al.*, 2010; Saclier *et al.*, 2013; Lund & Cornelison, 2013). The release of pro-inflammatory cytokines by activated resident MP and exudate myeloid cells may amplify the population of activated satellite cells (Brigitte *et al.*, 2010; Tidball, 2017). Thus, activated satellite cells and resident MP synergistically promote the initiation of inflammatory response.

At the perpetuation phase, the major infiltrated myeloid cells are neutrophils and M1 MP. These myeloid cells release pro-inflammatory signals that stimulate myoblast proliferation and migration, including TNF-α (Li, 2003; Otis *et al.*, 2014), IFNγ (Cheng *et al.*, 2008; Londhe & Davie, 2011), IL-6 (Serrano *et al.*, 2008; Muñoz-Cánoves *et al.*, 2013) and CCL2

(Yahiaoui *et al.*, 2008). Furthermore, these cytokines may facilitate the activation and migration of remote satellite cells to participate the regeneration process. In addition to the pro-proliferative and pro-migratory functions, cell-cell adhesion of macrophages with satellite cells protects satellite cells from apoptosis (Chazaud *et al.*, 2003; Sonnet *et al.*, 2006). For instance, Sonnet *et al.*, (2006) demonstrated the implication of platelet endothelial cell adhesion molecule 1 (PECAM1) homophilic interaction; and CX3CL1 (fractalkine)-CX3CR1 (fractalkine receptor). Given the proximity of macrophages and satellite cells during muscle regeneration, it is conceivable that cell-cell adhesion can promote satellite cell survival *in vivo* (Sonnet *et al.*, 2006; Lesault *et al.*, 2012; Bentzinger *et al.*, 2013).

During early resolution phase, M1 MP undergoes apoptosis in which activated satellite cells are implicated. A Fas cell surface death receptor (Fas), when activated by Fas ligand (FasL), triggers the downstream caspase activation and apoptotic cell death (Behrens *et al.*, 1997; Ramaswamy *et al.*, 2009). In response to muscle injury, Sandri *et al.*, (2001) demonstrated the predominant expression of FasL in myoblasts *in vitro* and MyoD+ cells (presumably activated satellite cells) *in vivo*. The upregulation of MyoD is correlated with macrophage apoptosis in muscle inflammation. The investigators also demonstrated that inhibition of FasL signaling resulted in undetectable phagocyte apoptosis and persistent inflammation (Sandri *et al.*, 2001). Besides, M2 MP directs myogenic differentiation by protecting differentiating myotubes (Sonnet *et al.*, 2006) and releasing growth factors such as IGF-1 (Arnold *et al.*, 2007; Tonkin *et al.*, 2015).

Table 1.1 Typical soluble factors involved in muscle regeneration. The potential sources, targeting cells and the responses are listed with references. Legend: ↑ promoting and ↓ suppressing the indicated effects. Abbreviation: IFNγ (interferon γ); IL- (interleukin) 4/ 6/ 8/ 10; TNF-α (tumor necrosis factor-α); NO (nitric oxide); CCL2 (C-C motif chemokine ligand 2); CXCL1 (C-X-C motif chemokine ligand 1); IGF-1 (insulin-like growth factor-1); HGF (hepatocyte growth factor); and TGF-β (transforming growth factor β).

(*Overleaf*)

Soluble factors	Potential sources	Target cells	Effects	References
Cytokine				
IFNγ	Macrophages	Macrophages	M1 polarization ↑	(Arnold *et al.*, 2007; Tidball *et al.*, 2014)
		Satellite cells	Proliferation ↑ Differentiation ↓	(Cheng *et al.*, 2008; Londhe & Davie, 2011)
IL-4	Macrophages	Macrophages	M2 polarization ↑	(Stein *et al.*, 1992; Tidball *et al.*, 2014; Tidball, 2017)
		Satellite cells	Differentiation ↑ Migration ↑	(Horsley *et al.*, 2003; Lafreniere *et al.*, 2006)
IL-6	Neutrophils Macrophages Satellite cells	Macrophages	Chemoattraction ↑	(Marino *et al.*, 2008; Zhang *et al.*, 2013; Muñoz-Cánoves *et al.*, 2013)
		Satellite cells	Proliferation ↑ Migration ↑ Differentiation ↑	(Serrano *et al.*, 2008; Zhang *et al.*, 2013; Muñoz-Cánoves *et al.*, 2013)
IL-8	Macrophages	Neutrophils	Chemoattraction ↑	(Hammond *et al.*, 1995)
IL-10	Macrophages	Macrophages	Pro-inflammatory cytokines & chemokines ↓ M2 polarization ↑	(Murray, 2005; Ouyang *et al.*, 2011; Villalta *et al.*, 2011; Philippou *et al.*, 2012; Deng *et al.*, 2012; Tidball, 2017)
		Satellite cells	Differentiation ↑	(Deng *et al.*, 2012)

(*Cont'd*)

TNF-α	Neutrophils Macrophages	Neutrophils	Chemoattraction ↑	(Collins & Grounds, 2001; Parameswaran & Patial, 2010; Tidball, 2017)
		Macrophages	M1 polarization ↑	
		Satellite cells	Chemoattraction ↑ Activation ↑ Proliferation ↑ Differentiation ↑	(Guttridge *et al.*, 1999; Torrente *et al.*, 2003; Li, 2003; Chen *et al.*, 2005, 2007; Palacios *et al.*, 2010; Otis *et al.*, 2014)
ROS/ RNS				
NO	Neutrophils Macrophages Myofibers	Neutrophils	Resolution ↑	(McCafferty *et al.*, 1997; Tidball & Villalta, 2010; Rigamonti *et al.*, 2013)
		Macrophages	Activation ↑ M1 polarization ↑	
		Satellite cells	Activation ↑ Differentiation ↑	(Lee *et al.*, 1994; Anderson, 2000; Tatsumi *et al.*, 2006; De Palma & Clementi, 2012; Rigamonti *et al.*, 2013; Hindi *et al.*, 2013)
Chemokines				
CCL2	Macrophages Satellite cells	Macrophages	Chemoattraction ↑	(Chazaud *et al.*, 2003; Deshmane *et al.*, 2009; Brigitte *et al.*, 2010; Lu *et al.*, 2011*a*, 2011*b*)
		Satellite cells	Chemoattraction ↑ Proliferation ↑	(Yahiaoui *et al.*, 2008)
CXCL1	Macrophages	Neutrophils	Chemoattraction ↑	(Hua *et al.*, 2005)

(*Cont'd*)

Growth factors				
IGF-1	Macrophages Myofibers	Neutrophils	Apoptosis ↓	(Kooijman *et al.*, 2002; Himpe *et al.*, 2008; Smith, 2010)
		Macrophages	Apoptosis ↓ M2 polarization ↑	(Smith, 2010; Tonkin *et al.*, 2015; Sciorati *et al.*, 2016)
		Satellite cells	Proliferation ↑ Differentiation ↑ Hypertrophy ↑	(Joe *et al.*, 2010; Schiaffino & Mammucari, 2011)
HGF	Interstitium Satellite cells	Satellite cells	Activation ↑	(Tatsumi *et al.*, 1998, 2006; Miller *et al.*, 2000)
TGF-β	Macrophages	Macrophages	M1 polarization ↓ iNOS activity ↓ M2 polarization ↑	(Wynn & Vannella, 2016; Tidball, 2017)
		Satellite cells	Activation ↓ Proliferation ↓ Differentiation ↓	(Allen & Boxhorn, 1987; Li *et al.*, 2004; Burks & Cohn, 2011)

1.4 INSULIN–LIKE GROWTH FACTOR

As described in Section 1.3, regulated inflammatory response is essential to muscle regeneration. Soluble factors mediate the regenerating process, in which IGF-1 displays dual-role in promoting satellite cell myogenesis and inflammatory resolution (Tidball & Welc, 2015). In this section, we describe in detail the insulin-like growth factor (IGF), in particular IGF-1 and its derivatives in muscle regeneration.

In the 30 years investigations, the "IGF" nomenclature is finally adopted over previous terminologies of "somatomedin", "non-suppressible insulin-like activity" and "multiplication stimulating activity" (Daughaday *et al.*, 1987; Daughaday & Rotwein, 1989; Puche & Castilla-Cortázar, 2012). The current nomenclature of IGF, "insulin-like" is given from the similarity with insulin in the aspect of sequence and metabolic activity; "growth factor" is originated from its promoting effect on tissue growth and development. Amongst all, IGF (particularly IGF-1) and the signaling is strongly implicated in tissue growth and development, metabolic homeostasis, survival, inflammatory modulation as well as skeletal muscle regeneration (Kooijman, 2006; Perrini *et al.*, 2010; Duan *et al.*, 2010; Puche & Castilla-Cortázar, 2012; Philippou & Barton, 2014).

The IGF family is composed of growth factors (IGF-1 and IGF-2), receptors (IGF-1R and IGF-2R) and binding proteins (IGFBP). Only the soluble factor IGF-1 is discussed in this thesis. Other members of IGF family will only be described briefly (see reviews: Mourkioti & Rosenthal, 2005; Duan *et al.*, 2010). IGF-1 gene and the peptide derivatives are firstly introduced followed by IGF-1/ IGF-1R signaling pathway. The expression of

IGF-1 in skeletal muscle regeneration is then described. Given that murine IGF-1 exists in two distinct isoforms, IGF-1Ea and mechano-growth factor (MGF or IGF-1Eb), the current understanding of the isoform functions are presented. Of note, MGF is used in this thesis to represent murine IGF-1Eb due to its upregulation in response to muscle injury (Yang *et al.*, 1996; McKoy *et al.*, 1999). It also avoids potential confusion from the similar terminology between IGF-1Ea and IGF-1Eb.

1.4.1 IGF-1 gene and peptides

The IGF-1 gene spans 80 kb of genomic DNA and contains six exons. Heterogeneous transcripts encoding distinct N-terminal signaling peptides and C-terminal E-peptides are generated by utilizing different leader sequences and alternative splicing. All isoforms possess the highly conserved mature IGF-1 peptide sequence (exon 3-4). By exclusive splicing of exon 1 or exon 2 to exon 3, the class 1 and class 2 IGF-1 N-terminal signaling peptide are respectively encoded. Class 2 IGF-1 is the circulatory form synthesized predominantly in liver for endocrine functions and not considered in this study (Temmerman *et al.*, 2010). There are two alternative splicing products of class 1 IGF-1 denoted by the E-domains including: exon 4-6 (IGF-1Ea) and exon 4-5-6 (MGF). For information regarding the full-length messenger RNA (mRNA) and peptide sequence, the GenBank accession numbers for murine IGF-1Ea (mRNA: AY878192; and peptide: AAX61179) and murine MGF (mRNA: AY878193; and peptide: AAX61180) are referred.

The putative peptide derivatives of murine IGF-1 are illustrated in Figure 1.4. The primary translation product of IGF-1 is a pre-pro-peptide called pre-pro-IGF-1 which contains the signal peptide, mature IGF-1 peptide and E-peptide. It later becomes the pro-peptide, pro-IGF-1, by post-transcriptional cleavage of signal peptide during secretory trafficking. Further cleavage of pro-IGF-1 yields common mature IGF-1 peptide but distinct E-peptides (Pfeffer *et al.*, 2009). The Ea-peptide is cleaved from IGF-1Ea whereas Eb-peptide is from MGF. *In vivo,* mature IGF-1, pro-IGF-1Ea and pro-MGF transcripts and peptides are detected in muscle (Matheny *et al.*, 2010; Durzyńska *et al.*, 2013; Philippou & Barton, 2014). Since muscle expresses mature IGF-1 peptide independently, it is presumable that the cleavage products Ea-peptide and Eb-peptide (from MGF) are also present *in vivo*. The sequence characteristics of E-peptides render the differences of IGF-1 isoforms in stability and optimal concentration (Brisson & Barton, 2012); ECM binding affinity and IGF-1 bioavailability (Hede *et al.*, 2012); post-translational modifications (Durzyńska *et al.*, 2013; Vassilakos *et al.*, 2014) and functions (Durzyńska *et al.*, 2013; Park *et al.*, 2014). The functional differentiation of IGF-1 isoforms and the cleaved E-peptides are described in Section 1.4.6.

To clarify the nomenclature used in this thesis, the term MGF is used to describe the murine pro-MGF and the putative derivatives: mature IGF-1 and Eb-peptide. Similar nomenclature is applied for another murine IGF-1 isoform, IGF-1Ea which composes of mature IGF-1 and Ea-peptide. IGF-1Ea and MGF are collectively represented by IGF-1 isoforms when appropriate.

Figure 1.4 Putative products of IGF-1 gene and the isoforms. (A) IGF-1 gene structure. The number in each rectangular block indicates the exon of IGF-1 gene. The transcription initiation sites are denoted by arrow heads above the exon 1 (343 and 245 base pair (bp) upstream of 3' end). Preferential initiation sites are marked by asterisks. At 5' end, exon 1-3 splicing gives rise to Class 1 transcripts. As for 3' end, exon 4-5-6 splicing results in Eb-domain whereas exon 4-6 yields Ea-domain. Notably, the 3' end portion of exon 4 is common to both E-domains. Exon 3-4 (5' portion) splicing is conserved in all isoforms which constitutes the mature IGF-1 sequence. (B) Translation products of IGF-1 vary with the E-peptides. Respectively, Class 1 pre-pro-IGF-1Ea contains 153 amino acid (aa) residues; Class 1 pre-pro-MGF contains 159 aa. The numbers of amino acid residue encoded by each exon sequence are indicated above the respective transcript region. (C) Putative peptides from pre-pro-IGF-1. After cleavage of N-terminal signal peptide, pro-IGF-1Ea (105 aa) and pro-MGF (111 aa) may undergo further cleavage to yield mature IGF-1 peptide (70 aa) and the corresponding E-peptides, Ea-peptide (35 aa) and Eb-peptide (41 aa). The dashed-box contains Class 1 (48 aa) signal peptides cleaved earlier from (B) to (C).

(*Overleaf*)

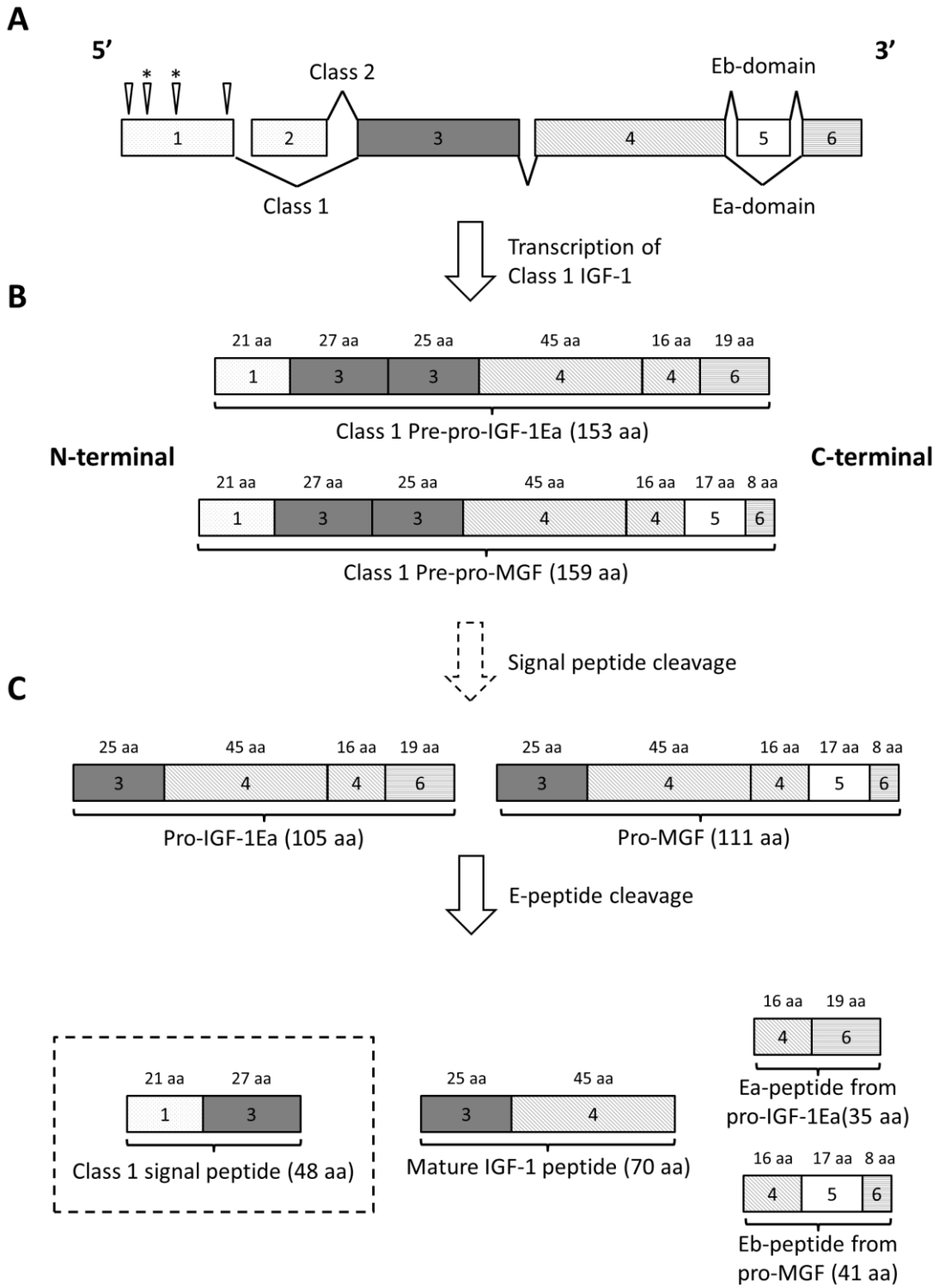
A
5'
3'
Class 2
Eb-domain
1
2
3
4
5
6
Class 1
Ea-domain
Transcription of
Class 1 IGF-1
B
21 aa
27 aa
25 aa
45 aa
16 aa
19 aa
Class 1 Pre-pro-IGF-1Ea (153 aa)
N-terminal
C-terminal
17 aa
8 aa
Class 1 Pre-pro-MGF (159 aa)
Signal peptide cleavage
C
Pro-IGF-1Ea (105 aa)
Pro-MGF (111 aa)
E-peptide cleavage
Class 1 signal peptide (48 aa)
Mature IGF-1 peptide (70 aa)
Ea-peptide from
pro-IGF-1Ea(35 aa)
Eb-peptide from
pro-MGF (41 aa)

1.4.2 IGF-1/ IGF-1R signaling

The bioactivity of IGF-1 is specifically mediated by IGF-1R, a ligand-activated transmembrane tyrosine kinase receptor. Although hybrid receptors formed by IGF-1R and insulin receptor are reported, the affinity of IGF-1 to these hybrid receptors and insulin receptor is far lower than insulin (see review: Belfiore *et al.*, 2009). The IGF-1R binding surface of IGF-1 locates at the mature IGF-1 sequence. Thus, pro-IGF-1Ea, pro-MGF and mature IGF-1 containing IGF-1R binding surface, but not the Ea-peptide and Eb-peptide, are able to bind IGF-1R to trigger downstream signaling. The IGF-1/ IGF-1R binding induce conformational change, activation and auto-phosphorylation of the tyrosine kinase domain. It subsequently leads to recruitment of the downstream docking proteins including insulin receptor substrate protein (IRS). The two major pathways implicated in muscle regeneration include: (i) IRS-1/ phosphatidylinositol-3 kinase/ protein kinase B (IRS-1/ PI3K/ Akt); (ii) mitogen activated protein kinases (MAPK) signaling cascade. The IGF-1/ IGF-1R signaling pathways in muscle regeneration are referred (see reviews: Smith, 2010; Schiaffino & Mammucari, 2011; Enguita-Germán & Fortes, 2014).

1.4.3 Expression of IGF-1 in muscle regeneration

Differential upregulation of IGF-1 transcripts has been demonstrated in human muscle after exercise-induced injury (Philippou *et al.*, 2009). While human IGF-1Ec transcript (equivalent to murine MGF) increases at 6 h post injury, human IGF-1Ea (equivalent to murine IGF-1Ea)

is upregulated from day 2 post injury. Thus, human IGF-1Ec transcript upregulation precedes that of human IGF-1Ea. However, in cardiotoxin (CTX)-induced muscle injury, murine IGF-1Ea and MGF display similar dynamic expression (Tonkin *et al.*, 2015). Both transcripts were induced day 2 post injury and further increased at day 5. Despite the discrepancy (probably due to differences in species and type of injury), it is in consensus that the transcripts upregulate from hours to days post injury while inflammatory response takes place (Tidball, 2017).

IGF-1 isoforms have been associated with muscle inflammation. Lu *et al.*, (2011*b*) reported that abolishment of macrophage infiltration by CCR2 knockout suppresses IGF-1 upregulation in injured muscle. Lysozyme M (LysM)-promoter driven myeloid cell-specific IGF-1 knockout also abolishes the upregulation of IGF-1 in response to muscle injury (Tonkin *et al.*, 2015). These findings highlighted myeloid cells including macrophages as the predominant source of IGF-1 in injured muscle. Yet, the contribution from other infiltrated myeloid cells (e.g. neutrophils) awaits to be confirmed (Tonkin *et al.*, 2015). Other sources of IGF-1 in injured muscle include myofibers (McKoy *et al.*, 1999; Hayashi *et al.*, 2004), satellite cells and fibroblasts (Tonkin *et al.*, 2015). It has been demonstrated that fibroblasts are the major source of IGF-1 transcript after inflammatory resolution. It may support tissue remodeling and hypertrophy of regenerating myofibers (Tonkin *et al.*, 2015). Dynamic cellular sources of IGF-1 isoforms in regenerating muscle are therefore suggested.

1.4.4 Functions of IGF-1 and IGF-1Ea in muscle regeneration

The anabolic roles of IGF-1/ IGF-1R signaling in meditating muscle regeneration are well acknowledged in the aspect of satellite cell myogenesis, angiogenesis, ECM remodeling and muscle inflammatory response (Coolican *et al.*, 1997; Barton, 2006*a*; Smith, 2010; Philippou & Barton, 2014). Macrophages/ myotubes co-culture model showed that macrophage-derived IGF-1 is supportive to myotube growth and myosin heavy chain (MHC) expression (Dumont & Frenette, 2010). Suppressed infiltration of myeloid cells and myeloid cell-specific IGF-1 knockout deplete IGF-1 in injured muscle and result in impaired muscle regeneration (Lu *et al.*, 2011*a*, 2011*b*; Tonkin *et al.*, 2015). Impaired IGF-1/ IGF-1R signaling also leads to accumulation of fibrous tissues in regenerating muscle (Zhang *et al.*, 2010*a*; Dong *et al.*, 2013). IGF-1 in particular derived from macrophages highlights the significance of soluble factor and inflammatory response to muscle regeneration.

Of note, previous investigations delineated the regenerative functions of IGF-1 mainly by overexpressing IGF-1Ea in skeletal muscle (Musarò *et al.*, 2001; Schertzer & Lynch, 2006; Pelosi *et al.*, 2007). IGF-1Ea transgenic mice exhibits activated MAPK-dependent signaling pathway that promotes satellite cell proliferation in CTX-injured muscle (Musarò *et al.*, 2001, 2004; Rabinovsky *et al.*, 2003; Pelosi *et al.*, 2007). The IGF-1Ea transgenic model also demonstrates the role of IGF-1 signaling in accelerating muscle regeneration and limiting muscle fibrosis after CTX-induced injury (Pelosi *et al.*, 2007). Similar pro-regenerative effect was also reported by viral-mediated IGF-1Ea overexpression in reloading-injured

muscle (Ye *et al.*, 2013). Moreover, IGF-1 facilitates the resolution by downregulating the expression of inflammatory cytokines and chemokines and promoting macrophage polarization to M2 phenotype (Pelosi *et al.*, 2007; Tonkin *et al.*, 2015). Taken together the concomitant upregulation of IGF-1Ea in inflammatory response to muscle injury, it is conceivable that IGF-1Ea physiologically mediates muscle regeneration by promoting satellite cell myogenesis and inflammatory resolution.

1.4.5 Function of MGF in muscle regeneration

The function of MGF was extensively investigated by the administration of synthetic peptide analog into injured tissue (Yang *et al.*, 1996; McKoy *et al.*, 1999; Yang & Goldspink, 2002). Yang & Goldspink, (2002) designed the "synthetic MGF peptide" (synthetic peptide hereafter) containing only the last 24 amino acids unique to human IGF-1Ec (equivalent to murine MGF) based on the predicted peptide sequence reported in 1995 (Chew *et al.*, 1995). Thereafter, *in vitro* and *in vivo* studies on the synthetic peptide suggested the prominent anabolic and pro-survival effects of MGF in skeletal muscle (Yang & Goldspink, 2002; Mills *et al.*, 2007; Ates *et al.*, 2007; Zabłocka *et al.*, 2012). The investigation of synthetic peptide was further extended to regeneration of other tissues including neurons (Dluzniewska *et al.*, 2005; Riddoch-Contreras *et al.*, 2009; Quesada *et al.*, 2011) and the heart (Carpenter *et al.*, 2008; Mavrommatis *et al.*, 2013). Although the synthetic peptide is effective in promoting tissue regeneration, the physiological relevance to MGF (containing mature IGF-1 and Eb-peptide) is questionable.

Firstly, the synthetic peptide designed by Yang & Goldspink, (2002) is a truncated peptide and shorter than the E-domain cleavage product of MGF i.e. Eb-peptide (see Figure 1.4 and Table 1.2). Even in the use of antibody raised from the synthetic peptide, proteins with size similar to the synthetic peptide has never been detected in any cell or tissue samples (Vassilakos *et al.*, 2017). It means that physiological cleavage of MGF unlikely yields any product similar to the synthetic peptide. Moreover, the amino acid sequence of the synthetic peptide is modified by amino acid stereoisomer substitution (Dluzniewska *et al.*, 2005; Ates *et al.*, 2007; Carpenter *et al.*, 2008; Quesada *et al.*, 2011). Specifically, L-arginine is substituted by D-arginine substitution. Studies in mammals have reported that D-arginine residues possess pharmacological actions (Navarro *et al.*, 2005; Vassilakos *et al.*, 2014). Besides, the synthetic peptide sequence is deviated from the E-domain of both human and murine MGF reference sequence in GenBank database (see Table 1.2). Of importance, these characteristic differences of synthetic peptide from MGF together can result in varying effects on the physiological functions. Lastly, independent research groups have synthesized the synthetic peptides based on Goldspink and investigators reported sequences and tested the bioactivity in promoting myoblast and satellite cell proliferation (Fornaro *et al.*, 2014; Janssen *et al.*, 2016). None of these experiments could reproduce previous findings. Thus the physiological relevance and functional significance of the synthetic peptide to MGF have been challenged (Matheny *et al.*, 2010; Vassilakos *et al.*, 2014; Rotwein, 2014).

In our investigation, we refer MGF to the full-length transcript and putative peptides as defined in Section 1.4.1 and shown in Figure 1.4, which is distinct from the synthetic peptide used by Goldspink and investigators. Distinguishing the difference between the synthetic peptide and the physiological MGF is indisputably critical for study of IGF-1 physiological functions (Vassilakos *et al.*, 2014). Although the synthetic peptide may be biologically active in various cells and tissues, the relevance of it to physiological MGF is questionable. In other words, the physiological role of MGF in muscle regeneration and the inflammatory response remains elusive. Experimental model other than synthetic peptide should be adopted, for instance MGF overexpression, to elucidate the role of MGF in muscle injury.

A	No. of amino acid residues	Estimated mass (kDa)	Residues
pre-pro-MGF	159	17.89	GenBank: AAX61180
pro-MGF	111	12.54	Residue 49-159
Mature IGF-1	70	7.69	Residue 49-118
Eb-peptide (Mouse)	41	4.88	Residue 119-159

B	Amino acid sequence (N-terminal to C-terminal)	Reference
Synthetic peptide (Goldspink)	YQPPSTNKNTKSQ- **RR**KGSTFEEHK	Mavrommatis *et al.*, 2013
Ec-peptide (Human)	…YQPPSTNKNTKSQ- RRKGSTFEERK	GenBank: NM_001111283.2
Eb-peptide (Mouse)	… SPSLSTNKKTKLQRRRKGSTFEEHK	GenBank: AAX61180

Table 1.2 Facts of MGF and the peptide derivatives. (A) The number of amino acid residues, the estimated mass and the corresponding residues of pre-pro-MGF (Residues 1-159; GenBank AAX61180 is referred) and each putative peptide products. (B) Differences of widely adopted Goldspink's synthetic peptide from putative human Ec-peptide and mouse Eb-peptide. Without the exon 4 extension, which is indicated as ellipses at N-terminal of putative E-peptides, synthetic peptide is composed of only 24 aa residues. The two bold Arginine residues (-RR-) in synthetic peptide are D-Arginine, the stereoisomer of L-arginine. There is one additional Arginine in mouse Eb-peptide. The red-colored residue indicates the amino acid residue discrepancy of synthetic peptide from the GenBank database.

1.4.6 Differential functions of IGF-1Ea and MGF

Studies by Barton and colleagues have investigated the functions of IGF-1 isoforms and the putative derivatives in the past 10 years (Barton, 2006*a*, 2006*b*). Taken into consideration of the physiological relevance of IGF-1, this group of investigators cloned full-length IGF-1 isoforms and overexpressed the clones in murine skeletal muscle. Various putative IGF-1 gene products are thus transcribed, translated and modified (both post-transcriptionally and post-translationally) in a physiologically relevant environment (Barton, 2006*b*; Pfeffer *et al.*, 2009; Barton *et al.*, 2010; Durzyńska *et al.*, 2013; Park *et al.*, 2014; Brisson *et al.*, 2014; Philippou & Barton, 2014). Such design is critical for the investigation on physiological roles of IGF-1 and the derivatives. We summarize the findings from Barton and colleagues to highlight the uniqueness of MGF over IGF-1Ea so as to address the elusive physiological function of MGF.

Barton *et al.*, (2010) compared the transcriptome of mature IGF-1, IGF-1Ea and MGF-overexpressed muscles in a microarray study. Amongst the 216 genes altered by overexpression of IGF-1Ea and MGF, 30 genes were altered uniquely by MGF and 66 genes only by IGF-1Ea (the remaining genes were commonly modified). For instance, anti-apoptotic gene B-cell lymphoma-2 like 1 (Bcl-X) was commonly upregulated by overexpression of both isoforms. Osteopontin (encoded by Spp-1 gene) was one of the unique genes remarkably upregulated by MGF (4 to 20 fold), compared to IGF-1Ea (2 to 4 fold) and mature IGF-1 (no change). Thus unique modulation of cell survival by MGF was suggested (Barton *et al.*, 2010). It is also noteworthy that the induction of metalloprotease 13 can be abolished in IGF-1Ea

overexpressed muscle by the administration of IGF-1R neutralizing antibody. However the same treatment only reduced the induction by MGF. This may imply alternative signaling mechanism for MGF (Barton *et al.*, 2010). For instance, Eb-peptide may modulate the internalization and localization of IGF-1R by direct interaction (Pfeffer *et al.*, 2009; Brisson & Barton, 2012). This modulation may prompt to the preferential activation of MAPK cascade by MGF (Barton, 2006*b*; Brisson & Barton, 2012). Eb-peptide was also suggested to interact with proteins in ECM due to the highly positively charged motifs (Hede *et al.*, 2012). Sequestration of MGF to the ECM in regulating IGF-1 bioavailability is thus plausible (Gallagher, 2001; Hede *et al.*, 2012).

Further *in vitro* studies also suggested the differences of IGF-1Ea and MGF. Optimal concentration required to activate Akt and MAPK pathway are 100 fold higher in IGF-1Ea (1 μM) than MGF (0.01 μM) (Brisson & Barton, 2012). Yet MGF stability (half-life: 20 min) in culture medium is much lower than that of IGF-1Ea (half-life: longer than 24 h) (Brisson & Barton, 2012). Recently, Brisson *et al.*, (2014) reported the use of viral constructs of IGF-1 isoforms with inactivating mutation at the mature IGF-1 peptide sequence. In other words, only the E-peptides were virtually overexpressed. The remarkable MGF hypertrophic effect from this model suggested unique bioactivity of Eb-peptide *in vivo* (Brisson *et al.*, 2014). The intrinsic differences of IGF-1Ea and MGF at least in part lead to the more prominent hypertrophic effect of MGF in muscle (Brisson *et al.*, 2014).

Extensive studies in the past decade suggested IGF-1Ea possesses pro-myogenic and anti-inflammatory functions in muscle regeneration. Despite the elegant studies carried out by Barton's group, the overexpression models were only used to evaluate the differential effects of IGF-1 isoforms in muscle hypertrophy instead of muscle regeneration. Besides, synthetic peptide analogous to MGF appears not an appropriate model to examine the physiological function of MGF. Thus, the physiological roles of MGF in muscle regeneration and inflammatory response are underexplored. Whether MGF shares similar pro-regenerative functions as IGF-1Ea or possesses distinct modulating roles in muscle inflammatory response and regeneration remains to be confirmed.

1.5 SUMMARY

Muscle regeneration is essential for restoring tissue homeostasis and muscle functional integrity following injury and tissue damage. Well-orchestrated cascade of activities paves to successful regeneration. These involve regulated inflammatory initiation, perpetuation and resolution; and concurrent with satellite cell activation, proliferation and differentiation. The release of soluble factors and clearance of necrotic tissue highlight the significance of the inflammatory response in satellite cell-mediated myogenesis. Inflammatory myeloid cells and particularly macrophages are implicated in satellite cell survival, migration and myogenesis. Amongst all, the release of growth factor IGF-1 is strongly implicated.

Recent findings from myeloid cell-specific IGF-1 knockout model suggested myeloid cells, in particular macrophages, are the major source of IGF-1 in muscle regeneration. Macrophage-derived IGF-1 not only promotes satellite cell activities but inflammatory resolution by virtue of its anti-inflammatory properties. However, this study did not examine other myeloid progenies such as neutrophils that were also subject to IGF-1 knockout and infiltrate prior to macrophages. These early infiltrate may also express IGF-1 to modulate initiation and perpetuation of muscle inflammation. We hypothesize that myeloid cells in addition to macrophages contribute to upregulation of IGF-1 in injured muscle.

IGF-1 signaling is essential to muscle regeneration by promoting myogenesis and regulating inflammatory response. Despite strong implication in muscle regeneration, IGF-1 expresses in two isoforms that potentially carries out distinct regenerative functions. For instance, overexpression of IGF-1 isoforms in non-injured muscle leads to differential muscle transcriptome and hypertrophic effects. In the context of muscle regeneration, extensive studies were carried out on IGF-1Ea only. IGF-1Ea is attributed to modulate inflammatory cytokine expression as well as inflammatory resolution. The roles of MGF in the modulation of inflammatory response, however, remain elusive.

Since both IGF-1 isoforms contain common mature IGF-1 peptide, MGF and IGF-1Ea may induce IGF-1 signaling similarly. Given the anti-inflammatory roles of IGF-1Ea, it is conceivable that MGF may also possess similar immunomodulating properties in muscle regeneration. The distinct functions of MGF due to the presence of unique E-peptide, however,

also suggest potentially varying physiological changes during muscle regeneration.

HYPOTHESIS OF THE INVESTIGATION

We hypothesize that MGF modulates muscle inflammatory response in muscle regeneration. The aims of this study are:

1. To examine the expression of IGF-1 isoforms in myeloid cell infiltration after muscle injury; and
2. To examine the roles of MGF in inflammatory response to muscle injury.

CHAPTER 2

General Methodology

2.1 INTRODUCTION

The experimental work described was performed in the Department of Rehabilitation Sciences of The Hong Kong Polytechnic University. BalbC mice were used in this investigation. Tibialis anterior (TA) were injured and/ or electroporated with plasmid DNA containing MGF transcript insert for further evaluation. The rationale of animal models, design of protocols and the general procedures were described in this Chapter 2.

2.2 PLASMID DNA FOR MGF OVEREXPRESSION

A custom designed plasmid namely pMGF encoding class 1 pre-pro-MGF transcript was custom-synthesized for both *in vitro* and *in vivo* MGF overexpression in this study. All the sub-cloning procedures were carried out and completed by our collaborator, Prof. Shannon AU (School of Life Science, The Chinese University of Hong Kong) and her team.

2.2.1 Sub-cloning

Skeletal muscle was reported to express IGF-1 transcripts (McKoy *et al.*, 1999; Yang & Goldspink, 2002; Hill *et al.*, 2003). The complementary DNA (cDNA) library was therefore generated by pooling the cDNA from TA of three untreated adult mice and passed to collaborator for generating the pre-pro-MGF insert. Synthesis of insert DNA was accomplished by routine polymerase chain reaction (PCR) using the cDNA library and custom designed primer pairs. The sequence of MGF-specific primer pairs were indicated in Figure 2.1. Restriction enzymes used for unidirectional cloning

were *Bam*HI (5'-GGATCC-3') and *Not*I (5'-GCGGCCGC-3') to create incompatible sticky ends at the cleavage site. The forward primer, BamHI-MGF, contained the first 24 bases of pre-pro-MGF transcript, including start codon, just after the *Bam*HI restriction site. In order to detect translated MGF peptides from pMGF, the 3'-end of the transcript sequence was modified by insertion of a hexahistidine epitode tag (6-HIS) sequence (5'-CATCACCATCACCATCAC-3') immediately before stop codon of the reverse primer, MGF-HIS-NotI. The final insert sequence was therefore expected to generate a fusion protein of MGF with a C-terminal 6-HIS tag. The tag directly links with the characteristic E-domain of MGF translation products.

The final insert was cloned into a commercial plasmid DNA vector, pcDNA 3.1(+) (Thermo Fisher Scientific, USA) containing constitutively active cytomegalovirus (CMV) promotor and ampicillin resistance sequence for selection in later transformation process. The product clone sequence was confirmed by DNA sequencing before sub-cloning was carried out.

Forward primer: BamHI-MGF

5' CTCA GGATCC ATGGGGAAAATCAGCAGCCTTCCA 3'

Overhang *Bam*HI Pre-pro-MGF-forward (24 bp)

Reverse primer: MGF-HIS-NotI:

5' CTCA GCGGCCGC CTA GTGATGGTGATGGTGATG

Overhang *Not*I Stop codon 6-HIS tag

CTTGTGTTCTTCAAATGTACTTCC 3'

Pre-pro-MGF-reverse (24 bp)

Figure 2.1 Sequences of primer pairs used for MGF sub-cloning. Restriction enzymes: *Bam*HI (Forward) and *Not*I (Reverse). Pre-pro-MGF-forward and pre-pro-MGF-reverse: pre-pro-MGF transcript-specific sequences in forward and reverse primers respectively. Hexahistidine epitope tag (6-HIS tag): reverse complementary sequence of the one mentioned in text.

2.2.2 Transformation and DNA amplification

The plasmid, pMGF (approximate 10 ng), was transformed into competent E.coli cells for amplification. Briefly, commercially available 5-alpha competent E.coli was firstly incubated with pMGF on ice for 30 min followed by heat shock treatment at 42 °C for 30 s. Afterward, the cells were chilled on ice for 5 min and diluted in LB (Luria-Bertani or lysogeny broth) medium for plating. The successfully transformed clone was selected by plating the cells on LB broth containing ampicillin (100 μg ml^{-1}). After overnight incubation at 37 °C, a single colony which was ampicillin-resistant due to co-expression of ampicillin-resistant gene and pMGF was picked and further incubated in 1,000 ml LB medium with 100 μg ml^{-1} ampicillin for overnight expansion.

2.2.3 Plasmid DNA purification and verification

Purification of plasmid DNA was performed using EndoFree plasmid maxi kit (QIAGEN, USA) following manufacturer manual. Briefly, the pMGF contained cells were lysed and filtered with the filter cartridge. Endotoxin removal buffer from the kit was used to eliminate endotoxin in the sample. After serial washing steps with gradient salt buffers to remove contaminants (e.g. proteins), DNA was eluted and further desalted with isopropanol. The precipitated DNA was collected and reconstituted in 500 μl endotoxin-free water. Aliquots were then stored at -20 °C until use. Part of the aliquots was reserved for further plasmid propagation as described in last section. The final product was a desalted plasmid DNA free of endotoxin and suitable for both *in vitro* and *in vivo* application. To confirm the correct

sequence identity, the product was sent for commercial sequencing every time after amplification. Only clone with 100% identity achieved from sequencing by both forward (T7) and reverse (BGH-rev) primers was used for experimental purposes.

Concentration of pMGF was measured using Varioskan FLASH multimode microplate reader equipped with μDrop plate (Thermo Fisher Scientific, USA). The use of μDrop plate allowed measurement of DNA or RNA that required only 2 μl loading volume to minimize sample usage. The absorbance reading at 230 nm, 260 nm, 280 nm and 320 nm were measured. The concentration, purity ratio 260/ 280 and ratio 260/ 230 were calculated by SkanIt software (Thermo Fisher Scientific, USA) and the equations of calculation were shown below. Pure DNA in the absence of proteins and organic solvents contamination usually gives ratio 260/ 280 and ratio 260/ 230 of 1.8-2.0 and above 2.0 respectively. The accordingly prepared pMGF plasmid DNA was usually of 2,000 to 4,000 ng μl^{-1} with ratio 260/ 280 at 1.8 and ratio 260/ 230 at 2.1 to 2.3. Thus the pMGF plasmid DNA used in this study was pure from proteins or organic solvents contamination.

DNA concentration (ng μl^{-1})= (Absorbance (Abs) 260 nm – Abs 320 nm) * double-stranded DNA extinction coefficient (ng μl^{-1}) * path length correction of μDrop plate; in turn,

DNA concentration (ng μl^{-1})= (Abs 260 nm – Abs 320 nm) * (50 ng μl^{-1}) * 20

Purity of plasmid DNA

Ratio 260/ 280= (Abs 260 nm – Abs 320 nm)/ (Abs 280 nm – Abs 320 nm)

Ratio 260/ 230= (Abs 260 nm – Abs 320 nm)/ (Abs 230 nm – Abs 320 nm)

2.2.4 Expected product peptides from pMGF clone

The primary product of pMGF clone refers to pre-pro-MGF-HIS (Figure 2.2). It is composed of N-terminal signal sequence, mature IGF-1 peptide sequence, characteristic MGF E-domain sequence and 6-HIS tag. The post-translational cleavage of pre-pro-MGF was reviewed in details (Philippou *et al.*, 2014) and confirmed in murine tissues (Vassilakos *et al.*, 2017). Without any processing, the expected size of pre-pro-MGF-HIS is 18.69 kDa. The N-terminal signal sequence facilitates the transfer of pre-pro-peptide into secretory pathway. It is cleaved to yield pro-MGF-HIS (13.36 kDa) and possibly without further biological significance (Lingappa *et al.*, 1980; Wallis, 2009; Philippou *et al.*, 2014). The pro-peptide can be cleaved by pro-protein convertase to synthesize the mature IGF-1 peptide (7.68 kDa) and Eb-HIS peptide (5.70 kDa) (Duguay *et al.*, 1995; Philippou *et al.*, 2014). Of note, protein lysate containing the putative pMGF translation products were subjected to immunoblotting with monoclonal antibody against the 6-HIS tag to confirm the translational activity of the custom synthesized clone (to be described in Section 2.6). Only the 6-HIS-tagged peptide products could be probed, including pre-pro-MGF-HIS, pro-MGF-HIS and Eb-peptide-HIS whereas the cleaved signal peptide and mature IGF-1 peptide could not be detected by the current design.

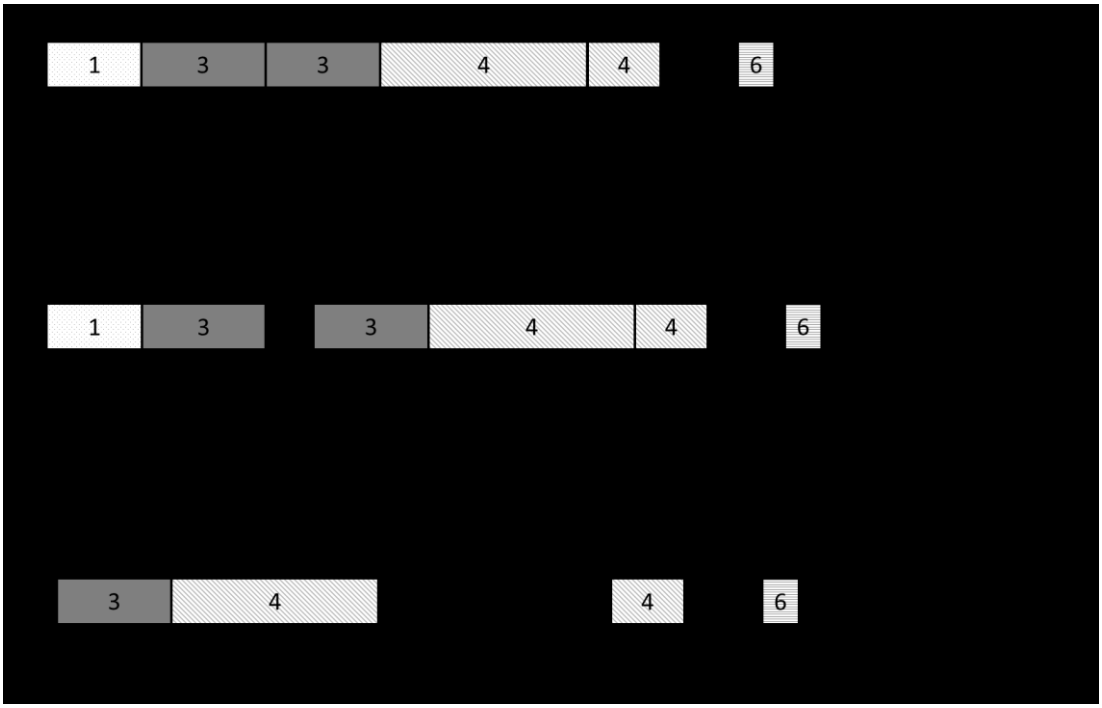

Figure 2.2 Putative translation products from pMGF clone. Each box refers to the corresponding exon sequence denoted by the exon number. The number above each exon portion of pre-pro-MGF-HIS sequence indicates the number of amino acid residues contained (aa= amino acid). After cleavage of signal peptide, the pro-MGF is yielded. Further cleavage generates the mature IGF-1 peptide and Eb-peptide-HIS. Of note, only peptide with 6-HIS tag could be detected by specific antibody against the 6-HIS tag.

2.3 ANIMAL MODELS

All animal care and experimental procedures performed in this study were approved by the Animal Subjects Ethics Sub-Committee of the Hong Kong Polytechnic University (ASESC no.: 12-09, 13-07, 13-08). Adult male BalbC mice (obtained from the Centralized Animal Facilities (CAF) of the Hong Kong Polytechnic University) were used in the present study. Adult male mice of 10 to 14 week old were used so as to minimize confounding effects from growth and hormonal fluctuation present in female mice.

All the animals were transferred to and housed in an animal holding room with 12:12 dark-light cycle and controlled temperature and humidity in CAF. Daily health monitoring activities were performed by qualified staff from CAF. Animals were fed with standard rat chow and disinfected water ad libitum (*ad lib*). Moreover, acclimation to the holding room for at least one week prior to experiments was essential to minimize any possible distress due to changes in housing environment. Additional monitoring of animal health conditions by the researcher was provided after every experimental treatment. When animals exhibited any sign of distress or demonstrated poor health conditions, they will be immediately excluded from the experiments and will be euthanized by rapid cervical dislocation.

2.3.1 Animal anesthesia

Before experimental manipulation, mice were anesthetized by inhalation of 1.5% isoflurane in oxygen. Complete anesthesia was confirmed by the lack of hindlimbs pedal withdrawal reflex. This anesthesia method was applied to all the animal experiments included in this study.

2.3.2 Rationale and protocol of muscle injury model – Cardiotoxin injection

CTX-induced muscle injury model was widely adopted in the studies of muscle regeneration (Musarò *et al.*, 2001; Pelosi *et al.*, 2007; Wang *et al.*, 2014; Tonkin *et al.*, 2015; Hardy *et al.*, 2016). Despite less physiological in comparison to contraction-induced injury, it is advantageous in the aspect of damage homogeneity and technical competence (Hardy *et al.*, 2016). CTX is a specific protein kinase C (PKC) inhibitor. Injection of CTX into skeletal muscle induces complete depolarization of sarcolemma and then myofiber contracture. Myofiber necrosis is the final outcome of CTX injection. Typical inflammatory response from acute infiltration of inflammatory cells to the resolution could also be clearly identified (Hardy *et al.*, 2016).

Although stereotypical responses could be observed amongst studies of CTX-induced muscle injury, the temporal dynamic of inflammatory response and muscle regeneration varied. It was attributable to the variation amongst injection protocols, such as the type of CTX used, dose and injection scheme etc. Therefore the timepoint design for CTX injury model has to be tested empirically to demonstrate the regeneration stages of research interest. In this study, injured muscles were collected at day 2, day 4 and day 7 post CTX injection. The harvest timepoint was designed to capture three distinct inflammatory phases observed from CTX-injured muscles respectively, namely (i) inflammatory; (ii) early resolution; and (iii) late resolution phase (referred to Sections 1.3.2-1.3.5).

2.3.3 Protocol of CTX injury model

In this study, CTX from venom of *Naja mossambica mossambica* (CTX III; Sigma Aldrich, USA) was used. Lyophilized CTX powder was reconstituted in normal saline to 400 mM, 0.22 μm filtered sterile and aliquots were stored at -20 °C. In each experiment, an aliquot of CTX was thawed and freshly diluted into working concentration (10 μM) with sterile normal saline. The half-maximal inhibitory concentration of this CTX to PKC should be at 9 μM (Chiou *et al.*, 1993). Our working concentration thus efficiently inhibited PKC activity. Simultaneously, it was reported not compromising satellite cell viability and muscle regenerative capacity (Couteaux *et al.*, 1988). Of note, elucidating the type of CTX used is essential as different potency might lead to variation in injury severity and recovery (Chiou *et al.*, 1993).

To induce muscle injury, animals were firstly anesthetized and the skin covering the TA was shaved and disinfected with 70% ethanol. Working solution of CTX was then intramuscularly injected into the mid-belly of TA (1 μl g^{-1} body mass) using insulin syringe (30 gauge; Terumo, USA). Sterile normal saline of the same injection volume, when appropriate, was injected into the contralateral TA to serve as experimental control. Successful intramuscular injection was indicated by immediate mild swelling of the injected TA which usually diminished within 30 min. Afterwards, the mice were allowed free-cage movement and food/ water access *ad lib* and euthanized at desired endpoints.

2.3.4 Skeletal muscle electroporation

Electroporation transiently raises cell permeability by applying electric field to induce formation of hydrophilic pores (Gehl, 2003; Weaver *et al.*, 2012). Exogenous material e.g. plasmid DNA thus migrates through the pores by electrophoretic movement. Our electroporation protocol was designed to maximize electroporation efficiency and the expression of MGF by choosing optimized parameters from previous protocols (McMahon *et al.*, 2001; Lee *et al.*, 2002; Schertzer & Lynch, 2006).

Mice were anaesthetized and the skin covering TA was shaved and disinfected with 70% ethanol. The muscles were intramuscularly injected with 20 µl (0.4 U μl^{-1} normal saline) filter-sterile bovine hyaluronidase (Sigma Aldrich, USA) using insulin syringe (30 gauge; Terumo, USA) (Schertzer *et al.*, 2006). Two hours after hyaluronidase treatment, one side of TA was injected with 25 µl pMGF (1 µg μl^{-1}) in sterile 0.45% m/v saline (Lee *et al.*, 2002). Immediately after each plasmid injection, a platinum tweezertrodes (5 mm diameter, BTX, USA) was placed in a longitudinal direction relative to TA. The contact sites of the electrodes and skin were wet with normal saline to increase conductivity. A total of 10 square-wave electrical pulses at 175 V cm^{-1} field strength (pulse duration= 20 ms and pulse interval= 1 Hz) were generated from electroporation apparatus ECM830 (BTX, USA) and locally delivered to the TA (McMahon *et al.*, 2001). The contralateral TA that electroporated with empty vector (pcDNA 3.1) in the same way served as negative control for comparison purpose. Afterwards, mice were allowed free-cage movement with food/ water access *ad lib*. Daily monitoring was given until euthanasia at desired endpoints.

2.3.5 Muscle dissection and harvest

At first the working area and all dissection tools were disinfected by spraying 70% ethanol. To harvest TA, mice were euthanized by cervical dislocation. The hindlimbs were sprayed with 70% ethanol and then the mouse was pinned onto dissecting board with ventral side up. Next the skin of lower limb was shaved and cut through with operating scissors to completely expose the TA underneath. The fascia covering TA was gently removed with fine forceps and dissecting scissors. Extra care was given to avoid any contact and damages to the muscle belly. The distal end of TA tendon was then exposed and released. After grasping the tendon with fine forceps, we cut the tendon with operating scissors at the insertion site and gently pulled up TA along the tibia. Attention was required to avoid stretching the muscle. Any connective tissues hindered the process could be carefully removed by dissecting scissors. Then, origin of TA at the proximal end was identified. Removal of surrounding connective tissue or part of the patella might help the exposure of TA origin. It was then cut with dissecting scissors as far from the muscle belly as possible.

Isolated TA was transferred onto a cotton wool soaked with sterile normal saline for the removal of residual connective, vascular and adipose tissues. The clean TA was then blot-dry with sterile gauze and ready for assay-specific processing. The same procedures applied on the contralateral TA. The procedures of assay-specific processing were described later in the respective section (referred to Sections 2.5-2.9).

2.4 IN VITRO CELL CULTURE

C2C12 cell line was purchased from American Type Culture Collection (USA). It is a mouse myoblast cell line capable of committing into myogenic differentiation to form contractile myotubes upon nutrient withdrawal or cell-cell contact. This cell line is commonly used in various skeletal muscle associated researches (Pfeffer *et al.*, 2009; Cheung *et al.*, 2011; Hede *et al.*, 2012; Fornaro *et al.*, 2014). Our in-house routine procedures of culturing C2C12 were detailed in this section (Cheung *et al.*, 2011). Moreover, all the following experimental procedures were performed inside a type IIA biological safety cabinet with aseptic techniques adopted to ensure culture sterility.

2.4.1 C2C12 cell thawing

A vial containing early passage 3 to passage 5 of C2C12 was quickly thawed from liquefied nitrogen (Liq. N) by putting the cryo-vial into 37 °C water bath with gentle shaking. When the cell suspension was almost thawed (a piece of ice left), cells were gently re-suspended in pre-warmed growth medium (GM) consisting of Dulbecco's Modified Eagle Medium (DMEM; Thermo Fisher Scientific, USA) supplemented with 10% fetal bovine serum (FBS; Thermo Fisher Scientific, USA) and antibiotics penicillin-streptomycin-glutamine (PSG; Thermo Fisher Scientific, USA).

The suspension was transferred into a sterile 100 mm tissue culture plate and incubated in humidified incubator (37 °C, 5% carbon dioxide, or CO_2). About 1 h from plating, attachment of viable cells should be observable under light microscope. GM was refreshed to remove the residual

freezing medium and non-attached cells or cellular debris. Cells were then returned to incubator and daily checked for morphology and confluency.

2.4.2 Proliferating cell culture

Proliferating C2C12 cell line was maintained in GM and should never be allowed to reach over 70% confluency. Sub-culture was performed by adding 0.25% Trypsin-EDTA (EDTA: Ethylenediaminetetraacetic acid; Thermo Fisher Scientific, USA) into phosphate buffer saline (PBS; Thermo Fisher Scientific, USA) washed cell plate and incubated at 37 °C for 4 min. Enzymatic dissociation was then stopped by adding two volumes of fresh GM. Cells should be easily detached by gentle tapping of the culture plate. The cell suspension was transferred to a 15 ml sterile centrifuge tube followed by gentle pipetting up-and-down for about 10 times. This step was important to dissociate any cell clumps into single cells. Cell pellet was collected by centrifugation (600 x g, 25 °C, 5 min) and re-suspended in 2 ml fresh GM. Cell counting using hemocytometer was performed to achieve desired cell number for cell passage. Usually, C2C12 at 2 x 10^5 per 100 mm plate growing in GM required sub-culture every two days and about 2 to 3 x 10^6 cells could be collected per plate. When passage 20 was reached, the cells were no longer used for further experiments and would be disposed.

2.4.3 Myogenic cell differentiation

Differentiation of C2C12 was induced by replacement of GM with differentiation medium containing DMEM supplemented with 2% normal

horse serum (Thermo Fisher Scientific, USA) and 1% PSG (Cheung *et al.*, 2011). Proliferating C2C12 culture were allowed to reach 80 to 90% confluency. After washing with PBS to remove residual GM, cells were cultured with differentiation medium to induce myogenic differentiation.

2.4.4 Transfection

To overcome cell membrane barrier against the charged plasmid DNA, commercial Lipofectamine, a reagent for *in vitro* delivery of plasmids into desired cells, was used in this study. Lipofectamine formulation allows formation of liposome containing desired plasmid in culture medium. It also allows fusion of the liposome molecules with cell membrane and thereafter release of the contained plasmid DNA into cells being transfected (Dalby *et al.*, 2004).

To prepare for transfection experiments, trypsinized C2C12 cells from proliferating culture was replated at desired cell density. PSG-free media were used in all transfection experiments because exposure to antibiotics might compromise cell viability and reduce transfection efficiency. Once desired confluency or cell status has reached, transfection experiment was performed using Lipofectamine 2000, following manufacturer instruction (Thermo Fisher Scientific, USA).

Transfection experiment started from separately incubating plasmid DNA (pMGF or empty vector) and Lipofectamine 2000 in transfection medium, OptiMEM (Thermo Fisher Scientific, USA) for 5 min at room temperature. Next the OptiMEM with plasmid DNA and Lipofectamine 2000 were mixed in 1:1 ratio to generate the working transfection mix and further

incubated at room temperature for additional 25 min. This procedure allowed liposome formation with plasmid DNA entrapped inside.

Prior to addition of transfection mix, cells were washed twice with PBS to get rid of serum included in PSG-free GM and plain DMEM was added. The cells were then treated with the transfection mix and incubated for transfection to take place (37 °C, 5% CO_2). To increase cell viability, serum was supplemented 6 h post transfection. Medium containing transfection mix was replaced after 24 h incubation with appropriate PSG-free media. Transfected cells were incubated and culture medium was refreshed every two days until harvest at desired timepoints.

2.5 EVALUATION OF TRANSCRIPT EXPRESSION

To evaluate the effects of different experimental paradigms on tissue or cell transcript expression, total RNA from muscle or cell samples was extracted, purified and reversely transcribed into cDNA for probe-based real-time quantitative PCR (RT-qPCR) assessments. Taqman assays were used to evaluate the expression of various genes. For details of the assays used in each experiment, please see corresponding methodology in experimental Chapter 3 and 4.

2.5.1 RNA extraction

All the RNA associated works were performed in an area restricted to molecular work. The working surface and instruments were wiped with 70% ethanol for disinfection followed by commercial ribonuclease (RNase)

cleaning regents (Thermo Fisher Scientific, USA). All the consumables used were nuclease-free. The pestle and mortar used for tissue disruption were overnight treated with 1% diethyl pyrocarbonate (Sigma Aldrich, USA) in ultrapure water followed by autoclave at 120 °C for 20 min to eliminate RNase on the tools. Special handling techniques were also used to avoid contamination of samples with exogenous DNA and RNA decomposition by RNase or high temperature. It included wearing new masks and gloves; avoiding any objects moving on uncapped samples and reagents; keeping RNA contained tubes on ice; and informing colleagues around not to approach the working area without prior notification. Total RNA in high yield and good quality was extracted following the above precautions. Purification of total RNA from contaminating genomic DNA and protein was accomplished by commercial purification kits following the manufacturer instruction. These were (i) PureLink RNA mini kit (Thermo Fisher Scientific, USA); (ii) SV total RNA isolation system (Promega, USA); and (iii) ReliaPrep RNA cell miniprep system (Promega, USA). Notably, all RNA samples were treated with deoxyribonuclease (DNase) during the purification procedures to get rid of genomic DNA.

To extract total RNA from C2C12 samples, PureLink RNA mini kit (Thermo Fisher Scientific, USA) was used. All reagents including RNA lysis buffer, DNase reaction mix and washing buffers were prepared according to manufacturer manual. Adhered cells were firstly washed three times with sterile PBS (Thermo Fisher Scientific, USA) to remove cell culture medium. Cells were then scratched off from the culture plate in the presence of ice-cool RNA lysis buffer supplemented with 1% v/v β-mercaptoethanol.

Homogenization was performed by passing the sample through a 23 gauge needle for no more than 5 times. The homogenate was diluted with one volume of molecular grade 70% ethanol and transferred into the kit provided spin cartridge. It was washed by centrifugation at 12,000 x g, room temperature (same centrifugation procedure applied to the following steps) for 15 s, followed by flow-through removal. Total RNA was now bound with the membrane of cartridge. After washing with 350 µl wash buffer I and centrifugation, the cartridge was then treated with column-compatible PureLink DNase treatment to remove genomic DNA (Thermo Fisher Scientific, USA). The same washing step was repeated after 15 min incubation at room temperature. The DNase-treated RNA was next washed twice with 700 µl wash buffer II with ethanol and centrifugation. In addition to 2 min high speed centrifugation suggested in the manufacturer manuals, the sample cartridges were air dried for 5 min. Both steps ensured complete removal of residual ethanol, which is potentially inhibitory to downstream enzyme treatments. The DNA-free purified total RNA was dissolved in 30 µl nuclease-free pure water, incubated for 1 min and eluted by centrifugation for 2 min. The final RNA concentration ranged from 200 to 800 ng μl^{-1}, depending on the starting amount and types of cells loaded. The manufacturer manual is available with detailed procedures:

https://tools.thermofisher.com/content/sfs/manuals/purelink_rna_mini_kit_man.pdf

(Page 19 to 20 for general purification procedure and page 63 to 65 for the modification required for on-column DNase treatment)

To extract RNA from muscle, isolated TA was snap-frozen in Liq. N and stored at -80 °C until further processing. Total RNA isolation from TA required the use of SV total RNA isolation system (Promega, USA) in which the lysis buffer worked well with fibrous tissues like skeletal muscle. All reagents were prepared following the manufacturer manual. To harvest total RNA, TA was grinded into powder by Liq. N chilled RNase-free pestle and mortar. The powder was then transferred into a pre-chilled microcentrifuge tube containing ice-cool RNA lysis buffer supplemented with 1% v/v β-mercaptoethanol. The lysate was homogenized by passing through 23 gauge needle until smooth passage (usually less than 20 times when sufficiently powdered). The homogenate was then mixed with 2 volume of RNA dilution buffer and heated at 70 °C for 3 min. The mixture was centrifuged at 14,000 x g, room temperature (same setting applied to the following centrifugation steps) for 4 min. Every 500 µl supernatant was mixed with 200 µl 95% ethanol by pipetting. The mixture was transferred into the spin cartridge and subjected to centrifugation for 1 min. The RNA-bound cartridge was washed with 600 µl RNA wash solution with centrifugation for 1 min. To eliminate genomic DNA, 50 µl DNase incubation mix was loaded onto the membrane and incubated at room temperature for 15 min. The digestion was stopped with DNase stop solution followed by centrifugation for 1 min. The DNA-free RNA was washed with 600 µl RNA wash solution with 1 min centrifugation and further washed by 250 µl RNA wash solution with 2 min centrifugation. Similarly, the spin cartridge was air-dried for 5 min before elution to ensure complete removal of ethanol residual from wash solution. The final DNA-free, pure total RNA

was eluted with 40 µl nuclease-free water. Approximately 600 ng μl^{-1} total RNA could be purified from a single TA isolated from adult male mice used in this study. The manufacturer manual is available with detailed procedures: https://www.promega.com/-/media/files/resources/protocols/technical-manuals/0/sv-total-rna-isolation-system-protocol.pdf
(Page 10, 13 to 14 for the column purification procedures)

To extract RNA from less abundant cell samples (below 10^5 cells), the ReliaPrep RNA cell miniprep system (Promega, USA) was used. It is a kit specialized for isolating total RNA from as low as 10^2 cells. The manufacturer protocol for reagents preparation and total RNA purification was strictly followed. Cell pellet collected from sorting experiment (referred to Section 2.9.2) was lysed by 100 µl BL buffer (supplemented with 1% v/v 1-thioglycerol) with brief vortexing. Afterward, 100% molecular grade isopropanol (Sigma Aldrich, USA) was added and mixed by 5 s vortexing. The mixture was transferred to the ReliaPrep mini-column and centrifuged at 14,000 x g, room temperature for 30 s (same centrifugation applied for following steps unless specified). Total RNA was washed with 500 µl RNA wash solution with ethanol and centrifuged. It was subsequently treated with DNase for 15 min at room temperature to remove genomic DNA, followed by 200 µl column wash solution to stop the DNase activity. The DNA-free total RNA was further washed by 500 µl RNA wash solution and centrifuged. The last washing step required 200 µl RNA wash solution and centrifugation for 2 min to remove the buffer completely. Lastly, the purified RNA was eluted with 10 µl nuclease-free water to maximize the concentration of

purified RNA. Further lowering the elution volume might compromise the total RNA yield and was not recommended by the manual. The manufacturer manual is available with detailed procedures:

https://www.promega.com/-/media/files/resources/protocols/technical-manuals/101/reliaprep-rna-cell-miniprep-system-protocol.pdf

(Page 9 to 11 for the column purification procedures)

2.5.2 First-strand cDNA synthesis

Concentration of purified total RNA samples isolated from cell line and muscle was determined by spectrophotometry using Varioskan FLASH multimode microplate reader equipped with µDrop plate (Thermo Fisher Scientific, USA) similar to method of DNA measurement as described in Section 2.2.3. The concentration and purity (ratio 260/ 280 and ratio 260/ 230) of RNA samples were calculated with the following formula:

RNA concentration (ng μl^{-1})= (Abs 260 nm – Abs 320 nm) * (40 ng μl^{-1}) * 20

Ratio 260/ 280= (Abs 260 nm – Abs 320 nm)/ (Abs 280 nm – Abs 320 nm)

Ratio 260/ 230= (Abs 260 nm – Abs 320 nm)/ (Abs 230 nm – Abs 320 nm)

To synthesize first-strand cDNA, 1 µg total RNA were reversely transcribed using GoScript reverse transcription system (Promega, USA). In the aspect of RNA from low abundant cell sample yielded below 1 µg, all eluted total RNA (about 9 µl) was loaded for cDNA synthesis to maximize cDNA yield. Constituents of the individual reaction mixes were summarized in Table 2.1. For the reaction conditions, reaction mix 1 was first incubated

at 42 °C for 5 min. Reaction mix 1 and 2 were then mixed into a single final mix. It underwent reverse transcription by incubating at 25 °C for 5 min, 42 °C for 60 min and 70 °C for 15 min. The reverse transcription reaction was carried out by CFX Connect Real Time PCR Detection System (Bio-Rad, USA). The cDNA samples were then stored at -20 °C prior to RT-qPCR assessment. For long-term storage, cDNA samples were kept at -80 °C.

2.5.3 RT-qPCR

To determine the transcript level of cDNA samples, probe-based RT-qPCR was conducted and carried out by CFX Connect Real-Time PCR Detection System (Bio-Rad, USA). All the probes used in this study were Taqman assays against mouse genome (Thermo Fisher Scientific, USA) and to be specified in the corresponding experimental Chapter 3 and 4. Commercial RT-qPCR master mix, namely GoTaq probe-based RT-PCR master mix (Promega, USA) contained all the required components for probe-based RT-qPCR. The composition of reaction mix and PCR running conditions were summarized in Table 2.2.

Reaction mix 1 (per sample)	**Reaction mix 2 (per sample)**
*Total RNA (1 µg)= X µl	GoScript 5X reaction buffer= 5 µl
Random primer (0.5 µg)= 1.25 µl	$MgCl_2$ (2 mM)= 3.625 µl
Oligo dT (0.5 µg)= 1.25 µl	dNTP mix (0.5 mM)= 1.25 µl
Nuclease-free water= (10 – X) µl	RNasin= 0.675 µl
	GoScript reverse transcriptase= 1.25 µl
	Nuclease-free water= 0.7 µl
Total volume= 12.5 µl	**Total volume= 12.5 µl**

Table 2.1 Reaction mixes of reverse transcription reaction. Total RNA was isolated from cell and muscle samples. *For less abundant cell sample, X was about 9 which was the volume of RNA eluted. All the listed components were provided by the GoScript reverse transcription system. Abbreviation: oligo-dT= deoxythymidine oligomer; $MgCl_2$= magnesium chloride; dNTP mix= deoxyribonucleotide mix; RNasin= ribonuclease inhibitor.

A

Components	Volume per reaction (µl)
2X GoTaq RT-PCR master mix	5
Taqman assay 1	0.5
*(Taqman assay 2)	(0.5)
*Nuclease-free water	3.5 (or 3)

* Adjustment for multiplex reaction

B

Steps	Temperature and duration	
1. Activation	95 °C, 5 min	
2. Denaturing	95 °C, 1 min	**Cycles:** 40
3. Annealing	60 °C, 30 s	
4. Extension and Measurement	42 °C, 1 min	
5. End	25 °C, forever	

Table 2.2 Protocol of probe-based RT-qPCR. A) Reaction mix recipe for a single reaction; B) PCR conditions.

2.5.4 Custom Taqman assay on MGF transcript

In addition, Taqman assay against mouse MGF was not commercially available and required custom synthesis (Thermo Fisher Scientific, USA). The designed sequences of primer pairs and probe were specific to the MGF E-domain to ensure detection of mouse MGF but not the other isoform, IGF-1Ea. The probe and reverse primers anneal to MGF transcript-specific exon 5 sequence only. In consideration of primer properties for RT-qPCR, there was only one nucleotide base spanning on exon 5 in forward primer. Signal released from each Taqman probe requires specific and ordered binding of primer pairs and probe simultaneously. Taken advantages of this probe-based method, the low coverage of exon 5 in forward primer should not compromise MGF Taqman assay specificity. This was supported by nucleotide BLAST (National Institutes of Health, USA) alignment tool showing no cross-reactivity of the primer pairs and probe sequences to other IGF-1 isoforms or genes. Besides, the primer design was conducted by online primer design tools (Thermo Fisher Scientific, USA). The algorithm only provides choices suitable for Taqman assay development and applicable in RT-qPCR. The custom MGF Taqman assay sequences were shown below:

Forward primer*:* 5'-GACATGCCCAAGACTCAGAAGT-3';

Reverse primer: 5"-CTTCTCCTTTGCAGCTTCGTTTT-3';

Probe sequence: MGB-FAM- 5"-TCCCTATCGACAAACAAG-3"

MGB is a non-fluorescent quencher conjugated directly with the fluorochrome. All Taqman probes were FAM dye conjugated including the MGF shown above. The only exception was the Taqman assay of ribosomal RNA 18S (18S rRNA), which was VIC dye conjugated and limited in primer amount. The use of two different dyes, FAM and VIC, allowed simultaneous detection (multiplex reaction) to be carried out for a given sample.

2.5.5 RT-qPCR data processing and analysis

To allow valid comparison amongst batches of experiments, the threshold line was set at relative fluorescence unit= 100 in all evaluations. It was empirically determined and found consistently located at the exponential phase of the PCR amplification curves. The cycle of threshold, Ct values, were then determined for each gene and sample reaction. Sample with Ct value of a gene above 35 cycles was regarded as not expressing that particular gene. The potential variation in the amount of starting material was corrected by normalizing the Ct value of interested gene with housekeeping genes.

The choices of housekeeping genes and their validity were identified and confirmed by NormFinder (Andersen *et al.*, 2004), an open algorithm with extensive usage and thousands citations. According to the original technical note, it ranks the set of candidate housekeeping genes based on their expression stability in a given sample set and experimental design. In this study, Glyceraldehyde 3-phosphate dehydrogenase (GAPDH; Assay ID: 4352932E), ribosomal protein S20 (RPS20; Assay ID: Mm02342828_g1) and 18S rRNA (Assay ID: 4448484) were the candidates

of housekeeping control and the Ct value from the corresponding Taqman assay (Thermo Fisher Scientific, USA) was input into NormFinder for evaluation. Single or a set of housekeeping gene determined to be stable and suitable by NormFinder would be used for normalization purposes. The choices of housekeeping genes used in the various experiments would be provided in the respective experimental methodology. When more than one housekeeping genes were needed, geomean of the Ct value would be calculated i.e. geomean Ct $_{\text{housekeeping genes}}$. Relative changes of interested gene expression comparing between groups, were calculated using the $2^{-\Delta\Delta Ct}$ ($\Delta\Delta$Ct: delta delta cycle of threshold) method of analysis. Statistical tests were performed on the delta Ct (dCt) values (Ct $_{\text{gene of interest}}$ − Ct $_{\text{housekeeping gene(s)}}$). The range of relative expression was calculated by mean dCT with ±1 standard error of mean (SEM) which represented the errors in relative expression (Livak & Schmittgen, 2001). The following example demonstrated the calculation of relative change and range of change between treatment and control group:

Relative change (treatment vs control)= 2^-(dCt of treatment- dCt of control)
Range of change= │Relative change - 2^-(dCt of treatment ± 1SEM of treatment - dCt of control) │

2.6 PROTEIN EXPRESSION

Expression of protein was evaluated by Western blotting coupled to targets-specific antibodies. In this study, protein expression from pMGF was examined in order to confirm the translational activity of the custom

synthesized clone in both *in vitro* and *in vivo* models. It was achieved by using specific antibody against the 6-HIS tag. The procedures from protein extraction to Western blotting were described as followed. The Western blotting procedures was based on our in-house protocol (Cheung *et al.*, 2011) and the Western blotting guide (Bio-rad, USA) at:

http://www.bio-rad.com/webroot/web/pdf/lsr/literature/Bulletin_2895.pdf

2.6.1 Protein extraction

Protein extraction of both cell and muscle samples used the same protein lysis buffer and the recipe was shown in Table 2.3. Particularly, phosphatase and protease inhibitors were included in the buffer. Phosphatase inhibitor suppresses protein dephosphorylation by endogenous phosphatases. Protease inhibitor on the other hand prevents protein decomposition by endogenous proteases. Precautions of using autoclaved and protease-free consumables and keeping protein samples on ice were followed.

To extract total protein from cell, adhered C2C12 cells were firstly washed with ice-cool PBS twice to remove residual culture media. Complete removal and thorough washing is critical to avoid sample contamination by abundant serum protein in culture media. Afterwards, ice-cool protein lysis buffer was directly applied to the cells. The lysate was then transferred to a microcentrifuge tube and homogenized by passing through a 23 gauge needle for 5 to 10 times. The homogenate was incubated at 4 °C for 30 min followed by centrifugation at 13,000 x g, 4 °C for 30 min. The supernatant containing total protein was then aliquoted, snap-frozen in Liq. N and stored at -80 °C until use.

As for protein extraction from muscle samples, frozen muscles were powdered by pestle and mortar. Sample powder was transferred to microcentrifuge tube containing ice-cool protein lysis buffer. Homogenization of muscle protein extract was accomplished by passing through a 23 gauge needle until smooth passage (usually less than 30 times). Generation of bubble during the process should be avoided. After homogenization step, the cell or muscle homogenates were incubated at 4 °C for 30 min followed by centrifugation at 13,000 x g, 4 °C for additional 30 min. The supernatant containing total protein was then aliquoted, snap-frozen in Liq. N and stored at -80 °C until use.

Components	Volume (µl) per 1 ml buffer
10X RIPA lysis buffer	100
10X PhosSTOP phosphatase inhibitor	100
10X cOmplete-ULTRA protease inhibitor	100
100 mM AEBSF	10
0.2 M Dithiothreitol (DTT)	2
ddH_2O	688

Table 2.3 Composition of protein lysis buffer for protein extraction. All components were purchased from Sigma Aldrich, USA except 10X RIPA (or Radioimmunoprecipitation assay) lysis buffer was from Cell Signaling Technology, USA. Tablets of PhosSTOP phosphatase inhibitor and cOmplete-ULTRA protease inhibitor were dissolved in double-distilled water (ddH_2O) at 10 times concentration. AEBSF, 4-(2-aminoethyl)-benzenesulfonyl fluoride hydrochloride, is a serine protease inhibitor.

2.6.2 Protein concentration determination

Aliquot of samples were thawed and subjected to protein quantification by Bradford protein assay (Bio-rad, USA) with bovine serum albumin (BSA) standards (Bio-rad, USA), following manufacturer manual. In brief, total protein samples were 10 times diluted with double-distilled water (ddH_2O) and then loaded, in duplicate, into 96-well plate containing working Bradford reagent. Similarly, standards were serially diluted into 4 concentrations and added into the same 96-well plate in duplicates per concentration. The plate was then scanned for absorbance at 595 nm using Varioskan FLASH multimode microplate reader (Thermo Fisher Scientific, USA). Absorbance of the duplicate was averaged and blank subtracted. Protein standard curve was established by plotting Abs 595 nm against standards concentration. Concentration of the protein sample was calculated based on the linear slope of standard curve established with BSA standards (M_{BSA}) as followed:

Sample dilution factor= 10

Sample protein concentration ($\mu g\ \mu l^{-1}$)= (Blank subtracted sample Abs 590 nm/ M_{BSA}) x 10

2.6.3 Sodium dodecyl sulfate-polyacrylamide gel electrophoresis

Unless specified, all the reagents and material used for sodium dodecyl sulfate (SDS)-polyacrylamide gel electrophoresis (PAGE), or SDS-PAGE were purchased from (Bio-Rad, USA). Tris-glycine-SDS running buffer was freshly prepared from 10X concentrated stock with ddH_2O.

Commercial 4-15% gradient gel of Mini-PROTEAN TGX precast gel was loaded into the Mini-PROTEAN tetra cell assembly. The inner and outer chambers were filled with the working running buffer. The comb within the gel was next removed and any bubble inside the well was removed by gentle flushing with running buffer. The gel assembly was ready for sample loading.

Prior to loading, Laemmli buffer (5X concentrated) supplemented with 500 mM dithiothreitol (DTT; Sigma Aldrich, USA) was mixed with 80 µg of sample total protein and topped up to 20 µl with ddH_2O. The sample-buffer mixes were then subjected to heating at 95 °C for 5 min followed by centrifugation at 1,000 x g, 30 s. The wells were then loaded with the denatured protein samples and dual-color protein ladder (10 to 250 kDa) for protein size reference. Any empty wells were loaded with working loading buffer of the same volume to avoid edge effects in gel running. The running condition was 80 V for 1 h. In running more than two gels, higher voltage or longer running time might be required. When the dye front reached 1 cm above the gel bottom, SDS-PAGE completed and the gel was removed from the gel cassettes.

2.6.4 Protein transfer

The aforesaid gel was washed twice with Tris-buffer saline for 5 min with gentle shaking (Bio-rad, USA) to get rid of residual SDS. The gel holder cassette with nitrocellulose membrane (0.2 µm, Bio-rad, USA), sponge pads and blotting filter papers included was pre-soaked with working transfer buffer containing 20% methanol (Sigma Aldrich, USA). The transfer

buffer was diluted from premixed 10X Tris-glycine buffer (Bio-rad, USA) with ddH_2O. The membrane at 0.2 µm was capable of entrapping proteins of small molecular size (below 15 kDa) and hence used for pMGF translated products with expected sizes below 20 kDa.

The gel was then equilibrated with working transfer buffer and sandwiched in the gel holder cassette for wet transfer. The gel-membrane sandwich arrangement from cathode (-) to anode (+) was: sponge pad→ filter papers → gel → nitrocellulose membrane → filter papers → sponge pad. The arrangement allowed the negatively charged protein mobilized from gel onto the membrane under the applied electric field**.** The cassette, with gel and membrane properly stacked, was loaded into gel tank containing working transfer buffer and transferred at constant voltage (100 V), 4 °C for 30 min. The complete transfer of colored ladder markers indicated successful transfer and the membrane was removed from the cassette and prepared for primary antibody incubation.

2.6.5 Membrane blocking and primary antibody incubation

After transfer, membrane was 5 min washed twice with Tris-buffered saline plus 0.1% Tween 20 (TBST; Tween 20 from Sigma Aldrich, USA) followed by blocking with TBST containing 5% non-fat dry milk (Bio-rad, USA) for 1 h at room temperature. The blocking solution was then refreshed and primary antibody, mouse THE^{TM} His tag monoclonal antibody (0.2 µg ml^{-1}; GenScript, USA) was applied to probe MGF with 6-HIS tag. The membrane was then incubated at 4 °C overnight with constant rolling.

2.6.6 Secondary antibody incubation and detection

After washing three times with TBST, the membrane was then incubated with horseradish peroxidase-conjugated secondary antibodies against mouse immunoglobulin G, or IgG (1:1,000; Cell Signaling Technology, USA) in 5% non-fat dry milk (in TBST) for 45 min at room temperature. With washing step repeated, the membrane was treated with enhanced chemiluminescent substrate and scanned by ChemiDoc imaging system (Bio-rad, USA) to visualize the chemiluminescence emitted. Membrane images of different exposure time were analyzed qualitatively to reveal the expression of MGF peptides with 6-HIS tag translated from pMGF clone compared with empty vector control.

2.7 MUSCLE HISTOLOGY

Histomorphological changes of injured muscle with or without MGF overexpression was evaluated by histological dye staining and immunohistochemical staining. For experiment-dependent image capturing criteria and the analyses, please see the corresponding experimental Chapter 3 and 4.

2.7.1 Muscle cryoblock preparation

Freshly isolated TA for histological evaluation were submerged into O.C.T embedding medium (Leica Biosystems, Germany) contained by curved plastic strip and slightly stretched. The curved plastic strip was made by cutting the bulb of plastic Pasteur pipette into half. The mid-belly was

located above an indicating label on the plastic strip. The assembly was then transferred and snap-frozen in Liq. N-chilled isopentane (Sigma Aldrich, USA). To indicate the mid-belly position on the cryoblock, additional label was added based on the indicating label on the plastic strip. Muscle cryoblocks embedded with O.C.T. medium with appropriate labeling were stored at -80 °C until cryosectioning and staining.

2.7.2 Muscle cryosectioning

The sample blocks from -80 °C were equilibrated for 1 h inside cryostat (Thermo Fisher Scientific, USA) set at -20 °C before cryosectioning. Later the muscle block was immobilized, at up-right position and distal end up, on a metal sample holder with freezing O.C.T. medium. The assembly was loaded on a specimen clamp perpendicular to the cutting edge. High-profile knife was mounted at 3° angle and used for sectioning. The muscle was then trimmed until the mid-belly mark reached.

Using brush technique, cryosections at 7 µm were collected at three longitudinal locations of the muscle mid-belly. Each location was separated from each other for about 200 µm. The collected cryosections were mounted onto warm Superfrost+++ glass slides (Thermo Fisher Scientific, USA). Afterwards, the slides were stored at -80 °C.

2.7.3 Hematoxylin and eosin staining

The cryosections were fixed with ice-cold 4% paraformaldehyde for 10 min and washed twice with PBS. To perform hematoxylin & eosin

(H&E) histological staining, fixed cryosections were firstly incubated in Harris-modified hematoxylin solution (Sigma Aldrich, USA) for 30 s and washed in running tap water for 1 min. The cryosections was then stained with fresh aqueous eosin solution (Sigma Aldrich, USA) for about 5 s and immediately washed with running tap water for 1 min. It was followed by dehydration in increasing %gradient of ethanol (70%, 90% and 100% for 3 times) and xylene (3 times). Stained slides were mounted with DPX mountant (Sigma Aldrich, USA) under glass coverslip. The slide was let dried at room temperature and later ready for microscopic examination.

2.7.4 Immunohistochemistry

For immunohistochemistry (IHC), the staining procedures below have been described in our previous publication (Cheung *et al.*, 2011). Cryosections were fixed with ice-cold 4% paraformaldehyde as described above. The fixed cryosections were permeabilized with 0.2% v/v Triton X-100 (Sigma Aldrich, USA) in PBS for 10 min. After washing three times with PBS, cryosections were covered and blocked with blocking solution (10% v/v normal horse serum in PBS) for 1 h at room temperature. Cryosections were then incubated with primary antibodies (diluted in blocking solution) in humidified chamber overnight at 4 °C.

Prior to secondary antibody incubation, the cryosections were washed three times with PBS to remove unbound primary antibodies. Fluorescent dye-conjugated, species-specific secondary antibodies diluted in blocking solution were added onto the cryosections. Light-shielded incubation was carried out for 45 min at room temperature. After the

washing steps, the cryosections were temporarily mounted with 4',6-diamidino-2-phenylindole (DAPI)-contained antifade mounting medium (Vector Laboratories, USA) covered by glass coverslip. The cryosections were ready for fluorescence microscopy. In addition, for each sample evaluated, no primary control was included by replacing the primary antibody incubation with antibody-free blocking solution while the rest of the procedures remained the same.

2.7.5 Microscopic imaging

All the prepared cryosections were observed under our eclipse 80i microscope (Nikon Instruments, USA) equipped with 4X to 40X objectives and fluorescence filter cubes of UV-2A, B-2A and G-2A (Nikon Instruments, USA). The light sources included halogen lamp and a pre-centered mercury fiber illumination system for epi-fluorescence (Intensilight, Nikon Instruments, USA). SPOT camera and SPOT advanced imaging software were used for image capturing (SPOT imaging, USA).

For bright field imaging, white balance was adjusted using the imaging software. As for fluorescent imaging, the exposure time were adjusted to achieve a reasonable signal-to-noise ratio. The noise or background signal, including non-specific antibody binding and auto-fluorescence, were identified by no primary control staining. Images of the no primary control at the same setting were captured for subsequent analyses. For quantitative measurement, multiple and non-overlapping images at 20X magnification were captured from the whole muscle cryosection. For qualitative comparison, images at 20X or 40X

magnification were captured to illustrate typical observations at region of interest. The criteria were applicable to both bright field and fluorescent imaging.

2.8 FLOW CYTOMETRY

2.8.1 Inflammatory cells isolation

Before starting the isolation procedures, the following reagents were prepared in a sterile tissue culture hood. Plain RPMI 1640 medium (Thermo Fisher Scientific, USA) was added into 12-well tissue culture plate (1 ml/ muscle/ well) and pre-incubated in humidified incubator at 37 °C, 5% CO_2 for pH and temperature equilibration. Moreover, digestion enzymes collagenase type II (Thermo Fisher Scientific, USA) and dispase (Worthington, USA) were freshly prepared at final concentration of 4 mg ml^{-1} and 0.5 mg ml^{-1} digestion medium respectively. The choices of digestion enzyme were reported to successfully and efficiently release inflammatory cells from muscle (Tonkin *et al.*, 2015).

To isolate inflammatory cells for evaluation purposes, injured TA were enzymatically digested to release the infiltrated cells. To begin with, isolated TA was rinsed twice in sterile PBS and subsequently equilibrated in the RPMI 1640 medium. Later the tendon structures were trimmed and the muscle belly was minced inside 1 ml of RPMI 1640 medium containing the freshly prepared digestion enzymes. The minced tissue was incubated in humidified incubator at 37 °C, 5% CO_2 for 30 min. Gentle shaking was applied every 10 min. After digestion, the disrupted tissue was transferred into a 15 ml falcon tube containing 2 volume of ice-cool cell buffer (PBS

supplemented with 1% FBS). To release cells from the disrupted muscle, the suspension was gently triturated by pipetting up-and-down through a 1 ml pipette tip for about 10 times. This was followed by centrifugation (500 x g, 4 °C, 5 min) to remove the enzyme solution. The cell pellet was re-suspended with 1 ml of cell buffer afterward. Undigested tissue and debris was removed by passing the cell suspension through a 40 μm cell strainer and collected into a new 15 ml falcon tube. The cell strainer was extensively washed by cell buffer (1 ml for 4 times) and the strain-through containing isolated cells was centrifuged at 500 x g, 4 ℃ for 5 min. The cell pellet was re-suspended in 500 μl cell buffer and 10 μl was taken for cell counting. Living cell number was counted using hemocytometer with 0.2% Trypan blue solution. Afterwards, the cells were centrifuged (500 x g, 4 ℃, 5 min) and reconstituted into 1 x 10^6 cells per 100 μl. The suspension was now ready for immunostaining.

2.8.2 Immunostaining of isolated cells

The flow cytometric analyses involved immunostaining of cells with specific antibodies conjugated with fluorochromes. Since the Fc-receptor expressing on inflammatory cells can bind non-specifically to the Fc region of primary antibodies, prior blocking of Fc-receptor should be performed to increase the specificity of flow cytometry. The Fc-receptor-mediated antibody binding was blocked by pre-incubation with Mouse FcBlock™ purified anti-mouse CD16/ CD32 antibody (BD Biosciences, USA) at 1 μg per 1 x 10^6 cells per 100 μl, 4 °C for 20 min.

For every flow cytometry experiment, a small portion of Fc-blocked cells (about 1 to 2 x 10^5 cells) was spared as unstained control i.e. no primary antibodies incubation. The remaining cells were then incubated with different fluorochrome-conjugated primary antibodies at 4 °C for 30 min. The panel of antibodies and the working concentration would be described in the corresponding experimental methodology in Chapter 3 and 4. After washing twice with cell buffer, the stained cells were re-suspended into 5 x 10^5 cells per 1 ml of cell buffer for flow cytometric analyses. Before loading for flow cytometry, cells were kept on ice to maintain low cell activity and antibodies stability.

2.8.3 Flow cytometry

Flow cytometry experiments were carried out by BD Accuri™ C6 flow cytometer (BD Biosciences, USA) equipped with red and blue laser. The system allowed scatter (forward and side scattering) and 4-color emission detection (emission from blue laser excitation: fluorochrome channel (FL)1-533/ 30 nm; FL2-585/ 40 nm; FL3> 670 nm and red laser excitation: FL4-675/ 25 nm). Before every experiment, the instrument was properly started up with 0.22 µm filtered ultrapure H_2O until event rate < 2 cell per second. The fluidic setting of cytometer was in "slow" mode with 14 µl min^{-1} flow rate and 10 µm core size. The sheath fluid used was 0.22 µm filtered ultrapure water with bacteriostatic solution (BD Biosciences, USA). Data were collected and analyzed with the Accuri C6 software (BD Biosciences, USA).

Stained samples were strained through 40 μm cell strainer to remove any cell clumps immediately prior to sample loading. At least 10,000 events were measured per sample with threshold detection set at height of forward scattering-height (FSC-H) > 80,000 or else discarded. The discarded signals (FSC-H< 80,000) represented the tiny cellular debris or other small particles within the suspension. The antibodies panel and the respective gating strategy as well as control staining were described in details in Chapter 3 and 4.

Since fluorochrome excitation and emission spectra inevitably overlap, fluorescence detected in a particular detector could be raised from different fluorochromes. It was controlled by proper compensation controls. All the primary antibodies for flow cytometry used in this study were of rat origin. Compensation control for every fluorochrome was hence performed by using anti-rat Igκ/ negative control compensation particles set (BD Biosciences, USA) following the manufacturer manual. Each antibody was independently incubated with the positive and negative beads mix at 4 °C, 30 min. After washing twice with PBS and centrifugation at 500 x g, 4 °C for 5 min, the antibody-bound beads were re-suspended with PBS and loaded onto AccuriC6. Compensation for each detection channels was adjusted using the software compensation control tool. Basically, no adjustment was required for FL4 because only one fluorochrome could emit light from red laser excitation. As for blue laser excited fluorochromes (3 in total), the signal spillover from one fluorochrome to other detectors was empirically adjusted until no spillover observed. The compensation setting was

antibody-specific and hence applied to all experiments of the same antibody panel.

2.9 FLUORESCENCE-ASSISTED CELL SORTING

The fluorescence-assisted cell sorting (FACS) technology was used to harvest cells with particular cell surface marker expression profile. The principles of cell identification including cell staining and gating were basically the same as in flow cytometry. Instead of straining the evaluated cells into waste, FACS allowed cells of interest differentially charged and displaced by electric field into the respective collection tubes.

2.9.1 Cell sorter setting and optimization

The FACS experiment was performed using BD FACSAria III cell sorter (BD Biosciences, USA) controlled by BD FACSDiva software. The sorter was installed with 488 nm and 633 nm laser for excitation. The detection panel allowed forward and side scattering and 5-color detection including emission from 488 nm excitation: FL1-530 nm/ FL2-585 nm/ FL3-695 nm/ FL4-760 nm; and 633 nm excitation: FL5-660 nm. The commercial BD FACSFlow sheath fluid was used (BD Biosciences, USA). To collect sorted cells, a 4-way assembly connected to water-cooling system (4 °C) was installed.

In order to collect specific and pure cells of interest, the conditions of sorter were checked every time before experiment with the use of BD FACS Diva CST beads (BD Biosciences, USA) and the build-in “CST”

program. A performance report was generated and the experiment was only run when all checked items passed. Since sorting was required, the sorter was calibrated before every experiment as well. Particularly, drop delay was the critical factor and should be fine adjusted with the use of BD FACS Accudrop beads (BD Biosciences, USA) and another build-in "auto drop delay" function. Once the drop delay was set appropriately, over 99.5% of positive beads would be charged and sorted.

In addition to the hardware checking mentioned above, cells were isolated from injured muscle, stained with antibodies of interest and run for experimental protocol optimization. The custom settings included the choice of neutral-density filter (2.0), nozzle size (100 μm), photomultiplier tube voltage for each fluorochrome channel (FL1-300; FL2-260; FL3-400; FL4-380; and FL5-460) as well as compensation controls. All these were empirically determined and set in the presence of a trained BD AriaIII cell sorter specialist.

2.9.2 Cell sorting

The cell samples were prepared and immunostained as described in Section 2.8.1-2.8.2. About 30 min before loading, individual sample was treated with viability dye 7-aminoactinomycin D, or 7-AAD (5 μl per 1 x 10^6 cells in 100 μl; BD Biosciences, USA). Then, 40 μm strained cell suspension was loaded into the cell chamber with agitation at 200 rpm and temperature at 4 °C. The flow rate was adjusted to be approximately 1,000 events per second and sorting started immediately. Cells were sorted into collection tubes containing cell buffer maintained at 4 °C. Every 20 min, the

suspension was unloaded and tap-mixed to prevent cell clumping until the sorting completed. The sorted cells were retrieved and centrifuged (500 x g, 4 °C, 5 min) and the cell pellets were washed twice with ice-cool PBS. After washing, supernatant was removed as much as possible and the final cell pellet was snap-frozen in Liq. N and stored at -80 °C until RNA extraction.

2.10 STATISTICAL ANALYSES

Data are presented in mean ± SEM. All statistical tests were performed by SPSS 20 (IBM analytic, USA). Student's t test (unpaired), Pearson's correlation, one-way analysis of variance (ANOVA) with Bonferroni correction and two-way ANOVA were used as appropriate. Significant differences were taken at $P< 0.05$.

CHAPTER 3

The Involvement of IGF-1Ea and MGF in the Inflammatory Response to Muscle Injury

3.1 INTRODUCTION

Inflammatory response plays indispensable roles in mediating muscle regeneration including scavenger, modulation of myogenesis and tissue remodeling (Tidball, 2011, 2017). Inflammatory cells, particularly myeloid cells like neutrophils and macrophages, are the major players of the inflammatory response. Numerous soluble factors including inflammatory cytokines and growth factors derived from myeloid cells are implicated in the inflammatory response of muscle regeneration (Bentzinger *et al.*, 2013; Musarò, 2014; Tidball, 2017). These soluble factors modulate the activities of myeloid cells and satellite cells, including recruitment (Chazaud *et al.*, 2003; Lu *et al.*, 2011*a*, 2011*b*), activation and proliferation (Teixeira *et al.*, 2003; Toumi *et al.*, 2006; Saclier *et al.*, 2013), survival (Chazaud *et al.*, 2003; Sonnet *et al.*, 2006) and differentiation (Mills *et al.*, 2000; Horsley *et al.*, 2003).

IGF-1 is amongst the most characterized soluble factor in skeletal muscle. In injured muscle, IGF-1 is released mainly from infiltrated myeloid cells and in particular, macrophages (Nathan, 1987; Arkins *et al.*, 1993; Smith, 2010; Lu *et al.*, 2011*b*; Tonkin *et al.*, 2015). The IGF-1/ IGF-1R signaling cascade is essential for satellite cell proliferation and myogenic differentiation in muscle regeneration (Semsarian *et al.*, 1999; Barton-Davis *et al.*, 1999; Machida & Booth, 2004; Jacquemin *et al.*, 2004). Indeed, impairment of IGF-1/ IGF-1R signaling leads to poor muscle regeneration (Lefaucheur & Sébille, 1995; Lu *et al.*, 2011*b*; Tonkin *et al.*, 2015). Overexpression of IGF-1 in injured muscle, on the other hand, improves muscle regeneration and facilitates inflammatory resolution (Musarò *et al.*,

2001, 2004; Takahashi *et al.*, 2003; Schertzer *et al.*, 2006; Pelosi *et al.*, 2007). Pelosi *et al.*, (2007) demonstrated that IGF-1 (IGF-1Ea specifically) exerts anti-inflammatory effects in regenerating muscle including reduced myeloid cell infiltration, inhibited expression of inflammatory cytokines and mediators 5 days after CTX-induced muscle injury.

IGF-1 exists in two isoforms, IGF-1Ea and MGF. Although myeloid cells and particularly macrophages are shown to be the predominant source of IGF-1, Tonkin *et al.*, (2015) have not delineated whether IGF-1 isoforms can be derived from early myeloid infiltrate (e.g. neutrophils) in their myeloid-specific IGF-1 knockout model. Since IGF-1 isoforms elevate within 24 h post muscle injury prior to macrophage infiltration (Philippou *et al.*, 2009), it is conceivable that other early infiltrated myeloid cells may contribute to the upregulation.

Moreover, the isoforms differentially regulate muscle transcript expression profile and demonstrate distinct effects on IGF-1 downstream signaling and bioavailability of mature IGF-1 peptide (Barton, 2006*b*; Pfeffer *et al.*, 2009; Barton *et al.*, 2010; Brisson & Barton, 2012; Philippou *et al.*, 2014). Yet, the characterization experiments of IGF-1 isoforms were carried out in non-injured skeletal muscle. Although previous studies suggested the anti-inflammatory roles of IGF-1 in injured muscle (Summan *et al.*, 2006; Pelosi *et al.*, 2007; Dumont & Frenette, 2010; Lu *et al.*, 2011*b*), only IGF-1Ea is evident to possess the anti-inflammatory effects (Pelosi *et al.*, 2007). Whether MGF modulates muscle inflammatory response in injured muscle is unclear.

3.1.1. Hypothesis and Aims of the study

The first aim of this study was to examine the expression of IGF-1 isoforms in myeloid cell infiltration after muscle injury. Before determining the contribution of IGF-1 isoforms from macrophages, Tonkin *et al.*, (2015) first demonstrated that IGF-1 upregulation temporally coincides with macrophage infiltration in CTX-injured muscle. It was also the first evidence that both IGF-1 isoforms are associated with muscle inflammatory response. However, there is potential variability in inflammatory response amongst CTX-induced muscle injury protocols (Musarò *et al.*, 2001; Pelosi *et al.*, 2007; Wang *et al.*, 2014; Tonkin *et al.*, 2015; Hardy *et al.*, 2016). We therefore decided to confirm the association of IGF-1 isoforms with muscle inflammatory response and myeloid cell infiltration in our CTX-induced muscle injury model, before investigating the expression of IGF-1 isoforms in infiltrated myeloid cells.

Although Tonkin *et al.*, (2015) attributed macrophages as the source of IGF-1, they could not rule out the potential contribution from other myeloid cells (including neutrophils and monocytes), which infiltrate prior to macrophages, due to the use of myeloid cell-specific IGF-1 knockout model. The expression of IGF-1 isoforms from infiltrated myeloid cells in muscle regeneration remains unclear. We thus hypothesize that (i) IGF-1Ea and MGF associate with inflammatory response during muscle regeneration; and (ii) IGF-1Ea and MGF are expressed by the infiltrated myeloid cells. The experimental aims of Chapter 3 were:

1. To confirm the association of IGF-1 isoforms, IGF-1Ea and MGF expression with muscle inflammatory response; and

2. To examine the expression of IGF-1Ea and MGF in infiltrated myeloid cells including neutrophils and macrophages in muscle injury

3.2 METHODOLOGY

Details of the methods including CTX-induced muscle injury, muscle histology, transcript expression profile and cell sorting have been described in Chapter 2.

3.2.1 Experimental design

To confirm the association of IGF-1Ea and MGF with muscle inflammatory response (experimental aim 1), we induced TA injury with CTX injection. The muscles were harvested at day 2, day 4 and day 7 post injection. These timepoints were designed to represent the distinct phases in CTX-induced muscle injury: the inflammatory (day 2), the early resolution (day 4) and the late resolution (day 7) phases.

To examine the expression of IGF-1Ea and MGF in infiltrated myeloid cells (experimental aim 2), CTX-injured muscles were enzymatically digested to dissociate infiltrated myeloid cells from the muscles at the timepoint when IGF-1 isoforms were mostly upregulated for transcript expression. The harvest timepoint was dependent on the expression profile determined in aim 1 experiments.

3.2.2 Skeletal muscle injury model

One TA was subjected to CTX injection whereas the contralateral TA was injected with saline as control. The muscles were collected at day 2, day 4 and day 7 post injection. The CTX working solution (10 μM) or sterile normal saline (as control) was intramuscularly injected into the mid-belly of TA (1 μl g^{-1} body mass) using insulin syringe (30 gauge; Terumo, USA). Untreated muscle was served as baseline control (day 0) and the reference for comparison.

3.2.3 Expression of IGF-1 isoforms and inflammatory cytokines in CTX-injured muscle

Total RNA from muscle samples (n= 4 to 5/ treatment/ timepoint) was purified for reverse transcription to yield cDNA. The cDNA samples were subjected to probe-based RT-qPCR assessment. The genes of interests included IGF-1 isoforms (i.e. IGF-1Ea and MGF) and inflammatory cytokines (i.e. TNF-α, IL-6 and IL-10). These inflammatory cytokines typically involve in the mediation of muscle inflammation (see Table 1.1). The respective Taqman assays were purchased from Thermo Fisher Scientific, USA and summarized in Table 3.1. The housekeeping gene was GAPDH. Relative expression, $2^{-\Delta\Delta Ct}$ analysis method was used to compare the expression between groups of sample. In addition, we tested the correlation of IGF-1 isoforms with inflammatory cytokines to evaluate the association of IGF-1 expression with inflammatory response.

Genes of interest	Assay ID	Gene ID	Assay designs
GAPDH	4352932E	NM_008084.2	*Exon spanning
IGF-1Ea	Mm00710307_m1	AY878192	
MGF	Custom synthesized	AY878193	
TNF-α	Mm00443258_m1	NM_013693	
IL-6	Mm00446190_m1	NM_031168	
IL-10	Mm01288386_m1	NM_010548	

Table 3.1 Taqman assays involved in profiling IGF-1 and inflammatory cytokine expression in injured muscle. All Taqman assays were purchased from Thermo Fisher Scientific, USA. *Exon spanning means that primer pairs span an exon-exon junction. Thus intron-containing genomic DNA would not be detected.

3.2.4 Histology of the CTX-injured muscle

CTX-injured muscles were collected for cryosectioning and H&E staining. Injured muscles demonstrated histological characteristics (Figure 3.1) including: (1) the presence of necrotic myofibers; (2) inflammatory cell-infiltrated myofibers; (3) inflammatory cell-infiltrated interstitial spaces; (4) regenerating myofibers; and (5) regenerated myofibers. Necrotic myofibers were pale pink in color compared with non-injured myofibers. Inflammatory cell infiltration was characterized with numerous mononuclear cells found within damaged myofibers and interstitial spaces. Presence of necrotic myofibers and infiltration of mononuclear cells indicated muscle inflammation (i.e. histological characteristic 1 to 3). Regenerating myofibers were small, basophilic and centrally nucleated. In addition, reduction of mononuclear cell infiltration indicated inflammatory resolution. These suggested regeneration and inflammatory resolution (i.e. histological characteristic 4). Later, regenerating myofibers underwent hypertrophy and became similar to non-injured myofibers in size. Mononuclear cells within interstitial space were scarce. It was the end stage of muscle regeneration (i.e. histological characteristic 5). These were the criteria of evaluating muscle regeneration from CTX-induced injury.

3.2.5 Infiltrated mononuclear cells in CTX-injured muscle

To examine the identity of infiltrated mononuclear cells histologically, cryosections of injured muscle (n= 4; same muscle samples used in histology) were immunostained. Rat anti-mouse monoclonal primary

antibodies against myeloid cell surface marker CD11b (1:100; BD Biosciences, USA) and macrophage surface marker F4/80 (1:100; Bio-rad, USA) were used for mapping cells of myeloid origin and macrophage phenotype respectively (Tonkin *et al.*, 2015). Anti-rat immunoglobulin antibody conjugated with Alexa Fluor (AF) 488 (1:300; Thermo Fisher Scientifics, USA) was used as the secondary antibody. The injured loci were identified by the intensive DAPI+ staining indicating infiltration of mononuclear cells. Images at 20X and 40X magnification of the injured loci for DAPI+ and CD11b+ (or F4/80+) were captured separately. Both CD11b and F4/80 are cell surface markers and thus not overlapped with DAPI signal after superimposing the images of CD11b/ DAPI and F4/80/ DAPI. Myeloid cells were DAPI+ (blue) surrounded by CD11b+ (green) staining. Macrophages, similarly, were DAPI+ (blue) surrounded by F4/80+ (green) staining.

Figure 3.1 Histological characteristics of CTX-injured muscle. The indicated numbers referred to the histological characteristics described in Section 3.2.4. (1) a pale and pink necrotic myofiber; (2) two myofibers infiltrated by mononuclear cells; (3) mononuclear cell infiltrated interstitial space; (4) two small, rounded and centrally nucleated myofibers; and (5) regenerated myofibers with central nucleation which was similar to adjacent non-centrally nucleated myofibers in size. All the images were captured at 40X magnification with scale bar= 50 μm.

(*Overleaf*)

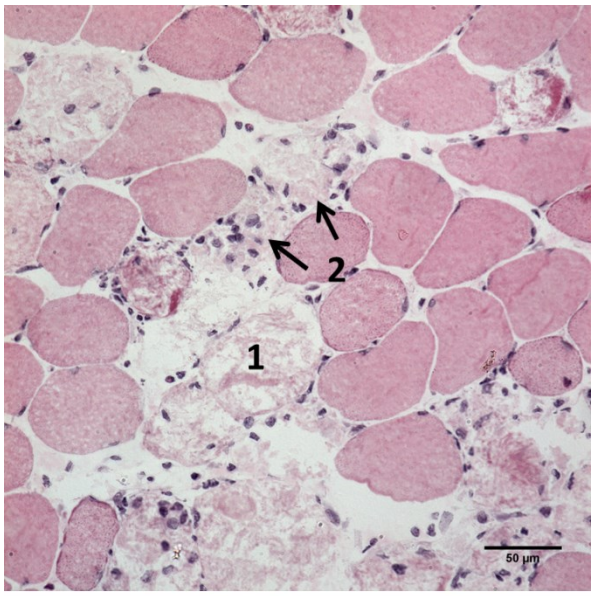
2
1
50 µm

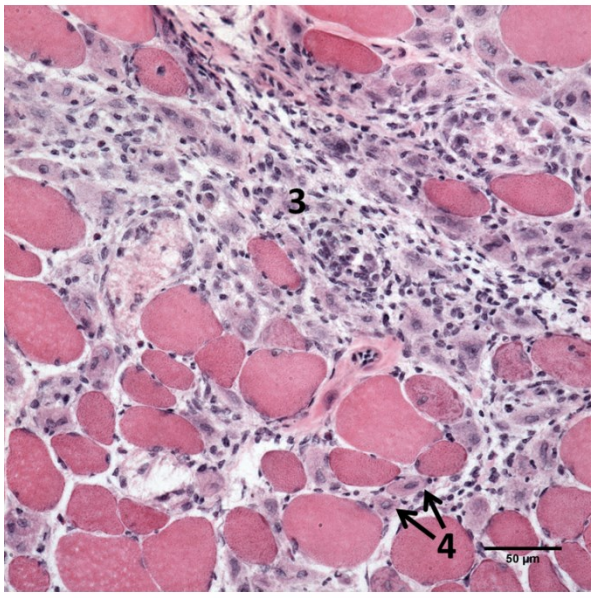
3
4
50 µm

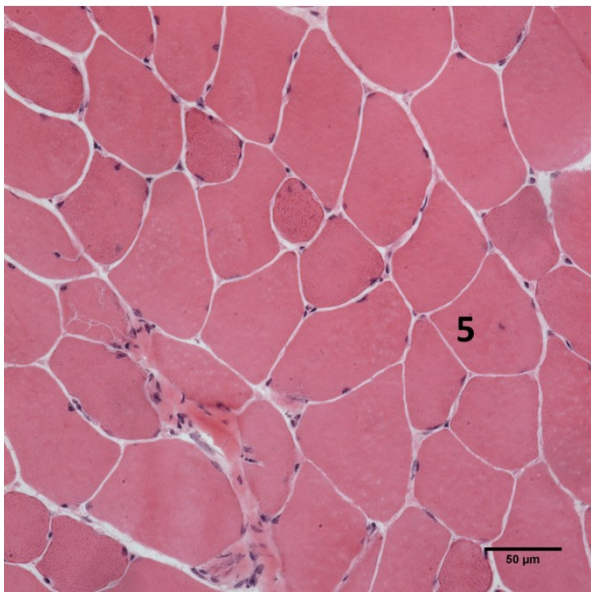
5
50 µm

3.2.6 Myeloid cell isolation and collection

Inflammatory cells were isolated from CTX-injured muscle 36 h post injury. Although day 2 (or 48 h) was the timepoint that IGF-1 isoforms reached its peak level (referred to Section 3.3.1), it might not allow simultaneous examination of IGF-1 isoforms in different types of myeloid cells. During the inflammatory phase, neutrophils peak within 24 h post injury while macrophages only dominate the tissue afterward (Tidball *et al.*, 2014; Sciorati *et al.*, 2016; Tidball, 2017). We thus selected 36 h post CTX injury, still within the inflammatory phase, which should provide sufficient population of neutrophils and macrophages for RT-qPCR assessment.

To harvest sufficient inflammatory cells for FACS analysis, TA, gastrocnemius and rectus femoris muscles for both legs of the same animal were CTX-injured. Regarding CTX injection into muscles other than TA, both heads of gastrocnemius muscles were injected twice with CTX working solution (1 μl g^{-1} body mass) while the rectus femoris was injected twice with 2 times the volume of the CTX working solution (2 μl g^{-1} body mass). The two injections were performed as followed: one injection at one-fourth from proximal end and another at one-fourth from the distal end.

The antibodies used for FACS were shown in Table 3.2. The two markers chosen to identify infiltrated myeloid cells were CD11b and Ly6C (lymphocyte antigen 6 complex, locus C). CD11b is a well-recognized cell surface marker for myeloid cells whereas Ly6C is present on infiltrating myeloid cells. The Ly6G and F4/80 are specific markers for neutrophils and macrophages respectively (Côté *et al.*, 2013; Tonkin *et al.*, 2015). After staining, the cell suspensions were gated to collect the desired cell

populations (Figure 3.2). Cells were first gated as P1 by size using forward scattering-area (FSC-A) and by granularity using side scattering-area (SSC-A). Single cells from P1 were further gated from spot blot of FSC-H against FSC-A. Viable cells were negative for 7AAD dye (7AAD−). Viable cells were first gated by the expression of Ly6G. The Ly6G+ cells double positive of Ly6C and CD11b (and negative for F4/80) were defined as neutrophils (7AAD−/ Ly6G+/ CD11b+/ Ly6C+/ F4/80−). As for the Ly6G− population, positivity of macrophage marker F4/80 determined the macrophages (7AAD−/ Ly6G−/ CD11b+/ Ly6C+/ F4/80+) whereas negativity for other myeloid cells (7AAD−/ Ly6G−/ CD11b+/ Ly6C+/ F4/80−). Other myeloid cells that collected at 36 h post injury are presumably monocytes (Shi & Pamer, 2011; Wang *et al.*, 2014) and eosinophils (Heredia *et al.*, 2013; Yu *et al.*, 2016). Distinguishing monocytes and eosinophils from other myeloid cells requires additional markers in the FACS antibody panel which are macrophage colony-stimulating factor 1 receptor (CD115) and sialic acid-binding Ig-like lectin (SiglecF), respectively (Heredia *et al.*, 2013; Yang *et al.*, 2014). Inclusion of additional markers was however technically unavailable for this study.

Based on the illustrated gating, viable neutrophils (7AAD−/ Ly6G+/ CD11b+/ Ly6C+/ F4/80−; n= 6), macrophages (7AAD−/ Ly6G−/ CD11b+/ Ly6C+/ F4/80+; n= 4) and other myeloid cells (7AAD−/ Ly6G−/ CD11b+/ Ly6C+/ F4/80−; n= 6) were collected for subsequent RNA extraction.

Antibody	Manufacturer	Clone (Isotype)	Working concentration (per 10^6 cells in 100 µl)	Fluorochromes (Sorter detection channel)
CD11b	BD Biosciences	M1/ 70 (Rat IgG2b, κ)	0.5 µg	BB515 (FL1)
Ly6C	Biolegend	HK1.4 (Rat IgG2c, κ)	1 µg	PE (FL2)
***7AAD**	BD Biosciences	N/ A	0.25 µg	N/ A (FL3)
Ly6G	Biolegend	1A8 (Rat IgG2a, κ)	1 µg	PE-Cy7 (FL4)
F4/80	BD Biosciences	T45-2342 (Rat IgG2a, κ)	2 µg	AF647 (FL5)

Table 3.2 Antibody panel used for identification of inflammatory cells from injured muscle. *7AAD is a viability dye included in the cell suspension buffer for living cell gating. Fluorochromes: BB515= BD Horizon BB515; PE= Phycoerythrin; PE-Cy7= Phycoerythrin-cyanine 7 tandem dye; and AF647= Alexa Fluor 647.

Figure 3.2 Gating strategy for FACS of inflammatory cells. P1 were gated from scatterplot of FSC-A against SSC-A. Single cells from P1 were further gated in spot blot of FSC-H against FSC-A. The single cells without 7AAD were regarded as viable cell fraction (7AAD−). It was further gated based on the expression of Ly6G, which is a specific neutrophil surface marker. Cells triple positive for Ly6G, Ly6C and CD11b were defined as neutrophils (7AAD−/ Ly6G+/ CD11b+/ Ly6C+/ F4/80−). As for Ly6G− population, double positivity in Ly6C and CD11b were further gated into macrophages (7AAD−/ Ly6G−/ CD11b+/ Ly6C+/ F4/80+) and other myeloid cells (7AAD−/ Ly6G−/ CD11b+/ Ly6C+/ F4/80−) based on the expression of specific macrophage marker F4/80. The final cell types that were FACS-collected and phenotypes were summarized at the bottom-left corner of the same figure.

(*Overleaf*)

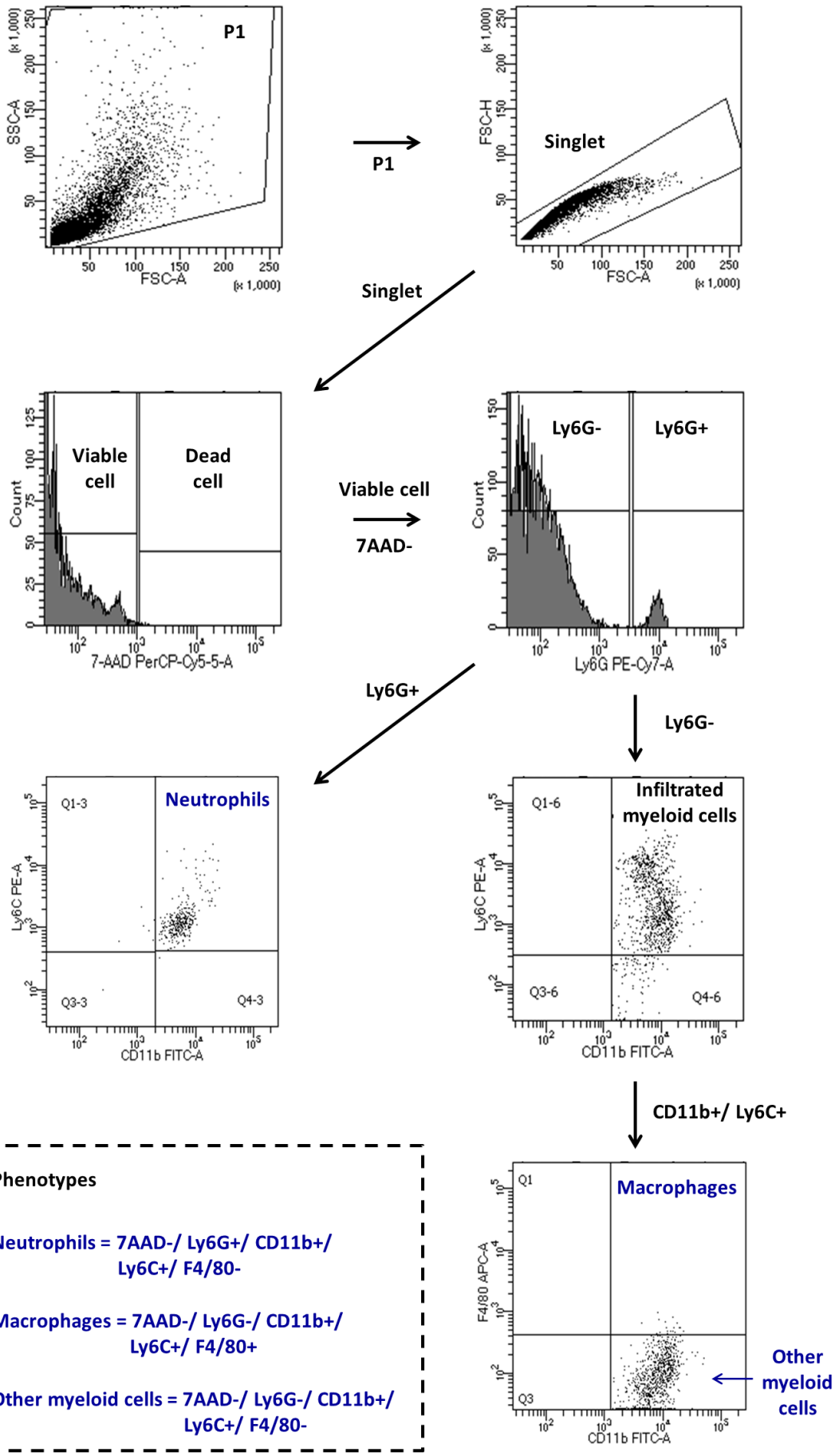
P1
SSC-A
FSC-A
(x 1,000)
P1
Singlet
FSC-H
FSC-A
(x 1,000)
Singlet
Viable cell
Dead cell
Count
7-AAD PerCP-Cy5-5-A
Viable cell
7AAD-
Ly6G-
Ly6G+
Count
Ly6G PE-Cy7-A
Ly6G+
Ly6G-
Q1-3
Neutrophils
Q3-3
Q4-3
Ly6C PE-A
CD11b FITC-A
Q1-6
Infiltrated myeloid cells
Q3-6
Q4-6
Ly6C PE-A
CD11b FITC-A
CD11b+/ Ly6C+
Q1
Macrophages
Q3
F4/80 APC-A
CD11b FITC-A
Other myeloid cells
Phenotypes
Neutrophils = 7AAD-/ Ly6G+/ CD11b+/ Ly6C+/ F4/80-
Macrophages = 7AAD-/ Ly6G-/ CD11b+/ Ly6C+/ F4/80+
Other myeloid cells = 7AAD-/ Ly6G-/ CD11b+/ Ly6C+/ F4/80-

3.2.7 Expression profile of FACS-collected cells

Purified RNA from each cell fraction was reversely transcribed and the cDNA samples were evaluated by RT-qPCR. Geometric means of GAPDH and 18S rRNA Ct values were used for normalization. The Taqman assays used included IGF-1 isoforms, TNF-α, IL-10 and CCL2 (gene ID: NM_011333 and assay ID: Mm00441242_m1; Thermo Fisher Scientific, USA). CCL2 is a well-recognized chemotactic factor of macrophages in muscle regeneration (Lu *et al.*, 2011*a*, 2011*b*).

3.2.8 Statistics

Quantitative data were presented in mean ± SEM. All statistical tests were performed by SPSS 20 (IBM analytic, USA). Significance level was set at $P< 0.05$.

The transcript expression profiles of CTX-injured muscle were analyzed by one-way ANOVA with post-hoc Bonferroni correction. The same statistical analysis was also used to compare the expression level of IGF-1 isoforms and inflammatory cytokines amongst FACS-collected cells from CTX-injured muscle.

We used Pearson correlation test to examine the strength of association between IGF-1 isoforms and inflammatory markers. The dCT values of each interested gene from CTX-injured muscle were analyzed.

3.3 RESULTS

All the timepoints described (i.e. day 2, day 4 and day 7) in this Chapter 3 referred to the days post CTX injury unless specified. The term IGF-1 isoforms referred to murine IGF-1Ea and MGF.

3.3.1 Positive correlation of IGF-1 isoforms and inflammatory cytokines in CTX-injured muscle

Macrophages express IGF-1 isoforms (Nathan, 1987; Arkins *et al.*, 1993; Smith, 2010). Macrophage-derived IGF-1 mediates muscle inflammatory response (Pelosi *et al.*, 2007; Tidball, 2017). However, the contribution of IGF-1 isoforms from different infiltrated inflammatory cells to muscle regeneration was yet to be defined. To confirm the association of IGF-1 isoforms expression with inflammatory response in muscle injury, we examined the transcript expression of IGF-1 isoforms as well as the inflammatory cytokines (i.e. TNF-α, IL-6 and IL-10) (n= 4 to 5/ treatment/ timepoint). Of note, the expression level of evaluated genes in saline control was essentially the same as the baseline control and unchanged amongst timepoints ($P > 0.05$). Any change in IGF-1 isoforms and inflammatory cytokines caused by injection of saline was thus negligible.

Our results demonstrated that the temporal profiles of IGF-1 isoforms and inflammatory cytokines were similar (Figure 3.3). Day 2 was the earliest peak of expression amongst all genes. It was significantly higher than baseline ($P < 0.01$ for both IGF-1 isoforms and $P < 0.001$ for all inflammatory cytokines). However, only the increased expression of

IGF-1Ea ($P< 0.01$), MGF ($P< 0.05$) and IL-10 ($P< 0.001$) persisted to day 4. Comparably, the upregulation of TNF-α and IL-6 appeared more transient, with expression significantly reduced from day 2 to day 4 (both genes, $P< 0.05$). Moreover, the expression level was not differed from baseline at day 4 ($P> 0.05$). None of the evaluated gene expression displayed significant difference from baseline at day 7.

We detected significant positive correlation, between IGF-1 isoforms (Figure 3.4), IGF-1Ea with all inflammatory cytokines (Figure 3.5) and MGF with all inflammatory cytokines (Figure 3.6). The respective Pearson coefficient (R-value) and significance (P-value) for each correlation were indicated in the corresponding figures. Thus, the detected positive correlation suggested simultaneous changes of IGF-1 isoforms with inflammatory cytokines in muscle regeneration.

Figure 3.3 IGF-1 and inflammatory cytokine transcript expression profiles of CTX-injured muscle. (A) IGF-1Ea; (B) MGF; (C) TNF-α; (D) IL-6; and (E) IL-10 (n= 4 to 5/ treatment/ timepoint). Expression level was relative to the baseline level without CTX-induced injury (mean ± SEM). One-way ANOVA with post-hoc Bonferroni correction, significant differences from baseline: *P< 0.05, **P< 0.01 and ***P< 0.001; day 2: ^P< 0.05, ^^P< 0.01, ^^^P< 0.001; day 4: #P< 0.05, ##P< 0.01. Abbreviation: RQ= relative quantification.

(*Overleaf*)

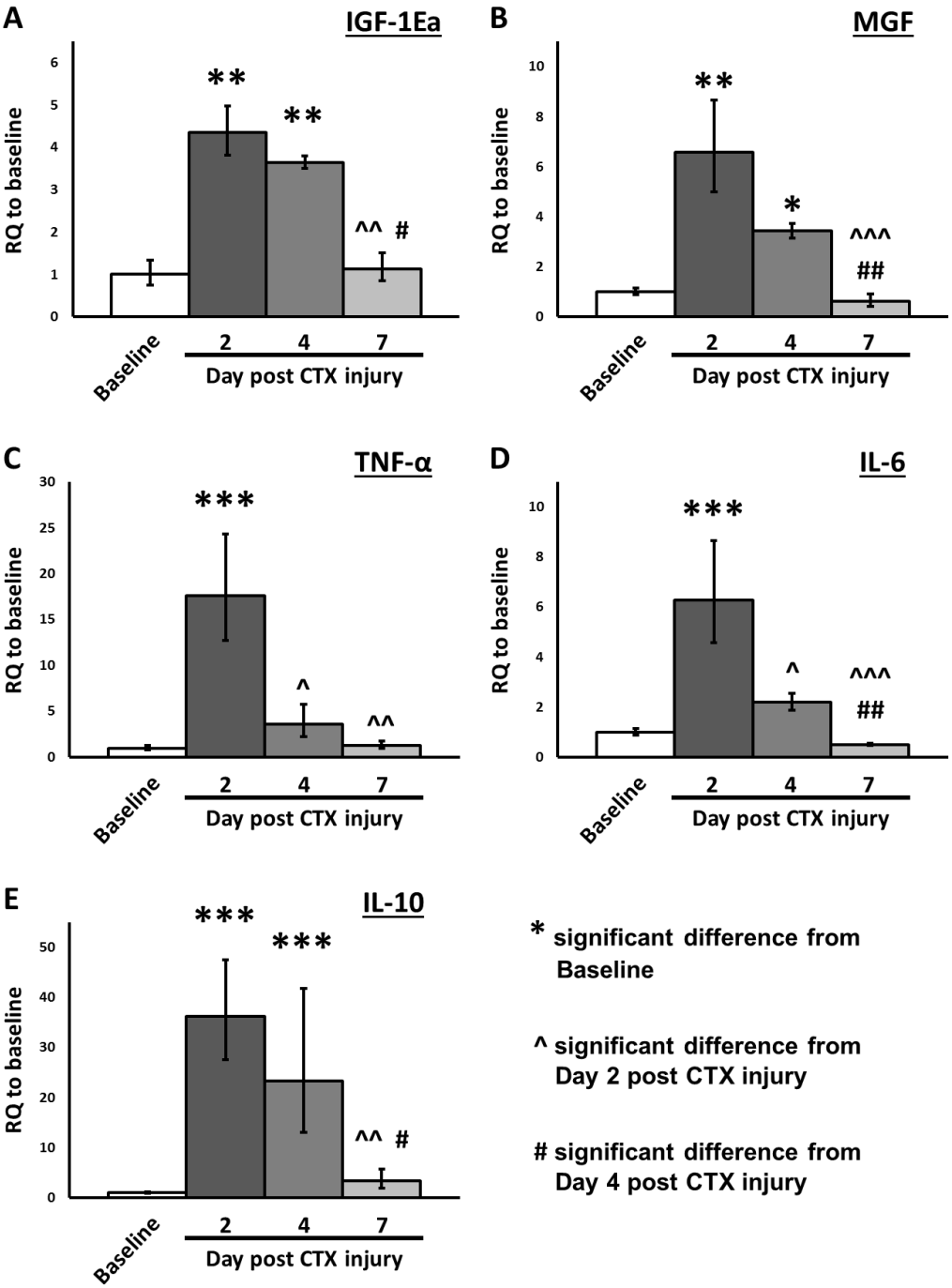
A
IGF-1Ea
RQ to baseline
**
**
^^ #
Baseline
2
4
7
Day post CTX injury
B
MGF
RQ to baseline
**
*
^^^
##
Baseline
2
4
7
Day post CTX injury
C
TNF-α
RQ to baseline
***
^
^^
Baseline
2
4
7
Day post CTX injury
D
IL-6
RQ to baseline
***
^
^^^
##
Baseline
2
4
7
Day post CTX injury
E
IL-10
RQ to baseline
***
***
^^ #
Baseline
2
4
7
Day post CTX injury
* significant difference from Baseline
^ significant difference from Day 2 post CTX injury
# significant difference from Day 4 post CTX injury

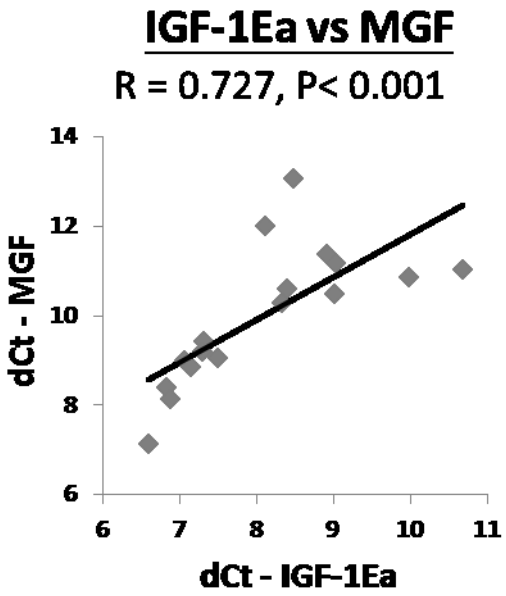

Figure 3.4 Scatter-plot of IGF-1 isoform expression level in CTX-injured muscle. Pearson coefficient (R-value) and significance (P-value) was shown above the linear best-fit trend line. Abbreviation: dCt= delta cycle of threshold.

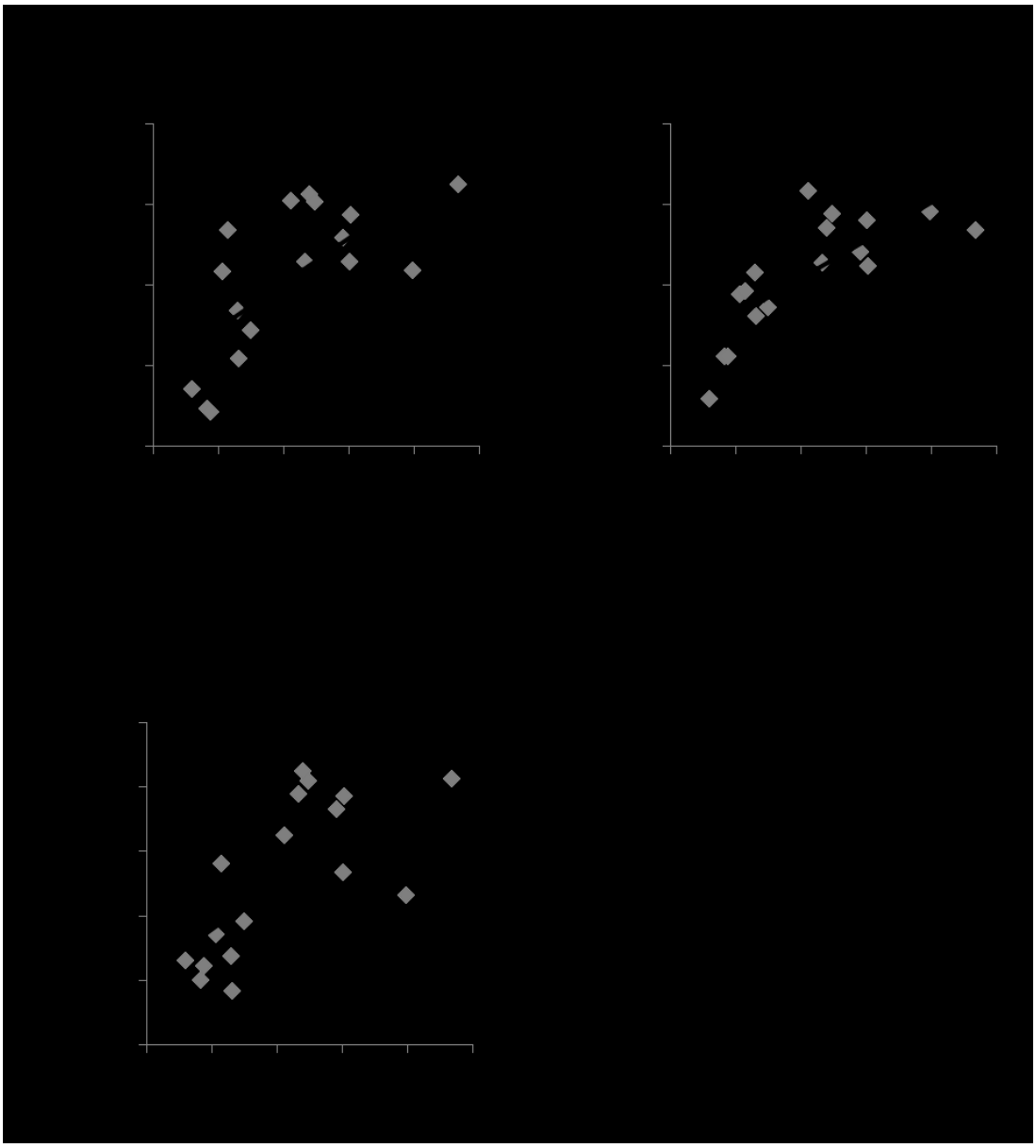

Figure 3.5 Scatter-plots of IGF-1Ea and inflammatory cytokine expression in CTX-injured muscle. (A) IGF-1Ea vs TNF-α; (B) IGF-1Ea vs IL-6; and (C) IGF-1Ea vs IL-10. The R-values and P-values were shown above the linear best-fit trend lines. Abbreviation: dCt= delta cycle of threshold.

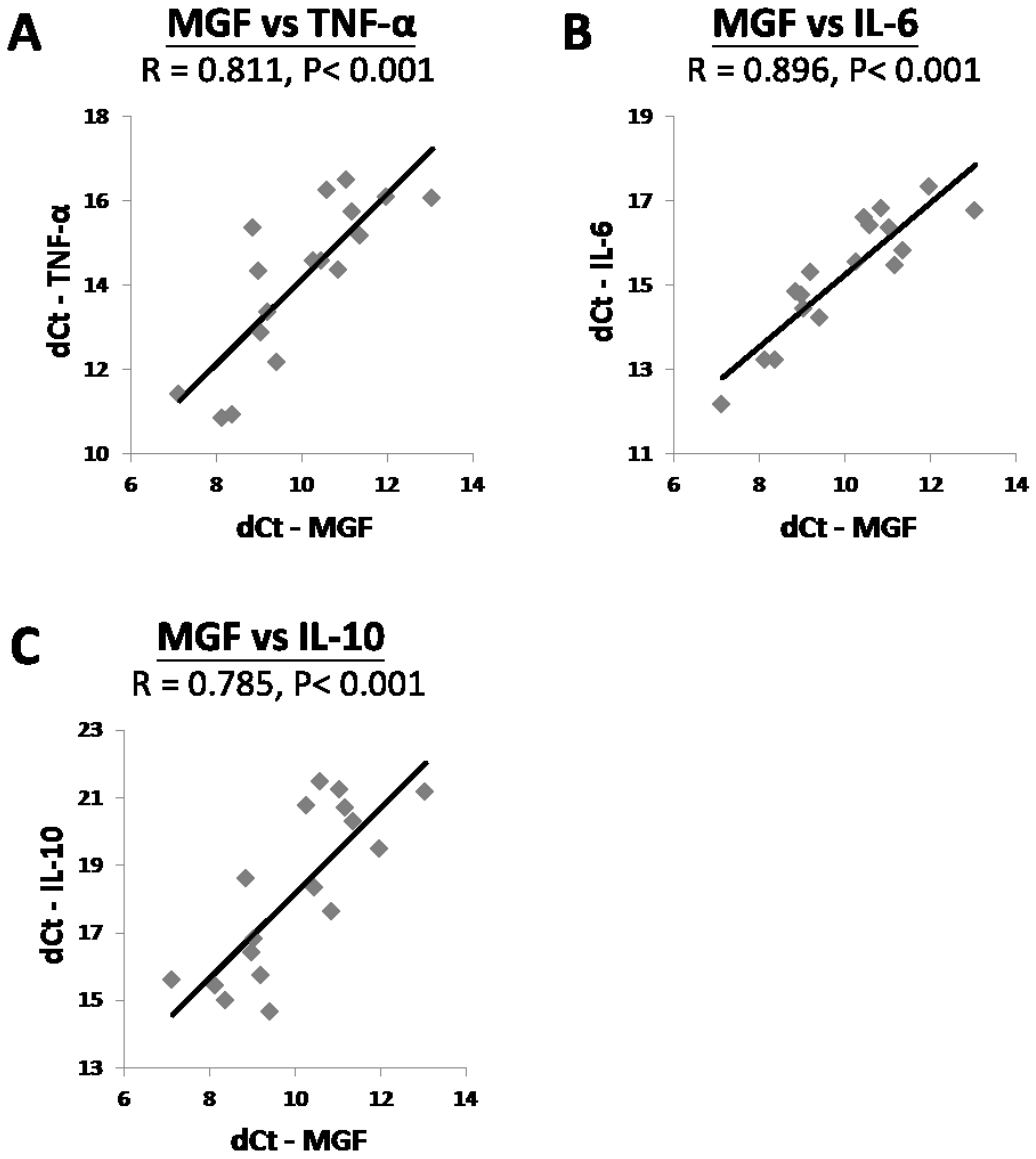

Figure 3.6 Scatter-plots of MGF and inflammatory cytokine expression in CTX-injured muscle. (A) MGF vs TNF-α; (B) MGF vs IL-6; and (C) MGF vs IL-10. The R-values and P-values were shown above the linear best-fit trend lines. Abbreviation: dCt= delta cycle of threshold.

3.3.2 Mononuclear cell infiltration coincided with IGF-1 upregulation

Inflammatory cytokines and IGF-1 isoforms expression were positively correlated. We next examined the association of IGF-1 upregulation with mononuclear cell infiltration. H&E staining of injured muscle cryosection was performed at day 2, day 4 and day 7. The representative cross-sectional images of injured muscle were illustrated in Figure 3.7 (n= 2/ treatment/ timepoint). The saline injection control did not demonstrate any tissue lesion and mononuclear cell infiltration at all and was histologically similar to untreated control.

At day 2, pale and swollen necrotic myofibers were observed in the CTX-injured muscle. Some of the myofibers as well as the interstitial space were massively infiltrated with mononuclear cells. The presence of mononuclear cell infiltration indicated the inflammatory phase.

At day 4, all myofibers in CTX-injured muscle were consistently stained with eosin. Pale or swollen myofibers were no longer observable. Mononuclear cells infiltrated into myofibers were absent, indicating the clearance of necrotic tissue. Nevertheless, mononuclear cells within interstitial spaces persisted particularly around the small and rounded centrally nucleated myofibers, representing the early resolution phase.

At day 7, interstitial infiltration was barely seen suggesting late or complete inflammatory resolution. Furthermore, centrally nucleated myofibers were larger than those observed at day 4 that suggested muscle hypertrophy. It indicated the end stage of muscle regeneration.

To demonstrate the concurrent IGF-1 expression and mononuclear cell infiltration, the histological images and the temporal profile of MGF in CTX-injured muscle was illustrated in parallel (Figure 3.8). Mononuclear cells infiltration observed at day 2 and day 4 coincided with the upregulation of inflammatory cytokines as well as IGF-1 expression.

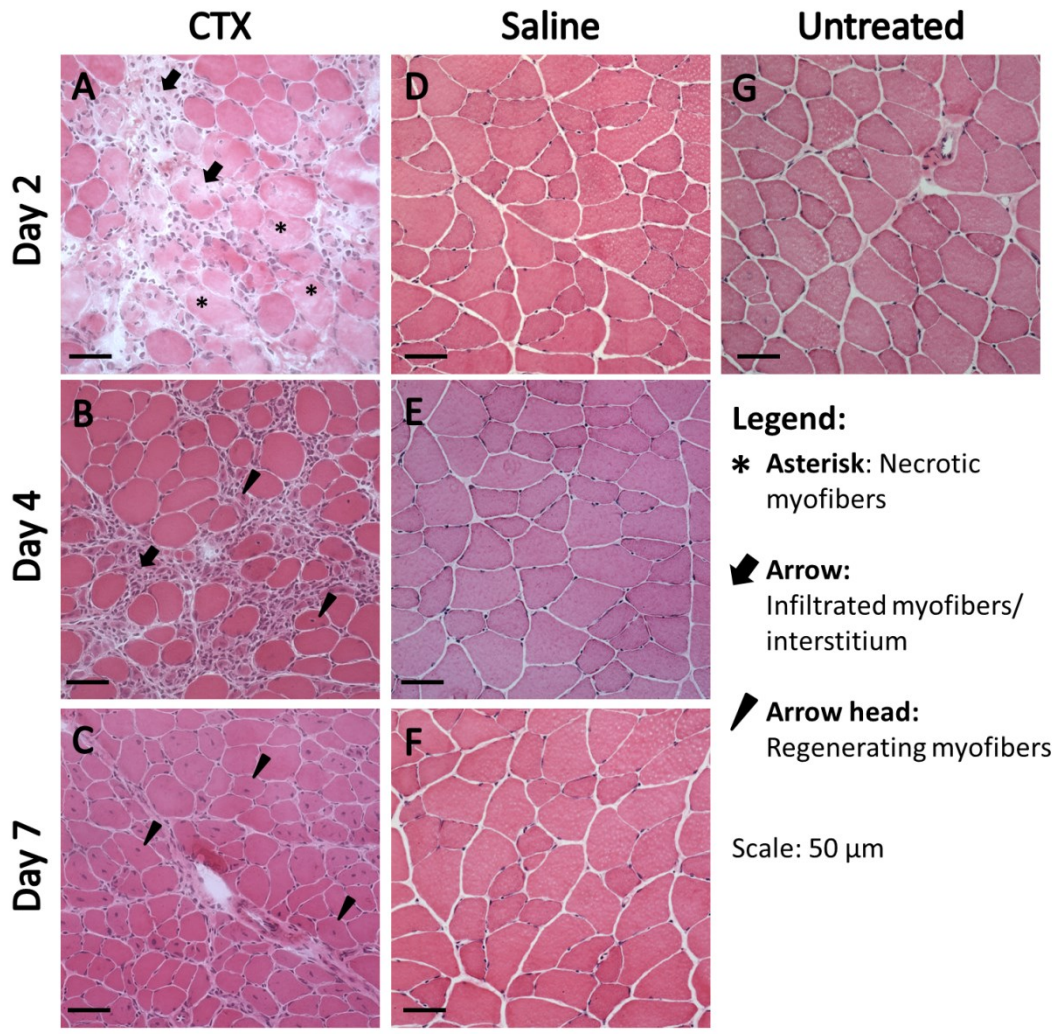

Figure 3.7 H&E staining of skeletal muscle. (A-C) CTX-injured; (D-F) saline injected and (G) untreated muscle (n= 2/ treatment/ timepoint). The rows from top-to-bottom were images of day 2 (A and D), day 4 (B and E) and day 7 (C and F) from the corresponding treatment. All the images were captured at 40X magnification with scale bar= 50 µm. Asterisks indicated the necrotic myofibers. Arrows indicated the infiltrated myofibers and interstitium. Arrow heads marked the regenerating myofibers.

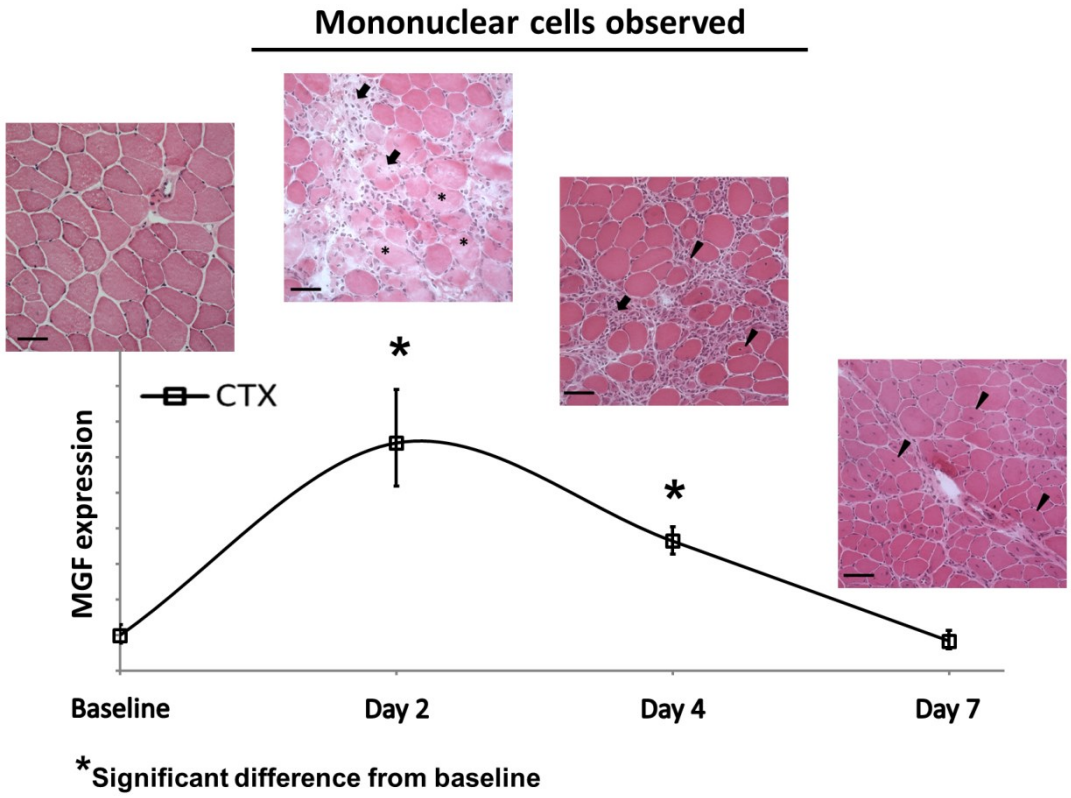

Figure 3.8 Mononuclear cell infiltration coincided with IGF-1 upregulation. The curve indicated IGF-1 expression. Of note, it was plotted using MGF data. Similar curve was achievable from IGF-1Ea and thus presented one to avoid confusion. Asterisks indicated significant upregulation. The H&E images above the curve were muscle histology at corresponding timepoints. Notably, the presence of mononuclear cells at day 2 and day 4 accompanied with significant upregulation of IGF-1 transcripts.

3.3.3 Myeloid cell and macrophage infiltration coincided with IGF-1 upregulation

Myeloid cells, including macrophages, infiltrate to injured muscle within 2 days from onset of injury (Tidball & Villalta, 2010; Novak *et al.*, 2014; Schiaffino *et al.*, 2017). Mononuclear cell infiltration from H&E staining likely represents these inflammatory progenies. We thus investigated the identity of mononuclear cells by immunostaining CD11b (myeloid cells) and F4/80 (macrophages) in muscle cryosections from day 2 (Figure 3.9; n= 4/ treatment). It was the timepoint that expression of all evaluated genes peaked and histologically mononuclear cell infiltrate dominated the injured site.

Both markers exhibited membrane staining restricted to the plasma membrane of mononuclear cells but not at the sarcolemma of peripherally nucleated normal myofibers. Numerous blue DAPI signal representing cell nuclei were found at interstitial spaces or inside myofibers. It indicated the injured site with prominent mononuclear infiltrate. These cells were mostly immunopositive for CD11b or F4/80. The mononuclear infiltrate at day 2 thus contained predominantly myeloid cells and macrophages. It might imply the infiltrated myeloid cells and macrophages contributed to the peak expression of inflammatory cytokines and IGF-1 isoforms.

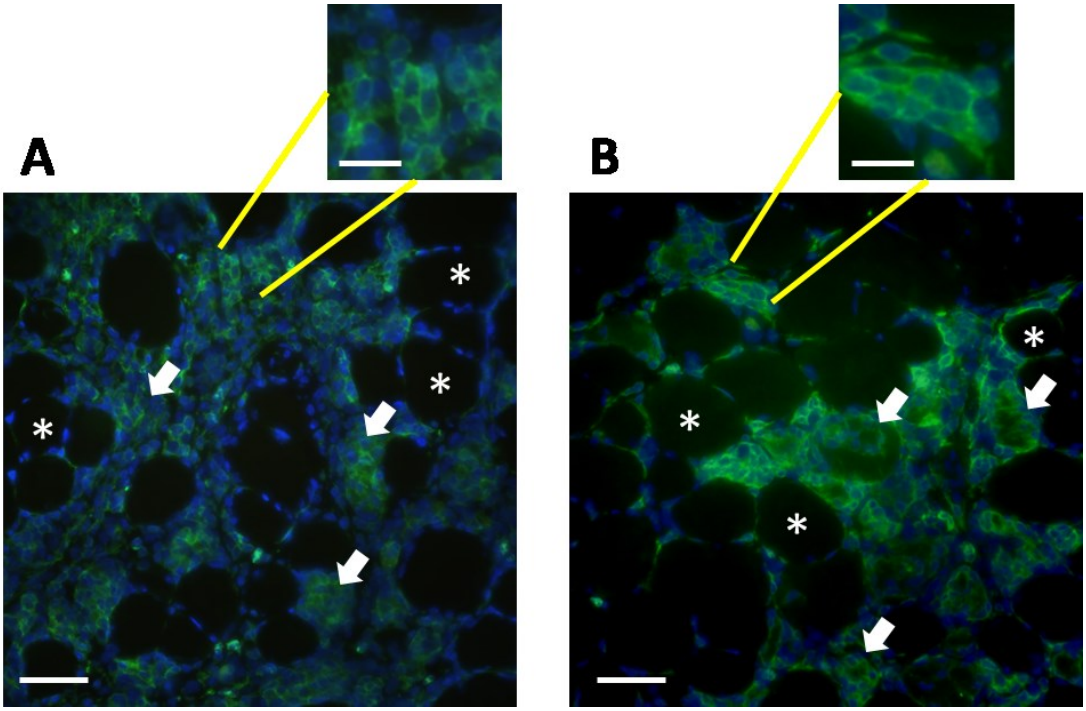

Figure 3.9 Representative IHC images of muscle with infiltrated myeloid cells and macrophages. (A) CD11b and (B) F4/80 staining of CTX-injured muscle at day 2 (n= 4). Both images were captured at 40X magnification with scale bar= 50 μm. The staining of CD11b (and F4/80) was green whereas DAPI signal was blue. The enlarged portions indicated membrane staining of both antigens (scale bar= 20 μm). The white arrows indicated the infiltrated myofibers and interstitial area. The asterisks indicated the non-infiltrated myofibers with peripheral nuclei and unstained cytoplasm.

3.3.4 Higher IGF-1 expression in macrophages than other infiltrated myeloid progenies

We demonstrated the association between IGF-1 expression and inflammatory response at both transcript and histological level. This was in agreement with previous findings that infiltrated myeloid cells or macrophages are the predominant sources of IGF-1 transcripts at inflammatory phase (Lu *et al.*, 2011*b*; Tonkin *et al.*, 2015). To confirm the expression of IGF-1 isoforms in macrophages, we sorted macrophages from CTX-injured muscle. In addition, previous studies did not rule out the contribution of IGF-1 isoforms from other infiltrated myeloid cells (Tonkin *et al.*, 2015). For example, neutrophils and monocytes infiltrated into the injured muscles, prior to macrophages, could also contribute to the IGF-1 expression. Expression of IGF-1 isoforms and inflammatory cytokines was assessed in all collected cell fractions i.e. macrophages, neutrophils and other myeloid cells (Figure 3.10).

Viable cells immunopositive for CD11b and Ly6C, representing the infiltrated cells of myeloid origin (CD11b+/ Ly6C+) from injured muscle were evaluated (n= 4/ cell type). Within the myeloid population, 26.68% ± 2.42% was neutrophils (CD11b+/ Ly6C+/ Ly6G+/ F4/80−); 1.61% ± 0.14% was macrophages (CD11b+/ Ly6C+/ Ly6G−/ F4/80+); and 71.7% ± 2.45% was other myeloid cells (CD11b+/ Ly6C+/ Ly6G−/ F4/80−). Amongst the three myeloid progenies, macrophages expressed the highest level of IGF-1Ea and MGF transcripts. Both isoforms in macrophages were 4 fold higher than neutrophils and other myeloid cells (all $P < 0.05$). For the inflammatory markers, expression of TNF-α transcript in neutrophils was 20

fold more than other myeloid cells ($P < 0.001$). Besides, the expression was also significantly higher (about 14 fold) than in macrophages ($P < 0.001$). In other words, expression of TNF-α in macrophages was 1.5 fold higher than that in other myeloid cells ($P < 0.05$). No difference in IL-10 and CCL2 expression was observed amongst the evaluated myeloid cells.

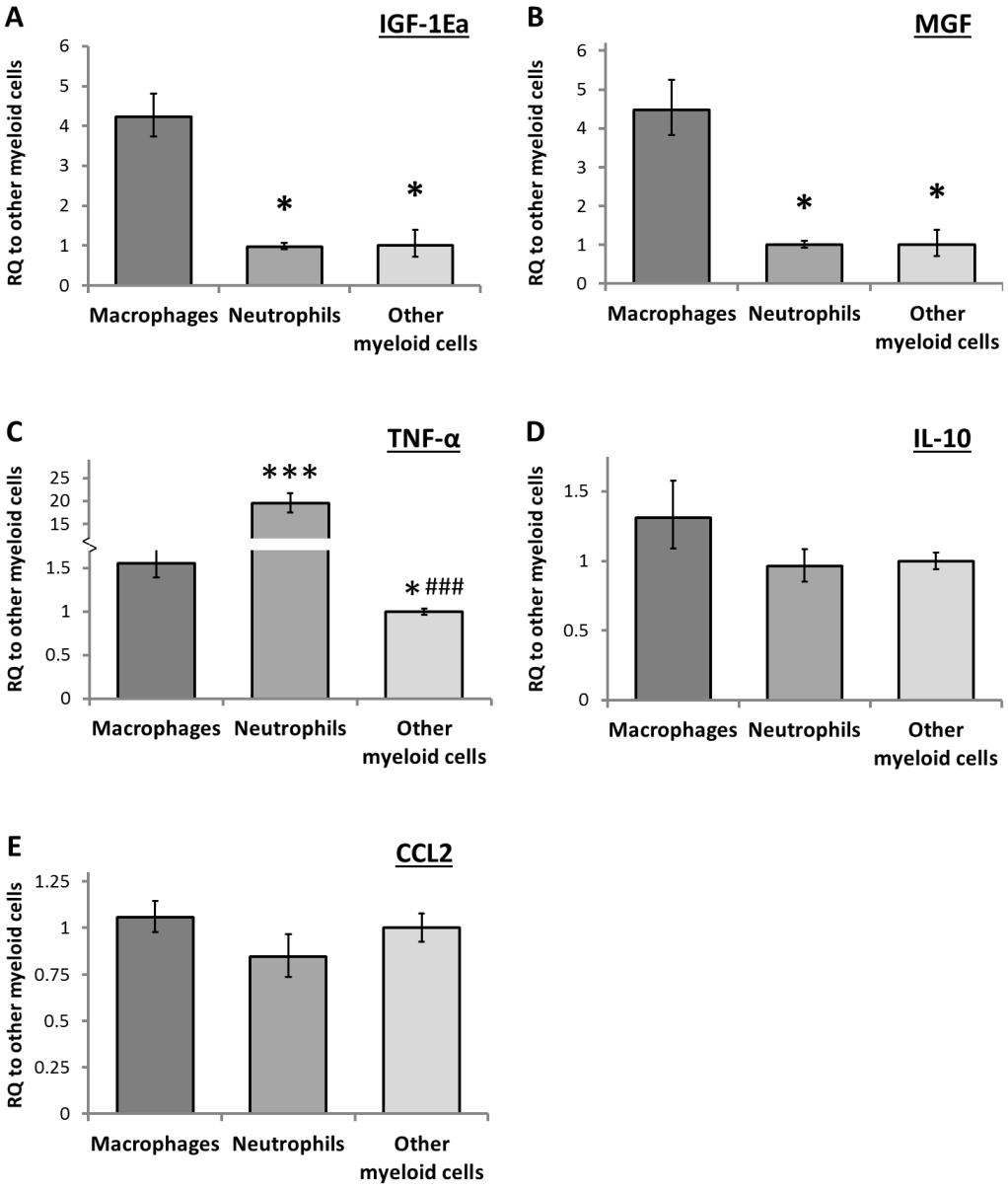

Figure 3.10 Transcript expression profiles of myeloid cells in CTX-injured muscle. Macrophages (n= 4), neutrophils and other myeloid cells (both n= 6) were isolated from CTX-injured muscle 36 h post injury (mean ± SEM). (A) IGF-1Ea; (B) MGF; (C) TNF-α; (D) IL-10; and (E) CCL2. Significant differences from macrophages: *P< 0.05 and ***P< 0.001; and significant difference from neutrophils: ###P< 0.001 tested by one-way ANOVA. Abbreviation: RQ= relative quantification.

3.4 DISCUSSION

In this Chapter, we confirmed the association of IGF-1 isoforms with inflammatory response at transcript and histological level. We showed that IGF-1 isoforms shared essentially the same temporal profile during muscle injury and were positively correlated. Both isoforms exhibited upregulation to peak at day 2 (inflammatory phase), persisted till day 4 (early resolution phase) and returned to baseline by day 7 (late resolution phase). Positive correlation of IGF-1 isoforms with typical inflammatory cytokines (TNF-α, IL-6 and IL-10) we also detected. Besides, increase of IGF-1 expression coincided with myeloid cell and macrophage infiltration. When inflammation resolved at day 7, IGF-1 isoforms had returned to baseline level. We therefore suggested that expression of IGF-1 isoforms were associated with muscle inflammatory response to injured muscle.

Expression of IGF-1 gene has been reported in macrophages infiltrated into injured muscle (Lu *et al.*, 2011*b*; Tonkin *et al.*, 2015). However the studies could not rule out the contribution from other infiltrated myeloid cells. As such, we also examined the transcript profile of infiltrated myeloid cells including neutrophils, macrophages and other myeloid cells. In addition to macrophages, which have been known to express IGF-1, neutrophils and other myeloid cells also expressed IGF-1Ea and MGF transcripts. Thus all isolated myeloid cells (CD11b+/ Ly6C+) contributed to IGF-1 upregulation in injured muscle. IGF-1 isoforms were most abundant in infiltrated macrophages that might suggest roles of IGF-1Ea and MGF in modulating macrophage activities in muscle regeneration, although the earliest infiltrating cells, the neutrophils, also contribute to IGF-1

expression. To our knowledge, it is the first report to demonstrate that neutrophils and other myeloid cells expressed both IGF-1 isoforms in injured muscle.

3.4.1. Myeloid cells as major sources of IGF-1 in the inflammatory phase of muscle regeneration

Myofibers are capable of expressing IGF-1Ea and MGF in response to eccentric injury (McKoy *et al.*, 1999). The expression of IGF-1 within myofibers was identified by *in situ* hybridization (McKoy *et al.*, 1999). Yet the myofibers that expressed IGF-1 appeared non-infiltrated or swollen (McKoy *et al.*, 1999). These myofibers likely escaped from injury and remained capable of expressing IGF-1. It was however questionable that ruptured and dying myofibers could release IGF-1 to signal satellite cell proliferation and differentiation as well as inflammatory mediation throughout regeneration process. Furthermore, damaged tissues are efficiently removed by infiltrated phagocytes like neutrophils within hours. Any release from injured myofibers is presumably limited and not sustainable. Intact myofibers that escaped from damage may support the neighboring regenerative events by paracrine IGF-1 signaling. However, intact myofibers can be rare in severe trauma. Injured site may then be deprived of IGF-1 which potentially impairs muscle regeneration. It requires other cellular sources to provide IGF-1.

Amongst cells that resided in skeletal muscle, satellite cells, endothelial cells and fibroblasts contribute to the endogenous IGF-1

expression (Christov *et al.*, 2007; Ceafalan *et al.*, 2014; Tonkin *et al.*, 2015). Yet, upregulation of IGF-1 isoforms during muscle inflammation is predominantly contributed by infiltrated macrophages (Tonkin *et al.*, 2015). Tonkin *et al.*, (2015) demonstrated that IGF-1 upregulation within muscle at day 2 post CTX injury, presumably inflammatory phase, was ablated by LysM promoter driven IGF-1 conditional knockout. Coincided with Tonkin *et al.*, (2015), macrophages analyzed in our study also expressed both IGF-1 isoforms and likely contributed to the upregulation of IGF-1 isoforms during inflammatory phase. Yet, LysM promotor is active in myeloid cells including neutrophils and monocytes (Goren *et al.*, 2009; Tonkin *et al.*, 2015). It is possible that IGF-1 expression in other infiltrated myeloid cells is also ablated to affect the upregulation of IGF-1 isoforms in injured muscle. Neutrophils infiltrate into the injured tissue prior to macrophages and peaked within 24 h post injury followed by resolution in the next 1 to 2 days (Wang *et al.*, 2014). We also showed in the sorting experiment that other myeloid cells and neutrophils composed of over 90% of the sorted cells 36 h post CTX injury. At 36 h post injury, only about 2% of myeloid cells were macrophages. Despite 4 fold higher IGF-1 isoform expression in macrophages at 36 h post injury, the upregulation of IGF-1 isoforms prior to macrophage infiltration should be attributed to the neutrophils and other myeloid cells.

To sum up, infiltrated myeloid cells were suggested to be the predominant source of both IGF-1 isoforms at the inflammatory phase of muscle regeneration. Sequentially, neutrophils and other myeloid cells (e.g. monocytes and eosinophils) were suggested to contribute to the early

upregulation of IGF-1 isoforms. It was followed by infiltration of macrophages that subsequently cleared the neutrophil population and thus became the predominant source of IGF-1 expression as previous study suggested (Tonkin *et al.*, 2015).

3.4.2. Potential functions of IGF-1 derived from neutrophils

The role of macrophage-derived IGF-1 in muscle regeneration has been extensively investigated (Pelosi *et al.*, 2007; Tidball & Welc, 2015; Tonkin *et al.*, 2015) but that of neutrophil-derived IGF-1 is unclear. The anti-apoptotic effect of IGF-1 on promoting neutrophil survival was demonstrated (Kooijman *et al.*, 2002; Kooijman, 2006). The investigators later reported that IGF-1 delays Fas-mediated apoptosis of neutrophils via PI3K pathway (Himpe *et al.*, 2008). In the same study, IGF-1 and TNF-α synergistically delay neutrophil apoptosis. We found that neutrophils in injured muscle expressed both IGF-1 and TNF-α. It is possible that infiltrated neutrophils express these soluble factors to inhibit apoptosis in autocrine or paracrine manner. Besides, IGF-1 increases phagocytosis and promotes respiratory burst (i.e. release of ROS/ RNS like NO) of neutrophils in the presence of inflammatory stimulus *in vitro* (Balteskard *et al.*, 1998). However, promotion of neutrophil survival and activities can be harmful to muscle cell especially in eccentric muscle injury (Pizza *et al.*, 2001; Nguyen & Tidball, 2003; Toumi & Best, 2003; Toumi *et al.*, 2006). Investigating and differentiating the roles of neutrophil-derived IGF-1 isoforms in mediating neutrophil activities and muscle regeneration would be recommended for further studies. To understand the importance of IGF-1 isoforms in

neutrophils, neutrophil-specific knockout of particular IGF-1 isoforms driven by Mrp8 promotor is suggested (Van Ziffle & Lowell, 2009). Muscle regeneration outcomes of these transgenic mice can also be compared. Notably neutrophils dominate injured muscle at the time satellite cells undergoing activation, proliferation and migration (Tidball & Rinaldi, 2012). Experiments on these aspects will elucidate the roles of neutrophil-derived IGF-1 of particular isoforms in muscle regeneration.

3.4.3. Association of IGF-1 with pro-inflammatory cytokines – TNF-α

Pro-inflammatory cytokines TNF-α and IL-6 upregulate predominantly at the inflammatory phase of muscle regeneration (Chen *et al.*, 2005; Meador *et al.*, 2008; Zhang *et al.*, 2013). We observed positive correlation of both IGF-1 isoforms with pro-inflammatory cytokines. Yet TNF-α and IL-6 significantly decreased to baseline level at day 4 while the upregulation of IGF-1 isoforms persisted. This apparent dissociation could be explained by the dynamic profile of myeloid infiltrates.

All myeloid cells collected 36 h post injury expressed TNF-α and IGF-1 isoforms. Common myeloid source might explain their simultaneous expression peak at day 2 at tissue level. However, it cannot explain the apparent dissociation at day 4. Intriguingly, TNF-α was much more abundant in neutrophils than macrophages (14 fold) and other myeloid cells (20 fold); whereas both IGF-1 isoforms were found higher in macrophages compared with neutrophils and other myeloid cells (both 4 fold higher). Given the abundance of TNF-α in neutrophils, resolution of neutrophils after day 2 post

injury (Sciorati *et al.*, 2016) might underlie the baseline reaching decrease of TNF-α at day 4. Besides, expression of TNF-α by macrophages is downregulated upon M2 polarization (Arnold *et al.*, 2007; Tidball, 2017). M2 MP-derived IL-10 further represses the expression of TNF-α (Strle *et al.*, 2007). Although neutrophils express IGF-1, its expression level was comparatively lower than macrophages. Moreover, macrophages become the predominant myeloid cells after neutrophil clearance (Tidball, 2011). Macrophages continued to express high level of IGF-1 isoforms. Collectively, expression of IGF-1 isoforms (and TNF-α) in injured muscle at day 2 were contributed by all myeloid cells but that at day 4 should be attributed to macrophages.

3.4.4. Functional cross-talk of pro-inflammatory cytokines with IGF-1 in muscle regeneration

Upregulation of TNF-α plays a pivotal role in the induction of pro-inflammatory cytokines (e.g. IL-6), mediation of phagocytosis by phagocytes and chemotaxis of macrophages (Collins & Grounds, 2001; Chen *et al.*, 2005, 2007; Parameswaran & Patial, 2010). Notably, apoptosis of neutrophils is synergistically suppressed by TNF-α and IGF-1 (Himpe *et al.*, 2008). We found that neutrophils expressed both TNF-α and IGF-1. Such co-expression with anti-apoptotic effects may prolong the phagocytic activities of neutrophils in injured muscle.

In addition to inflammatory modulation, TNF-α is also essential for activation of satellite cells and myogenesis during muscle regeneration.

Depending on the downstream signaling pathway, TNF-α modulates myoblast proliferation (Otis *et al.*, 2014) and differentiation (Chen *et al.*, 2005; Grounds *et al.*, 2008). Dual mitogenic and myogenic roles of IGF-1 are well-acknowledged (Coolican *et al.*, 1997; Smith, 2010). Apparently, TNF-α and IGF-1 coordinate to facilitate myogenesis and muscle regeneration. Activation of NF-κB signaling pathway by TNF-α is suggested to enhance proliferation (Guttridge *et al.*, 1999; Otis *et al.*, 2014). Similarly, IGF-1 promotes proliferation by activation of MAPK signaling cascade (Smith, 2010; Schiaffino & Mammucari, 2011; Enguita-Germán & Fortes, 2014). Differentiation is negatively regulated by TNF-α by inhibiting IGF-1/ IRS-1 and the downstream PI3K/ Akt signaling (O'Connor *et al.*, 2008). Specifically, TNF-α signaling induces ceramide synthesis (Strle *et al.*, 2004) followed by activating c-jun N-terminal kinase (JNK) to inhibit tyrosine phosphorylation of IRS-1 by IGF-1R (Frost *et al.*, 2003; Strle *et al.*, 2006). Upregulation of differentiation markers such as MyoD, Myog and MHC is thus suppressed. Besides, anabolic effect of IGF-1 in myoblast protein synthesis is abolished by treatment with TNF-α (Frost *et al.*, 1997). Although TNF-α represses IGF-1 activities, the inhibition appears restricted to IGF-1-induced myogenic differentiation but not on myoblast proliferation.

Besides, TNF-α induces the expression of other pro-inflammatory cytokines including IL-6 (Strle *et al.*, 2007). Our finding of synchronous expression of IL-6 and TNF-α at tissue level might support this notion. Moreover, IL-6 positively correlated with IGF-1 expression. Myoblast proliferation is promoted by IL-6 via cyclin D1 and c-myc (Serrano *et al.*, 2008). Activation of signal transducer and activator of transcription 3

(STAT3) by IL-6 promotes satellite cell proliferation in injured muscle (Toth *et al.*, 2011). Interaction of IGF-1 with IL-6 via STAT3 has been suggested (Zong *et al.*, 2000). Collectively, pro-inflammatory cytokines (TNF-α and IL-6) facilitate myoblast proliferation and negatively regulate differentiation induced by IGF-1. Inhibition of pro-inflammatory cytokine signaling leads to pre-mature myogenic differentiation that impairs muscle regeneration (Muñoz-Cánoves *et al.*, 2013). However, interaction of specific IGF-1 isoforms with pro-inflammatory cytokines (both TNF-α and IL-6) remains elusive. Given distinct signaling induced by IGF-1 isoforms (Barton, 2006*b*), differential regulation and interaction of IGF-1Ea and MGF with inflammatory cytokines is conceivable.

3.4.5. Association of IGF-1 with anti-inflammatory cytokine, IL-10

As a potent anti-inflammatory cytokine, IL-10 is pivotal in resolving muscle inflammatory response (Meador *et al.*, 2008; Ouyang *et al.*, 2011; Villalta *et al.*, 2011; Deng *et al.*, 2012; Sciorati *et al.*, 2016). Upregulation of IL-10 suppresses the expression of pro-inflammatory cytokines like TNF-α (Strle *et al.*, 2007; Deng *et al.*, 2012). It skews macrophage polarization to anti-inflammatory phenotype (i.e. M2 MP) which is supportive to myogenesis (Deng *et al.*, 2012). Although IL-10 cannot induce upregulation of MRF like Myog directly (Strle *et al.*, 2007; Deng *et al.*, 2012), it is key to abolish the inhibitory effects of TNF-α/ JNK signaling on IGF-1-mediated myogenic differentiation (Strle *et al.*, 2007). As a result, IGF-1/ PI3K/ Akt signaling is restored to induce MRF expression and myoblast differentiation. Besides, *in vitro* treatment of recombinant IGF-1

peptide induces upregulation of IL-10 in bone marrow derived macrophages. The investigators however did not provide the sequence details of the IGF-1 peptide used (Tonkin *et al.*, 2015). In a cardiac injury model, overexpression of IGF-1Ea induced upregulation of IL-10 as soon as one day post injury coupled with suppression of pro-inflammatory IL-1β and CCL2 (Gallego-Colon *et al.*, 2015). The role of MGF on IL-10 expression was not reported yet. Given the observed simultaneous upregulation of IL-10 and MGF (as well as IGF-1Ea), it is conceived that MGF could modulate the expression of IL-10 as well. Similar model by MGF overexpression might elucidate the function of MGF on anti-inflammatory cytokine expression in skeletal muscle injury.

3.5 CONCLUSION

In this Chapter, we examined the expression of IGF-1 isoforms in myeloid cells infiltrated into injured muscles. We evaluated the expression of IGF-1Ea and MGF in CTX-injured muscle and confirmed their association with upregulation of inflammatory cytokines and infiltration of myeloid cells. Expression of inflammatory cytokines was positively correlated with IGF-1 isoforms. The upregulation of IGF-1 isoforms coincided with the presence of myeloid cells and macrophages histologically. The FACS data indicated that IGF-1 isoforms expression level was 4 fold higher in macrophages compared to that of neutrophils and other myeloid cells. Yet, the relative abundance of neutrophils and monocytes prior to macrophage infiltration highlighted these IGF-1 expressing cells as the early source of

IGF-1 isoforms in injured muscle. However, the specific role of each IGF-1 isoforms could not be suggested from the results due to essentially the same expression profile of IGF-1Ea and MGF at tissue level and amongst inflammatory cells. Further investigation on the roles of specific isoforms was required to delineate their functions in muscle inflammatory response and consequently to muscle regeneration.

CHAPTER 4

Role of MGF in Modulating Inflammatory Response to Muscle Injury

4.1 INTRODUCTION

IGF-1 is predominantly derived from infiltrated myeloid cells or macrophages during the inflammatory phase of muscle regeneration (Lu *et al.*, 2011*b*; Tonkin *et al.*, 2015). This coincides with our findings reported in Chapter 3 that all myeloid cells (e.g. neutrophils and macrophages) express both IGF-1 isoforms in injured muscle. However, the role of MGF, in modulating inflammatory response to muscle injury remains elusive.

In addition to a previous study from Pelosi *et al.*, (2007) on the involvement of IGF-1Ea in the regenerative process of injured muscle, Tonkin *et al.*, (2015) has elucidated the significance of IGF-1Ea and MGF in muscle inflammatory response, which was not addressed in previous reports (Summan *et al.*, 2006; Dumont & Frenette, 2010; Lu *et al.*, 2011*b*). In that study, the ablation of myeloid cell-derived IGF-1 led to enhanced macrophage infiltration, downregulated anti-inflammatory transcripts expression, decreased macrophage polarization into M2 MP (anti-inflammatory phenotype) and ultimately impaired muscle regeneration (Tonkin *et al.*, 2015). When MGF was systemically ablated, muscle regenerated without any histological differences when compared to control. The authors therefore claimed that IGF-1Ea is attributed to the anti-inflammatory properties whereas MGF was dispensable for muscle regeneration (Tonkin *et al.*, 2015). Indeed, MGF contributes only 10% of total IGF-1 transcript (Brisson & Barton, 2012), and may therefore explain why MGF systemic knockout did not lead to perinatal lethality (Tonkin *et al.*, 2015), which was however the case in IGF-1 systemic knockout (Baker *et al.*, 1993; Liu *et al.*, 1993, 2000; Powell-Braxton *et al.*, 1993).

Furthermore, compensatory mechanism may exist in the systemic MGF ablation model that leads to complete muscle regeneration. Yet, overexpression of MGF in non-injured muscle induces transcript expression and activation of downstream signaling distinct from that by IGF-1Ea (Barton, 2006*b*; Barton *et al.*, 2010; Brisson & Barton, 2012). Differential temporal profile of IGF-1Ea and MGF in response to eccentric injury was also reported (Yang & Goldspink, 2002; Hill *et al.*, 2003; Philippou *et al.*, 2009). Collectively, it is still conceivable that MGF possesses unique roles and regulatory mechanism in skeletal muscle and potentially muscle inflammatory response.

Previous studies on MGF functions however relied predominantly on the physiologically irrelevant synthetic peptide (see Section 1.4.5). Alternative approach should be used to delineate the roles of MGF in modulating inflammatory response to muscle injury. We therefore decided to generate plasmid DNA overexpressing the full-length MGF cDNA. When full-length MGF was transcribed, it will be translated into pre-pro-MGF followed by post-translational modification under physiological control. Besides, application of plasmid DNA does not require any special facilities as in the case of viral-mediated gene transfer (Barton, 2006*b*; Barton *et al.*, 2010; Brisson *et al.*, 2014). To facilitate plasmid-based gene overexpression, the plasmid was injected into muscle followed by electroporation. It was an effective approach to locally overexpress a gene of interest within skeletal muscle (McMahon *et al.*, 2001; Lee *et al.*, 2002; Schertzer *et al.*, 2006), including IGF-1 (Schertzer & Lynch, 2006).

4.1.1. Hypothesis and aims

IGF-1 is essential for proper muscle regeneration. We demonstrated in Chapter 3 that all infiltrated myeloid progenies expressed IGF-1 isoforms, coincided with previous findings (Lu *et al.*, 2011*b*; Tonkin *et al.*, 2015). Although macrophage-derived IGF-1Ea has been attributed to the anti-inflammatory properties of IGF-1 while MGF was suggested to be dispensable for muscle regeneration (Pelosi *et al.*, 2007; Tonkin *et al.*, 2015), compensatory mechanism for the systemic loss of MGF might exist which could account for the absence of phenotypic changes in muscle regeneration. Furthermore, unique roles and signaling of MGF have been suggested (Barton, 2006*b*; Barton *et al.*, 2010; Brisson & Barton, 2012). Given the upregulation of MGF transcript coincided with the infiltration of myeloid cells including macrophages in response to CTX injury; and macrophages displayed higher MGF expression amongst infiltrated myeloid cells (see Chapter 3), we hypothesize that MGF modulates the inflammatory response in muscle regeneration. This study was thus undertaken to examine the roles of MGF in modulating muscle inflammatory response and muscle regeneration by overexpressing MGF.

Overexpression could be established by electroporation of plasmid DNA encoding MGF cDNA transcript into muscle (Schertzer & Lynch, 2006). By this mean, MGF was expressed by the myofibers and likely enacted on infiltrated macrophages in paracrine manner, similar to the muscle cell-driven IGF-1Ea overexpression model (Pelosi *et al.*, 2007). Muscle injury was then induced by CTX injection. Inflammatory response of MGF-overexpressed muscle subjected to CTX-induced injury would be

evaluated at transcript, cellular and histological level. Altered inflammatory response might influence muscle regeneration (Tidball, 2017). Thus, assessments of muscle regeneration outcomes were included. The experimental aims of Chapter 4 were:

1. To assess the effect of MGF overexpression on inflammatory transcript profiles at tissue level;
2. To evaluate the infiltrated macrophage and sub-population profiles in response to MGF overexpression; and
3. To demonstrate the association of inflammatory response with muscle regeneration outcomes upon MGF overexpression

4.2 METHODOLOGY

The synthesis of plasmid encoding MGF, protocol of muscle electroporation and CTX-induced muscle injury and *in vitro* cell culture were described in Chapter 2. Similarly, the general procedures of performing the following assessments, including RT-qPCR, Western blotting, histology, flow cytometry and cell sorting were also referred.

4.2.1 Experimental design

The experiments began with the verification of MGF overexpression model using custom-made MGF clone, i.e. pMGF. Our electroporation protocol and pMGF transcription and translation in skeletal muscle were evaluated. The efficiency of our electroporation protocol was demonstrated *in vivo* using reporter plasmid pEGFP-N1 (Clontech, USA). In

addition, possible muscle injury caused by the electroporation procedures was evaluated by immunostaining of myeloid cells in electroporated muscle. In use of a verified *in vivo* electroporation protocol, the transcription and translation of pMGF was evaluated by RT-qPCR and Western blotting respectively. Moreover, *in vitro* C2C12 myoblast and myotube were transfected with pMGF to examine the clone activities again by RT-qPCR and Western blotting.

For aim 1, the effect of MGF overexpression on inflammatory transcript profiles of injured muscle was assessed. The evaluated inflammatory markers included a number of inflammatory cytokines and antigens presented on pro-inflammatory macrophages (M1 MP) and anti-inflammatory macrophages (M2 MP) (Tidball, 2017). Muscles harvesting was based on the three inflammatory phases in CTX-injured muscle (Hardy *et al.*, 2016). The timepoints included day 1 (pre-injury), day 3 (inflammatory phase), day 5 (early resolution phase) and day 8 (late resolution phase) post electroporation. Comparison between pMGF and empty vector control on the expression profiles of inflammatory cytokines might yield valuable information on the gross effects of MGF overexpression on cytokine expression and macrophage polarization.

M1 MP and M2 MP appear sequentially and interact to modulate distinct inflammatory process (Mills *et al.*, 2000; Tidball, 2005, 2017). For aim 2, we employed flow cytometry and immunohistochemistry (IHC) techniques to evaluate the effects of MGF overexpression on the recruitment, polarization and resolution of macrophages. The population of M1 MP and M2 MP was analyzed by flow cytometry daily from the day of CTX injection

to the end of early resolution phase (day 1 to day 6 post electroporation). The late resolution phase (day 6 and day 8) would be examined by IHC assessment. For aim 3, regeneration outcomes in MGF-overexpressed muscle were evaluated at the transcript and histological level.

No previous studies have reported the potential regulatory interaction of IGF-1Ea and MGF, it is possible that overexpression of MGF would alter the expression level of IGF-1Ea and thus confound the findings and interpretation. As such, the transcript expression of IGF-1Ea was evaluated whenever possible.

4.2.2 Evaluations of *in vivo* electroporation model

The evaluations of *in vivo* electroporation model included electroporation efficiency and possible damages induced by electroporation. The efficiency of electroporation was evaluated with the use of pEGFP-N1 plasmid DNA (Clontech, USA). It is a clone for constitutive expression of green fluorescent protein (GFP) and allows direct evaluation by *in vivo* imaging and histological assessment. Muscle for the evaluation of electroporation efficiency was collected at day 4 post electroporation. *In vivo* imaging would focus on the lower limb of animal. Presence of GFP signal in TA but not in other adjacent tissues indicated successfully confined delivery of plasmid DNA by electroporation. The distribution of GFP+ myofibers suggested the efficiency of the current protocol. It would be evaluated by comparing with literature reports (McMahon *et al.*, 2001; Lee *et al.*, 2002; Schertzer *et al.*, 2006)

Besides, the severity of tissue damage induced by electroporation was evaluated by histology. Empty vector plasmid DNA was identically injected into both side of TA followed with electrical stimulation on only one of them. The other TA was not electrically stimulated and thus served as no electroporation control (negative control). Inflammatory myeloid cell infiltration reflected the damages induced by electrical stimuli. It was assessed at day 2 post electroporation by IHC staining against CD11b. Muscle damages were indicated by CD11b immunopositivity. The potential damages observed from the negative control represented the minimal damages and inflammatory response caused by injections *per se*. Additional damages in electroporated TA, if any, suggested the tissue injury induced by electrical stimulation in addition to injections.

4.2.3 Transcriptional and translational activity of pMGF plasmid DNA

The transcriptional and translational activities of pMGF were evaluated *in vivo* by electroporation and *in vitro* by transfection of C2C12 cell line, using RT-qPCR and Western blotting respectively.

In vivo electroporation was performed as described in last section. One side of TA was electroporated with pMGF plasmid and the contralateral TA was electroporated with empty vector. The latter served as negative control. Samples were harvested at day 1, day 3, day 5 and day 8 post electroporation for RNA evaluation. RT-qPCR and Western blot analyses were used to evaluate the expression of MGF transcript and peptide

respectively. Of note, our custom Taqman assay for MGF could not distinguish endogenous and plasmid-derived MGF transcript. Overexpression was thus confirmed by comparison with the corresponding vector control. The protein examination was conducted at day 2 and day 4 post electroporation instead. Comparisons were made between pMGF and vector electroporated muscles to demonstrate the overexpression of MGF peptides within muscle. With the use of anti-6-HIS antibody, pMGF-derived putative MGF peptides, but not the endogenous MGF, could be specifically identified.

Transfection of C2C12 cells with pMGF or vector was achieved using lipofectamine-mediated transfection system (Lipofectamine 2000; Thermo Fisher Scientific, USA) according to the manufacturer instruction. For RNA evaluation, C2C12 cells were separately transfected in proliferating and differentiated cultures. In proliferating C2C12, 3 x 10^4 cells were plated in 12-well plate. Transfection, using 2 µg pMGF or empty vector and 3 µl Lipofectamine 2000, was performed on the next day and harvested separately 24 h and 48 h post transfection. For transfection of differentiated C2C12, 1 x 10^5 cells were plated in 12-well plate and allowed to differentiate for 4 days when myotubes became observable. Transfection and harvest were then performed identically as in proliferating culture. For protein examination, 2.5 x 10^5 cells were plated in 6-well plate and transfected the next day with 5 µg pMGF or empty vector and 7.5 µl of Lipofectamine 2000 regent. The cells were harvested for Western blotting 24 h and 48 h post transfection. Comparison of MGF expression was made between pMGF and vector control similar to that for *in vivo*.

4.2.4 Combined model of MGF overexpression and CTX-induced injury

In order to examine the roles of MGF in muscle inflammatory response, we designed and established the MGF overexpression with CTX-induced injury model. In this model, MGF overexpression by electroporation established high MGF microenvironment within the electroporated muscle. The CTX-induced injury model led to tissue rupture and induced infiltration of inflammatory cells. The combination of these two models thus exposed the infiltrated inflammatory cells to high MGF microenvironment. Specifically, MGF overexpression was performed on one side of TA. The contralateral TA electroporated with vector plasmid DNA served as negative control. One day after electroporation, CTX injection was performed on both electroporated TA to induce tissue injury and the subsequent inflammatory response. The workflows of CTX injection and MGF overexpression were exactly the same as described before. To avoid confusion from the sole MGF overexpression model, pMGF-electroporated muscle with CTX-induced injury was designated as "pMGF+ CTX injury" whereas as that for vector control was "vector+ CTX injury".

Muscles were harvested at day 1, day 3, day 5 and day 8 post electroporation. Notably, CTX injection was performed one day after electroporation. In other words, the harvest timepoints were equivalent to pre-injury and day 2, day 4 and day 7 post CTX injury respectively. These timepoints represented different phases of muscle regeneration. Again, from the day of CTX injection, these were inflammatory phase (day 2), early resolution (day 4) and then the late resolution (day 7). In combination with

MGF overexpression model, the effects of MGF on the three phases of muscle inflammatory responses were examined.

The injection of CTX at day 1 post electroporation was determined empirically from the MGF expression profile of pMGF-electroporated muscle (see Figure 4.7). We observed drastic downregulation of MGF transcript from approximately 700 fold at day 1 to about 15 fold at day 3 post electroporation, compared with the corresponding vector control. Thereafter, the expression level was stably downregulating to about 10 fold at day 8 post electroporation. The injection of CTX at day 1 post electroporation captured the earliest timepoint that exhibited intense MGF upregulation. Inflammatory cells including macrophages were thus exposed to the highest possible level of MGF achieved from the current electroporation model.

We acknowledged a limitation to our model that injection of CTX might damage the transfected myofibers, if not all, and compromised the efficiency of MGF overexpression. In view of this, MGF transcript expression was evaluated at all evaluation timepoints and compared between pMGF+ CTX injury with vector+ CTX injury. Overexpression of MGF was confirmed throughout the evaluation time window. Moreover, we mentioned at the end of Section 4.2.2 about our objective of evaluating the injury caused by electroporation. Injection of CTX was presumed as the only inducing factor of muscle damages in this model. However, injury from electroporation is basically inevitable, e.g. intramuscular injections (Lee *et al.*, 2002; Schertzer *et al.*, 2006). The problem thus become whether the electroporation procedures led to negligible injury compared with that

resulted from CTX injection. To address this concern, inflammatory cell infiltration was compared between: (i) vector with and without electrical stimulation; and (ii) vector and vector+ CTX injury, at day 2 post electroporation. The extent of injury induced by electroporation and CTX-induced injury would be demonstrated.

4.2.5 *In vivo* imaging

Muscle electroporated with pEGFP-N1 clone was assessed by *in vivo* imaging to reveal the expression of GFP protein *in situ*. The experiment was performed at day 4 post electroporation to evaluate the electroporation efficiency of the current protocol. To allow *in vivo* imaging, animals were anesthetized, limb hair shaved and fixed inside the imaging chamber of *in vivo* Xtreme II (Bruker, USA). X-ray scanning and fluorescence imaging were performed in focus of the lower limbs. The radiograph and fluorescence images were next overlaid for anatomical identification of TA and co-localization with GFP signals.

4.2.6 Histology of GFP+ myofibers

After *in vivo* imaging, the pEGFP-N1 electroporated TA were collected and processed for histological evaluation. Cryosections were collected at the mid-belly of the muscle. Myofibers with GFP expression should emit green fluorescence under blue laser excitation which was observable under epi-fluorescence microscope. The entire muscle cryosection was evaluated. Images taken at 20X magnification were then

assessed for the number of GFP+ myofibers and the total number of myofibers. The percentage of GFP+ myofibers within muscle served as the quantitative indicator of the electroporation efficiency.

4.2.7 RT-qPCR

Purified total RNA were reverse transcribed to generate the first strand cDNA for RT-qPCR assessment. It included samples from MGF overexpression model, MGF overexpression with CTX-induced injury model, *in vitro* C2C12 model as well as cells collected from FACS. The genes of interest were categorized into housekeeping, IGF-1 isoforms, inflammation and regeneration-related markers. The respective Taqman assays were summarized in Table 4.1. Housekeeping genes including GAPDH, 18S rRNA and RPS20, were evaluated for the determination of internal control. It was performed by NormFinder (Andersen *et al.*, 2004) in which the most stable gene(s) would be empirically chosen for normalization purpose. The $2^{-\Delta\Delta Ct}$ method (Livak & Schmittgen, 2001) was adopted for the quantitative analysis of RT-qPCR data.

The inflammatory markers included a number of cytokines, cell surface antigens and cytokine receptors. The pro-inflammatory cytokines were TNF-α, IL-6 and the anti-inflammatory marker was IL-10. A chemokine that investigated was CCL2. The expression of macrophage surface antigens as well as cytokine receptors allowed detection of various macrophage subsets, M1 MP and M2 MP. Particularly, CD86 (B-lymphocyte antigen B7-2) and IFNγR1 (interferon gamma receptor 1) were two transcripts

preferentially expressed in M1 MP whereas CD206 (mannose receptor C-type 1) and IL-4Ra (interleukin-4 receptor, alpha) were in M2 MP (Lai *et al.*, 1998; Martinez & Gordon, 2014; Tidball, 2017). The regeneration-related markers included a satellite cell marker, Pax7; two MRF genes: MyoD and Myog; and two MHC genes: Myh3 (myosin heavy chain, embryonic form) and Myh8 (myosin heavy chain, neonatal form) (Marsh *et al.*, 1997; Serrano *et al.*, 2008; McKay *et al.*, 2008; Villalta *et al.*, 2011). Myh3 and Myh8 are expressed predominantly by regenerating myofibers which will be substituted by slow MHC in mature myofibers (Musarò, 2014).

4.2.8 Western blot

Western blot was used for verifying the translation of pMGF clone. Total protein extracted from pMGF-electroporated muscle and the vector control was subjected to SDS-PAGE and Western blotting (the same applied for *in vitro* samples). Since 6-HIS tag sequence was inserted at the C-terminal end of MGF insert sequence, anti-6-HIS tag antibody was used to identify those C-terminal sequence-inclusive peptides (Figure 2.2). The expected sizes of the putative peptides from pMGF were about 18.69 kDa (pre-pro-MGF-HIS), 13.36 kDa (pro-MGF-HIS) and 5.70 kDa (Eb-peptide-HIS). Detection of the 6-HIS tag with the relevant molecular weight indicated the form of MGF peptides expressed from pMGF.

Table 4.1 Taqman assays involved in studying the effect of MGF overexpression on muscle inflammatory response. All Taqman assays were purchased from Thermo Fisher Scientific, USA. Abbreviation: GAPDH: Glyceraldehyde 3-phosphate dehydrogenase; 18S rRNA: ribosomal RNA 18S; RPS20: ribosomal protein S20; MGF: mechano-growth factor; IGF-1Ea: insulin-like growth factor-1 Ea isoform; TNF-α: tumor necrosis factor-α; IL-6: interleukin 6; IL-10: interleukin 10; CCL2: C-C motif chemokine ligand 2; CD86: B-lymphocyte antigen B7-2; CD206: mannose receptor C-type 1; IFNγR1: interferon gamma receptor 1; IL-4Ra: interleukin-4 receptor, alpha; Pax7: paired box 7; MyoD: myogenic differentiation protein 1; Myog: myogenin; Myh3: myosin heavy chain, embryonic form; Myh8: myosin heavy chain, neonatal form.

(*Overleaf)*

	Genes of interest	Assay ID	Gene ID
Housekeeping gene	GAPDH	4352932E	NM_008084.2
	18S rRNA	4448484	X03205.1
	RPS20	Mm02342828_g1	NM_026147.5
IGF-1 isoform	MGF	Custom	AY878193
	IGF-1Ea	Mm00710307_m1	NM_001111275.1
Inflammatory cytokine and chemokine	TNF-α	Mm00443258_m1	NM_013693.3
	IL-6	Mm00446190_m1	NM_031168.1
	IL-10	Mm01288386_m1	NM_010548.2
	CCL2	Mm00441242_m1	NM_011333.3
Macrophage surface antigen	CD86	Mm00444543_m1	NM_019388.3
	CD206	Mm01329362_m1	NM_008625.2
Cytokine receptor	IFNγR1	Mm00599890_m1	NM_010511.2
	IL-4Ra	Mm01275139_m1	NM_001008700.3
Satellite cells	Pax7	Mm01354484_m1	NM_011039.2
Myogenic regulatory factor	MyoD	Mm00440387_m1	NM_010866.2
	Myog	Mm00446194_m1	NM_031189.2
Myosin heavy chain	Myh3	Mm01332463_m1	NM_001099635.1
	Myh8	Mm01329494_m1	NM_177369.3

4.2.9 Myeloid cell and macrophage measurement in skeletal muscle cryosection

The presence of myeloid cells and macrophages were assessed by IHC using specific antibodies against CD11b and F4/80 respectively. Fluorescent images of DAPI staining and immunostaining at 20X magnification were taken from the entire muscle cryosection. Images at 40X magnification were taken to demonstrate the representative staining of myeloid cells and macrophages in the injured muscle. Besides, no primary antibody control determining the background fluorescence was included in all samples. Analyses were performed by ImageJ image analysis software (National Institutes of Health, USA). Depending on the phase of muscle regeneration i.e. the inflammatory phase and the late resolution phase, intensity and extensiveness of immunopositive signal were distinct which favored two different quantification approaches elaborated as followed.

During inflammatory phase (day 2), the injured loci that infiltrated with myeloid cells and macrophages demonstrated intensive and extensive immunopositivity of CD11b and F4/80 respectively. Although the number of infiltrated cells should be the most accurate reflective of the infiltration process, cell counting was technically not possible. It was hindered by extensive overlapping DAPI fluorescent signals due to the extraordinarily high density of infiltrated cells present at this phase. The measurement of immunopositive area was the alternative to reflect the extent of infiltration. Besides, the relatively high signal-to-noise ratio of these acutely inflamed muscle samples favored the area measurement as well. Specifically, the area measurement began with defining a threshold signal of individual samples.

The threshold was set using the no primary control of the same muscle by ImageJ. The threshold represented the background signal of that particular sample. After threshold signal determination, any signal with intensity above the threshold were treated as immunopositivity and measured by the ImageJ software. The immunopositive and total area of the muscle cryosection were quantified.

As for the analyses of myeloid cells and macrophages at late resolution phase, direct counting on the immunopositive cells was performed instead. The density of inflammatory progenies has been massively reduced due to inflammatory resolution. The technical hindrance from overlapping DAPI signal no longer existed. In addition, the signal-to-noise ratio for both CD11b and F4/80 staining decreased at this phase. It became difficult to define a signal threshold for area measurement. Thus direct counting of myeloid cells and macrophages was more favorable. Besides, sub-analyses were also conducted based on the localization of the immunopositive cells. Epimysium-resided macrophages represent the muscle resident MP (Brigitte *et al.*, 2010). Macrophages identified at the interstitial spaces were likely the remaining infiltrated progeny. The typical identification of resident MP and interstitial myeloid cells or macrophages was shown in Figure 4.1. Similarly, no primary control was firstly evaluated for the background signal of individual samples. Signal stronger than the background and associated with DAPI staining was taken as an immunopositive cell. The number of immunopositive cells at epimysium and interstitial space was counted. Data were expressed as number of immunopositive cells per total myofibers.

Figure 4.1 Identification of epimysial and interstitial myeloid cells and macrophages. Epimysium represented the outermost structure of muscle and identified at the cryosection outer boundary. Epimysial cells aligned and concentrated along epimysium and appeared elongated in shape. It is distinct from the relatively random distribution of myonuclei and interstitial cells. By this mean, epimysial and interstitial (A) CD11b+ and (B) F4/80+ cells were analyzed. Images were captured at 20X magnification with scale bar= 100 μm. The staining of CD11b (and F4/80) was green whereas DAPI signal was blue. The arrows and the arrow heads indicated the immunopositive cells at interstitial space and epimysium respectively. The inset regions were enlarged for clear illustration of cells resided at epimysium (left) and interstitial space (bottom), scale bar= 200 μm.

(*Overleaf)*

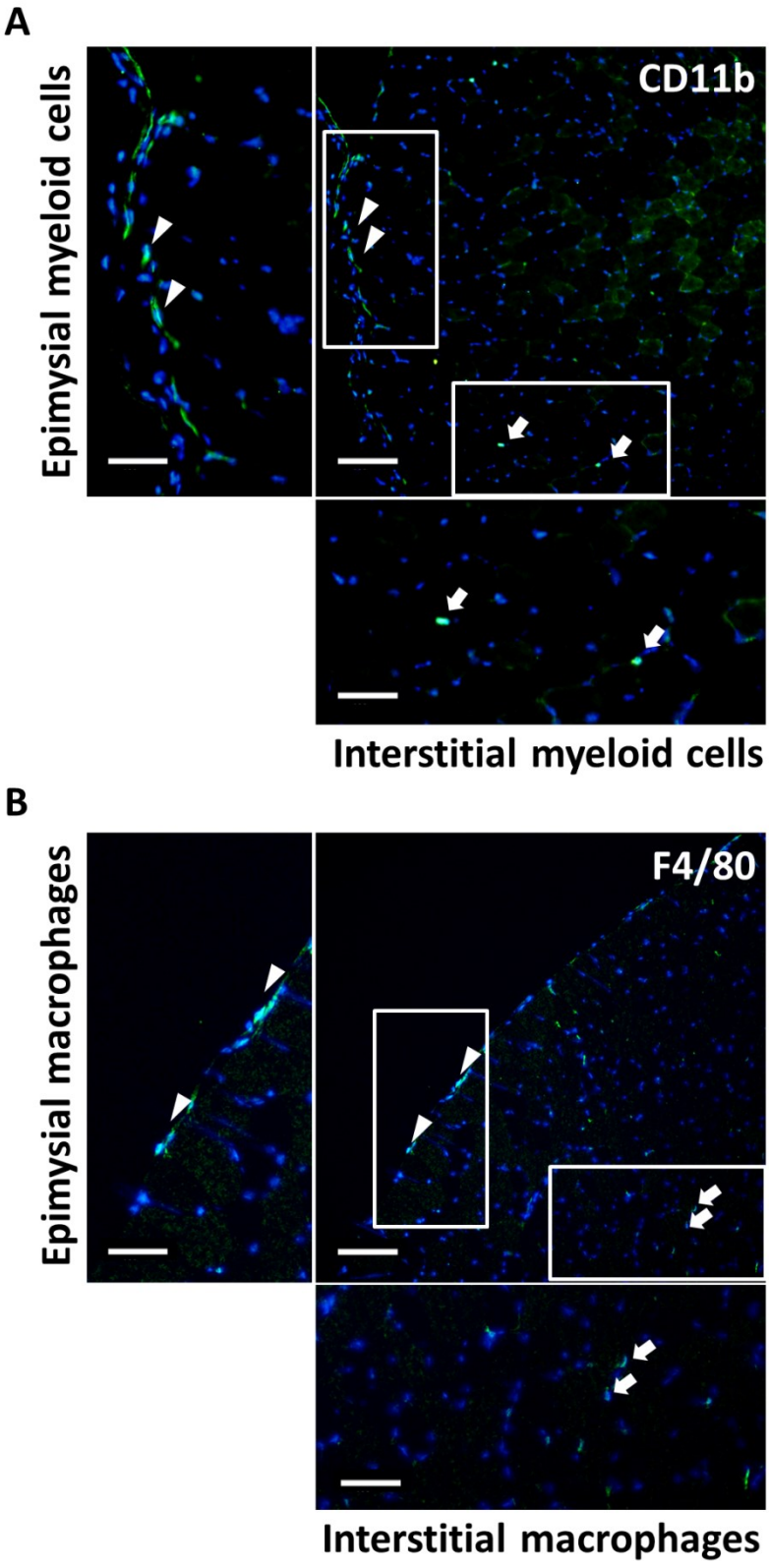
A
Epimysial myeloid cells
CD11b
Interstitial myeloid cells
B
Epimysial macrophages
F4/80
Interstitial macrophages

4.2.10 Histology of regenerating muscle

The regeneration outcome of muscle from MGF overexpression with CTX-induced injury model was evaluated to demonstrate the effect of MGF overexpression on muscle regeneration. Number of centrally nucleated myofibers that represented the number of regenerating myofibers, and the cross-sectional area (CSA) that reflected the progress of hypertrophy of the regenerating myofibers, were counted and measured. H&E staining was performed on cryosections followed by microscopic imaging. Images at 20X magnification were taken from the entire cryosection for analyses.

Normal myofibers are peripherally nucleated whereas regenerating myofibers are centrally nucleated. The nuclear staining was indicated by hematoxylin in blue and cytoplasmic staining with eosin in red. Thus myofibers with blue nuclei located at the inner periphery of sarcolemma was defined as normal myofibers and counted, while the myofibers with at least one nucleus at the cytoplasmic region was regarded as centrally nucleated myofibers. The total myofibers represented the sum of normal myofibers and regenerating myofibers. The data would be presented as centrally nucleated myofibers per total myofibers (%centrally nucleated myofibers per total myofibers).

The CSA of centrally nucleated myofibers was next measured by ImageJ software using polygon tool. The centrally nucleated myofibers were first identified as described above. The outer surface of the centrally nucleated myofibers was then outlined by the polygon tool. The size of the final polygon indicating the CSA of that particular centrally nucleated myofiber was measured by ImageJ. The mean CSA and the distribution of

centrally nucleated myofibers were then computed. To demonstrate the CSA distribution, four categories were defined based on the resulting range of centrally nucleated myofiber CSA which were: (i) below 550 μm^2; (ii) ≥550 μm^2 to 1100 μm^2; (iii) ≥1100 μm^2 to 1650 μm^2; and (iv) greater than 1650 μm^2. The frequency of centrally nucleated myofibers within each category was computed and plotted against the area categories.

4.2.11 Macrophage profiling by flow cytometry

The macrophage profile of samples from the MGF overexpression with CTX-induced injury model was evaluated by flow cytometry. Muscles were harvested daily from day 1 post electroporation till day 6 post electroporation in order to establish a temporal profile of macrophages and the sub-populations. Of note, day 1 post electroporation was not CTX-injured and served as the baseline level of macrophages within the electroporated muscle. The information and staining conditions of antibodies used in macrophage profiling were summarized in Table 4.2.

The gating strategy of the flow cytometric analyses was graphically illustrated in Figure 4.2. Macrophages were defined as cells with high granularity (High-SSC) and double positivity for CD11b and F4/80. Sub-populations of macrophages were defined by the exclusive expression pattern of Ly6C and CD206. Pro-inflammatory M1 MP were positive for Ly6C but negative for CD206 and vice versa in anti-inflammatory M2 MP (Italiani & Boraschi, 2014; Martinez & Gordon, 2014; Tonkin *et al.*, 2015). In total 5 x 10^4 events were measured for each cell suspension. The number

of total myeloid cells (High-SSC/ CD11b+), total macrophages (High-SSC/ CD11b+/ F4/80+), M1 MP (High-SSC/ CD11b+/ F4/80+/ Ly6C+/ CD206−) and M2 MP (High-SSC/ CD11b+/ F4/80+/ Ly6C−/ CD206+) were all counted. Other macrophages were calculated by subtracting M1 MP and M2 MP from the total macrophages and should be either double positive or double negative for Ly6C and CD206. The number of macrophages was divided by the total number of myeloid cells and expressed in %total macrophages, %M1 MP, %M2 MP and %other macrophages.

The profiling of macrophages and the sub-populations delineated the effects of MGF overexpression on their infiltration, expansion and resolution during the regeneration process. The inflammatory status of the muscle could also be deduced from the temporal dynamic of each sub-population, which formed the basis of our result interpretation.

4.2.12 Fluorescent-assisted cell sorting

Fluorescent-assisted cell sorting (FACS) was used to isolate macrophages and other myeloid cells. The isolated cells were collected and subjected to RT-qPCR analyses. The cell staining (Table 3.2) and gating strategy (Figure 3.2) for macrophages and other myeloid cells was identical to that described in Section 3.2.6 except neutrophils was not sorted. Single cells of high granularity were gated by forward scattering (FSC) and side scattering (SSC). Only viable cells (7AAD−) were then negatively gated with Ly6G to exclude neutrophils from collection. Positive gates with CD11b and Ly6C identified the infiltrated myeloid cells. Depending on the

immunoactivity with macrophage-specific F4/80 antibody, macrophages (7AAD−/ Ly6G−/ CD11b+/ Ly6C+/ F4/80+) and other myeloid cells (7AAD−/ Ly6G−/ CD11b+/ Ly6C+/ F4/80−) were separately collected. In order to have sufficient inflammatory cells for RT-qPCR analysis, three sorted cell samples of the same treatment were pooled and processed as a single RNA sample for RT-qPCR analyses.

4.2.13 Statistics

Quantitative data were presented in mean ± standard error (SEM). All statistical tests were performed by SPSS 20 (IBM analytic, USA). Significance level was set at $P< 0.05$.

Two-way ANOVA was used to compare between treatments (pMGF and vector) and between or amongst harvest timepoints (day post electroporation). Interaction between the two independent variables was determined simultaneously. Post-hoc tests were performed only when significant major effect was found by two-way ANOVA. Post-hoc Student's t test or one-way ANOVA were used to identify the particular timepoints demonstrating differences between pMGF and vector control as well as the temporal changes during regeneration process as appropriate.

Antibody	Manufacturer	Clone (Isotype)	Working concentration (per 10^6 cells in 100 µl)	Fluorochrome (Sorter detection channel)
CD11b	BD Biosciences	M1/ 70 (Rat IgG2b, κ)	0.5 µg	BB515 (FL1)
Ly6C	Biolegend	HK1.4 (Rat IgG2c, κ)	1 µg	PE (FL2)
CD206	Biolegend	C068C2 (Rat IgG2a κ)	1 µg	PE-Cy7 (FL3)
F4/80	BD Biosciences	T45-2342 (Rat IgG2a, κ)	2 µg	AF647 (FL4)

Table 4.2 Antibody panel used for profiling macrophages from injured muscle. Fluorochromes: BB515= BD Horizon BB515; PE= Phycoerythrin; PE-Cy7= Phycoerythrin-cyanine 7 tandem dye; and AF647= Alexa Fluor 647.

Figure 4.2 Gating strategy for macrophage profiling. The plots were exported from one of the sample analyses. (A) Size (FSC-A) and granularity (SSC-A) gating with cells of high granularity gate-included as “High-SSC”; (B) Single cell gating by FSC-H and FSC-A with cells from “High-SSC’ further gate-included as “Singlet”; (C) Individual antigen plots and gating with cells from “Singlet”. The gating line for each antigen was adjusted by unstained control or isotype control which served as reference for following quadrant-gates; (D) Scatter-plot of cells from “Singlet” with double positivity for CD11b and F4/80 in "Quadrant-gate-I"= macrophages (CD11b+/ F4/80+); (E) Scatter-plot of macrophages (CD11b+/ F4/80+) for sub-population gating and measurement. "Quadrant-gate-II"= M2 MP (CD11b+/ F4/80+/ Ly6C−/ CD206+) whereas "Quadrant-gate-III"= M1 MP (CD11b+/ F4/80+/ Ly6C+/ CD206−). The macrophages with double positivity or double negativity for Ly6C and CD206 were designated as “other macrophages”.

(*Overleaf*)

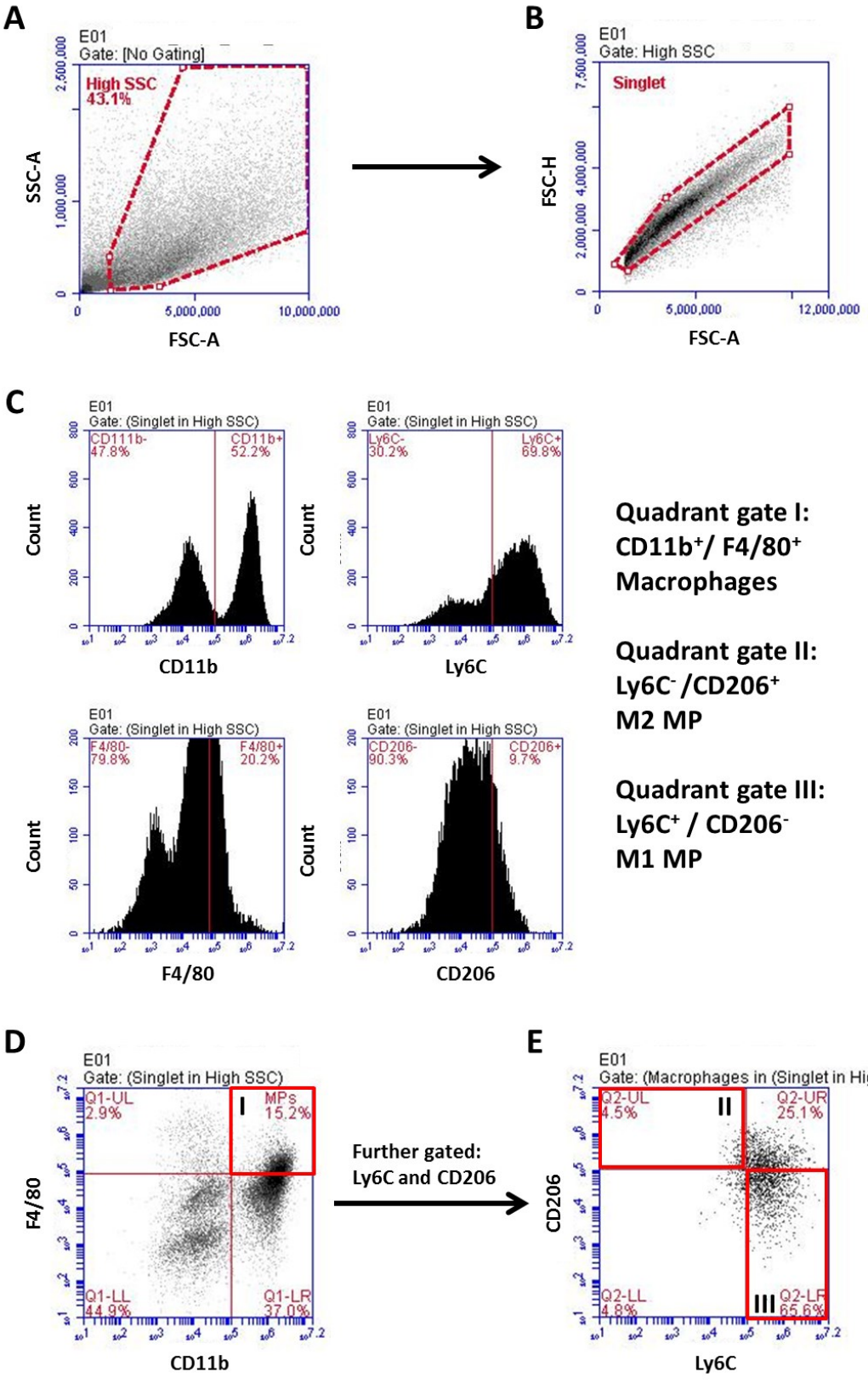
A
E01
Gate: [No Gating]
High SSC
43.1%
SSC-A
FSC-A
B
E01
Gate: High SSC
Singlet
FSC-H
FSC-A
C
E01
Gate: (Singlet in High SSC)
CD111b-
47.8%
CD11b+
52.2%
Count
CD11b
Ly6C-
30.2%
Ly6C+
69.8%
Ly6C
F4/80-
79.8%
F4/80+
20.2%
F4/80
CD206-
90.3%
CD206+
9.7%
CD206
Quadrant gate I:
CD11b+/ F4/80+
Macrophages
Quadrant gate II:
Ly6C- /CD206+
M2 MP
Quadrant gate III:
Ly6C+ / CD206-
M1 MP
D
E01
Gate: (Singlet in High SSC)
Q1-UL
2.9%
I
MPs
15.2%
Q1-LL
44.9%
Q1-LR
37.0%
F4/80
CD11b
Further gated:
Ly6C and CD206
E
E01
Gate: (Macrophages in (Singlet in High
Q2-UL
4.5%
II
Q2-UR
25.1%
Q2-LL
4.8%
III
Q2-LR
65.6%
CD206
Ly6C

4.3 RESULTS

The results of this study would be separately presented in four parts. First, it began with the evaluation of electroporation efficiency. The transcription and translation of pMGF was confirmed *in vitro* and *in vivo*. Second, the electroporation protocol and pMGF clone were then applied to investigate roles of MGF in muscle inflammatory response during regeneration. The third part was about the examination of regeneration outcomes of MGF-overexpressed muscle. Further experiments designed based on the major findings were presented at the end.

In the following results, timepoints were represented as day post electroporation e.g. day 5 post electroporation (or simply day 5). Besides, "CTX" must be designated when CTX injection was performed on the electroporated muscle e.g. pMGF+ CTX injury referred to muscle overexpressing MGF with CTX-induced injury.

4.3.1. Evaluation of electroporation protocol

We modified electroporation protocols of other studies in order to improve electroporation efficiency in skeletal muscle (referred to Section 2.3.4). The efficiency of our protocol was demonstrated followed by assessment of electroporation-induced muscle injury. We next assessed the transcription and translation of our custom made MGF-overexpressing plasmid DNA, pMGF, *in vitro* and *in vivo*.

4.3.1.1 Electroporation efficiency

In order to demonstrate the efficiency of our *in vivo* overexpression model, TA was electroporated with plasmid pEGFP-N1 and collected at day 4 post electroporation for *in vivo* imaging and histological assessment (n= 2).

The radiograph and fluorescence images were overlaid and shown in Figure 4.3 which allowed simultaneous identification of TA and co-localization with GFP signal. TA was identified and labeled on the radiograph. Intense GFP signal was detected focally and specifically on the lateral side of the tibia but not elsewhere nearby. This result indicated that the current electroporation protocol achieved focal expression of the injected plasmid in TA. It was worth noting that the green signal over the mouse body was due to the autofluorescence emitted by the animal fur. Such autofluorescence was absent at the hindlimbs when the fur was shaved. Afterwards, the animal was harvested for histological evaluation. The GFP expression at histological level was examined and shown in Figure 4.4. The green polygonal structures of the TA cryosections represented the myofibers successfully transfected with pEGFP-N1. High transfection efficiency of the current protocol is confirmed (n = 5; 55.56% ± 18.64% GFP+ area/ total cross-sectional area). Remarkably, GFP signal was not found in the interstitial space, indicating that the preferential transfection of plasmid was within myofibers. To summarize, the results from *in vivo* imaging and histological imaging verified the efficiency of our electroporation protocol. Therefore the stated electroporation protocol was used in the following experiments.

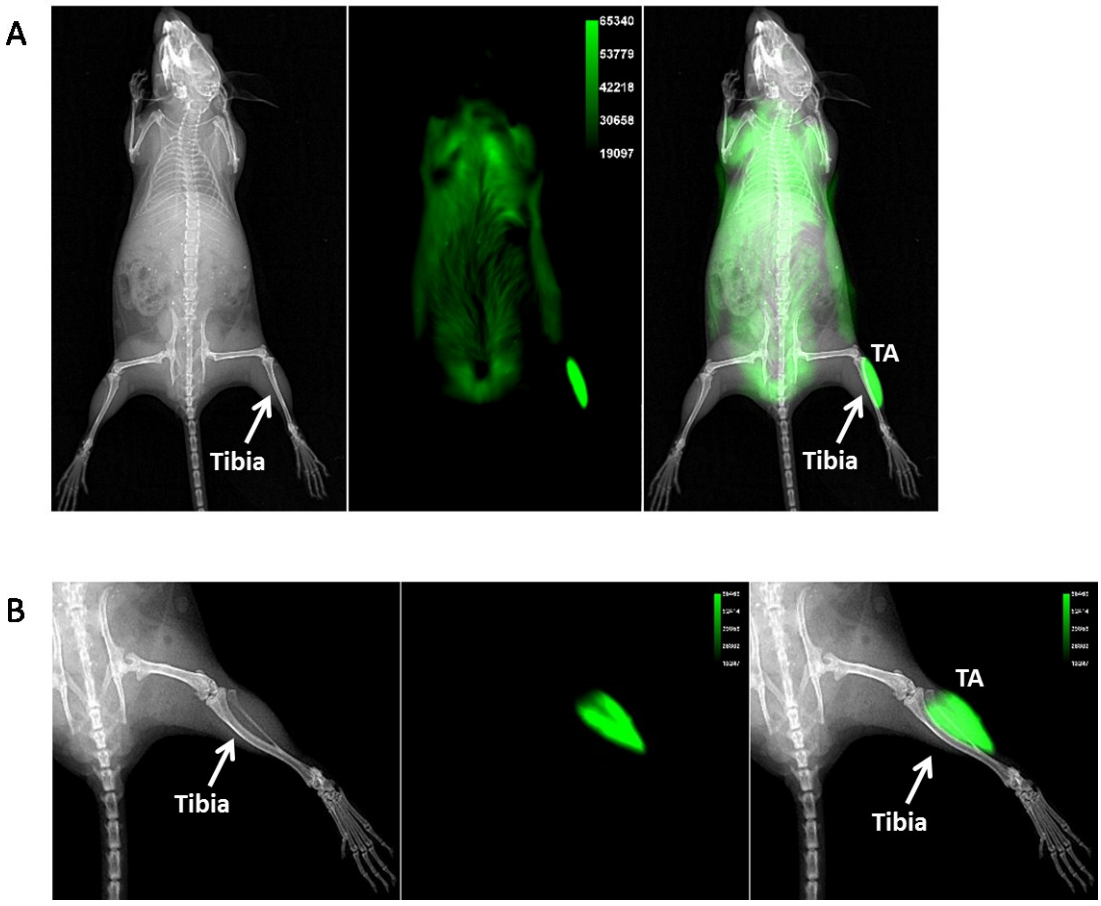

Figure 4.3 *In vivo* imaging of pEGFP-N1 electroporated TA. (A) Whole body imaging and (B) lower limb imaging (n= 2, day 4 post electroporation). From left to right were the radiograph, fluorescence image and the overlaid image. Abbreviation: TA= tibialis anterior.

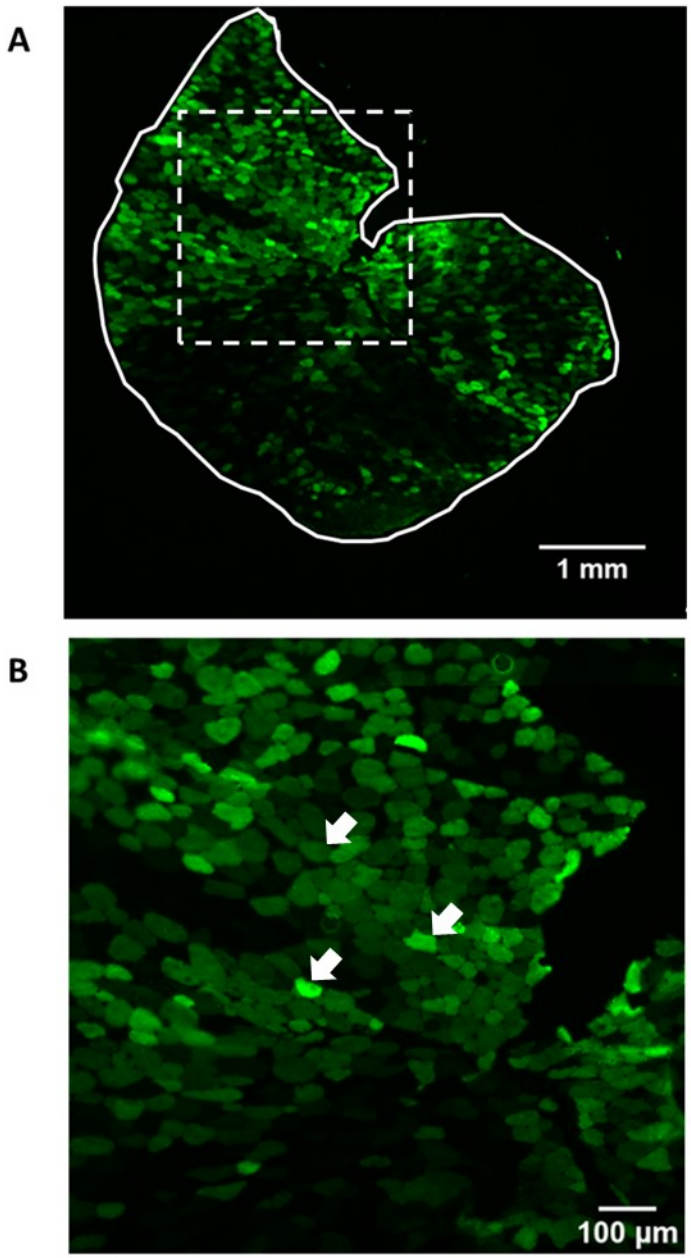

Figure 4.4 Fluorescence imaging of cryosections from pEGFP-N1 electroporated TA. (A) Low magnification image (4X; scale bar= 1 mm) with muscle outline in white; (B) magnified image of the inset in (A) and scale bar= 100 µm (n= 5, day 4 post electroporation). The green polygonal structures represented the GFP+ myofibers (indicated by white arrows).

4.3.1.2 Muscle inflammatory response due to electroporation

Electroporation inevitably leads to tissue damage due to electrical pulses and reagent injections (Lee *et al.*, 2002; Schertzer *et al.*, 2006). Despite high efficiency of our current protocol, significant injury arising from electroporation might induce muscle inflammatory response and confound data interpretation based on the established understanding of CTX-induced muscle injury model. To evaluate muscle inflammatory response caused by electroporation, both sides of TA were pretreated with hyaluronidase and injected with vector plasmid DNA but only one TA was electroporated. Muscle inflammatory response was analyzed 2 days after treatment by IHC against CD11b+ myeloid cells to indicate tissue injury. The representative images were shown in Figure 4.5.

The inflammatory loci in TA without CTX injection were small and sparse in which only a few myofibers were affected as shown in the 40X image. Inflammation in muscles with and without electroporation was indistinguishable. It suggested that electrical stimulation itself did not exaggerate tissue inflammation. The observed inflammatory response was likely attributed to injections of hyaluronidase and plasmid DNA. Needle puncture was a known physical insult and led to tissue damages (Lee *et al.*, 2002). Compared to CTX-induced injury with extensive CD11b+ staining, the inflammatory response induced by electroporation was minimal and negligible. Electroporation *per se* would not influence CTX-induced inflammatory response and regeneration.

Figure 4.5 Extent of tissue injury in electroporated muscle. Images were taken at two magnification 10X (left, scale bar= 200 μm) and 40X (right, scale bar= 50 μm) at day 2 post electroporation. From top to bottom were images from no electroporation (i.e. only injected with hyaluronidase and vector), electroporation (injections with electroporation) and electroporation with CTX injection. The IHC staining of CD11b was green whereas DAPI signal was blue. The 40X image could be referred to the inset in 10X image.

(*Overleaf)*

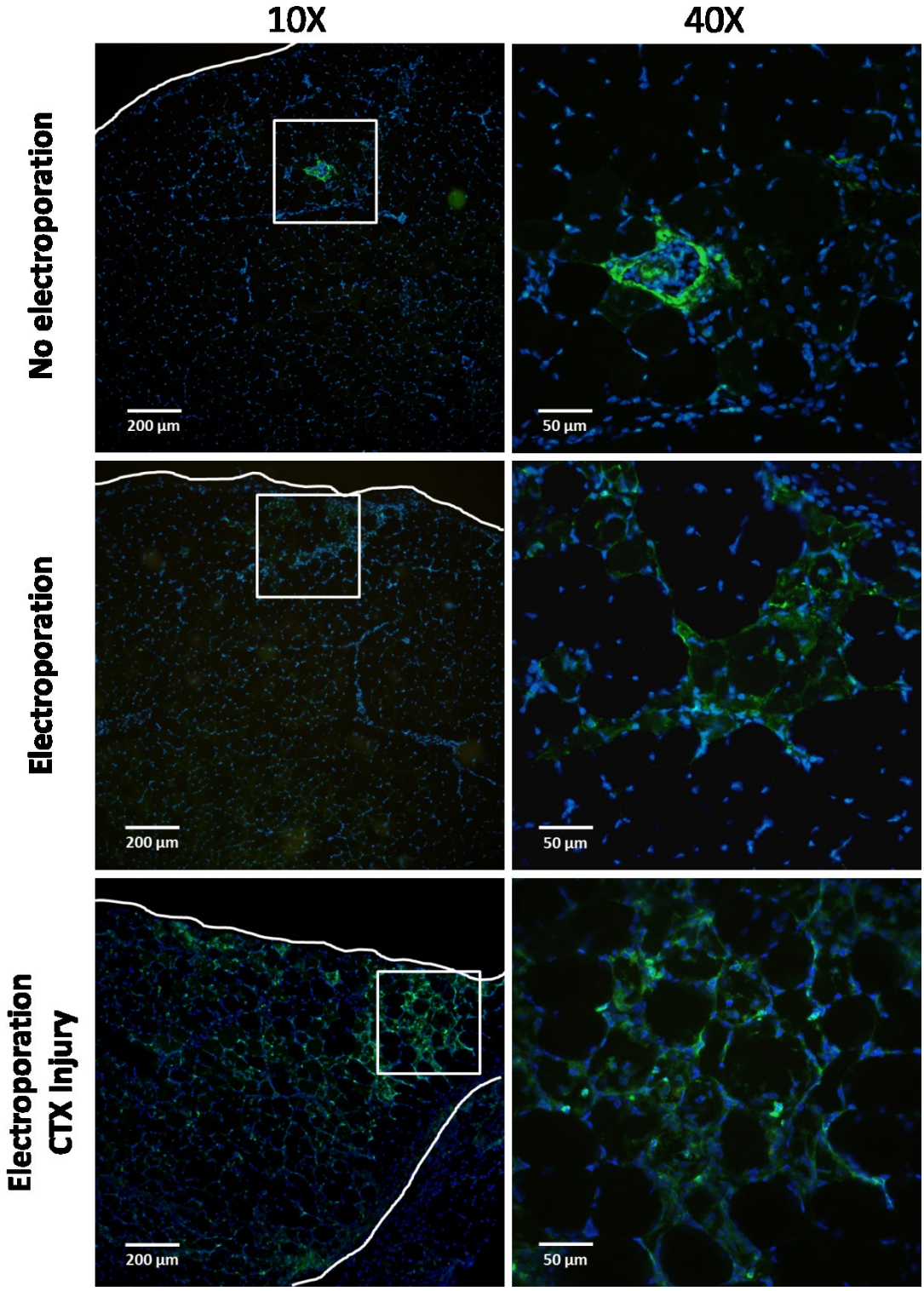
10X
40X
No electroporation
Electroporation
Electroporation
CTX Injury
200 µm
50 µm
200 µm
50 µm
200 µm
50 µm

4.3.1.3 Transcription of pMGF plasmid *in vitro* and *in vivo*

We have confirmed the efficiency of electroporation protocol by examining GFP expression. We next tested the transcription activity of our custom-made pMGF plasmid DNA *in vivo* using the same electroporation method. In addition, the transcription of pMGF was also demonstrated *in vitro* by transfecting C2C12 proliferating and differentiating culture. *In vitro* and *in vivo* MGF overexpression were shown in Figure 4.6 and Figure 4.7 respectively. Besides, the expression level of IGF-1Ea transcript in response to MGF overexpression was included as well.

In vitro, the expression of MGF in pMGF-transfected proliferating C2C12 cells reached thousands fold higher than the corresponding vector control 24 h post transfection. Despite decreasing in the next 24 h, it remained approximately 280 fold higher than the vector control. As for differentiating C2C12, similarly, significant upregulation was observed 24 h (20 fold) and 48 h (10 fold) post transfection. Intriguingly, MGF overexpression led to modest induction of IGF-1Ea (2.7 fold) at 24 h but slight repression (0.8 fold) at 48 h in proliferating C2C12. No change in IGF-1Ea was detected in differentiating C2C12. Collectively, we achieved MGF overexpression in both proliferating and differentiating C2C12.

In vivo, muscles were collected at day 1, day 3, day 5 and day 8 for MGF transcript evaluation. Overexpression of MGF transcript in pMGF remained higher than vector control for at least eight days (all $P < 0.001$). At day 1, there was about 600 fold higher MGF expression in pMGF than the corresponding vector control ($P < 0.001$). Significant downregulation of MGF was observed from day 1 to day 3 and day 1 to day 5 (both $P < 0.001$) in

pMGF but the downregulation was most drastic from day 1 to day 3. The expression of MGF at day 5 was not different from that at day 8. Unlike *in vitro* model, *in vivo* MGF overexpression did not alter IGF-1Ea expression. Thus, the subsequent finding from *in vivo* model was unlikely confounded by altered IGF-1Ea expression.

4.3.1.4 Translation of pMGF plasmid *in vitro* and *in vivo*

Western blotting using anti-6-HIS tag antibody determined the expression of MGF peptides from pMGF plasmid but not the endogenous source. The blot scanning images were shown in Figure 4.8. A clear single immunoreactive band at 15 to 20 kDa was consistently identified from all pMGF samples but not from the vector controls. It should be pre-pro-MGF-HIS peptide (18.69 kDa). *In vitro,* expression of MGF peptide was most dominant at 24 h but barely detectable at 48 h. *In vivo*, both electroporated muscles harvested at day 2 and day 4 expressed MGF peptide. Notably, bands representing pro-MGF-HIS (13.36 kDa) and Eb-HIS peptide (5.70 kDa) were again not detected in all blots. Similar results has been reported (Pfeffer *et al.*, 2009) and was likely attributed to their short half-life after cleavage and release (Brisson & Barton, 2012; Zabłocka *et al.*, 2012). To summarize, pMGF was translationally active *in vitro* and *in vivo* in which pre-pro-MGF-HIS was the only detectable form.

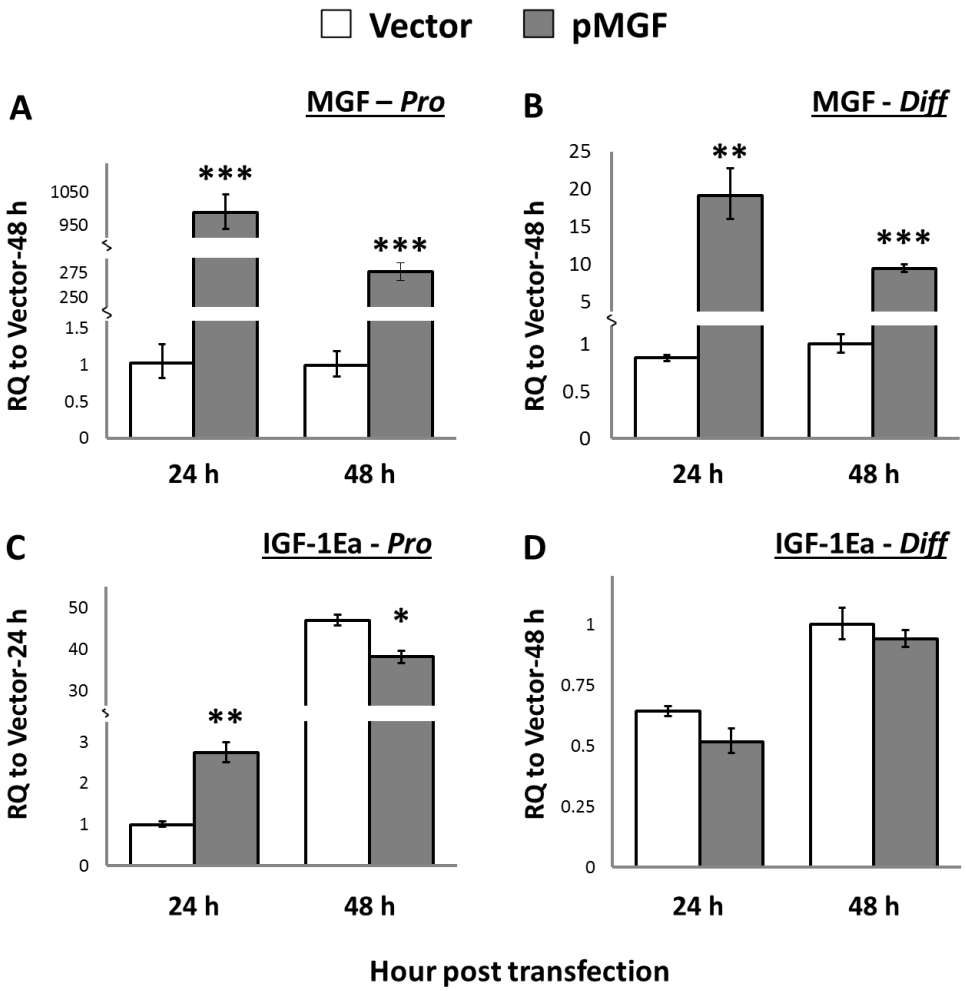

Figure 4.6 IGF-1 isoforms expression in MGF-overexpressed C2C12 cells. Expression of MGF transcript in (A) proliferating and (B) differentiating C2C12; Expression of IGF-1Ea transcript in (C) proliferating and (D) differentiating C2C12. The empty bars represented the vector and the filled bars represented pMGF (n= 3/ cell/ treatment/ timepoint). Expression level was relative to the 48 h vector except (C) to 24 h vector (mean ± SEM). Comparison between pMGF and vector at each timepoint by post-hoc Student's t-test: *P< 0.05, **P< 0.01 and ***P< 0.001. Abbreviation: RQ= relative quantification; h= hour; Pro= proliferating C2C12; Diff= differentiating C2C12.

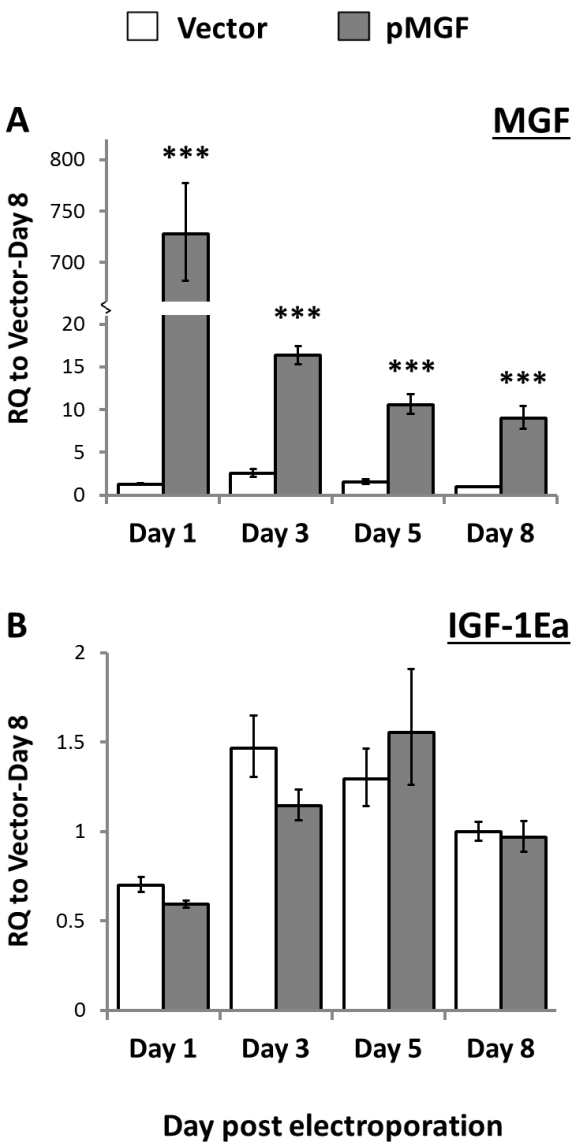

Figure 4.7 IGF-1 isoforms expression in TA harvested from day 1 to day 8 post electroporation. (A) MGF and (B) IGF-1Ea. The empty bars represented the vector and the filled bars represented pMGF (n= 5/ treatment/ timepoint). Expression level was relative to the vector at day 8 post electroporation (mean ± SEM). Significant differences between pMGF and vector control: ***P< 0.001 by Student's t-test. Abbreviation: RQ= relative quantification.

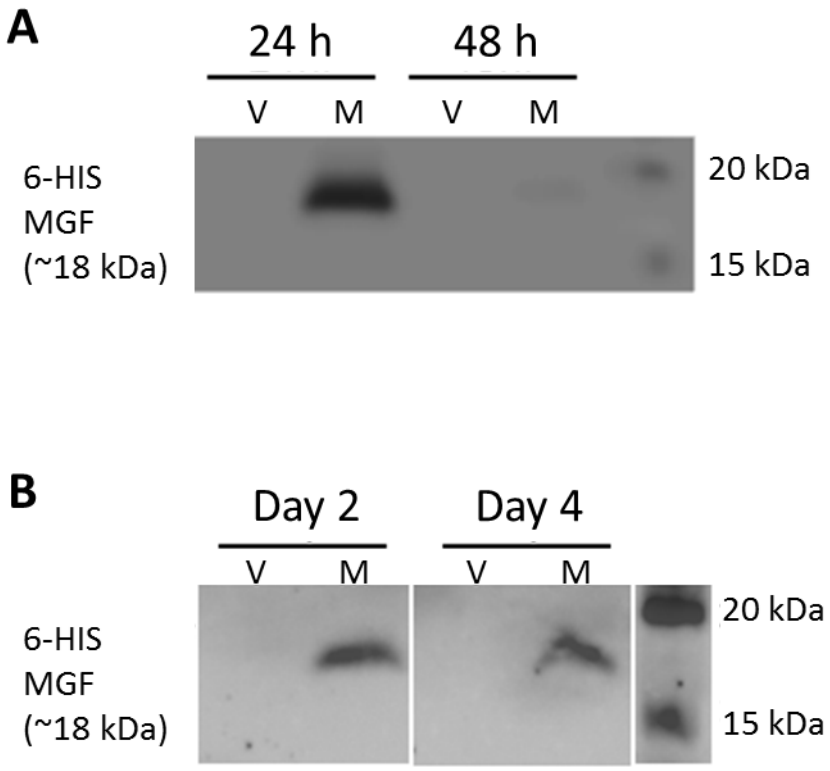

Figure 4.8 Western blotting of 6-HIS-tagged MGF peptide. Equal protein amount (80 µg) was loaded into each lane. Expression of 6-HIS-tagged MGF peptide from (A) proliferating C2C12 harvested 24 h and 48 h post pMGF transfection; and (B) TA harvested at day 2 and day 4 post pMGF electroporation. A single band was observed at about 18 kDa and no other band below that was detected within the same blot. Abbreviation: V= empty vector control; M= pMGF; h= hour; kDa= kilodalton.

4.3.1.5 Summary

Our electroporation protocol efficiently overexpressed GFP in over 60% of myofibers. The protocol did not induce significant damage to muscle as indicated from the minimal infiltration of myeloid cells. With the efficient electroporation protocol, pMGF was confirmed to overexpress MGF transcript and peptide *in vivo*. In addition, the transcript and translation of pMGF was also evident in proliferating and differentiating C2C12 cell culture. We therefore applied the verified electroporation protocol and pMGF for the following experiments.

4.3.2. Effect of MGF overexpression on muscle inflammatory response to injury

After confirming MGF overexpression *in vivo*, we combined the CTX-induced injury model to evaluate the effects of MGF overexpression on muscle inflammatory response. The transcript profile was first evaluated. Macrophage and the sub-population profiles were used to refine the inflammatory phases of the current model. The histology or flow cytometry results were presented following the sequence of refined inflammatory phases, which were inflammatory phase, early resolution phase and late resolution phase.

4.3.2.1 Upregulation of inflammatory markers in MGF-overexpressed CTX-injured muscle

Muscles subjected to MGF overexpression and CTX-induced injury were harvested at day 3, day 5 and day 8 (n= 6/ treatment/ timepoint) to assess the effect of MGF overexpression on inflammatory transcript profiles at tissue level. Again, the timepoints should reflect the inflammatory, early resolution and late resolution phase of CTX-induced muscle injury respectively. The expression profiles of IGF-1 isoforms and altered inflammatory genes were illustrated in Figure 4.9 whereas those of other genes were summarized in Figure 4.10.

Overexpression of MGF transcript was confirmed in which expression of MGF in pMGF+ CTX injury was sustainably higher than that of vector+ CTX injury throughout the evaluation window (all $P < 0.001$). CTX-induced muscle injury performed one day after electroporation did not abolish MGF overexpression. Moreover, the expression of IGF-1Ea transcript was not altered, which was coincided with the *in vivo* finding described in Section 4.3.1.3. Thus, it was conceived that the inflammatory phases were under the influence of overexpressing MGF within the injured muscle.

In vector control, expression of all inflammatory genes were the highest at day 3 among the timepoints examined (day 3, day 5 and day 8), but was then reduced from day 3 onwards. Upon overexpression of MGF, instead of downregulating as in vector control from day 3, expression of TNF-α, IL-10 and CD86 was maintained ($P > 0.05$, day 3= day 5). In addition, TNF-α, IL-10, CD86 and CCL2 were significantly higher than the corresponding vector control at day 5 (all $P < 0.05$) (Figure 4.9). Such upregulation in TNF-α and IL-10, but not CD86 or CCL2, remained

significant at day 8 in pMGF+ CTX injury. As mentioned, decreasing inflammatory markers were observed from day 3 to day 8 in vector+ CTX injury control, but that for pMGF+ CTX injury began at day 5, except CCL2 which began at day 3. However, the decrease in pMGF+ CTX injury appeared smaller and thus higher level was observed at day 5. Apparently, MGF overexpression delayed the downregulation of these inflammatory markers.

Other inflammatory markers, IL-6 and CD206, also demonstrated significant major effect of MGF from two-way ANOVA (pMGF+ CTX injury > vector+ CTX injury; both $P < 0.05$). However, no significant difference was found from the post-hoc tests. In other words, these two genes only demonstrated a trend of higher expression in pMGF+ CTX injury. Expression of cytokine receptors, IFNγR1 and IL-4Ra, was not altered by MGF overexpression.

Figure 4.9 Transcript expression profiles of altered inflammatory markers in MGF-overexpressed CTX-injured muscle. Samples were collected from day 3 to day 8 post electroporation. The illustrated genes were (A) MGF; (B) IGF-1Ea; (C) TNF-α; (D) IL-10; (E) CD86; and (F) CCL2. The empty bars represented the vector+ CTX injury and the filled bars represented pMGF+ CTX injury (n= 6/ treatment/ timepoint). Expression level was relative to day 8 vector+ CTX injury (mean ± SEM). Comparison between pMGF+ CTX injury and vector+ CTX injury at each timepoint by post-hoc Student's t-test: *P< 0.05 and ***P< 0.001. Abbreviation: RQ= relative quantification.

(*Overleaf)*

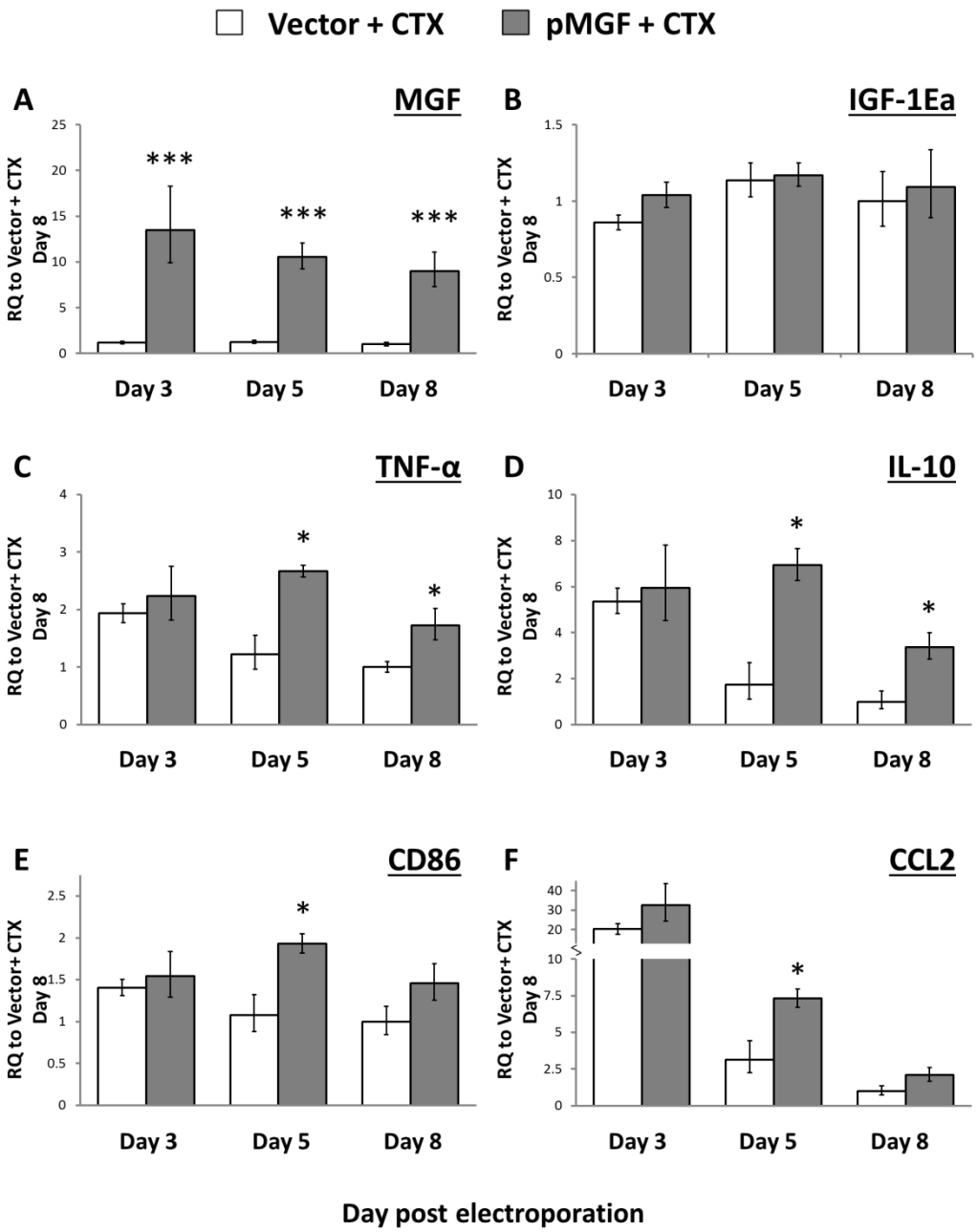
Vector + CTX
pMGF + CTX
A
MGF
B
IGF-1Ea
C
TNF-α
D
IL-10
E
CD86
F
CCL2
RQ to Vector + CTX Day 8
Day 3
Day 5
Day 8
***
*
Day post electroporation

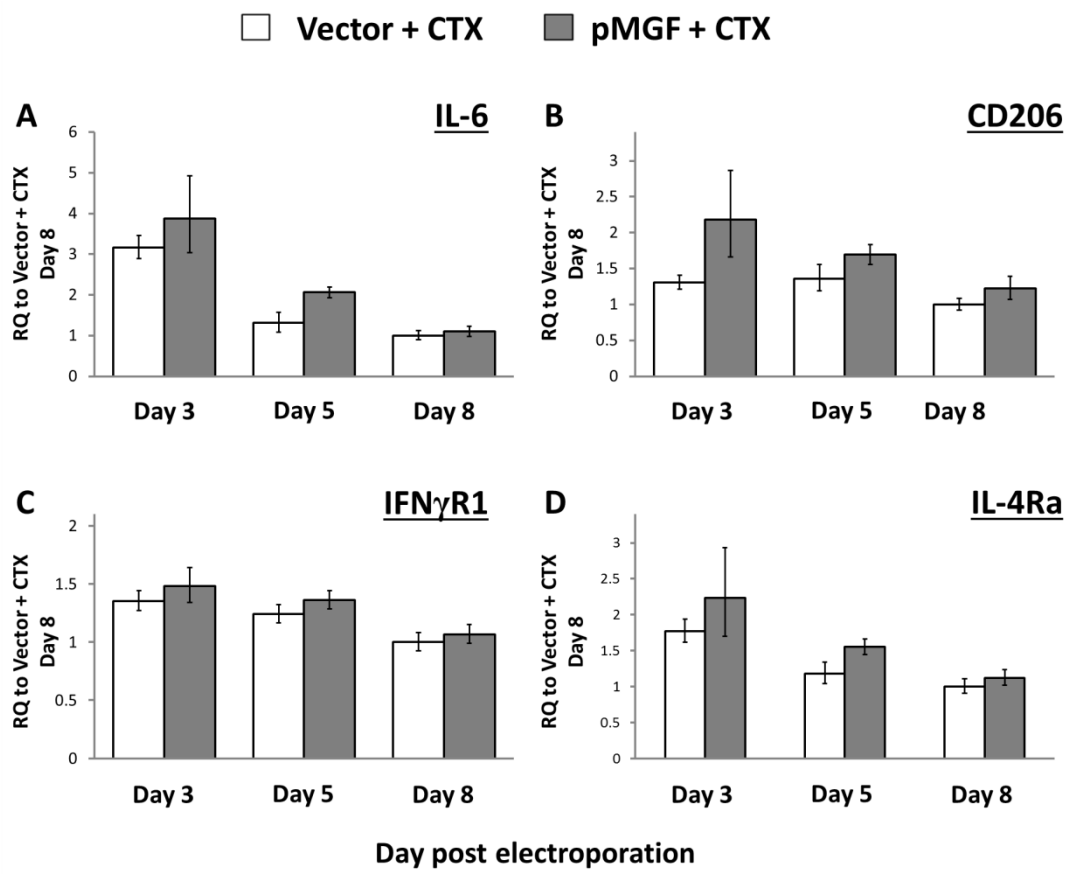

Figure 4.10 Transcript expression profiles of other inflammatory markers in MGF-overexpressed CTX-injured muscle. Samples were collected from day 3 to day 8 post electroporation. The illustrated genes were (A) IL-6; (B) CD206; (C) IFNγR1; and (D) IL-4Ra. The empty bars represented the vector+ CTX injury and the filled bars represented pMGF+ CTX injury (n= 6/ treatment/ timepoint). Expression level was relative to day 8 vector+ CTX injury (mean ± SEM). Significant major effects of MGF overexpression were found in IL-6 and CD206 ($P < 0.05$) but no significance from post-hoc Student's t-test. Abbreviation: RQ= relative quantification.

4.3.2.2 Refined inflammatory phases of muscle regeneration based on inflammatory macrophage profile

We showed that overexpression of MGF delayed the downregulation of inflammatory markers. Macrophage markers CD86 and CD206 (in trend) were upregulated implying that more macrophages might be present within the injured muscle. To demonstrate the roles of MGF on macrophage population, flow cytometry was carried out on mononuclear cells isolated from MGF-overexpressed CTX-injured muscles from day 1 to day 6. The percentages of macrophages and its sub-populations were shown in Figure 4.11. We previously denoted inflammatory phase by single timepoint in Chapter 3 based on the expression of inflammatory markers. Here we refined the designation by day post electroporation based on the control macrophage profiles in vector+ CTX injury muscle.

During muscle injury, increasing total macrophages was observed from day 1 to day 4 indicating infiltration and expansion of macrophages within the injured muscle. The major constituent of the macrophage population was pro-inflammatory M1 MP which accounted for more than 50% of total macrophages. The increase of M1 MP began at day 1 followed by other macrophages (day 2) and M2 MP (day 3). Given the profound infiltration and expansion of different macrophage populations, day 1 to day 4 should be referred to as inflammatory phase of muscle regeneration (Tidball, 2005; Tidball & Villalta, 2010; Martinez & Gordon, 2014). In Chapter 3, it was denoted by a single timepoint as day 2 post CTX injury.

The total macrophages reached peak at day 4 followed by sharp drop on the next day that indicated the commencement of inflammatory

resolution from day 4 onward. The resolution have not been completed at day 6 and total macrophages remained higher than the baseline level (day 6> day 1, P< 0.01). Yet, when the sub-population analysis was taken into consideration, day 6 was in fact the time when resolution of M1 MP completed. A drastic drop of M1 MP was evident from day 4 to day 5 whereas M2 MP and other macrophages were increasing modestly. As the resolution of M1 MP coincided with rising anti-inflammatory M2 phenotype, day 4 to day 6 should be referred to as the early resolution phase. It is characterized by macrophage polarization into M2 phenotype and resolution of pro-inflammatory cells to support the upcoming regeneration activities (Tidball, 2005, 2011; Tidball & Villalta, 2010). This phase was previously denoted as day 4 post CTX injury in Chapter 3.

Although the cytometry profiles could not demonstrate the resolution of M2 MP, this population was presumably resolved after day 6 post electroporation (i.e. about day 7 post CTX injury in Chapter 3). The late resolution phase was evaluated by IHC staining (Section 4.3.2.5). To summarize, the inflammatory phases of MGF overexpression CTX-induced muscle injury model were inflammatory phase: day 1 to day 4 post electroporation; early resolution phase: day 4 to day 6 post electroporation and late resolution phase: likely after day 6 post electroporation.

4.3.2.3 Unaffected infiltration and expansion of macrophages at the inflammatory phase

As described in the last section, inflammatory phase was referred to day 1 to day 4 characterized by increasing macrophage populations. The increasing trends were similar between pMGF+ CTX injury and vector+ CTX injury (pMGF+ CTX injury= vector+ CTX injury at day 1, day 2, day 3 and day 4; all P> 0.05). Thus, the overexpression of MGF appeared not affecting infiltration or expansion of total macrophages and the sub-populations (i.e. M1 MP, M2 MP and other macrophages) at the inflammatory phase. To confirm the finding, we analyzed myeloid cell and macrophage infiltration at day 3 by IHC staining using specific CD11b and F4/80 antibodies. The representative images and the quantitative analysis of immunopositive area were shown in Figure 4.12.

Muscle inflammatory response was prominent after CTX-induced muscle injury. Immunopositive staining of CD11b and F4/80 were intense and abundant within the injured loci. Interstitial and myofiber invasion by myeloid cells (CD11b+) and macrophages (F4/80+) were evident. It was noteworthy that a few myofibers within the injured loci appeared morphologically normal with peripheral nuclei and immunonegative for both CD11b and F4/80. In quantitative analysis, immunopositive area of CD11b and F4/80 were measured separately. Similar to flow cytometry data, no difference was found between pMGF+ CTX injury and the corresponding control despite the prevalent invasion of inflammatory cells at day 3 (Student's t-test, P> 0.05). Flow cytometry and IHC assessment provided consistent findings and solid evidence that MGF overexpression did not modulate the infiltration or expansion of myeloid cells and macrophages (i.e. inflammatory phase) in response to CTX-induced muscle injury.

Figure 4.11 Macrophage profile in MGF-overexpressed CTX-injured muscle. Samples were collected from day 1 to day 6 post electroporation. (A) %Total macrophages (CD11b+/ F4/80+); (B) %M1 MP (CD11b+/ F4/80+/ Ly6C+/ CD206−); (C) %M2 MP (CD11b+/ F4/80+/ Ly6C−/ CD206+); (D) %Other macrophages (CD11b+/ F4/80+/ Ly6C+/ CD206+ and CD11b+/ F4/80+/ Ly6C−/ CD206−). The grey line represented the vector+ CTX injury and the black line represented pMGF+ CTX injury (n= 4/ treatment from day 1 to day 3 and n= 6/ treatment from day 4 to day 6). Data are expressed in mean ± SEM. Comparison between pMGF+ CTX injury and vector+ CTX injury at each timepoint by post-hoc Student's t-test: *P< 0.05, **P< 0.01.

(*Overleaf*)

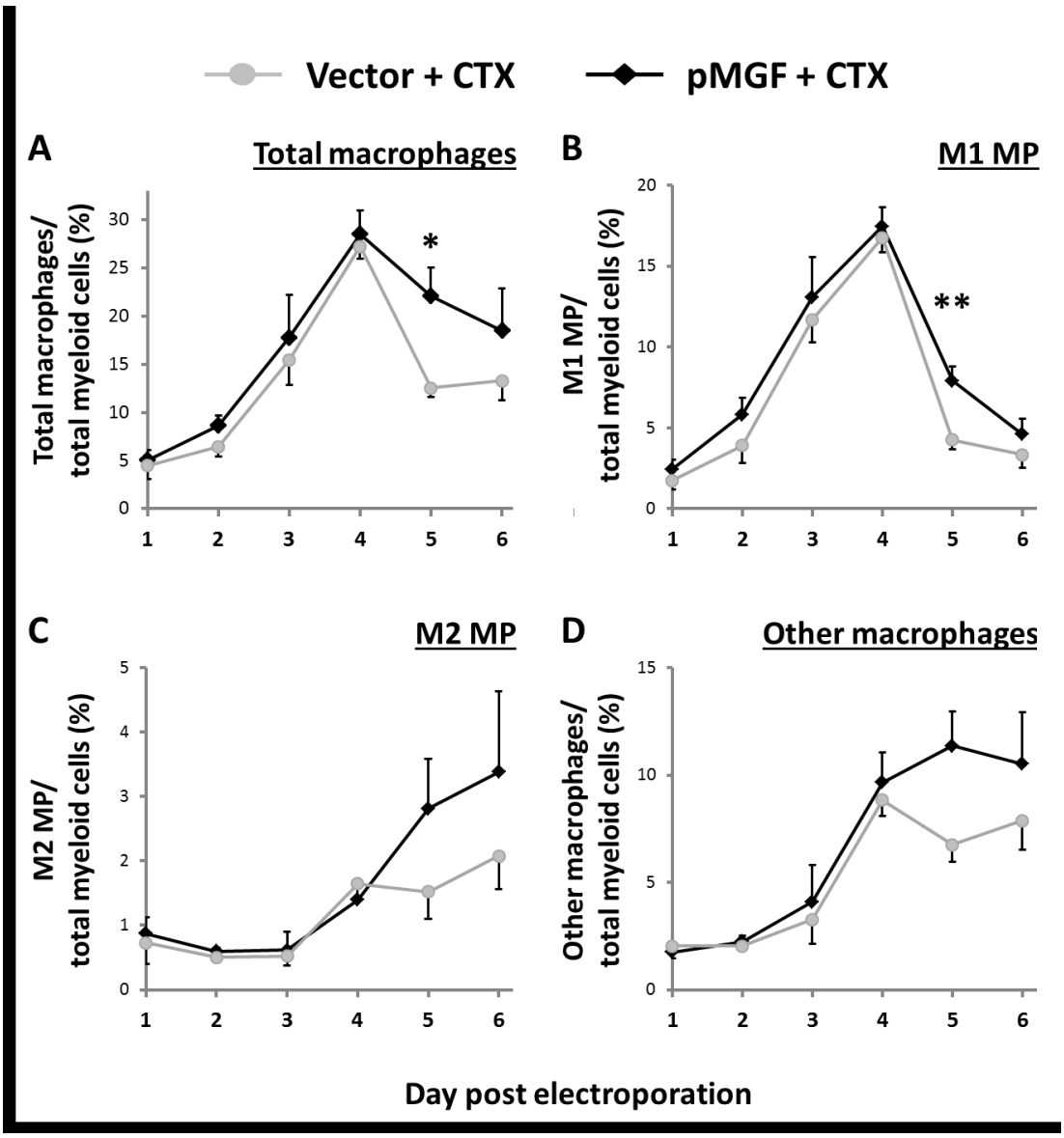
Vector + CTX
pMGF + CTX
A
Total macrophages
Total macrophages/ total myeloid cells (%)
*
B
M1 MP
M1 MP/ total myeloid cells (%)
**
C
M2 MP
M2 MP/ total myeloid cells (%)
D
Other macrophages
Other macrophages/ total myeloid cells (%)
Day post electroporation

Figure 4.12 Infiltration of myeloid cells and macrophages in MGF-overexpressed CTX-injured muscle. Samples were collected at day 3 post electroporation. (A) Representative images of CD11b (Upper) and F4/80 (lower) immunostaining on muscle of day 3 post electroporation. All the images were captured at 40X magnification with scale bar= 50 μm. The staining of CD11b (myeloid cells) and F4/80 (macrophages) were fluorescence green whereas DAPI signal was blue. The white arrows indicated the infiltrated myofibers and interstitial area. The asterisks indicated the non-infiltrated myofibers with peripheral nuclei and unstained cytoplasm. (B) Quantitative measurement of immunopositive area. Data were divided by total measured area and expressed in percentage (mean ± SEM). The empty bars represented the vector+ CTX injury and the filled bars represented pMGF+ CTX injury (n= 4/ treatment). No significant difference was detected between groups in both CD11b and F4/80 immunostaining.

(*Overleaf*)

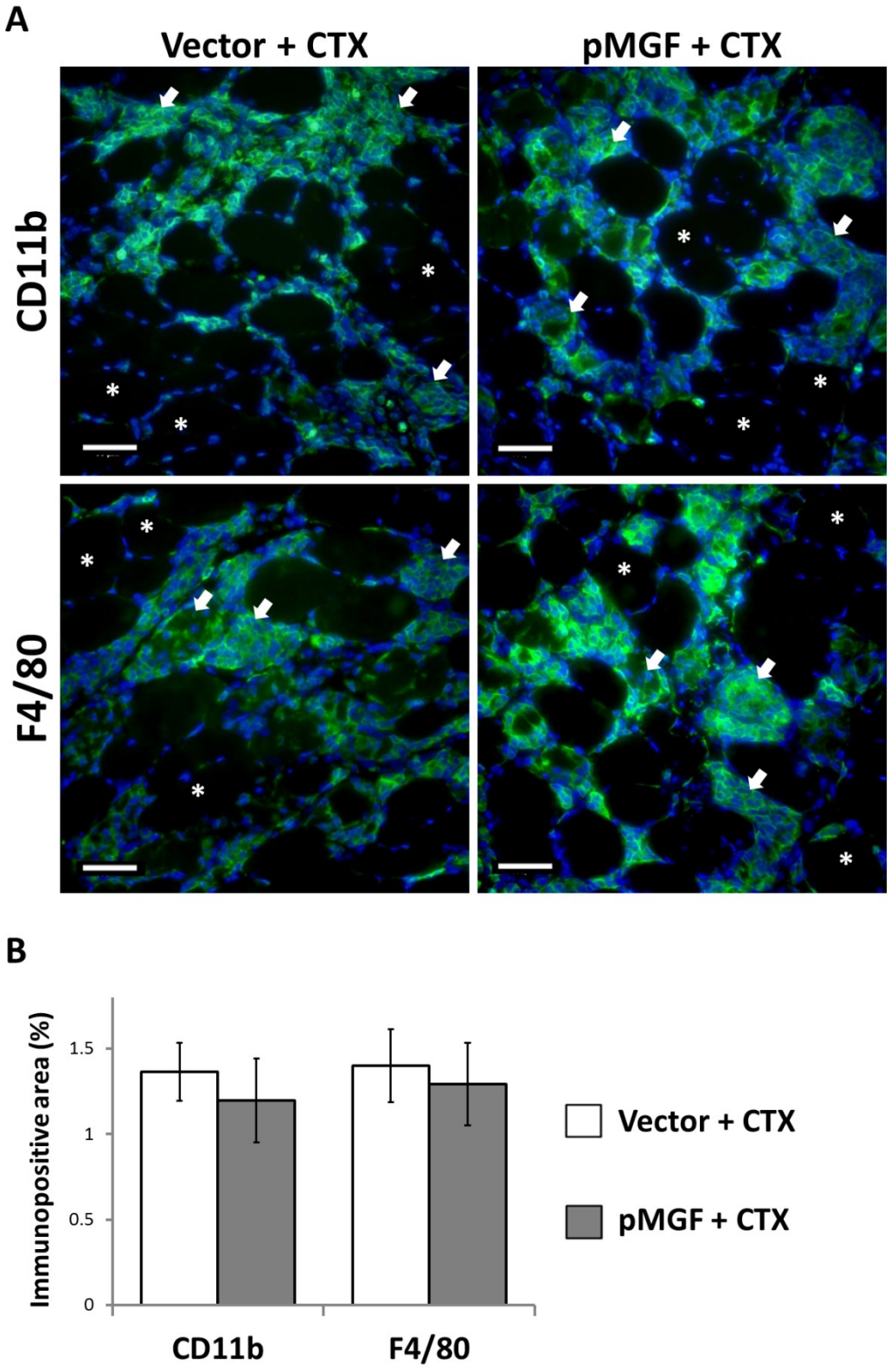
A
Vector + CTX
pMGF + CTX
CD11b
F4/80
B
Immunopositive area (%)
1.5
1
0.5
0
CD11b
F4/80
Vector + CTX
pMGF + CTX

4.3.2.4 Prolonged presence of M1 MP during early resolution phase

Early resolution phase was characterized by the decrease of total macrophages and M1 MP from day 4 to day 6 (referred to Figure 4.11). At day 4, total macrophages and sub-populations were not different between pMGF+ CTX injury and vector+ CTX injury. However, significant effect was observed at day 5 in which there were more total macrophages in MGF-overexpressed CTX-injured muscle ($P < 0.05$). Sub-population analyses indicated more abundant M1 MP in day 5 pMGF+ CTX injury ($P < 0.01$). Apparently, M1 MP should account for the changes in total macrophage population at the same timepoint. At day 6, the percentages of both total and M1 MP were no longer different between pMGF+ CTX injury and vector+ CTX injury. Besides, M1 MP has returned to baseline level (day 1) at day 6 in both groups. Overexpression of MGF thus transiently prolonged the presence of M1 MP which also accounted for the increase of total macrophages during early resolution phase (i.e. day 5). In addition, M2 MP began increasing at day 3 and peaked at about day 5 or day 6. Similarly, other macrophages predominantly double positive of both M1 and M2 markers increased at day 2 and peaked at about day 5 or day 6. The increasing trends were the same between pMGF+ CTX injury and vector+ CTX injury until day 5. The increase appeared to be promoted by MGF overexpression although the difference did not reach statistical significance.

4.3.2.5 Comparable myeloid cells and macrophages at the late phase of resolution

We deduced from the flow cytometry profiles (Section 4.3.2.2) that the late resolution phase should take place from day 6. To confirm this postulate and also to evaluate the potential effect of MGF overexpression on late resolution phase, we evaluated muscle cryosections at day 6 and day 8 by IHC staining against myeloid cells (CD11b+) and macrophages (F4/80+). Compared with flow cytometry, IHC staining allowed separate counting of resident MP from the infiltrated interstitial population based on their spatial location (Brigitte *et al.*, 2010). Macrophages on epimysium, indicating resident MP, were readily identified. Infiltrated macrophages could be identified at interstitium only. The results of counting were summarized in Figure 4.13. The numbers of CD11b+ myeloid cells at epimysium, interstitial space and the total count were not different between pMGF+ CTX injury and vector+ CTX injury control (all $P > 0.05$). The same applied to the results of F4/80+ macrophages (all $P > 0.05$). Therefore, late resolution of myeloid cells and macrophages was not affected by MGF overexpression.

Figure 4.13 Resolution of myeloid cells and macrophages in MGF-overexpressed CTX-injured muscle. Samples were collected at day 6 and day 8 post electroporation. The count data are divided by total number of myofibers (mean ± SEM). The empty bars represented the vector+ CTX injury and the filled bars represented pMGF+ CTX injury (n= 4/ treatment/ timepoint). No significant difference was detected amongst comparisons.

(*Overleaf*)

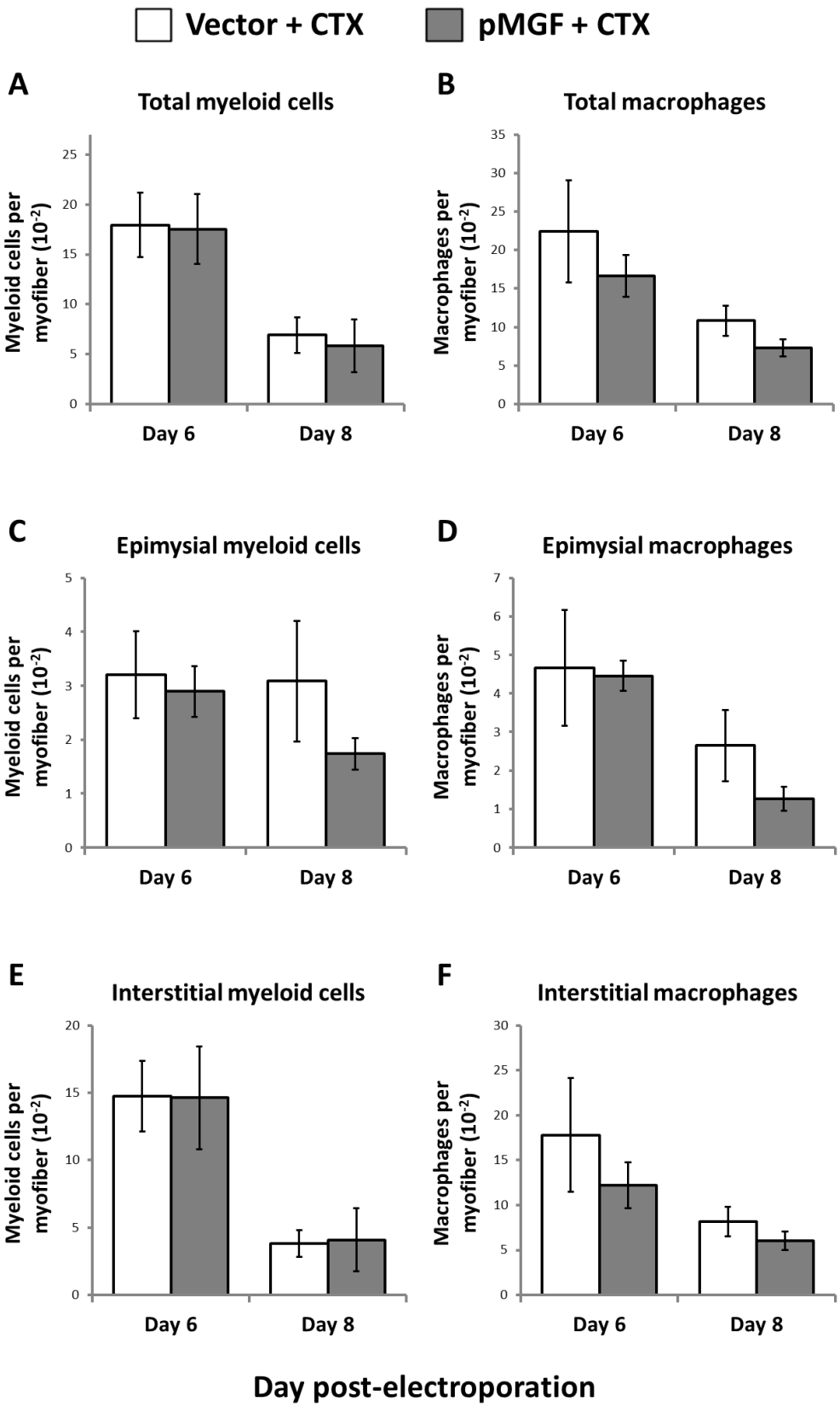
Vector + CTX
pMGF + CTX
A
Total myeloid cells
Myeloid cells per myofiber (10-2)
Day 6
Day 8
B
Total macrophages
Macrophages per myofiber (10-2)
C
Epimysial myeloid cells
D
Epimysial macrophages
E
Interstitial myeloid cells
F
Interstitial macrophages
Day post-electroporation

4.3.2.6 Summary

Overexpression of MGF was achievable even in the presence of CTX-induced injury. We refined the inflammatory phases based on the macrophage profiles. No difference was observed in the inflammatory phase (day 1 to day 4) in terms of inflammatory marker expression and macrophage profiles. However, downregulation of inflammatory markers taking place in early resolution phase (day 4 to day 6) was delayed in muscles of pMGF+ CTX injury group. More macrophages, particularly M1 MP, were detected at day 5 in MGF-overexpressed CTX-injured muscle which coincided with upregulated M1 marker CD86. Role of MGF in early resolution was thus suggested. As for late resolution phase (after day 6), inflammatory markers remained significantly higher in pMGF+ CTX injury. Yet, we observed no difference in resident MP and interstitial macrophages from histology. Lastly, the overexpression of MGF did not modulate the expression of IGF-1Ea during muscle regeneration. The aforesaid changes should be attributed to MGF overexpression.

4.3.3. Muscle regeneration outcomes apparently not influenced by MGF overexpression

We observed delayed downregulation of inflammatory markers and transient change of macrophage sub-populations in previous section. Aim 3 of this study was to demonstrate the association of muscle regeneration with these alterations in inflammatory response due to MGF overexpression. We

thus investigated the effect of MGF overexpression on muscle regeneration outcomes at histological and transcript level.

4.3.3.1 Unaltered histology of regenerating muscle

Histologically, the representative H&E staining of injured muscle at day 8 post electroporation was shown in Figure 4.14. Presence of centrally nucleated myofibers was evident. The CSA of centrally nucleated myofibers varied in both pMGF+ CTX injury and vector+ CTX injury groups. The CSA of some centrally nucleated myofibers was similar to the adjacent peripherally nucleated normal myofibers. Quantitative measurement showed that MGF overexpression had no effects on the percentage or mean CSA of centrally nucleated myofibers, on both day 6 and day 8 (Figure 4.15). The same percentage of centrally nucleated myofibers implied that MGF overexpression and the altered inflammatory response might not affect the formation of centrally nucleated myofibers.

Despite the same mean CSA of centrally nucleated myofibers ($P > 0.05$), further analyses based on the distribution of CSA were conducted. Significant increase in CSA was observed from day 6 to day 8 reflecting the regeneration process. For instance, centrally nucleated myofibers of smallest CSA (below 550 μm^2) decreased significantly from day 6 to day 8 in both treatment groups (both $P < 0.05$). Significant increases of $\geq$550 – 1100 μm^2 and $\geq$1100 – 1650 μm^2 categories from day 6 to day 8 were also observed in pMGF+ CTX injury and vector+ CTX injury respectively.

There was, however, no difference between pMGF+ CTX injury and vector+ CTX injury at each CSA category suggesting MGF overexpression did not modify the hypertrophy of centrally nucleated myofibers. It was noteworthy that most of the centrally nucleated myofibers (> 80%) in both pMGF+ CTX injury and vector+ CTX injury group fell into the two smallest categories (i.e. below 550 μm^2 and $\geq$ 550 μm^2 to 1100 μm^2). Thus, ongoing muscle regeneration and myofiber hypertrophy was suggested. Whether pMGF+ CTX injury and vector+ CTX injury displayed difference at later timepoints was unclear.

Collectively, regeneration and hypertrophy of CTX-injured myofibers appeared not to be affected by MGF overexpression at the evaluation timepoints chosen.

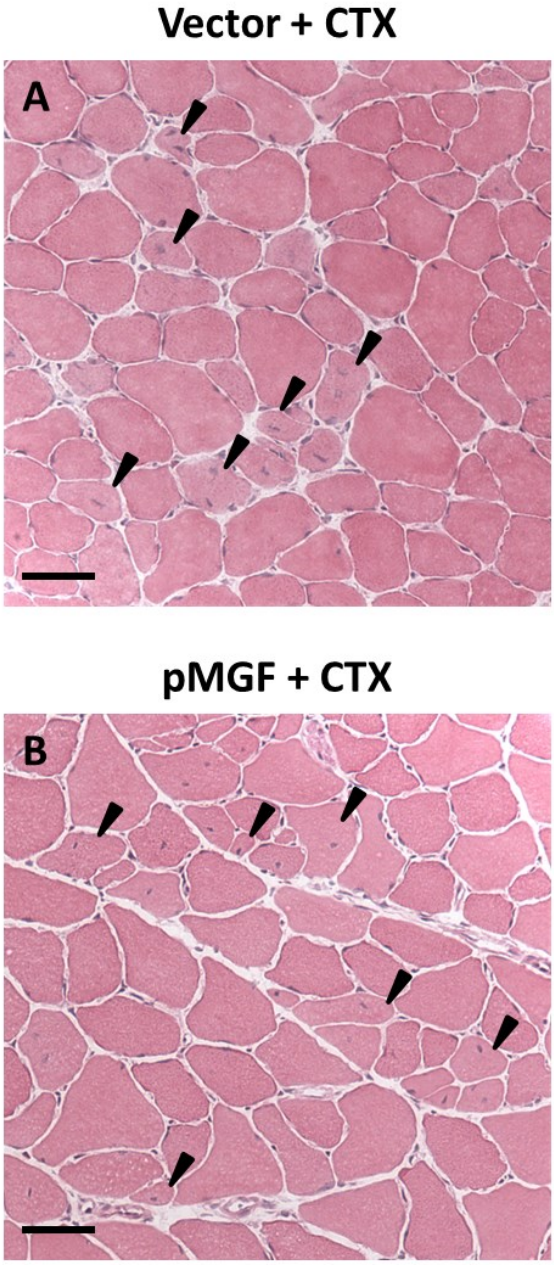

Figure 4.14 H&E staining of MGF-overexpressed CTX-injured muscle. Samples were collected at day 8 post electroporation (n= 8/ treatment). (A) Vector+ CTX injury and (B) pMGF+ CTX injury. All the images were captured at 40X magnification with scale bar= 50 µm. Arrow heads represented the centrally nucleated myofibers of various sizes.

Figure 4.15 Quantitative analyses on the histology of MGF-overexpressed CTX-injured muscle. (A) Percentage of centrally nucleated myofibers and (B) mean CSA of centrally nucleated myofibers. The empty bars represented the vector+ CTX injury and the filled bars represented pMGF+ CTX injury. (C) CSA distribution of centrally nucleated myofibers. Data are expressed in mean ± SEM (n= 4/ treatment/ timepoint). Comparison between day 6 and day 8 by post-hoc Student's t-test in vector+ CTX injury: *P< 0.05; and pMGF+ CTX injury: ^p<0.05. Abbreviation: CN myofibers= centrally nucleated myofibers; CSA= cross-sectional area.

(*Overleaf*)

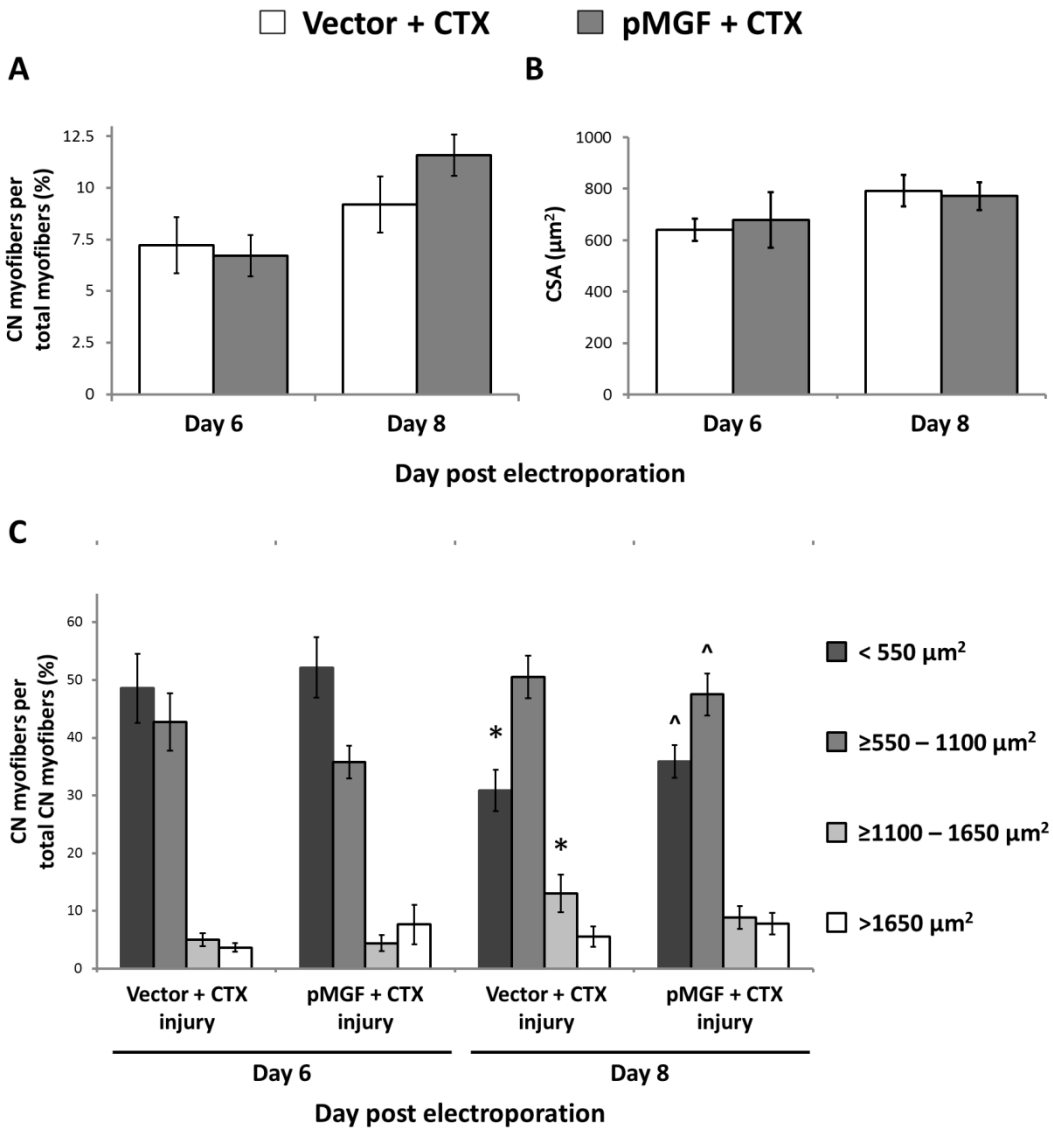
Vector + CTX
pMGF + CTX
A
B
CN myofibers per total myofibers (%)
12.5
10
7.5
5
2.5
0
Day 6
Day 8
CSA (µm²)
1000
800
600
400
200
0
Day 6
Day 8
Day post electroporation
C
CN myofibers per total CN myofibers (%)
60
50
40
30
20
10
0
< 550 µm²
≥550 – 1100 µm²
≥1100 – 1650 µm²
>1650 µm²
*
*
^
^
Vector + CTX injury
pMGF + CTX injury
Vector + CTX injury
pMGF + CTX injury
Day 6
Day 8
Day post electroporation

4.3.3.2 Unaltered expression of regeneration markers

The expression profiles of regeneration markers were illustrated in Figure 4.16 including satellite cell marker (Pax7); MRF including MyoD and Myog; and MHC isoforms including Myh3 (embryonic form) and Myh8 (neonatal form). Amongst all the investigated genes examined, none of them was altered by MGF overexpression. The expression of Pax7 remained unchanged throughout the evaluation window. Satellite cell population appeared not affected by MGF overexpression and muscle regeneration. All other genes showed major effect of time (all $P< 0.001$) suggesting alternation of these genes during regeneration. High level of MRF could be observed from day 3 indicating myogenesis. The level of MRF decreased with time which was followed by upregulation of MHC at day 5. The MHC isoforms, Myh3 and Myh8, predominantly express in regenerating myofibers (Shavlakadze *et al.*, 2004; Musarò, 2014). The sequential upregulation of MRF and MHC isoforms suggested the muscle was undergoing regeneration. However, MGF overexpression has no observable effect on this process.

Figure 4.16 Transcript expression profiles of regeneration markers in MGF-overexpressed CTX-injured muscle. Samples were collected from day 3 to day 8 post electroporation. The respective genes were (A) Pax7; (B) MyoD; (C) Myog; (D) Myh3; and (E) Myh8. The empty bars represented the vector+ CTX injury and the filled bars represented pMGF+ CTX injury (n= 6/ treatment/ timepoint). Expression level was relative to the day 8 vector+ CTX injury. None of the comparison resulted in significant major effect of MGF overexpression. Abbreviation: RQ= relative quantification.

(*Overleaf*)

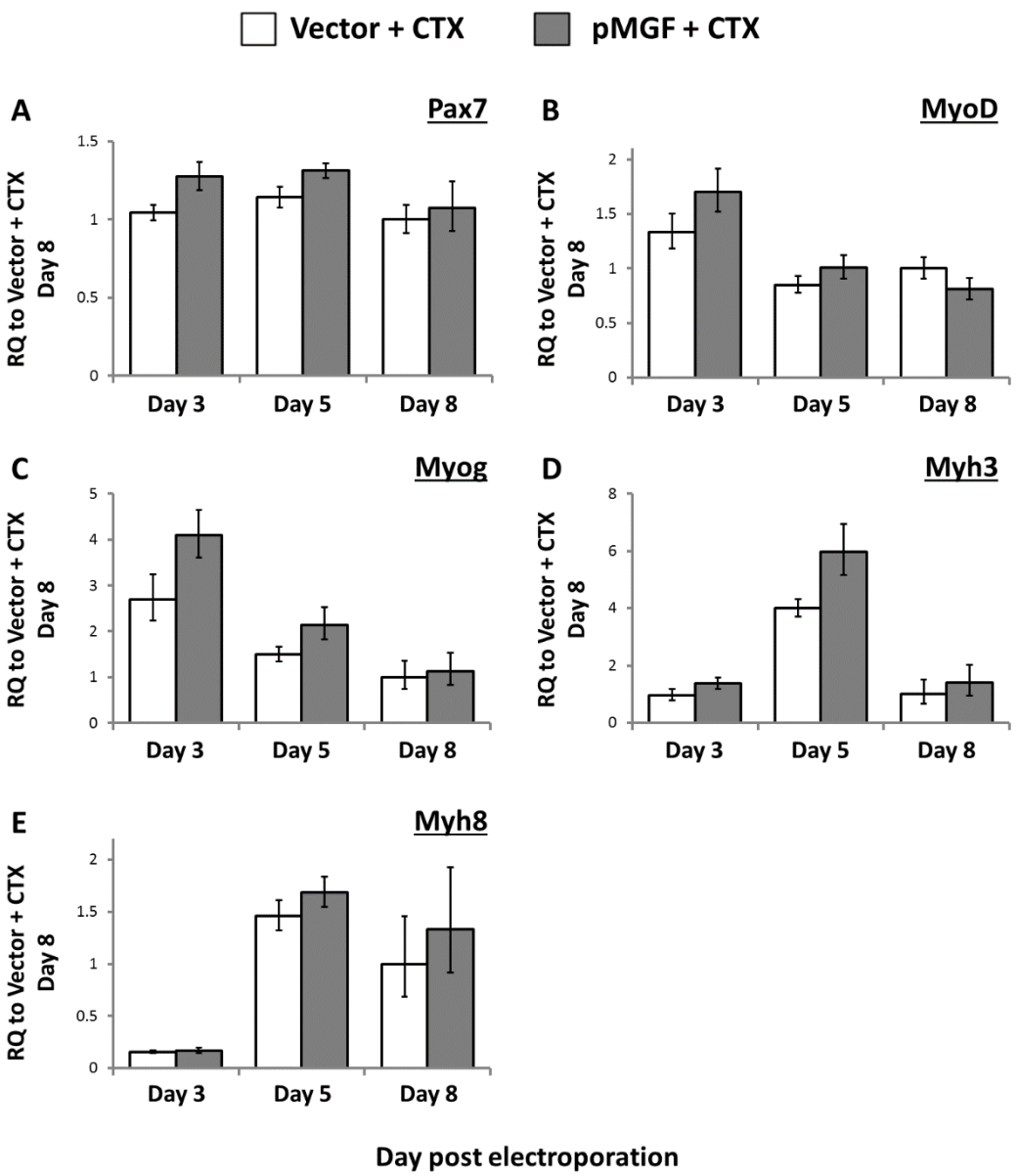
Vector + CTX
pMGF + CTX
A
Pax7
B
MyoD
C
Myog
D
Myh3
E
Myh8
RQ to Vector + CTX Day 8
Day 3
Day 5
Day 8
Day post electroporation

4.3.4. Contributing cells to inflammatory marker upregulation by MGF overexpression

We observed upregulation of inflammatory markers (i.e. TNF-α, IL-10, CD86 and CCL2) at tissue level at day 5 (Section 4.3.2.1). It coincided with more total and M1 MP in pMGF+ CTX injury at day 5 (Section 4.3.2.4). The temporal association might suggest that the presence of macrophages was prolonged by MGF overexpression which contributed to upregulation of inflammatory markers at tissue level.

Although macrophages are able to express the aforesaid inflammatory markers in injured muscle (Lai *et al.*, 1998; Martinez & Gordon, 2014; Tidball, 2017), it was unclear whether the macrophages were still expressing those inflammatory markers in MGF-overexpressed CTX-injured muscle at day 5. Thus, macrophages were FACS-collected from day 5 MGF-overexpressed CTX-injured muscle for transcript expression profiling. Moreover, comparison between cells isolated from muscles of pMGF+ CTX injury and vector+ CTX injury might suggest if MGF overexpression *in vivo* regulated the expression of these transcripts in macrophages.

Beside macrophages, it was also possible that other skeletal muscle resident cells (e.g. satellite cells, myofibers, fibroblasts, FAP) were responsive to MGF overexpression and upregulated these markers. In particular, cytokines like TNF-α and CCL2 were known to be expressed by muscle cells in response to injury or mechanical stimulation (Collins & Grounds, 2001; Peake *et al.*, 2015). Myofibers were electroporated with pMGF where availability of MGF was presumably the highest. Moreover,

muscle cells are responsive to IGF-1 signaling (see reviews in Section 1.4.4-1.4.6). It was thus possible that muscle cells might potentially contribute to the upregulation. To evaluate the potential contribution from muscle cells, we assessed the expression of aforesaid inflammatory markers in MGF-overexpressed C2C12 cells (both proliferating and differentiating culture). As for the potential involvement of other resident cells, we evaluated MGF-overexpressed non-injured muscle. Infiltration of myeloid cells was minimal in these samples compared with CTX-induced injury (Section 4.3.1.2). Accompanying with the *in vitro* data on C2C12 cells, the significance of infiltrated macrophages in contribution of inflammatory marker upregulation in response to MGF overexpression was suggested.

To summarize, the goal of the experiments was to elucidate the contribution of infiltrated macrophages to the upregulation of inflammatory markers in response to MGF overexpression. The evaluation included: (i) the transcript profile of infiltrated macrophages in muscle from day 5 pMGF+ CTX injury; (ii) the transcript profile of MGF-overexpressed muscle cells *in vitro*; and (iii) the transcript profile of MGF-overexpressed non-injured muscle.

4.3.4.1 Unaltered inflammatory marker expression in macrophages

To confirm altered macrophage abundance leading to changes in muscle inflammatory marker expression, we FACS-collected macrophages and other myeloid cells at day 5 (i.e. the timepoint displayed significantly more M1 MP and higher inflammatory marker expression *in vivo*) and evaluated their inflammatory marker expression. The genes that responded to MGF overexpression, including TNF-α, IL-10, CD86 and CCL2, were again evaluated. In addition, evaluation of IGF-1Ea was included to determine if MGF altered IGF-1Ea expression in macrophages. The data were demonstrated in Figure 4.17.

All the evaluated genes were readily detected in macrophages and other myeloid cells collected from day 5 MGF-overexpressed CTX-injured muscle. It implied that more macrophages within the muscle potentially led to the upregulation of inflammatory markers at tissue level. Whether the cells examined were macrophages or other myeloid cells, the assessed inflammatory genes exhibited no differences between pMGF+ CTX injury and vector+ CTX injury (all $P > 0.05$). Thus it should most likely be the increase in macrophage population but not promoting transcription in these cells that accounted for the upregulation of inflammatory markers at tissue level. Of note, expression of IGF-1Ea could be detected from the two isolated myeloid progenies but it was not altered by MGF overexpression.

Figure 4.17 Transcript expression profiles of inflammatory markers in myeloid cells and macrophages. Cells were isolated from MGF-overexpressed CTX-injured muscle at day 5 post electroporation. The sample cell identity of the graphs was (A) macrophages and (B) other myeloid cells. The empty bars represented the vector+ CTX injury and the filled bars represented pMGF+ CTX injury (n= 3/ cell/ treatment). Expression level was relative to the corresponding vector+ CTX injury (mean ± SEM). In both cell types, none of the comparison exhibited significant difference. Abbreviation: RQ= relative quantification.

(*Overleaf*)

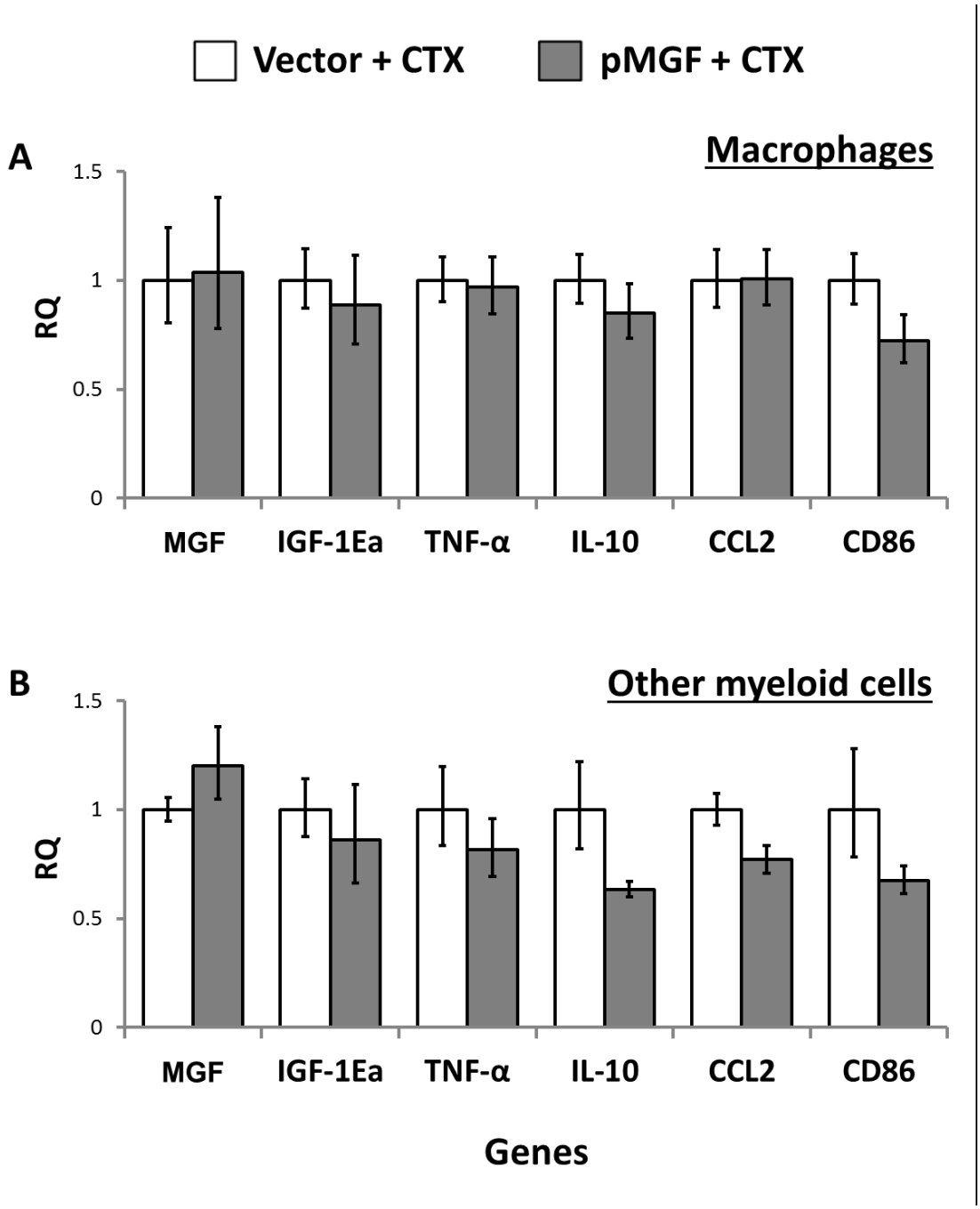
Vector + CTX
pMGF + CTX
A
Macrophages
RQ
1.5
1
0.5
0
MGF
IGF-1Ea
TNF-α
IL-10
CCL2
CD86
B
Other myeloid cells
RQ
1.5
1
0.5
0
MGF
IGF-1Ea
TNF-α
IL-10
CCL2
CD86
Genes

4.3.4.2 Muscle cells - *in vitro* evaluation

To evaluate the potential contribution from muscle cells, inflammatory marker expression in MGF-overexpressed C2C12 was evaluated. The samples were the same as in Section 4.3.1.3 in which *in vitro* MGF overexpression had been confirmed. The expression of genes TNF-α, IL-10 and CCL2 in proliferating and differentiating C2C12 were illustrated in Figure 4.18. Of note, CD86 is a macrophage marker and thus not evaluated in this experiment despite the altered expression *in vivo*. Remarkably, IL-10 transcript was undetectable in C2C12 cells whether in the proliferating or the differentiating culture, coincided with human myoblast (Nagaraju *et al.*, 1998; Peake *et al.*, 2015). Instead of upregulation, intriguingly, proliferating C2C12 cells with MGF overexpression demonstrated suppression of TNF-α and CCL2 transcript expression 48 h post transfection. Differentiating C2C12 was however irresponsive to the MGF overexpression. To summarize, muscle cells like myoblasts and myofibers were less likely to be the contributing cells for the upregulated inflammatory markers observed *in vivo*.

Figure 4.18 TNF-α and CCL2 transcript expression in MGF-overexpressed C2C12 cells. Expression level in proliferating culture (A, C and E) and differentiating culture (B, D and F). Genes evaluated: (A, B) MGF; (C, D) TNF-α; (E, F) CCL2. IL-10 transcript was undetectable from all samples. The empty bars represented the vector and the filled bars represented pMGF (n= 3/ cell/ treatment/ timepoint). Expression level was relative to the 48 h vector (mean ± SEM). Comparison between pMGF and vector at each timepoint by post-hoc Student's t-test: *P< 0.05, **P< 0.01 and ***P< 0.001. Abbreviation: RQ= relative quantification; h= hour; Pro= proliferating C2C12; Diff= differentiating C2C12.

(*Overleaf*)

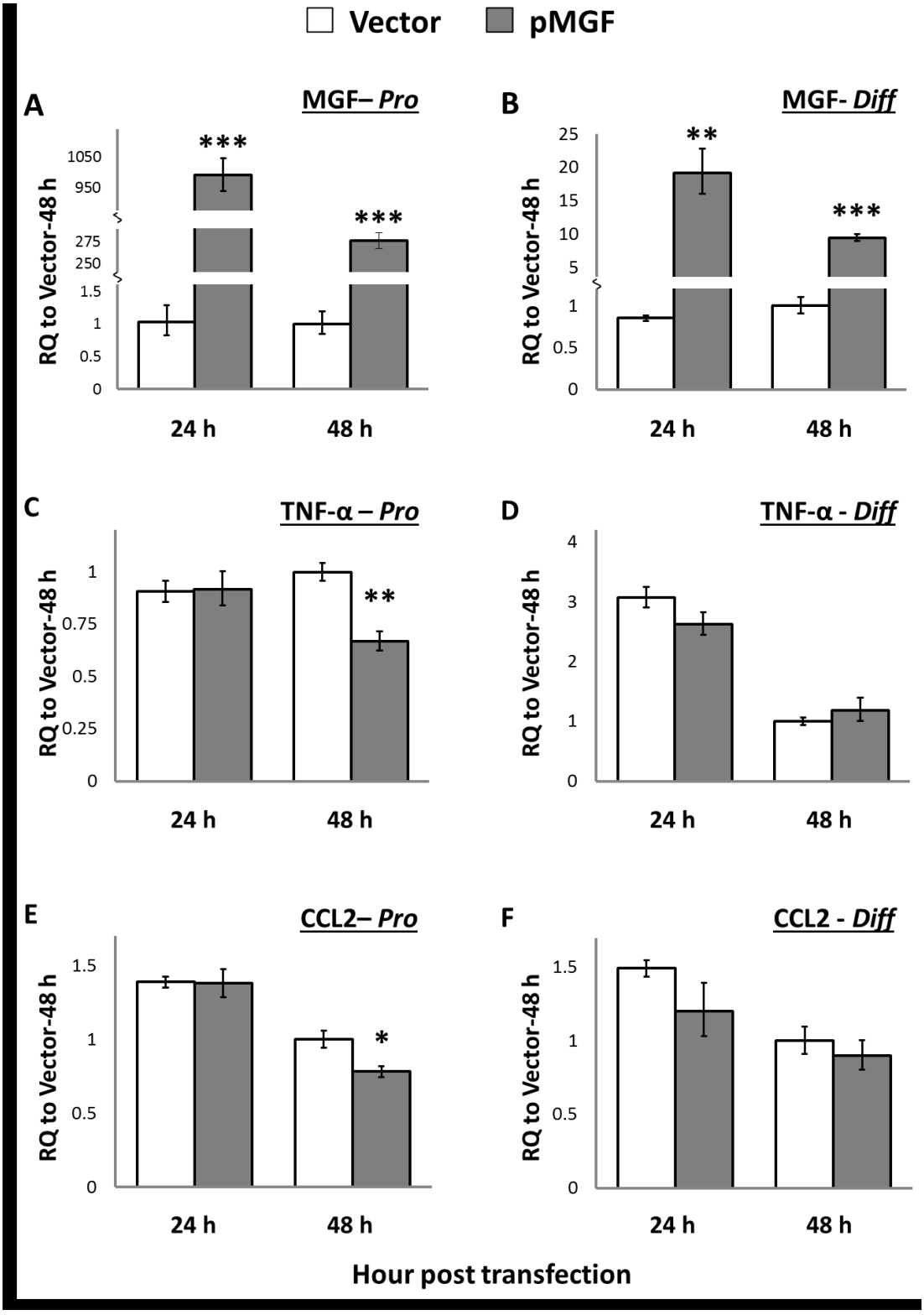
Vector
pMGF
A
MGF– Pro
RQ to Vector-48 h
1050
950
275
250
1.5
1
0.5
0
***
***
24 h
48 h
B
MGF- Diff
25
20
15
10
5
1
0.5
0
**
***
24 h
48 h
C
TNF-α – Pro
1
0.75
0.5
0.25
0
**
24 h
48 h
D
TNF-α - Diff
4
3
2
1
0
24 h
48 h
E
CCL2– Pro
1.5
1
0.5
0
*
24 h
48 h
F
CCL2 - Diff
1.5
1
0.5
0
24 h
48 h
Hour post transfection

4.3.4.3 Potential involvement of resident cells in injured muscle

From the last two sections, we suggested the possibility that upregulation of inflammatory cytokines in muscle of day 5 pMGF+ CTX injury was not due to the transcriptional upregulation in muscle cells or macrophages. Apparently, the prolonged presence of macrophages at day 5 accounted for the upregulation. To confirm the essence of infiltrated macrophages, MGF-overexpressed non-injured muscle was evaluated in which MGF overexpression had been confirmed (Section 4.3.1.3). Tissue damages and the subsequent macrophage infiltration within these samples were minimal and presumably negligible when compared to those with CTX-induced injury (Section 4.3.1.2 and Figure 4.5). Thus, the effect of MGF overexpression on upregulation of inflammatory marker should diminish in the absence of CTX injection, unless infiltrated macrophages were not the sole mediating cells. The expression profile of pMGF and vector (no CTX injection) electroporated muscle was illustrated in Figure 4.19. Of note, MGF transcript had been confirmed overexpressing throughout the evaluation timeframe without altering IGF-1Ea expression (Figure 4.7).

Inflammatory marker expression level was the highest at day 1. It implied initiation of muscle inflammatory response (Tidball, 2017) despite the minimal inflammatory infiltration at later timepoint (day 2; Figure 4.5). Besides, the upregulation of TNF-α and CCL2 at day 1 was enhanced by MGF overexpression. Notably, macrophage infiltration was minimal at day 1 and gradually increased to peak at day 4 in the context of CTX-induced injury (Figure 4.11). Cells already existed in the muscle before day 1 and

capable of expressing inflammatory cytokines might mediate the enhanced upregulation of inflammatory markers by MGF overexpression. The enhancement observed at day 1 implicated early infiltrated cells or muscle resident cells as the mediators. Further experiments at timepoints shorter than day 1 were suggested to identify the responsive cell type.

Moreover, it was intriguing to identify the same set of genes upregulated (TNF-α, IL-10, CD86 and CCL2) or unaltered (IL-6, CD206, IFNγR1 and IL-4Ra) in response to MGF overexpression at equivalent timepoints (day 5 and day 8) in the absence of CTX-induced muscle injury. Overexpression of MGF without CTX-induced injury exhibited significantly higher inflammatory marker expression at day 5 and day 8. While decreasing trend was observed from day 1 to day 8 in vector control, the downregulation appeared inhibited in MGF-overexpressed muscle. The similar transcript profiles of MGF-overexpressed muscles with or without CTX-induced injury was unlikely a coincidence but may imply specific responses from muscle resident cells. Yet, it might also suggest CTX-induced injury and infiltrated macrophages were not the sole factors for the effect of MGF overexpression. The contribution of infiltrated and resident progenies could be elucidated by comparing between MGF-overexpressed muscles with and without CTX-induced muscle injury.

Figure 4.19 Transcript expression profiles of inflammatory markers in MGF-overexpressed muscle. Samples were not CTX-injured and collected from day 1 to day 8 post electroporation. Overexpression of MGF had been confirmed from day 1 to day 8 (Figure 4.7). The illustrated genes were (A) TNF-α; (B) IL-10; (C) CD86; (D) CCL2; (E) IL-6; (F) CD206; (G) IFNγR1; and (H) IL-4Ra. The empty bars represented the vector and the filled bars represented pMGF (n= 5/ treatment/ timepoint). Expression level was relative to the day 8 vector (mean ± SEM). Comparison between pMGF and vector at each timepoint by post-hoc Student's t-test: *P< 0.05, **P< 0.01 and ***P< 0.001. Abbreviation: RQ= relative quantification.

(*Overleaf*)

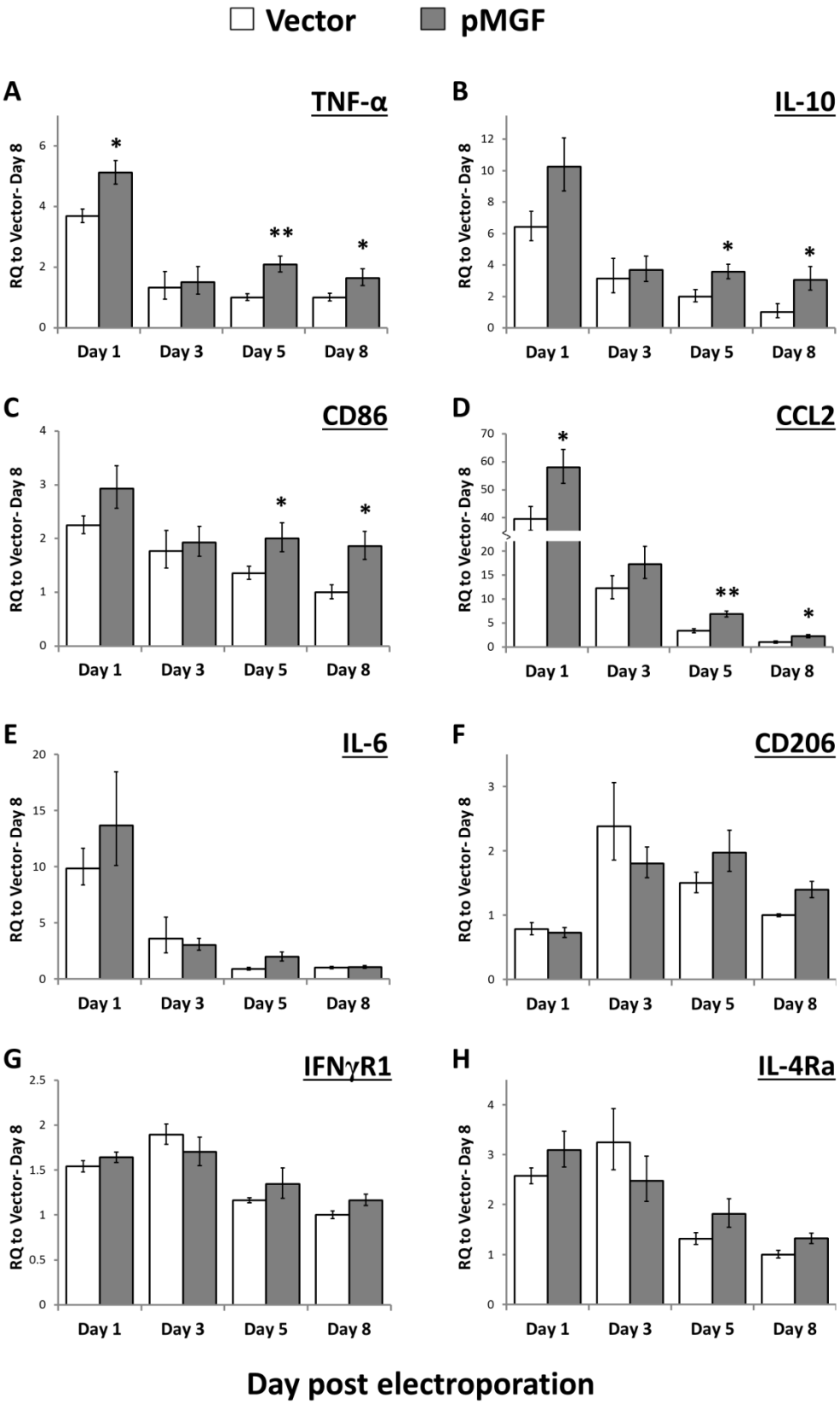
Vector
pMGF
A
TNF-α
B
IL-10
C
CD86
D
CCL2
E
IL-6
F
CD206
G
IFNγR1
H
IL-4Ra
RQ to Vector- Day 8
Day 1
Day 3
Day 5
Day 8
Day post electroporation

4.3.4.4 Contribution of resident and infiltrated cells to inflammatory marker expression in response to MGF overexpression

We confirmed that MGF overexpression induced the same set of inflammatory marker expression (i.e. TNF-α, IL-10, CD86 and CCL2) in both CTX-injured (Figure 4.9) and non-injured muscle (Figure 4.19), in particular, day 5 post electroporation. It was thus possible that both the prolonged presence of M1 MP and muscle resident cells could contribute to higher inflammatory marker expression at day 5. We therefore compared the expression of inflammatory markers between MGF-overexpressed muscles with and without CTX-induced muscle injury (Figure 4.20). The effect of MGF overexpression and CTX injection was compared by two-way ANVOA. Of note, the significant effect of MGF overexpression on the induction of inflammatory markers in CTX-injured and non-injured muscles has been described in Section 4.3.2.1 and 4.3.4.3 respectively.

The major influence of CTX-induced injury was in the expression of TNF-α. The upregulation of TNF-α in MGF-overexpressed CTX-injured muscle was significantly higher than that of MGF-overexpressed non-injured muscle ($P < 0.01$). Such difference suggested that prolonged presence of M1 MP in MGF-overexpressed CTX-injured muscle contributed to further upregulation of inflammatory marker, in addition to resident cells. IL-10, CD86 and CCL2, yet insignificant, displayed similar trends of increased expression in MGF overexpressed CTX-injured muscle.

To summarize, both resident cells and prolonged presence of M1 MP rendered the upregulation of inflammatory markers in MGF-overexpressed muscle.

Figure 4.20 Comparison of transcript expression in MGF-overexpressed muscles with and without CTX-induced injury. (A) MGF; (B) TNF-α; (C) IL-10; (D) CD86; and (E) CCL2. The empty bars represented the vector and the filled bars represented pMGF (n= 5/ treatment/ timepoint). The injection of CTX was indicated at the horizontal axis. Expression level was relative to the vector no CTX control (mean ± SEM). Comparison between pMGF and vector by post-hoc Student's t-test: *P< 0.05, **P< 0.01 and ***P< 0.001; and between no CTX control and CTX-injured: ##P< 0.01. Abbreviation: RQ= relative quantification.

(*Overleaf*)

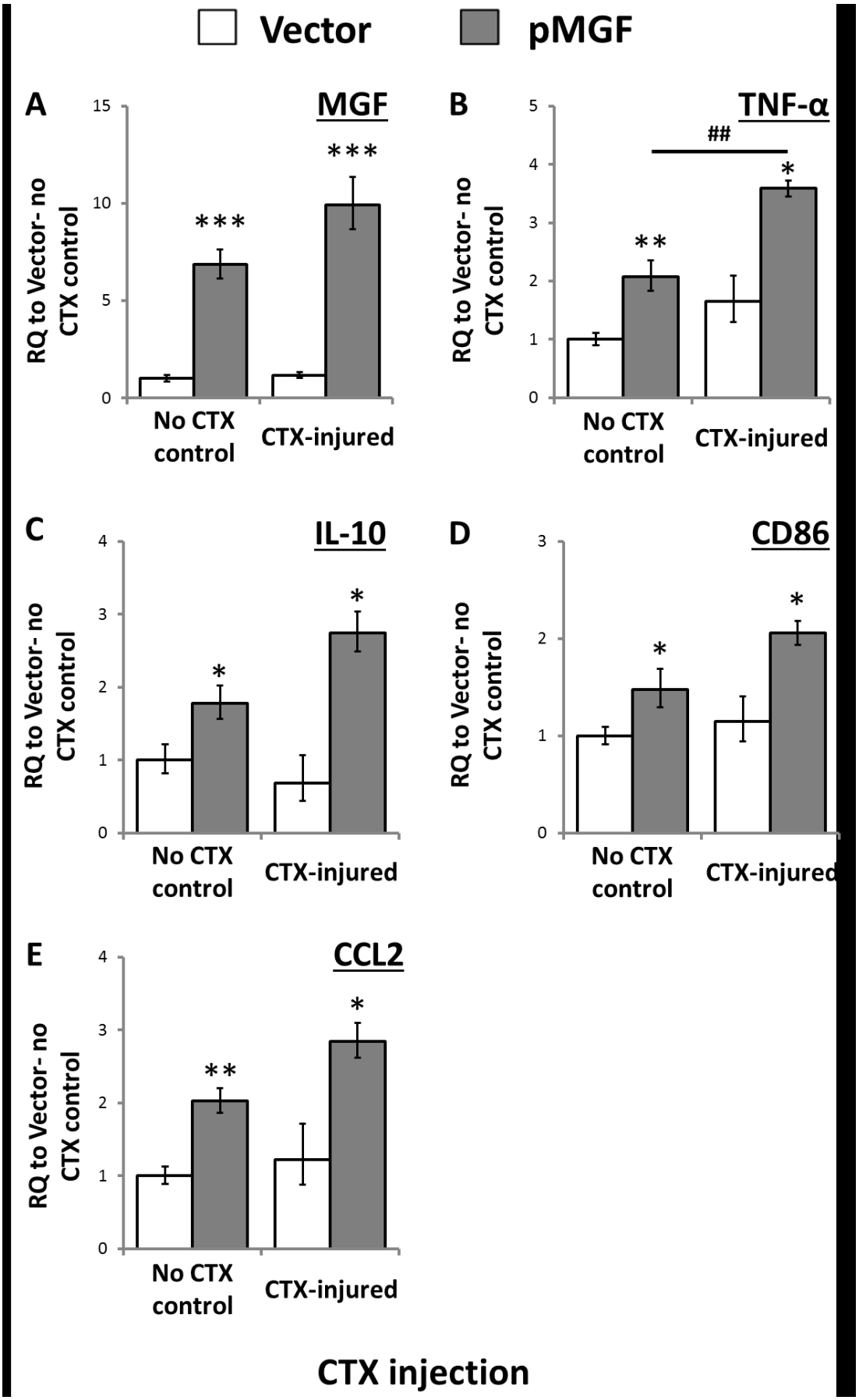
Vector
pMGF
A
MGF
RQ to Vector- no CTX control
No CTX control
CTX-injured
B
TNF-α
##
C
IL-10
D
CD86
E
CCL2
CTX injection

4.4 DISCUSSION

Our electroporation model was verified to efficiently overexpress GFP protein locally in over 60% myofibers with only negligible damage (compared with CTX-induced injury). Sustainable overexpression of MGF transcript was achieved by pMGF custom plasmid. Translation of MGF peptide from the clone was also detected. CTX-induced muscle injury did not abolish MGF overexpression as we observed myofibers survived from the injury even within the injured site. Notably, MGF overexpression did not alter IGF-1Ea expression in all *in vivo* models. Any phenotypic changes in our study were thus attributable to MGF instead of IGF-1Ea. To sum up, our overexpression model was effective in upregulating MGF locally in myofibers which was used to investigate the role of MGF in modulating muscle inflammatory response.

Overexpression of MGF extended the duration of inflammatory marker expression at the early resolution phase (day 4 to day 6). It was also the same phase that M1 MP increased in response to MGF overexpression. In other words, the postponed downregulation of inflammatory markers coincided with the delayed resolution of macrophages, particularly M1 sub-population. These inflammatory markers altered at tissue level however were not changed by MGF overexpression in the FACS-collected macrophages at the same timepoint (i.e. day 5). It prompted us to suggest that the increased population of macrophages or M1 MP led to enhanced cytokine expression in early resolution phase. However, we observed the same set of inflammatory markers upregulated at the same timepoints in the absence of CTX-induced muscle injury. The upregulation thus could also be

contributed by skeletal muscle resident cells, precluding myoblasts and myofibers from our *in vitro* experiments. Despite the modulation of inflammatory response, we could not observe changes in muscle regeneration outcomes by MGF overexpression at the evaluation timepoints.

To sum up, MGF appeared to regulate the resolution of M1 MP and modulate inflammatory marker expression in muscle but with no notable changes in muscle regeneration outcomes. Both infiltrated macrophages and resident cells were implicated in mediating the effect of MGF overexpression on inflammatory marker expression. The above findings were discussed with respect to the order of inflammatory phases in muscle regeneration.

4.4.1. Inflammatory phase

In this study, the inflammatory phase was empirically determined as day 1 to day 4 post electroporation (or day 0 to day 3 post CTX injury). The inflammatory phase of muscle regeneration involved a sequence of activities: the initiation of innate immune responses, infiltration of exudate myeloid cells and perpetuation of pro-inflammatory response (Tidball, 2005, 2011). Upregulation of inflammatory cytokines could be observed as early as one day after electroporation even in the absence of CTX-induced injury, indicating the initiation of innate immune responses (Brigitte *et al.*, 2010). In response to CTX-induced muscle injury, infiltration of M1 MP began at day 1 and peaked at day 4, coincided with previous reports (Radley & Grounds, 2006; Dumont *et al.*, 2007; Brigitte *et al.*, 2010; Lu *et al.*, 2011*a*,

2011*b*). We also demonstrated the invasion of macrophages into necrotic myofibers at day 3 by IHC. It is one of the pro-inflammatory activities to remove tissue debris. Thus, the histological findings suggested the active involvement of macrophages, likely M1 MP, within the inflammatory phase of inflammation. The decrease of total macrophages and M1 MP from day 4 implied inflammatory resolution and the end of inflammatory phase (Tidball, 2011; Sciorati *et al.*, 2016).

4.4.1.1 Implications of MGF in initiation of innate immune response

TNF-α and CCL2 are key inflammatory cytokines for the initiation and perpetuation of innate inflammatory response with well-recognized chemotactic property to recruit circulatory leukocytes into injured muscle (Ming *et al.*, 1987; Warren *et al.*, 2002; Radley & Grounds, 2006; Deshmane *et al.*, 2009; Brigitte *et al.*, 2010; Tidball & Villalta, 2010; Lu *et al.*, 2011*a*). We observed remarkably high level of TNF-α and CCL2 in both vector control and pMGF at day 1 post electroporation (without CTX-induced injury). It suggested that the electroporation *per se* activated the innate inflammatory response despite minimal myeloid cell infiltration on the next day. Minimal injury is attributable to the injections of hyaluronidase and plasmid DNA (Lee *et al.*, 2002). Moreover, the expression of TNF-α and CCL2 in pMGF at the same timepoint was approximately 1.5 fold higher than that in the vector control. Upregulation of MGF transcript within 1 day post injury has been reported (Philippou *et al.*, 2009). Implication of MGF in the initiation of innate immune response was thus suggested. Cells

responsible for the cytokine upregulation in the initiation process on the first day might be MGF responsive and mediate the changes.

There are at least three leukocyte candidates including resident MP, neutrophils and monocytes presented within 24 h to initiate and perpetuate innate immune response. Resident MP in skeletal muscle detects damage associated molecular patterns (DAMP) and initiates muscle inflammatory response (Brigitte *et al.*, 2010; Bosurgi *et al.*, 2011; Tidball, 2017). For instance, injured myofibers release HMGB1 that detected by TLR-4 on resident MP (Sciorati *et al.*, 2016). It in turn activates the NF-κB pro-inflammatory signaling cascade (Verstak *et al.*, 2009; Tidball, 2017). The activated resident MP expressed and released TNF-α, as well as chemokine CCL2 (Radley *et al.*, 2008; Brigitte *et al.*, 2010) that orchestrates the recruitment of leukocytes from the circulation (Modur *et al.*, 1996; Lu *et al.*, 2011*a*). The other two candidates are mainly exudate neutrophils and monocytes that dominate the early inflammatory infiltrate. They also release TNF-α and CCL2 to the injured site to perpetuate the pro-inflammatory response (Deshmane *et al.*, 2009; Tecchio *et al.*, 2014).

Notably, the enhanced expression of TNF-α and CCL2 was transient and the difference no longer existed at day 3 post electroporation while MGF remained overexpressing. The resolution of the responsive leukocytes within this period of time, for instance neutrophils, might account for the transient upregulation of inflammatory cytokines (TNF-α and CCL2). Neutrophils infiltrate injured muscle within a few hours and essentially resolved within 48 h from the insult (Teixeira *et al.*, 2003; Tidball & Villalta, 2010). Resolution of neutrophils concurred with the diminished effects of

MGF on the cytokines upregulation. Neutrophils appeared to be the mediating cells of MGF modulation on inflammatory marker expression. Yet, simultaneous downregulation of MGF transcript was evident from day 1 to day 3 post electroporation in pMGF+ CTX injury. The absence of change at day 3 might also reflect a dose-dependent response to reduction in MGF. Whether the effect of MGF was neutrophil-mediated or not required further confirmation. We suggested evaluating leukocytes within 24 h post electroporation which mainly include resident MP, neutrophils and monocytes.

4.4.1.2 TNF-α and CCL2 induction in satellite cells by MGF overexpression?

In addition to leukocytes, activated satellite cells were capable of releasing TNF-α and CCL2 to chemoattract and recruit macrophages to the injured area (Chazaud *et al.*, 2003). Temporally satellite cells are activated within the first 24 h post injury and presumably express the cytokines (Nagaraju *et al.*, 1998; Chazaud *et al.*, 2003). It was thus possible that activated satellite cells could also contribute to the enhanced expression of TNF-α and CCL2 at day 1 by MGF overexpression. From our *in vitro* study, actively proliferating C2C12 myoblasts, resembling the activated satellite cells, did not upregulate TNF-α and CCL2 upon MGF overexpression after 24 h culture. Instead a mild suppression was observed in the next 24 h. Moreover, IGF-1 appears not an activation signal to quiescent satellite cells (Matheny *et al.*, 2010). We also observed unaltered expression of the satellite cell activation marker, MyoD, by MGF overexpression *in vivo*. It

means that MGF overexpression should not enhance the cytokine expression by activating more satellite cells in injured muscle. To sum up, the upregulation of TNF-α and CCL2 within muscle observed at day 1 post electroporation was unlikely mediated by activated satellite cells.

4.4.1.3 Independence of inflammatory perpetuation on MGF signaling

Initiation of inflammation was considered completed within the first 24 h. The perpetuation could be reflected from the increasing macrophage population from day 1 till day 4 post electroporation with CTX-induced injury. Despite the enhanced expression of TNF-α and CCL2 by MGF overexpression, macrophage population from day 1 to day 4 was similar between pMGF+ CTX injury and vector+ CTX injury control. The transient enhancement of these chemoattractants (only at day 1) unlikely promoted macrophage infiltration till day 4 the end of inflammatory phase. Sustained infiltration of macrophages relied mainly on the constitutive release of TNF-α and CCL2 from the infiltrated macrophages (particularly M1 MP), which took over the roles of early infiltrated neutrophils and monocytes (Deshmane *et al.*, 2009; Lu *et al.*, 2011*a*). The expression level observed at day 3 might reflect the contribution from these infiltrated M1 MP. As the transcript level was not altered at day 3, M1 MP might not respond to MGF overexpression in the aspect of TNF-α and CCL2 expression. In summary, MGF was not involved in the perpetuation of inflammatory response as indicated in the unchanged cytokine expression level and macrophage infiltration and expansion

4.4.1.4 Phagocytosis by macrophages

Although cytokines induction in M1 MP appeared insensitive to MGF, other pro-inflammatory functions might be affected. For instance, M1 MP actively engulfed dead cells such as apoptotic neutrophils and tissue debris primarily by phagocytosis (El Kebir & Filep, 2013; Xiao *et al.*, 2013; Martinez & Gordon, 2014; Sciorati *et al.*, 2016). Implication of IGF-1 in macrophage phagocytic activities has been suggested (Xiao *et al.*, 2013; Han *et al.*, 2016). Phagocytic activities of macrophage cell lines and primary macrophages derived from bone marrow and peritoneum were not altered by treating with mature IGF-1 peptide (without the E-domain), (Han *et al.*, 2016). Conversely, the synthetic peptide analogous to Eb-peptide (despite the lack of physiological relevance) was inhibitory to phagocytic activities of peritoneal macrophages (Xiao *et al.*, 2013). The presence of characteristic E-domain in MGF might be accountable for the differential findings. Since we did not examine changes in phagocytic activity, concluding the roles of MGF on macrophage phagocytosis was not possible. Yet, it was believed that MGF should not suppress the process because necrotic or infiltrated myofibers were not observed at day 6 or day 8 and regeneration was not affected by MGF overexpression. Suppression of phagocytosis likely prolongs the presence of necrotic tissues and delays muscle regeneration.

4.4.2. Early resolution phase

After the peak at day 4, M1 MP in vector+ CTX injury returned to baseline level in two days i.e. day 6 post electroporation. Concurrently,

rising population of M2 MP was observed. In addition to macrophage profiling, resolution of inflammatory response was also evident from the decreasing inflammatory cytokine expression. The key characteristic of early resolution phase is the resolution of pro-inflammatory response. It is indicated with drastic decrease of M1 MP with simultaneous emergence and expansion of M2 MP (Tidball, 2011; Sciorati *et al.*, 2016). Early resolution phase was characterized as day 4 to day 6 post electroporation in this study. During this phase, MGF overexpression appeared to transiently delay the resolution of M1 MP. We suggested that MGF may modulate the cell fate of infiltrated macrophages in injured muscle.

4.4.2.1 Anti-apoptotic effect of IGF-1 and resolution of M1 MP

We observed more M1 MP at day 5 in MGF-overexpressed CTX-injured muscle. It was possible that MGF suppressed the clearance process of M1 MP during early resolution. Apoptosis is the major pathway for the clearance of M1 MP (Tidball & St Pierre, 1996; Horiguchi *et al.*, 2002; Gautier *et al.*, 2013; Sciorati *et al.*, 2016). IGF-1/ IGF-1R signaling is protective to various cell types against apoptosis (Kooijman, 2006; Smith, 2010). Its active roles in mediating inflammatory response and apoptosis of macrophages and neutrophils have been reviewed (Smith, 2010). Effect of MGF against cell death was suggested in studies of ischemic heart and viral-mediated MGF-overexpressed muscle (Carpenter *et al.*, 2008; Barton *et al.*, 2010). In a microarray study, Spp1 gene encoding osteopontin, a potent inflammatory mediator of macrophage activities and their survival, is upregulated by full-length MGF for 4 to 20 fold, but unchanged in mature

IGF-1 and only 2 to 4 fold by full-length IGF-1Ea (Barton *et al.*, 2010). In addition, all the three IGF-1 isoforms are able to upregulate the major anti-apoptotic gene Bcl-X normally found in skeletal muscle (Dominov *et al.*, 2001; Barton *et al.*, 2010). The potential anti-apoptotic effect of MGF might prolong the survival of M1 MP during early resolution. The anti-apoptotic effect of full-length MGF on macrophages warrants further investigation.

4.4.2.2 Quick restoration of M1 MP population potentially by promoting M2 polarization

The population of M1 MP transiently increased at day 5 due to MGF overexpression but returned baseline simultaneously with vector control at day 6. Notably, the return of M1 MP to baseline level coincided with further yet insignificant increase of M2 MP. In addition to M1 clearance by apoptosis, the resolution of M1 MP can be achieved by polarization into M2 MP (Tidball & St Pierre, 1996; Horiguchi *et al.*, 2002; Gautier *et al.*, 2013; Sciorati *et al.*, 2016). In a LysM promoter (myeloid cell-specific) driven IGF-1 knockout model, persistent infiltration of M1 MP with reduction of M2 MP was evident. Thus, IGF-1 autocrine signaling skews macrophage polarization into reparative M2 phenotype (Tonkin *et al.*, 2015). In our model, increasing M2 progenies was detected as early as day 3 post electroporation. It suggested that muscle microenvironment from day 3 was becoming anti-inflammatory and favoring M2 polarization. Other macrophages double positive with M1 and M2 markers emerged in between the M1 MP and M2 MP suggesting its polarizing phenotypes from M1 to M2.

The modulation of polarization by IGF-1 (Tonkin *et al.*, 2015), the presence of anti-inflammatory niche and increasing trend of polarizing macrophages prompted us to suggest that the increased M1 MP due to MGF overexpression might polarize into M2 MP under the anti-inflammatory niche. Thus, M1 MP returned to baseline level at the same time of the vector control.

4.4.2.3 Resident MP-mediated MGF-induced upregulation of inflammatory markers during resolution

We found that the inflammatory marker upregulation upon MGF overexpression was not attributable to CTX-induced injury. The same set of inflammatory markers at similar timepoints was upregulated by MGF overexpression which implied the mediation by resident cells, but not exclusively by exudate progenies. In previous discussion on inflammatory phase (Section 4.4.1), we have suggested that MGF overexpression potentially enhanced expression of TNF-α and CCL2 transcript by resident MP in the initiation of innate inflammatory response. Resident MP might respond to MGF and upregulate the two cytokines even when macrophage infiltration was minimal in the absence of CTX-induced injury. Furthermore, resident MP possesses migratory ability from epimysium into the injured site to undergo phagocytosis (Brigitte *et al.*, 2010), similar to infiltrated macrophages. The minimal macrophage invasion into myofibers observed at day 2 post electroporation without CTX-induced injury might be contributed by resident MP, but not necessarily by the exudate counterpart.

Resident MP thus appeared to be one of the MGF responsive cells mediating the upregulation of inflammatory markers in this CTX-absent model.

Certainly, we could not rule out the possibility that the CTX-absent model (electroporation only) was actually a milder injury model (due to electroporation and needle puncture) compared with that induced by CTX injection. Whether resident MP or exudate macrophages were the predominant cells mediating the effects of MGF overexpression remains elusive. Using approaches like exudate macrophage-specific depletion with clodronate liposome (Summan *et al.*, 2006; Côté *et al.*, 2013) and bone marrow transplantation model (Brigitte *et al.*, 2010) may help delineate the differential response of resident and exudate progenies toward MGF upregulation in muscle injury. The former model eliminates the contribution from exudate macrophages whereas the latter allows distinguishing the resident and exudate cells by either labeling the donor or receiver cells.

4.4.3. Late resolution phase

The late resolution phase was defined as day 6 to day 8 post electroporation in this study. We observed the lowest level of inflammatory transcripts at day 8 post electroporation amongst the evaluated timepoints. Moreover, decreasing number of macrophages shown in IHC indicated the on-going inflammatory resolution during the period. All these findings coincided with previous observations and represented the ending stage of inflammatory response in injured muscle (Chargé & Rudnicki, 2004; Warren *et al.*, 2007; Tonkin *et al.*, 2015; Hardy *et al.*, 2016).

The effect of MGF overexpression on the upregulation of TNF-α and IL-10 persisted from the early to late resolution phase i.e. day 5 to day 8 post electroporation. Since M1 MP was essentially resolved by day 6, the upregulation observed at day 8 should not be attributed to altering M1 availability. As for M2 MP, it became predominant after M1 resolution. The macrophages identified at day 8 within muscle cryosections was likely of M2 phenotype (Kharraz *et al.*, 2013; Martinez & Gordon, 2014). However, it was unclear if M2 MP responded to MGF overexpression and upregulated inflammatory cytokines at the late resolution phase. At least in physiological context, it should not be the case. Upon CTX-induced muscle injury, endogenous upregulation of MGF did not persist till this end stage of inflammation but returned to baseline level by day 7 post CTX injury (see Chapter 3). The temporal dynamic of MGF matched with that of M1 MP but not the M2 MP. Again, resident MP might be responsive to MGF overexpression since the progeny remains active until restoration of tissue homeostasis (Brigitte *et al.*, 2010). MGF overexpression might enhance the cytokine expression of these resident cells and resulted in the upregulated inflammatory markers at late resolution phase.

4.5 CONCLUSION

In this Chapter, we examine the role of MGF in muscle inflammatory response using the MGF overexpression model. We have successfully delivered MGF gene locally into skeletal muscles prior to CTX-induced muscle injury. We demonstrated the effect of MGF overexpression on inflammatory transcript profile and macrophage

availability from inflammatory phase, early resolution and late resolution phase in the injured muscle. The effect of MGF overexpression on muscle regeneration was also examined. First, our MGF overexpression with CTX-induced injury model clearly demonstrated the effects of MGF in prolonging the presence of M1 MP when it was supposed to get resolved. Anti-apoptotic effect of IGF-1 signaling might render the increased population but this hypothesis requires further investigation. Primarily, we attributed the extended presence of M1 macrophage to the concomitant increase of inflammatory markers. However, the same modification of inflammatory transcript profile was observed from MGF-overexpressed muscle without CTX-induced injury. We thus suggested in addition to M1 MP, the involvement of resident cells in mediating the cytokine upregulation. Besides, MGF overexpression appeared enhancing the initiation of innate immune response by upregulating TNF-α and CCL2, despite the lack of changes in the early infiltration of macrophages. Further investigation on the mechanistic pathway of MGF in regulating resolution of M1 MP was suggested. The identity of MGF responsive cells in upregulating inflammatory cytokines also warrants further studies. Finally, although inflammatory response was altered by MGF overexpression, muscle regeneration outcomes were not affected, probably due to the presence of feedback correction mechanisms.

CHAPTER 5

General Discussion and Conclusion

5.1 MUSCLE INJURY, INFLAMMATION AND IGF-1

Skeletal muscles undergo regeneration to restore functional integrity upon injury, during which inflammatory response plays an indispensable role. Muscle inflammatory response to injury involves number of typical phases and each phase is mediated by particular inflammatory progenies, including resident MP, neutrophils, M1 MP and M2 MP. These distinct but overlapping inflammatory phases include (i) initiation: resident MP detects DAMP and activates inflammatory signaling cascade (e.g. NF-κB) to initiate the inflammatory response; (ii) perpetuation: neutrophils and M1 MP remove tissue debris and release pro-inflammatory cytokines to feedforward inflammation; (iii) early resolution: pro-inflammatory myeloid cells undergo apoptosis and part of M1 MP polarizes into pro-reparative M2 MP; (iv) late resolution: M2 MP promotes regenerating myofiber growth and tissue remodeling followed by resolution that indicates complete muscle regeneration.

IGF-1 is a potent growth factor that facilitates muscle regeneration derived primarily from inflammatory cells. It participates in promoting myogenic cell proliferation and differentiation; and also resolving muscle inflammatory response. It was mainly expressed and released by infiltrated myeloid cells or macrophages. Yet, alternative splicing gives rise to different IGF-1 isoforms that display distinct biological activities. To date, the predominant isoform IGF-1Ea is attributed to most of the documented functions of IGF-1 in muscle regeneration, including enhancement of myogenesis and promotion of anti-inflammatory response. Although another

isoform MGF is also implicated in myogenesis, the source and the role of MGF in muscle inflammatory response remain elusive.

We hypothesize that: (i) MGF is expressed by infiltrated myeloid cells including macrophages and neutrophils; and (ii) MGF possesses immunomodulating functions in muscle regeneration. The aims of this study were: (1) to examine the expression of MGF in the inflammatory response of muscle regeneration and; (2) to examine the role of MGF in modulating inflammatory response during early muscle injury.

For Aim 1, we examined the source of MGF in injured muscles and the association with inflammatory response. For Aim 2, we investigated the differential changes on the profiles of inflammatory cytokines, the population of inflammatory cells, and the potential effects on muscle regeneration upon *in vivo* MGF overexpression by electroporation.

5.2 MAJOR FINDINGS AND SIGNIFICANCE

Using the CTX-injured muscle model, our findings showed that the expression of MGF is associated with muscle inflammatory response. We observed that MGF is predominantly derived by inflammatory cells of myeloid origin during muscle inflammation. Thus, it is conceivable that MGF may play a role in modulating inflammatory response for muscle regeneration. Moreover, we confirmed the expression of MGF in macrophages (Lu *et al.*, 2011*b*; Tonkin *et al.*, 2015) and showed the first time that neutrophils likely contributes to the upregulation of MGF in injured muscle. Since neutrophils dominate the early inflammatory infiltrate

prior to macrophage infiltration, it may be the earliest source of MGF in the injured muscle. The function of MGF derived from neutrophils is however unknown and warrants further investigation.

Tonkin *et al.*, (2015) suggested that MGF appears dispensable for muscle regeneration in a systemic knockout model. Given the distinct effects of MGF overexpression on skeletal muscle and the aforesaid association, we overexpressed MGF and evaluated its role in modulating inflammatory response during muscle regeneration. It is noteworthy that MGF overexpression did not lead to alteration of IGF-1Ea expression. The results indicated that (i) the phenotypic changes observed upon MGF overexpression *in vivo* is solely due to MGF and is not contributed by IGF-1Ea; (ii) expression of IGF-1Ea *in vivo* does not depend on the upregulation of MGF. Overexpression of MGF in the injured muscle (i) prolonged the upregulation of inflammatory cytokines; (ii) delayed the resolution of pro-inflammatory macrophages (M1 MP); and (iii) modulated the transcript profile of muscle resident cells. The modulation did not however lead to any observable differences in muscle regeneration outcomes. We speculated that the modulated inflammatory response might be corrected by a potential feedback upregulation of anti-inflammatory cytokine and enhanced polarization to M2 MP, which is consistent with our experimental data on the increased IL-10 expression and increasing trend of M2 MP. Yet, MGF may not be implicated in infiltration and expansion of M1 MP, or the resolution of M2 MP.

Since different isoforms display differential roles in skeletal muscle, our findings about the possible role of MGF contribute to the

understanding of IGF-1 isoforms in muscle regeneration. IGF-1Ea has been suggested to modulate anti-inflammatory response in muscle regeneration. It is implicated in the repression of inflammatory cell infiltration, promotion of M2 polarization and modulation of inflammatory cytokine profiles (Pelosi *et al.*, 2007; Tonkin *et al.*, 2015). Our findings showed that MGF may have pro-inflammatory function. MGF transiently enhanced the upregulation of pro-inflammatory cytokine (TNF-α) and chemokine (CCL2) at day 1 after overexpression. Despite significantly more M1 MP during early resolution phase, M1 resolution in the MGF-overexpressed CTX-injured muscle was restored within one day. We speculated the presence of feedback correction mechanism by increasing anti-inflammatory cytokines (IL-10) and macrophages (i.e. M2 MP). However, the lack of observable changes in muscle regeneration outcomes might be accounted by the evaluation timepoints selected in the study. Timepoints later than day 8 post electroporation (or 7 days post injury) are required to confirm the effects of MGF on muscle regeneration outcomes.

5.3 LIMITATIONS

5.4.1. MGF overexpression model

In our MGF *in vivo* overexpression model, we were only able to detect the pre-pro-MGF peptide but not the two putative secretory forms i.e. pro-MGF or Eb-peptide (Pfeffer *et al.*, 2009). However if MGF could not be cleaved and released from myofibers, it was unlikely that the observed changes in inflammatory response were directly mediated by MGF peptides.

Failure in detection was probably due to their short half-life (Brisson & Barton, 2012). Recently an antibody against MGF is confirmed to identify pro-MGF and Eb-peptide *in vivo* after optimizing Western blotting protocol (Vassilakos *et al.*, 2017). Adaptation of the optimized protocol as well as the MGF antibody might confirm the presence of pro-MGF and Eb-peptide in our samples. The effects of MGF reported in this study can be confirmed by loss-of-function experiment model. Given MGF is predominantly expressed by infiltrated macrophages, transgenic model of MGF-flexed mice crossed macrophage-Cre lines can be established to demonstrate the roles of MGF in inflammatory response of muscle injury.

5.4.2. Inflammatory marker expression of macrophages in response to MGF overexpression

We suggested that transcription of inflammatory markers by macrophages was not affected by MGF overexpression from our FACS findings. FACS has been used to purify various cells from muscle for IGF-1 investigation (Fornaro *et al.*, 2014; Tonkin *et al.*, 2015). However, MGF overexpression was induced in myofibers. We could not rule out the possibility that transcript alteration in macrophages had been diminished after isolation.

In vitro culture of macrophage cell line (Iida *et al.*, 2002; Han *et al.*, 2016) or primary macrophages (Tonkin *et al.*, 2015) with recombinant MGF peptides (pro-MGF or Eb-peptide) may demonstrate the response of macrophages to MGF signaling (Janssen *et al.*, 2016). Conditional knockout

of MGF in macrophages by Cre/loxP system targeting the MGF-specific exon 5 sequence may confirm the essence of MGF signaling in macrophages (Liu *et al.*, 2000; Tonkin *et al.*, 2015).

5.4 FUTURE INVESTIGATIONS

5.5.1. Neutrophil-derived MGF in early muscle inflammatory response

Neutrophils were able to express MGF. As neutrophils are the earliest infiltrated myeloid cells, the upregulation of MGF within first 24 h from muscle injury might be attributable to neutrophils. IGF-1 signaling has been suggested to enhance neutrophil survival (Kooijman *et al.*, 2002; Kooijman, 2006; Himpe *et al.*, 2008), respiratory burst and phagocytic activities (Balteskard *et al.*, 1998; Han *et al.*, 2016). Besides, neutrophils infiltrate injured muscle at a similar timepoint when satellite cells undergo activation and proliferation (Tidball & Rinaldi, 2012). It may be possible that the neutrophil-derived MGF enacts in autocrine manner to modulate neutrophil survival and phagocytosis; and in paracrine manner to modulate satellite cell myogenesis in injured muscle.

To confirm if neutrophils contribute to the upregulation of MGF during early phase of inflammation, we propose experiments of *in vivo* depletion of neutrophils using clone 1A8 anti-Ly6G antibody (Daley *et al.*, 2008). Muscles of neutrophil-depleted mice were then subjected to injury and MGF expression can be evaluated (both transcript and protein level) within 24 h post injury. To investigate MGF-mediated neutrophil activities in

muscle regeneration, we propose the use of gene knockout model driven by Mrp8 neutrophil-specific promoter (Van Ziffle & Lowell, 2009). The interaction of MGF knockout neutrophils with myoblasts can be demonstrated by co-culture models (e.g. transwell and conditioned medium). Assessment of apoptosis, release of ROS/ RNS and phagocytosis of MGF knockout neutrophils in injured muscle are suggested. Furthermore, satellite cell myogenesis and muscle regeneration outcomes in the proposed model should be evaluated. It will demonstrate the impact of modified neutrophil activities on muscle regeneration.

5.5.2. Anti-apoptotic effects of MGF on M1 MP

The clearance of M1 MP at early resolution phase was transiently delayed in MGF-overexpressed CTX-injured muscle. We propose that the potential anti-apoptotic effect of MGF might underline the observation (Carpenter *et al.*, 2008; Barton *et al.*, 2010).

To examine the anti-apoptotic effects of MGF on M1 MP infiltrated into injured muscle, immunostaining of the MGF-overexpressed CTX-injured muscle can be performed. Using our IHC protocol, macrophages can be identified by anti-F4/80 within muscle samples. Apoptotic cells can be identified from the same cryosection by TUNEL (terminal transferase-mediated dUTP nick end-labeling) assay (Negoescu *et al.*, 1998). Double-labeling for TUNEL and F4/80 indicates the apoptotic MP (TUNEL+/ F4/80+) *in situ*. To specifically measure apoptotic M1 MP, flow cytometric analysis described in this study can be performed in couple with

Annexin-V staining (Wlodkowic *et al.*, 2009). Other parameters for apoptosis evaluation include tissue expression of caspases and Fas that are implicated in macrophage apoptosis (Sandri *et al.*, 2001).

5.5 CONCLUSION

This study aims to elucidate the role of MGF in the inflammatory response of muscle regeneration upon injury. Our findings are:

i. All isolated myeloid cells, including neutrophils and macrophages, from CTX-injured muscle expressed MGF.

ii. Injured muscle with MGF overexpression demonstrated more pro-inflammatory macrophages (M1 MP) during early resolution phase (day 5) when compared with vector control.

iii. Inflammatory markers (mainly cytokines) were upregulated by MGF overexpression and such upregulation is contributed by muscle resident cells and increased M1 MP availability.

The inflammatory modulating effects of MGF in muscle injury warrant further investigation, particularly on the neutrophil activities and resolution of M1 MP.

REFERENCES

Allen RE & Boxhorn LK (1987). Inhibition of skeletal muscle satellite cell differentiation by transforming growth factor-beta. *J Cell Physiol* **133,** 567–572.

Andersen CL, Jensen JL & Ørntoft TF (2004). Normalization of real-time quantitative reverse transcription-PCR data: a model-based variance estimation approach to identify genes suited for normalization, applied to bladder and colon cancer data sets. *Cancer Res* **64,** 5245–5250.

Anderson JE (2000). A role for nitric oxide in muscle repair: nitric oxide-mediated activation of muscle satellite cells. *Mol Biol Cell* **11,** 1859–1874.

Arkins S, Rebeiz N, Biragyn A, Reese DL & Kelley KW (1993). Murine macrophages express abundant insulin-like growth factor-I class I Ea and Eb transcripts. *Endocrinology* **133,** 2334–2343.

Arnold L, Henry A, Poron F, Baba-Amer Y, van Rooijen N, Plonquet A, Gherardi RK & Chazaud B (2007). Inflammatory monocytes recruited after skeletal muscle injury switch into antiinflammatory macrophages to support myogenesis. *J Exp Med* **204,** 1057–1069.

Arnold L, Perrin H, de Chanville CB, Saclier M, Hermand P, Poupel L, Guyon E, Licata F, Carpentier W, Vilar J, Mounier R, Chazaud B, Benhabiles N, Boissonnas A, Combadiere B & Combadiere C (2015). CX3CR1 deficiency promotes muscle repair and regeneration by enhancing macrophage ApoE production. *Nat Commun* **6,** 8972.

Ates K, Yang SY, Orrell RW, Sinanan ACM, Simons P, Solomon A, Beech S, Goldspink G & Lewis MP (2007). The IGF-I splice variant MGF increases progenitor cells in ALS, dystrophic, and normal muscle. *FEBS Lett* **581,** 2727–2732.

Baker J, Liu JP, Robertson EJ & Efstratiadis A (1993). Role of insulin-like growth factors in embryonic and postnatal growth. *Cell* **75,** 73–82.

Balteskard L, Unneberg K, Halvorsen D, Hansen JB & Revhaug A (1998). Effects of insulin-like growth factor 1 on neutrophil and monocyte functions in normal and septic states. *JPEN J Parenter Enteral Nutr* **22,** 127–135.

Barton-Davis ER, Shoturma DI & Sweeney HL (1999). Contribution of satellite cells to IGF-I induced hypertrophy of skeletal muscle. *Acta Physiol Scand* **167,** 301–305.

Barton ER (2006*a*). The ABCs of IGF-I isoforms: impact on muscle hypertrophy and implications for repair. *Appl Physiol Nutr Metab* **31,** 791–797.

Barton ER (2006*b*). Viral expression of insulin-like growth factor-I isoforms promotes different responses in skeletal muscle. *J Appl Physiol* **100,** 1778–1784.

Barton ER, DeMeo J & Lei H (2010). The insulin-like growth factor (IGF)-I E-peptides are required for isoform-specific gene expression and muscle hypertrophy after local IGF-I production. *J Appl Physiol* **108,** 1069–1076.

Behrens L, Bender A, Johnson MA & Hohlfeld R (1997). Cytotoxic mechanisms in inflammatory myopathies. Co-expression of Fas and protective Bcl-2 in muscle fibres and inflammatory cells. *Brain* **120,** 929–938.

Belfiore A, Frasca F, Pandini G, Sciacca L & Vigneri R (2009). Insulin receptor isoforms and insulin receptor/insulin-like growth factor receptor hybrids in physiology and disease. *Endocr Rev* **30,** 586–623.

Bentzinger CF, Wang YX, Dumont NA & Rudnicki MA (2013). Cellular dynamics in the muscle satellite cell niche. *EMBO Rep* **14,** 1062–1072.

Berkes CA & Tapscott SJ (2005). MyoD and the transcriptional control of myogenesis. *Semin Cell Dev Biol* **16,** 585–595.

Bosurgi L, Manfredi AA & Rovere-Querini P (2011). Macrophages in injured

skeletal muscle: a perpetuum mobile causing and limiting fibrosis, prompting or restricting resolution and regeneration. *Front Immunol* **2,** 62.

Brigitte M, Schilte C, Plonquet A, Baba-Amer Y, Henri A, Charlier C, Tajbakhsh S, Albert M, Gherardi RK & Chrétien F (2010). Muscle resident macrophages control the immune cell reaction in a mouse model of notexin-induced myoinjury. *Arthritis Rheum* **62,** 268–279.

Brisson BK & Barton ER (2012). Insulin-like growth factor-I E-peptide activity is dependent on the IGF-I receptor. *PLoS One* **7,** e45588.

Brisson BK, Spinazzola J, Park S & Barton ER (2014). Viral expression of insulin-like growth factor I E-peptides increases skeletal muscle mass but at the expense of strength. *Am J Physiol Endocrinol Metab* **306,** E965–E974.

Burks TN & Cohn RD (2011). Role of TGF-β signaling in inherited and acquired myopathies. *Skelet Muscle* **1,** 19.

Burzyn D, Kuswanto W, Kolodin D, Shadrach JL, Cerletti M, Jang Y, Sefik E, Tan TG, Wagers AJ, Benoist C & Mathis D (2013). A special population of regulatory T cells potentiates muscle repair. *Cell* **155,** 1282–1295.

Butterfield TA, Best TM & Merrick MA (2006). The dual roles of neutrophils and macrophages in inflammation: a critical balance between tissue damage and repair. *J Athl Train* **41,** 457–465.

Carpenter V, Matthews K, Devlin G, Stuart S, Jensen J, Conaglen J, Jeanplong F, Goldspink P, Yang S-Y, Goldspink G, Bass J & McMahon C (2008). Mechano-growth factor reduces loss of cardiac function in acute myocardial infarction. *Heart Lung Circ* **17,** 33–39.

Ceafalan LC, Popescu BO & Hinescu ME (2014). Cellular players in skeletal muscle regeneration. *Biomed Res Int* **2014,** 957014.

Chargé SBP & Rudnicki MA (2004). Cellular and molecular regulation of

muscle regeneration. *Physiol Rev* **84,** 209–238.

Charles JP, Cappellari O, Spence AJ, Hutchinson JR & Wells DJ (2016). Musculoskeletal geometry, muscle architecture and functional specialisations of the mouse hindlimb. ed. Phillips WD. *PLoS One* **11,** e0147669.

Chazaud B, Sonnet C, Lafuste P, Bassez G, Rimaniol A-C, Poron F, Authier F-J, Dreyfus PA & Gherardi RK (2003). Satellite cells attract monocytes and use macrophages as a support to escape apoptosis and enhance muscle growth. *J Cell Biol* **163,** 1133–1143.

Chen S-E, Gerken E, Zhang Y, Zhan M, Mohan RK, Li AS, Reid MB & Li Y-P (2005). Role of TNF-{alpha} signaling in regeneration of cardiotoxin-injured muscle. *Am J Physiol Cell Physiol* **289,** C1179–C1187.

Chen S-E, Jin B & Li Y-P (2007). TNF-alpha regulates myogenesis and muscle regeneration by activating p38 MAPK. *Am J Physiol Cell Physiol* **292,** C1660–C1671.

Cheng M, Nguyen M-H, Fantuzzi G & Koh TJ (2008). Endogenous interferon-gamma is required for efficient skeletal muscle regeneration. *Am J Physiol Cell Physiol* **294,** C1183–C1191.

Cheung K-K, Yeung SS, Au SW, Lam LS, Dai Z-Q, Li Y-H & Yeung EW (2011). Expression and association of TRPC1 with TRPC3 during skeletal myogenesis. *Muscle Nerve* **44,** 358–365.

Chew SL, Lavender P, Clark AJ & Ross RJ (1995). An alternatively spliced human insulin-like growth factor-I transcript with hepatic tissue expression that diverts away from the mitogenic IBE1 peptide. *Endocrinology* **136,** 1939–1944.

Chiou SH, Raynor RL, Zheng B, Chambers TC & Kuo JF (1993). Cobra venom cardiotoxin (cytotoxin) isoforms and neurotoxin: comparative potency of protein kinase C inhibition and cancer cell cytotoxicity and modes of enzyme inhibition. *Biochemistry* **32,** 2062–2067.

Christov C, Chrétien F, Abou-Khalil R, Bassez G, Vallet G, Authier F-J, Bassaglia Y, Shinin V, Tajbakhsh S, Chazaud B & Gherardi RK (2007). Muscle satellite cells and endothelial cells: close neighbors and privileged partners. *Mol Biol Cell* **18,** 1397–1409.

Collins RA & Grounds MD (2001). The role of tumor necrosis factor-alpha (TNF-alpha) in skeletal muscle regeneration. Studies in TNF-alpha(-/-) and TNF-alpha(-/-)/LT-alpha(-/-) mice. *J Histochem Cytochem* **49,** 989–1001.

Coolican SA, Samuel DS, Ewton DZ, McWade FJ & Florini JR (1997). The mitogenic and myogenic actions of insulin-like growth factors utilize distinct signaling pathways. *J Biol Chem* **272,** 6653–6662.

Côté CH, Bouchard P, van Rooijen N, Marsolais D & Duchesne E (2013). Monocyte depletion increases local proliferation of macrophage subsets after skeletal muscle injury. *BMC Musculoskelet Disord* **14,** 359.

Couteaux R, Mira JC & D'Albis A (1988). Regeneration of muscles after cardiotoxin injury. I. Cytological aspects. *Biol cell* **62,** 171–182.

Dalby B, Cates S, Harris A, Ohki EC, Tilkins ML, Price PJ & Ciccarone VC (2004). Advanced transfection with Lipofectamine 2000 reagent: primary neurons, siRNA, and high-throughput applications. *Methods* **33,** 95–103.

Daley JM, Thomay AA, Connolly MD, Reichner JS & Albina JE (2008). Use of Ly6G-specific monoclonal antibody to deplete neutrophils in mice. *J Leukoc Biol* **83,** 64–70.

Daughaday WH, Hall K, Salmon WD, Van den Brande JL & Van Wyk JJ (1987). On the nomenclature of the somatomedins and insulin-like growth factors. *Endocrinology* **121,** 1911–1912.

Daughaday WH & Rotwein P (1989). Insulin-like growth factors I and II. Peptide, messenger ribonucleic acid and gene structures, serum, and tissue concentrations. *Endocr Rev* **10,** 68–91.

Deng B, Wehling-Henricks M, Villalta SA, Wang Y & Tidball JG (2012). IL-10 triggers changes in macrophage phenotype that promote muscle growth and regeneration. *J Immunol* **189,** 3669–3680.

Deshmane SL, Kremlev S, Amini S & Sawaya BE (2009). Monocyte chemoattractant protein-1 (MCP-1): an overview. *J Interferon Cytokine Res* **29,** 313–326.

Dluzniewska J, Sarnowska A, Beresewicz M, Johnson I, Srai SKS, Ramesh B, Goldspink G, Górecki DC & Zabłocka B (2005). A strong neuroprotective effect of the autonomous C-terminal peptide of IGF-1 Ec (MGF) in brain ischemia. *FASEB J* **19,** 1896–1898.

Dominov JA, Houlihan-Kawamoto CA, Swap CJ & Miller JB (2001). Pro- and anti-apoptotic members of the Bcl-2 family in skeletal muscle: a distinct role for Bcl-2 in later stages of myogenesis. *Dev Dyn* **220,** 18–26.

Dong Y, Lakhia R, Thomas SS, Dong Y, Wang XH, Silva KAS & Zhang L (2013). Interactions between p-Akt and Smad3 in injured muscles initiate myogenesis or fibrogenesis. *Am J Physiol Endocrinol Metab* **305,** E367–E375.

Duan C, Ren H & Gao S (2010). Insulin-like growth factors (IGFs), IGF receptors, and IGF-binding proteins: roles in skeletal muscle growth and differentiation. *Gen Comp Endocrinol* **167,** 344–351.

Duguay SJ, Lai-Zhang J & Steiner DF (1995). Mutational analysis of the insulin-like growth factor I prohormone processing site. *J Biol Chem* **270,** 17566–17574.

Dumont N, Bouchard P & Frenette J (2008). Neutrophil-induced skeletal muscle damage: a calculated and controlled response following hindlimb unloading and reloading. *Am J Physiol Regul Integr Comp Physiol* **295,** R1831–R1838.

Dumont N & Frenette J (2010). Macrophages protect against muscle atrophy and promote muscle recovery in vivo and in vitro: a mechanism partly

dependent on the insulin-like growth factor-1 signaling molecule. *Am J Pathol* **176,** 2228–2235.

Dumont N, Lepage K, Côté CH & Frenette J (2007). Mast cells can modulate leukocyte accumulation and skeletal muscle function following hindlimb unloading. *J Appl Physiol* **103,** 97–104.

Durzyńska J, Philippou A, Brisson BK, Nguyen-McCarty M & Barton ER (2013). The pro-forms of insulin-like growth factor I (IGF-I) are predominant in skeletal muscle and alter IGF-I receptor activation. *Endocrinology* **154,** 1215–1224.

Enguita-Germán M & Fortes P (2014). Targeting the insulin-like growth factor pathway in hepatocellular carcinoma. *World J Hepatol* **6,** 716–737.

Fadok VA, Bratton DL & Henson PM (2001). Phagocyte receptors for apoptotic cells: recognition, uptake, and consequences. *J Clin Invest* **108,** 957–962.

Fadok VA, Warner ML, Bratton DL & Henson PM (1998). CD36 is required for phagocytosis of apoptotic cells by human macrophages that use either a phosphatidylserine receptor or the vitronectin receptor (alpha v beta 3). *J Immunol* **161,** 6250–6257.

Farup J, Madaro L, Puri PL & Mikkelsen UR (2015). Interactions between muscle stem cells, mesenchymal-derived cells and immune cells in muscle homeostasis, regeneration and disease. *Cell Death Dis* **6,** e1830.

Fornaro M, Hinken AC, Needle S, Hu E, Trendelenburg A-U, Mayer A, Rosenstiel A, Chang C, Meier V, Billin AN, Becherer JD, Brace AD, Evans WJ, Glass DJ & Russell AJ (2014). Mechano-growth factor peptide, the COOH terminus of unprocessed insulin-like growth factor 1, has no apparent effect on myoblasts or primary muscle stem cells. *Am J Physiol Endocrinol Metab* **306,** E150–E156.

Frost RA, Lang CH & Gelato MC (1997). Transient exposure of human myoblasts to tumor necrosis factor-alpha inhibits serum and insulin-like

growth factor-I stimulated protein synthesis. *Endocrinology* **138,** 4153–4159.

Frost RA, Nystrom GJ & Lang CH (2003). Tumor necrosis factor-alpha decreases insulin-like growth factor-I messenger ribonucleic acid expression in C2C12 myoblasts via a Jun N-terminal kinase pathway. *Endocrinology* **144,** 1770–1779.

Gallagher JT (2001). Heparan sulfate: growth control with a restricted sequence menu. *J Clin Invest* **108,** 357–361.

Gallego-Colon E, Sampson RD, Sattler S, Schneider MD, Rosenthal N & Tonkin J (2015). Cardiac-Restricted IGF-1Ea Overexpression Reduces the Early Accumulation of Inflammatory Myeloid Cells and Mediates Expression of Extracellular Matrix Remodelling Genes after Myocardial Infarction. *Mediators Inflamm* **2015,** 484357.

Gautier EL, Ivanov S, Lesnik P & Randolph GJ (2013). Local apoptosis mediates clearance of macrophages from resolving inflammation in mice. *Blood* **122,** 2714–2722.

Gehl J (2003). Electroporation: theory and methods, perspectives for drug delivery, gene therapy and research. *Acta Physiol Scand* **177,** 437–447.

Godman GC (1957). On the regeneration and redifferentiation of mammalian striated muscle. *J Morphol* **100,** 27–81.

Goren I, Allmann N, Yogev N, Schürmann C, Linke A, Holdener M, Waisman A, Pfeilschifter J & Frank S (2009). A transgenic mouse model of inducible macrophage depletion: effects of diphtheria toxin-driven lysozyme M-specific cell lineage ablation on wound inflammatory, angiogenic, and contractive processes. *Am J Pathol* **175,** 132–147.

Grounds MD, Radley HG, Gebski BL, Bogoyevitch MA & Shavlakadze T (2008). Implications of cross-talk between tumour necrosis factor and insulin-like growth factor-1 signalling in skeletal muscle. *Clin Exp Pharmacol Physiol* **35,** 846–851.

Guttridge DC (2012). Skeletal muscle regeneration. In *Muscle: Fundamental Biology and Mechanisms of Disease*, 1st edn., ed. Hill J & Olson EN, pp. 921–933. Elsevier, New York, NY.

Guttridge DC, Albanese C, Reuther JY, Pestell RG & Baldwin AS (1999). NF-kappaB controls cell growth and differentiation through transcriptional regulation of cyclin D1. *Mol Cell Biol* **19,** 5785–5799.

Hammond ME, Lapointe GR, Feucht PH, Hilt S, Gallegos CA, Gordon CA, Giedlin MA, Mullenbach G & Tekamp-Olson P (1995). IL-8 induces neutrophil chemotaxis predominantly via type I IL-8 receptors. *J Immunol* **155,** 1428–1433.

Han CZ, Juncadella IJ, Kinchen JM, Buckley MW, Klibanov AL, Dryden K, Onengut-Gumuscu S, Erdbrügger U, Turner SD, Shim YM, Tung KS & Ravichandran KS (2016). Macrophages redirect phagocytosis by non-professional phagocytes and influence inflammation. *Nature* **539,** 570–574.

Hardy D, Besnard A, Latil M, Jouvion G, Briand D, Thépenier C, Pascal Q, Guguin A, Gayraud-Morel B, Cavaillon J-M, Tajbakhsh S, Rocheteau P & Chrétien F (2016). Comparative study of injury models for studying muscle regeneration in mice. ed. Kumar A. *PLoS One* **11,** e0147198.

Hayashi S, Aso H, Watanabe K, Nara H, Rose MT, Ohwada S & Yamaguchi T (2004). Sequence of IGF-I, IGF-II, and HGF expression in regenerating skeletal muscle. *Histochem Cell Biol* **122,** 427–434.

Hede MS, Salimova E, Piszczek A, Perlas E, Winn N, Nastasi T & Rosenthal N (2012). E-peptides control bioavailability of IGF-1. *PLoS One* **7,** e51152.

Heredia JE, Mukundan L, Chen FM, Mueller AA, Deo RC, Locksley RM, Rando TA & Chawla A (2013). Type 2 innate signals stimulate fibro/adipogenic progenitors to facilitate muscle regeneration. *Cell* **153,** 376–388.

Hill M, Wernig A & Goldspink G (2003). Muscle satellite (stem) cell

activation during local tissue injury and repair. *J Anat* **203,** 89–99.

Himpe E, Degaillier C, Coppens A & Kooijman R (2008). Insulin-like growth factor-1 delays Fas-mediated apoptosis in human neutrophils through the phosphatidylinositol-3 kinase pathway. *J Endocrinol* **199,** 69–80.

Hindi SM, Tajrishi MM & Kumar A (2013). Signaling mechanisms in mammalian myoblast fusion. *Sci Signal* **6,** re2.

Horiguchi T, Shibata M-A, Ito Y, Eid NAS, Abe M & Otsuki Y (2002). Macrophage apoptosis in rat skeletal muscle treated with bupivacaine hydrochloride: possible role of MCP-1. *Muscle Nerve* **26,** 79–86.

Horsley V, Jansen KM, Mills ST & Pavlath GK (2003). IL-4 acts as a myoblast recruitment factor during mammalian muscle growth. *Cell* **113,** 483–494.

Hua HT, Al-Badawi H, Entabi F, Stoner MC, Diamond RE, Bonheur JA, Houser S & Watkins MT (2005). CXC chemokine expression and synthesis in skeletal muscle during ischemia/reperfusion. *J Vasc Surg* **42,** 337–343.

Iida KT, Suzuki H, Sone H, Shimano H, Toyoshima H, Yatoh S, Asano T, Okuda Y & Yamada N (2002). Insulin inhibits apoptosis of macrophage cell line, THP-1 cells, via phosphatidylinositol-3-kinase-dependent pathway. *Arterioscler Thromb Vasc Biol* **22,** 380–386.

Italiani P & Boraschi D (2014). From Monocytes to M1/M2 Macrophages: Phenotypical vs. Functional Differentiation. *Front Immunol* **5,** 514.

Jacquemin V, Furling D, Bigot A, Butler-Browne GS & Mouly V (2004). IGF-1 induces human myotube hypertrophy by increasing cell recruitment. *Exp Cell Res* **299,** 148–158.

Janssen JAMJL, Hofland LJ, Strasburger CJ, van den Dungen ESR & Thevis M (2016). Potency of full-length MGF to induce maximal activation of the IGF-IR is similar to recombinant human IGF-I at high equimolar

concentrations. *PLoS One* **11,** e0150453.

Järvinen TAH, Järvinen TLN, Kääriäinen M, Kalimo H & Järvinen M (2005). Muscle injuries: biology and treatment. *Am J Sports Med* **33,** 745–764.

Joe AWB, Yi L, Natarajan A, Le Grand F, So L, Wang J, Rudnicki MA & Rossi FM V (2010). Muscle injury activates resident fibro/adipogenic progenitors that facilitate myogenesis. *Nat Cell Biol* **12,** 153–163.

Kawakami Y, Ichinose Y & Fukunaga T (1998). Architectural and functional features of human triceps surae muscles during contraction. *J Appl Physiol* **85,** 398–404.

Kawanishi N, Mizokami T, Niihara H, Yada K & Suzuki K (2016). Neutrophil Depletion Attenuates Muscle Injury after Exhaustive Exercise. *Med Sci Sports Exerc* **48,** 1917–1924.

El Kebir D & Filep JG (2013). Modulation of Neutrophil Apoptosis and the Resolution of Inflammation through β2 Integrins. *Front Immunol* **4,** 60.

Kharraz Y, Guerra J, Mann CJ, Serrano AL & Muñoz-Cánoves P (2013). Macrophage plasticity and the role of inflammation in skeletal muscle repair. *Mediators Inflamm* **2013,** 491497.

Kooijman R (2006). Regulation of apoptosis by insulin-like growth factor (IGF)-I. *Cytokine Growth Factor Rev* **17,** 305–323.

Kooijman R, Coppens A & Hooghe-Peters E (2002). Igf-I inhibits spontaneous apoptosis in human granulocytes. *Endocrinology* **143,** 1206–1212.

Lacy P & Stow JL (2011). Cytokine release from innate immune cells: association with diverse membrane trafficking pathways. *Blood* **118,** 9–18.

Lafreniere JF, Mills P, Bouchentouf M & Tremblay JP (2006). Interleukin-4 improves the migration of human myogenic precursor cells in vitro and in vivo. *Exp Cell Res* **312,** 1127–1141.

Lai L, Alaverdi N, Maltais L & Morse HC (1998). Mouse cell surface antigens: nomenclature and immunophenotyping. *J Immunol* **160,** 3861–3868.

Lee KH, Baek MY, Moon KY, Song WK, Chung CH, Ha DB & Kang MS (1994). Nitric oxide as a messenger molecule for myoblast fusion. *J Biol Chem* **269,** 14371–14374.

Lee M-J, Cho S-S, Jang H-S, Lim YS, You J-R, Park J, Suh H, Kim J-A, Park J-S & Kim D-K (2002). Optimal salt concentration of vehicle for plasmid DNA enhances gene transfer mediated by electroporation. *Exp Mol Med* **34,** 265–272.

Lefaucheur JP & Sébille A (1995). Muscle regeneration following injury can be modified in vivo by immune neutralization of basic fibroblast growth factor, transforming growth factor beta 1 or insulin-like growth factor I. *J Neuroimmunol* **57,** 85–91.

Lesault P-F, Theret M, Magnan M, Cuvellier S, Niu Y, Gherardi RK, Tremblay JP, Hittinger L & Chazaud B (2012). Macrophages improve survival, proliferation and migration of engrafted myogenic precursor cells into MDX skeletal muscle. *PLoS One* **7,** e46698.

Li Y-P (2003). TNF-alpha is a mitogen in skeletal muscle. *Am J Physiol Cell Physiol* **285,** C370-6.

Li Y, Foster W, Deasy BM, Chan Y, Prisk V, Tang Y, Cummins J & Huard J (2004). Transforming growth factor-beta1 induces the differentiation of myogenic cells into fibrotic cells in injured skeletal muscle: a key event in muscle fibrogenesis. *Am J Pathol* **164,** 1007–1019.

Lightfoot AP & Cooper RG (2016). The role of myokines in muscle health and disease. *Curr Opin Rheumatol* **28,** 661–666.

Lingappa VR, Lingappa JR & Blobel G (1980). Signal sequences for early events in protein secretion and membrane assembly. *Ann N Y Acad Sci* **343,** 356–361.

Liu JL, Yakar S & LeRoith D (2000). Conditional knockout of mouse insulin-like growth factor-1 gene using the Cre/loxP system. *Proc Soc Exp Biol Med* **223,** 344–351.

Liu JP, Baker J, Perkins AS, Robertson EJ & Efstratiadis A (1993). Mice carrying null mutations of the genes encoding insulin-like growth factor I (Igf-1) and type 1 IGF receptor (Igf1r). *Cell* **75,** 59–72.

Livak KJ & Schmittgen TD (2001). Analysis of relative gene expression data using real-time quantitative PCR and the 2(-Delta Delta C(T)) Method. *Methods* **25,** 402–408.

Londhe P & Davie JK (2011). Gamma interferon modulates myogenesis through the major histocompatibility complex class II transactivator, CIITA. *Mol Cell Biol* **31,** 2854–2866.

Lu H, Huang D, Ransohoff RM & Zhou L (2011*a*). Acute skeletal muscle injury: CCL2 expression by both monocytes and injured muscle is required for repair. *FASEB J* **25,** 3344–3355.

Lu H, Huang D, Saederup N, Charo IF, Ransohoff RM & Zhou L (2011*b*). Macrophages recruited via CCR2 produce insulin-like growth factor-1 to repair acute skeletal muscle injury. *FASEB J* **25,** 358–369.

Lund DK & Cornelison DDW (2013). Enter the matrix: shape, signal and superhighway. *FEBS J* **280,** 4089–4099.

Machida S & Booth FW (2004). Insulin-like growth factor 1 and muscle growth: implication for satellite cell proliferation. *Proc Nutr Soc* **63,** 337–340.

Marino M, Scuderi F, Provenzano C & Bartoccioni E (2011). Skeletal muscle cells: from local inflammatory response to active immunity. *Gene Ther* **18,** 109–116.

Marino M, Scuderi F, Provenzano C, Scheller J, Rose-John S & Bartoccioni E (2008). IL-6 regulates MCP-1, ICAM-1 and IL-6 expression in human myoblasts. *J Neuroimmunol* **196,** 41–48.

Marsh DR, Criswell DS, Carson J a & Booth FW (1997). Myogenic regulatory factors during regeneration of skeletal muscle in young, adult, and old rats. *J Appl Physiol* **83,** 1270–1275.

Martinez FO & Gordon S (2014). The M1 and M2 paradigm of macrophage activation: time for reassessment. *F1000Prime Rep* **6,** 13.

Matheny RW, Nindl BC & Adamo ML (2010). Minireview: Mechano-growth factor: a putative product of IGF-I gene expression involved in tissue repair and regeneration. *Endocrinology* **151,** 865–875.

Mauro A (1961). Satellite cell of skeletal muscle fibers. *J Biophys Biochem Cytol* **9,** 493–495.

Mavrommatis E, Shioura KM, Los T & Goldspink PH (2013). The E-domain region of mechano-growth factor inhibits cellular apoptosis and preserves cardiac function during myocardial infarction. *Mol Cell Biochem* **381,** 69–83.

McCafferty DM, Mudgett JS, Swain MG & Kubes P (1997). Inducible nitric oxide synthase plays a critical role in resolving intestinal inflammation. *Gastroenterology* **112,** 1022–1027.

McKay BR, O'Reilly CE, Phillips SM, Tarnopolsky MA & Parise G (2008). Co-expression of IGF-1 family members with myogenic regulatory factors following acute damaging muscle-lengthening contractions in humans. *J Physiol* **586,** 5549–5560.

McKoy G, Ashley W, Mander J, Yang SY, Williams N, Russell B & Goldspink G (1999). Expression of insulin growth factor-1 splice variants and structural genes in rabbit skeletal muscle induced by stretch and stimulation. *J Physiol* **516,** 583–592.

McMahon JM, Signori E, Wells KE, Fazio VM & Wells DJ (2001). Optimisation of electrotransfer of plasmid into skeletal muscle by pretreatment with hyaluronidase -- increased expression with reduced muscle damage. *Gene Ther* **8,** 1264–1270.

Meador BM, Krzyszton CP, Johnson RW & Huey KA (2008). Effects of IL-10 and age on IL-6, IL-1beta, and TNF-alpha responses in mouse skeletal and cardiac muscle to an acute inflammatory insult. *J Appl Physiol* **104,** 991–997.

Mescher AL (2013). Muscle Tissue. In *Junqueira's Basic Histology*, 14e edn., ed. Mescher AL. The McGraw-Hill, New York, NY.

Miller KJ, Thaloor D, Matteson S & Pavlath GK (2000). Hepatocyte growth factor affects satellite cell activation and differentiation in regenerating skeletal muscle. *Am J Physiol Cell Physiol* **278,** C174–C181.

Mills CD, Kincaid K, Alt JM, Heilman MJ & Hill AM (2000). M-1/M-2 macrophages and the Th1/Th2 paradigm. *J Immunol* **164,** 6166–6173.

Mills P, Lafrenière J-F, Benabdallah BF, El Fahime EM & Tremblay J-P (2007). A new pro-migratory activity on human myogenic precursor cells for a synthetic peptide within the E domain of the mechano growth factor. *Exp Cell Res* **313,** 527–537.

Ming WJ, Bersani L & Mantovani A (1987). Tumor necrosis factor is chemotactic for monocytes and polymorphonuclear leukocytes. *J Immunol* **138,** 1469–1474.

Miyatake S, Shimizu-Motohashi Y, Takeda S & Aoki Y (2016). Anti-inflammatory drugs for Duchenne muscular dystrophy: focus on skeletal muscle-releasing factors. *Drug Des Devel Ther* **10,** 2745–2758.

Modur V, Zimmerman GA, Prescott SM & McIntyre TM (1996). Endothelial cell inflammatory responses to tumor necrosis factor alpha. Ceramide-dependent and -independent mitogen-activated protein kinase cascades. *J Biol Chem* **271,** 13094–13102.

Mojumdar K, Giordano C, Lemaire C, Liang F, Divangahi M, Qureshi ST & Petrof BJ (2016). Divergent impact of Toll-like receptor 2 deficiency on repair mechanisms in healthy muscle versus Duchenne muscular dystrophy. *J Pathol* **239,** 10–22.

Montarras D, Lindon C, Pinset C & Domeyne P (2000). Cultured myf5 null and myoD null muscle precursor cells display distinct growth defects. *Biol cell* **92,** 565–572.

Mourkioti F & Rosenthal N (2005). IGF-1, inflammation and stem cells: interactions during muscle regeneration. *Trends Immunol* **26,** 535–542.

Muñoz-Cánoves P, Scheele C, Pedersen BK & Serrano AL (2013). Interleukin-6 myokine signaling in skeletal muscle: a double-edged sword? *FEBS J* **280,** 4131–4148.

Murray PJ (2005). The primary mechanism of the IL-10-regulated antiinflammatory response is to selectively inhibit transcription. *Proc Natl Acad Sci U S A* **102,** 8686–8691.

Musarò A (2014). The Basis of Muscle Regeneration. *Adv Biol* **2014,** 1–16.

Musarò A, Giacinti C, Borsellino G, Dobrowolny G, Pelosi L, Cairns L, Ottolenghi S, Cossu G, Bernardi G, Battistini L, Molinaro M & Rosenthal N (2004). Stem cell-mediated muscle regeneration is enhanced by local isoform of insulin-like growth factor 1. *Proc Natl Acad Sci U S A* **101,** 1206–1210.

Musarò A, McCullagh K, Paul A, Houghton L, Dobrowolny G, Molinaro M, Barton ER, Sweeney HL & Rosenthal N (2001). Localized Igf-1 transgene expression sustains hypertrophy and regeneration in senescent skeletal muscle. *Nat Genet* **27,** 195–200.

Nagaraju K, Raben N, Merritt G, Loeffler L, Kirk K & Plotz P (1998). A variety of cytokines and immunologically relevant surface molecules are expressed by normal human skeletal muscle cells under proinflammatory stimuli. *Clin Exp Immunol* **113,** 407–414.

Nathan CF (1987). Secretory products of macrophages. *J Clin Invest* **79,** 319–326.

Navarro E, Alonso SJ, Martín FA & Castellano MA (2005). Toxicological and pharmacological effects of D-arginine. *Basic Clin Pharmacol*

Toxicol **97,** 149–154.

Negoescu A, Guillermet C, Lorimier P, Brambilla E & Labat-Moleur F (1998). Importance of DNA fragmentation in apoptosis with regard to TUNEL specificity. *Biomed Pharmacother* **52,** 252–258.

Nguyen HX & Tidball JG (2003). Interactions between neutrophils and macrophages promote macrophage killing of rat muscle cells in vitro. *J Physiol* **547,** 125–132.

Nielsen S & Pedersen BK (2008). Skeletal muscle as an immunogenic organ. *Curr Opin Pharmacol* **8,** 346–351.

Novak ML, Weinheimer-Haus EM & Koh TJ (2014). Macrophage activation and skeletal muscle healing following traumatic injury. *J Pathol* **232,** 344–355.

O'Connor JC, McCusker RH, Strle K, Johnson RW, Dantzer R & Kelley KW (2008). Regulation of IGF-I function by proinflammatory cytokines: at the interface of immunology and endocrinology. *Cell Immunol* **252,** 91–110.

Olguin HC, Yang Z, Tapscott SJ & Olwin BB (2007). Reciprocal inhibition between Pax7 and muscle regulatory factors modulates myogenic cell fate determination. *J Cell Biol* **177,** 769–779.

Ortega-Gómez A, Perretti M & Soehnlein O (2013). Resolution of inflammation: an integrated view. *EMBO Mol Med* **5,** 661–674.

Otis JS, Niccoli S, Hawdon N, Sarvas JL, Frye MA, Chicco AJ & Lees SJ (2014). Pro-inflammatory mediation of myoblast proliferation. *PLoS One* **9,** e92363.

Ouyang W, Rutz S, Crellin NK, Valdez PA & Hymowitz SG (2011). Regulation and functions of the IL-10 family of cytokines in inflammation and disease. *Annu Rev Immunol* **29,** 71–109.

Ownby CL, Fletcher JE & Colberg TR (1993). Cardiotoxin 1 from cobra (Naja naja atra) venom causes necrosis of skeletal muscle in vivo.

Toxicon **31,** 697–709.

Ownby CL, Powell JR, Jiang MS & Fletcher JE (1997). Melittin and phospholipase A2 from bee (Apis mellifera) venom cause necrosis of murine skeletal muscle in vivo. *Toxicon* **35,** 67–80.

Paiva-Oliveira EL, da Silva RF, Bellio M, Quirico-Santos T & Lagrota-Candido J (2017). Pattern of cardiotoxin-induced muscle remodeling in distinct TLR-4 deficient mouse strains. *Histochem Cell Biol* **148,** 49–60.

Palacios D, Mozzetta C, Consalvi S, Caretti G, Saccone V, Proserpio V, Marquez VE, Valente S, Mai A, Forcales S V, Sartorelli V & Puri PL (2010). TNF/p38α/polycomb signaling to Pax7 locus in satellite cells links inflammation to the epigenetic control of muscle regeneration. *Cell Stem Cell* **7,** 455–469.

De Palma C & Clementi E (2012). Nitric oxide in myogenesis and therapeutic muscle repair. *Mol Neurobiol* **46,** 682–692.

Parameswaran N & Patial S (2010). Tumor necrosis factor-α signaling in macrophages. *Crit Rev Eukaryot Gene Expr* **20,** 87–103.

Park S, Brisson BK, Liu M, Spinazzola JM & Barton ER (2014). Mature IGF-I excels in promoting functional muscle recovery from disuse atrophy compared with pro-IGF-IA. *J Appl Physiol* **116,** 797–806.

Peake JM, Della Gatta P, Suzuki K & Nieman DC (2015). Cytokine expression and secretion by skeletal muscle cells: regulatory mechanisms and exercise effects. *Exerc Immunol Rev* **21,** 8–25.

Pelletier M, Maggi L, Micheletti A, Lazzeri E, Tamassia N, Costantini C, Cosmi L, Lunardi C, Annunziato F, Romagnani S & Cassatella MA (2010). Evidence for a cross-talk between human neutrophils and Th17 cells. *Blood* **115,** 335–343.

Pelosi L, Giacinti C, Nardis C, Borsellino G, Rizzuto E, Nicoletti C, Wannenes F, Battistini L, Rosenthal N, Molinaro M & Musarò A (2007). Local expression of IGF-1 accelerates muscle regeneration by rapidly

modulating inflammatory cytokines and chemokines. *FASEB J* **21,** 1393–1402.

Perdiguero E, Sousa-Victor P, Ruiz-Bonilla V, Jardí M, Caelles C, Serrano AL & Muñoz-Cánoves P (2011). p38/MKP-1-regulated AKT coordinates macrophage transitions and resolution of inflammation during tissue repair. *J Cell Biol* **195,** 307–322.

Perrini S, Laviola L, Carreira MC, Cignarelli A, Natalicchio A & Giorgino F (2010). The GH/IGF1 axis and signaling pathways in the muscle and bone: mechanisms underlying age-related skeletal muscle wasting and osteoporosis. *J Endocrinol* **205,** 201–210.

Pfeffer LA, Brisson BK, Lei H & Barton ER (2009). The insulin-like growth factor (IGF)-I E-peptides modulate cell entry of the mature IGF-I protein. *Mol Biol Cell* **20,** 3810–3817.

Philippou A & Barton ER (2014). Optimizing IGF-I for skeletal muscle therapeutics. *Growth Horm IGF Res* **24,** 157–163.

Philippou A, Maridaki M, Pneumaticos S & Koutsilieris M (2014). The complexity of the IGF1 gene splicing, posttranslational modification and bioactivity. *Mol Med* **20,** 202–214.

Philippou A, Maridaki M, Theos A & Koutsilieris M (2012). Cytokines in muscle damage. *Adv Clin Chem* **58,** 49–87.

Philippou A, Papageorgiou E, Bogdanis G, Halapas A, Sourla A, Maridaki M, Pissimissis N & Koutsilieris M (2009). Expression of IGF-1 isoforms after exercise-induced muscle damage in humans: characterization of the MGF E peptide actions in vitro. *In Vivo* **23,** 567–575.

Pizza FX, McLoughlin TJ, McGregor SJ, Calomeni EP & Gunning WT (2001). Neutrophils injure cultured skeletal myotubes. *Am J Physiol Cell Physiol* **281,** C335–C341.

Powell-Braxton L, Hollingshead P, Warburton C, Dowd M, Pitts-Meek S,

Dalton D, Gillett N & Stewart TA (1993). IGF-I is required for normal embryonic growth in mice. *Genes Dev* **7,** 2609–2617.

Puche JE & Castilla-Cortázar I (2012). Human conditions of insulin-like growth factor-I (IGF-I) deficiency. *J Transl Med* **10,** 224.

Quesada A, Ogi J, Schultz J & Handforth A (2011). C-terminal mechano-growth factor induces heme oxygenase-1-mediated neuroprotection of SH-SY5Y cells via the protein kinase Cϵ/Nrf2 pathway. *J Neurosci Res* **89,** 394–405.

Rabinovsky ED, Gelir E, Gelir S, Lui H, Kattash M, DeMayo FJ, Shenaq SM & Schwartz RJ (2003). Targeted expression of IGF-1 transgene to skeletal muscle accelerates muscle and motor neuron regeneration. *FASEB J* **17,** 53–55.

Radley HG, Davies MJ & Grounds MD (2008). Reduced muscle necrosis and long-term benefits in dystrophic mdx mice after cV1q (blockade of TNF) treatment. *Neuromuscul Disord* **18,** 227–238.

Radley HG & Grounds MD (2006). Cromolyn administration (to block mast cell degranulation) reduces necrosis of dystrophic muscle in mdx mice. *Neurobiol Dis* **23,** 387–397.

Ramaswamy M, Cleland SY, Cruz AC & Siegel RM (2009). Many checkpoints on the road to cell death: regulation of Fas-FasL interactions and Fas signaling in peripheral immune responses. *Results Probl Cell Differ* **49,** 17–47.

Rath M, Müller I, Kropf P, Closs EI & Munder M (2014). Metabolism via Arginase or Nitric Oxide Synthase: Two Competing Arginine Pathways in Macrophages. *Front Immunol* **5,** 532.

Relaix F & Zammit PS (2012). Satellite cells are essential for skeletal muscle regeneration: the cell on the edge returns centre stage. *Development* **139,** 2845–2856.

Riddoch-Contreras J, Yang S-Y, Dick JRT, Goldspink G, Orrell RW &

Greensmith L (2009). Mechano-growth factor, an IGF-I splice variant, rescues motoneurons and improves muscle function in SOD1(G93A) mice. *Exp Neurol* **215,** 281–289.

Rigamonti E, Touvier T, Clementi E, Manfredi AA, Brunelli S & Rovere-Querini P (2013). Requirement of inducible nitric oxide synthase for skeletal muscle regeneration after acute damage. *J Immunol* **190,** 1767–1777.

Rotwein P (2014). Editorial: the fall of mechanogrowth factor? *Mol Endocrinol* **28,** 155–156.

Sabourin LA, Girgis-Gabardo A, Seale P, Asakura A & Rudnicki MA (1999). Reduced differentiation potential of primary MyoD-/- myogenic cells derived from adult skeletal muscle. *J Cell Biol* **144,** 631–643.

Saclier M, Cuvellier S, Magnan M, Mounier R & Chazaud B (2013). Monocyte/macrophage interactions with myogenic precursor cells during skeletal muscle regeneration. *FEBS J* **280,** 4118–4130.

Sambasivan R, Yao R, Kissenpfennig A, Van Wittenberghe L, Paldi A, Gayraud-Morel B, Guenou H, Malissen B, Tajbakhsh S & Galy A (2011). Pax7-expressing satellite cells are indispensable for adult skeletal muscle regeneration. *Development* **138,** 3647–3656.

Sandri M, Sandri C, Brun B, Giurisato E, Cantini M, Rossini K, Destro C, Arslan P & Carraro U (2001). Inhibition of fasL sustains phagocytic cells and delays myogenesis in regenerating muscle fibers. *J Leukoc Biol* **69,** 482–489.

Schertzer JD & Lynch GS (2006). Comparative evaluation of IGF-I gene transfer and IGF-I protein administration for enhancing skeletal muscle regeneration after injury. *Gene Ther* **13,** 1657–1664.

Schertzer JD, Plant DR & Lynch GS (2006). Optimizing plasmid-based gene transfer for investigating skeletal muscle structure and function. *Mol Ther* **13,** 795–803.

Schiaffino S & Mammucari C (2011). Regulation of skeletal muscle growth by the IGF1-Akt/PKB pathway: insights from genetic models. *Skelet Muscle* **1,** 4.

Schiaffino S, Pereira MG, Ciciliot S & Rovere-Querini P (2017). Regulatory T cells and skeletal muscle regeneration. *FEBS J* **284,** 517–524.

Sciorati C, Rigamonti E, Manfredi AA & Rovere-Querini P (2016). Cell death, clearance and immunity in the skeletal muscle. *Cell Death Differ* **23,** 927–937.

Segawa M, Fukada S ichiro, Yamamoto Y, Yahagi H, Kanematsu M, Sato M, Ito T, Uezumi A, Hayashi S, Miyagoe-Suzuki Y, Takeda S, Tsujikawa K & Yamamoto H (2008). Suppression of macrophage functions impairs skeletal muscle regeneration with severe fibrosis. *Exp Cell Res* **314,** 3232–3244.

Semsarian C, Sutrave P, Richmond DR & Graham RM (1999). Insulin-like growth factor (IGF-I) induces myotube hypertrophy associated with an increase in anaerobic glycolysis in a clonal skeletal-muscle cell model. *Biochem J* **339,** 443–451.

Serrano AL, Baeza-Raja B, Perdiguero E, Jardí M & Muñoz-Cánoves P (2008). Interleukin-6 is an essential regulator of satellite cell-mediated skeletal muscle hypertrophy. *Cell Metab* **7,** 33–44.

Shavlakadze T, Davies M, White JD & Grounds MD (2004). Early regeneration of whole skeletal muscle grafts is unaffected by overexpression of IGF-1 in MLC/mIGF-1 transgenic mice. *J Histochem Cytochem* **52,** 873–883.

Shi C & Pamer EG (2011). Monocyte recruitment during infection and inflammation. *Nat Rev Immunol* **11,** 762–774.

Smith TJ (2010). Insulin-like growth factor-I regulation of immune function: a potential therapeutic target in autoimmune diseases? *Pharmacol Rev* **62,** 199–236.

Sonnet C, Lafuste P, Arnold L, Brigitte M, Poron F, Authier F-J, Chrétien F, Gherardi RK & Chazaud B (2006). Human macrophages rescue myoblasts and myotubes from apoptosis through a set of adhesion molecular systems. *J Cell Sci* **119,** 2497–2507.

Spoor CW, van Leeuwen JL, van der Meulen WJ & Huson A (1991). Active force-length relationship of human lower-leg muscles estimated from morphological data: a comparison of geometric muscle models. *Eur J Morphol* **29,** 137–160.

Stein M, Keshav S, Harris N & Gordon S (1992). Interleukin 4 potently enhances murine macrophage mannose receptor activity: a marker of alternative immunologic macrophage activation. *J Exp Med* **176,** 287–292.

Stout RD, Jiang C, Matta B, Tietzel I, Watkins SK & Suttles J (2005). Macrophages sequentially change their functional phenotype in response to changes in microenvironmental influences. *J Immunol* **175,** 342–349.

Strle K, Broussard SR, McCusker RH, Shen W-H, Johnson RW, Freund GG, Dantzer R & Kelley KW (2004). Proinflammatory cytokine impairment of insulin-like growth factor I-induced protein synthesis in skeletal muscle myoblasts requires ceramide. *Endocrinology* **145,** 4592–4602.

Strle K, Broussard SR, McCusker RH, Shen W-H, LeCleir JM, Johnson RW, Freund GG, Dantzer R & Kelley KW (2006). C-jun N-terminal kinase mediates tumor necrosis factor-alpha suppression of differentiation in myoblasts. *Endocrinology* **147,** 4363–4373.

Strle K, McCusker RH, Tran L, King A, Johnson RW, Freund GG, Dantzer R & Kelley KW (2007). Novel activity of an anti-inflammatory cytokine: IL-10 prevents TNFalpha-induced resistance to IGF-I in myoblasts. *J Neuroimmunol* **188,** 48–55.

Summan M, Warren GL, Mercer RR, Chapman R, Hulderman T, Van Rooijen N & Simeonova PP (2006). Macrophages and skeletal muscle regeneration: a clodronate-containing liposome depletion study. *Am J*

Physiol Regul Integr Comp Physiol **290,** R1488–R1495.

Swentik A (2016). Pathophysiology of Skeletal Muscle Injury. In *Muscular Injuries in the Posterior Leg*, ed. Dixon JB, pp. 35–47. Springer US, Boston, MA.

Takahashi T, Ishida K, Itoh K, Konishi Y, Yagyu K-I, Tominaga A, Miyazaki J-I & Yamamoto H (2003). IGF-I gene transfer by electroporation promotes regeneration in a muscle injury model. *Gene Ther* **10,** 612–620.

Tatsumi R, Anderson JE, Nevoret CJ, Halevy O & Allen RE (1998). HGF/SF is present in normal adult skeletal muscle and is capable of activating satellite cells. *Dev Biol* **194,** 114–128.

Tatsumi R, Liu X, Pulido A, Morales M, Sakata T, Dial S, Hattori A, Ikeuchi Y & Allen RE (2006). Satellite cell activation in stretched skeletal muscle and the role of nitric oxide and hepatocyte growth factor. *Am J Physiol Cell Physiol* **290,** C1487–C1494.

Tecchio C, Micheletti A & Cassatella MA (2014). Neutrophil-derived cytokines: facts beyond expression. *Front Immunol* **5,** 508.

Teixeira CFP, Zamunér SR, Zuliani JP, Fernandes CM, Cruz-Hofling MA, Fernandes I, Chaves F & Gutiérrez JM (2003). Neutrophils do not contribute to local tissue damage, but play a key role in skeletal muscle regeneration, in mice injected with Bothrops asper snake venom. *Muscle Nerve* **28,** 449–459.

Temmerman L, Slonimsky E & Rosenthal N (2010). Class 2 IGF-1 isoforms are dispensable for viability, growth and maintenance of IGF-1 serum levels. *Growth Horm IGF Res* **20,** 255–263.

Tidball JG (2005). Inflammatory processes in muscle injury and repair. *Am J Physiol Regul Integr Comp Physiol* **288,** R345–R353.

Tidball JG (2011). Mechanisms of Muscle Injury, Repair, and Regeneration. In *Comprehensive Physiology*, ed. David M. Pollock, pp. 2029–2062.

John Wiley & Sons, Inc., Hoboken, NJ, USA.

Tidball JG (2017). Regulation of muscle growth and regeneration by the immune system. *Nat Rev Immunol* **17,** 165–178.

Tidball JG, Dorshkind K & Wehling-Henricks M (2014). Shared signaling systems in myeloid cell-mediated muscle regeneration. *Development* **141,** 1184–1196.

Tidball JG & Rinaldi C (2012). Immunological Responses to Muscle Injury. In *Muscle: Fundamental Biology and Mechanisms of Disease*, 1st edn., ed. Hill JA & Olson EN, pp. 899–909. Elsevier, New York, NY.

Tidball JG & St Pierre BA (1996). Apoptosis of macrophages during the resulution of muscle inflammation. *J Leukoc Biol* **59,** 380–388.

Tidball JG & Villalta SA (2010). Regulatory interactions between muscle and the immune system during muscle regeneration. *Am J Physiol Regul Integr Comp Physiol* **298,** R1173–R1187.

Tidball JG & Welc SS (2015). Macrophage-derived IGF-1 is a potent coordinator of myogenesis and inflammation in regenerating muscle. *Mol Ther* **23,** 1134–1135.

Tonkin J, Temmerman L, Sampson RD, Gallego-Colon E, Barberi L, Bilbao D, Schneider MD, Musarò A & Rosenthal N (2015). Monocyte/Macrophage-derived IGF-1 Orchestrates Murine Skeletal Muscle Regeneration and Modulates Autocrine Polarization. *Mol Ther* **23,** 1189–1200.

Torrente Y, El Fahime E, Caron NJ, Del Bo R, Belicchi M, Pisati F, Tremblay JP & Bresolin N (2003). Tumor necrosis factor-alpha (TNF-alpha) stimulates chemotactic response in mouse myogenic cells. *Cell Transplant* **12,** 91–100.

Toth KG, McKay BR, De Lisio M, Little JP, Tarnopolsky MA & Parise G (2011). IL-6 induced STAT3 signalling is associated with the proliferation of human muscle satellite cells following acute muscle

damage. *PLoS One* **6,** e17392.

Toumi H & Best TM (2003). The inflammatory response: friend or enemy for muscle injury? *Br J Sports Med* **37,** 284–286.

Toumi H, F'guyer S & Best TM (2006). The role of neutrophils in injury and repair following muscle stretch. *J Anat* **208,** 459–470.

Vassilakos G, Philippou A & Koutsilieris M (2017). Identification of the IGF-1 processing product human Ec/rodent Eb peptide in various tissues: Evidence for its differential regulation after exercise-induced muscle damage in humans. *Growth Horm IGF Res* **32,** 22–28.

Vassilakos G, Philippou A, Tsakiroglou P & Koutsilieris M (2014). Biological activity of the e domain of the IGF-1Ec as addressed by synthetic peptides. *Hormones (Athens)* **13,** 182–196.

Verstak B, Nagpal K, Bottomley SP, Golenbock DT, Hertzog PJ & Mansell A (2009). MyD88 adapter-like (Mal)/TIRAP interaction with TRAF6 is critical for TLR2- and TLR4-mediated NF-kappaB proinflammatory responses. *J Biol Chem* **284,** 24192–24203.

Villalta SA, Rinaldi C, Deng B, Liu G, Fedor B & Tidball JG (2011). Interleukin-10 reduces the pathology of mdx muscular dystrophy by deactivating M1 macrophages and modulating macrophage phenotype. *Hum Mol Genet* **20,** 790–805.

Wallis M (2009). New insulin-like growth factor (IGF)-precursor sequences from mammalian genomes: the molecular evolution of IGFs and associated peptides in primates. *Growth Horm IGF Res* **19,** 12–23.

Wang H, Melton DW, Porter L, Sarwar ZU, McManus LM & Shireman PK (2014). Altered macrophage phenotype transition impairs skeletal muscle regeneration. *Am J Pathol* **184,** 1167–1184.

Warren GL, Hulderman T, Jensen N, McKinstry M, Mishra M, Luster MI & Simeonova PP (2002). Physiological role of tumor necrosis factor alpha in traumatic muscle injury. *FASEB J* **16,** 1630–1632.

Warren GL, Summan M, Gao X, Chapman R, Hulderman T & Simeonova PP (2007). Mechanisms of skeletal muscle injury and repair revealed by gene expression studies in mouse models. *J Physiol* **582,** 825–841.

Weaver JC, Smith KC, Esser AT, Son RS & Gowrishankar TR (2012). A brief overview of electroporation pulse strength-duration space: a region where additional intracellular effects are expected. *Bioelectrochemistry* **87,** 236–243.

Whitham M & Febbraio MA (2016). The ever-expanding myokinome: discovery challenges and therapeutic implications. *Nat Rev Drug Discov* **15,** 719–729.

Wlodkowic D, Skommer J & Darzynkiewicz Z (2009). Flow cytometry-based apoptosis detection. *Methods Mol Biol* **559,** 19–32.

Wynn TA & Vannella KM (2016). Macrophages in Tissue Repair, Regeneration, and Fibrosis. *Immunity* **44,** 450–462.

Xiao W, Chen P, Wang R & Dong J (2013). Overload training inhibits phagocytosis and ROS generation of peritoneal macrophages: role of IGF-1 and MGF. *Eur J Appl Physiol* **113,** 117–125.

Yahiaoui L, Gvozdic D, Danialou G, Mack M & Petrof BJ (2008). CC family chemokines directly regulate myoblast responses to skeletal muscle injury. *J Physiol* **586,** 3991–4004.

Yang J, Zhang L, Yu C, Yang X-F & Wang H (2014). Monocyte and macrophage differentiation: circulation inflammatory monocyte as biomarker for inflammatory diseases. *Biomark Res* **2,** 1.

Yang S, Alnaqeeb M, Simpson H & Goldspink G (1996). Cloning and characterization of an IGF-1 isoform expressed in skeletal muscle subjected to stretch. *J Muscle Res Cell Motil* **17,** 487–495.

Yang SY & Goldspink G (2002). Different roles of the IGF-I Ec peptide (MGF) and mature IGF-I in myoblast proliferation and differentiation. *FEBS Lett* **522,** 156–160.

Ye F, Mathur S, Liu M, Borst SE, Walter GA, Sweeney HL & Vandenborne K (2013). Overexpression of insulin-like growth factor-1 attenuates skeletal muscle damage and accelerates muscle regeneration and functional recovery after disuse. *Exp Physiol* **98,** 1038–1052.

Yin H, Price F & Rudnicki MA (2013). Satellite cells and the muscle stem cell niche. *Physiol Rev* **93,** 23–67.

Yu Y-RA, O'Koren EG, Hotten DF, Kan MJ, Kopin D, Nelson ER, Que L & Gunn MD (2016). A protocol for the comprehensive flow cytometric analysis of immune cells in normal and inflamed murine non-lymphoid tissues. ed. Mueller SN. *PLoS One* **11,** e0150606.

Zabłocka B, Goldspink PH, Goldspink G & Górecki DC (2012). Mechano-Growth Factor: an important cog or a loose screw in the repair machinery? *Front Endocrinol (Lausanne)* **3,** 131.

Zhang C, Li Y, Wu Y, Wang L, Wang X & Du J (2013). Interleukin-6/signal transducer and activator of transcription 3 (STAT3) pathway is essential for macrophage infiltration and myoblast proliferation during muscle regeneration. *J Biol Chem* **288,** 1489–1499.

Zhang L, Wang XH, Wang H, Du J & Mitch WE (2010*a*). Satellite cell dysfunction and impaired IGF-1 signaling cause CKD-induced muscle atrophy. *J Am Soc Nephrol* **21,** 419–427.

Zhang Q, Raoof M, Chen Y, Sumi Y, Sursal T, Junger W, Brohi K, Itagaki K & Hauser CJ (2010*b*). Circulating mitochondrial DAMPs cause inflammatory responses to injury. *Nature* **464,** 104–107.

Van Ziffle JA & Lowell CA (2009). Neutrophil-specific deletion of Syk kinase results in reduced host defense to bacterial infection. *Blood* **114,** 4871–4882.

Zong CS, Chan J, Levy DE, Horvath C, Sadowski HB & Wang LH (2000). Mechanism of STAT3 activation by insulin-like growth factor I receptor. *J Biol Chem* **275,** 15099–15105.